Molecular mechanisms controlling excitatory synaptic transmission

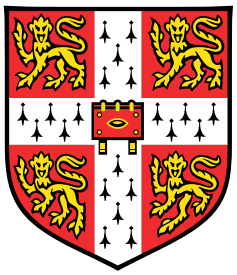

Jake Frederick Watson

Supervisor: Dr. Ingo H. Greger

MRC Laboratory of Molecular Biology
University of Cambridge

This dissertation is submitted for the degree of
Doctor of Philosophy

Pembroke College March 2018

On the importance of large ornaments

Preface

This thesis is the result of my own work and includes nothing which is the outcome of work done in collaboration except as declared below and specified in the text.

The development of IVA Cloning (Chapter 3) was a collaborative project conceived through discussions with Dr Javier García-Nafría, and a subset of experiments were performed by Dr García-Nafría. Chapters 4 and 5 were conducted with support from Mr Hinze Ho, who aided the preparation and maintenance of organotypic slice cultures, performed the majority of single-cell electroporation and conducted a subset of electrophysiological recordings to independently confirm important findings. Investigations were conducted under the supervision of Dr Ingo Greger.

This thesis is not substantially the same as any that I have submitted, or, is being concurrently submitted for a degree or diploma or other qualification at the University of Cambridge or any other University or similar institution. I further state that no substantial part of my dissertation has already been submitted, or, is being concurrently submitted for any such degree, diploma or other qualification at the University of Cambridge or any other University or similar institution.

This thesis contains less than 60,000 words excluding the bibliography, appendix and figure legends.

Jake Frederick Watson
March 2018

A subset of results, figures and ideas presented in this document have been published in the following:

Articles

García-Nafría, J., Watson, J. F.*, and Greger, I. H. 2016. IVA cloning: A single-tube universal cloning system exploiting bacterial* In Vivo *Assembly. Scientific reports. 6, 27459; doi: 10.1038/srep27459*. (* authors contributed equally)

Watson, J. F., Ho, H., and Greger, I. H. 2017. Synaptic transmission and plasticity require AMPA receptor anchoring via its N-terminal domain. eLife, 6:471-484.

Reviews

García-Nafría, J., Herguedas, B., Watson, J. F., and Greger, I. H. 2016. The dynamic AMPA receptor extracellular region: A platform for synaptic protein interactions. The Journal of physiology, 594(19):5449-5458.

Greger, I. H., Watson, J. F., and Cull-Candy, S.G. 2017. Structural and Functional Architecture of AMPA-Type Glutamate Receptors and Their Auxiliary Proteins. Neuron, 94(4):713-730.

Acknowledgements

Firstly, I thank the Medical Research Council for funding this study. I would very much like to thank Dr Ingo Greger for his supervision throughout this research, and whose ideas, advice and enthusiasm have been essential for this investigation. It has been an entertaining experience. I am very grateful to Hinze Ho for his collaboration and technical support on this project, without which it would certainly not have been as efficient or productive. I also thank Dr Javier García-Nafría, with whom I have enjoyed developing many optimistic ideas, of which at least a few actually appear to be of some value. I have had valuable electrophysiological advice from Prof. Ole Paulsen, for which I am very grateful.

I have enjoyed and benefitted from working with many members of the Greger Lab both past and present, in particular Dr Alexandra Pinggera, who regularly offers interesting and productive discussions, and has proofread sections of this study, Dr James Krieger, whose thoughtful suggestions often prompt new ideas, and Drs Beatriz Herguedas and Ondrej Cais, whose technical expertise have been important to this work. The exchanges with Professor Terunaga Nakagawa during his time in Cambridge have been both insightful and thought-provoking. Many thanks also to Dr Tanja Fuchsberger for collaboration and numerous interesting discussions, and Dr Katharina Strege for her valuable advice. I am greatly indebted to the biomedical staff at the LMB and Ares for their essential technical support, and a variety of staff at the LMB for their assistance, in particular Dr Nick Barry and the Light Microscopy team. I am also thankful to Dr Alina Guna and Maria Daly for flow cytometry support, and Dr Ana González Rueda for initial assistance with P0 viral injections.

I am grateful to a number of members of the wider scientific community for provision of animals, tools, reagents and advice. I am very thankful to Dr Andrew Penn for providing custom NSFA scripts, and both Dr Penn and Dr Tim Benke for great support in their application. I am thankful to Prof. Yasunori Hayashi, who offered useful advice and protocols on transfection of dissociated neuronal cultures, and Prof. Helmut Kessels for insightful discussions on mEPSC and LTP recordings. Dr Rolf Sprengel provided *Gria1, 2 and 3*$^{fl/fl}$ mice, and various plasmids were provided by Dr José A. Esteban, Dr Jonathan Hanley, Dr Andrew Penn and Prof. Bong-Kiun Kaang, as mentioned throughout.

Finally, I am thankful to the many public houses of Cambridge for provision of abundant refreshments in support of invariably constructive discussions.

Abstract

At synapses, the sites of communication between neurons, neurotransmitter is released from the presynaptic cell and binds to postsynaptic receptors on another. In the case of excitatory synapses, the predominant neurotransmitter, L-glutamate, binds to postsynaptic AMPA receptors (AMPARs). Crucially, synaptic strength is plastic, and control of this strength is essential for fundamental brain functions such as the processing and storage of information.

Synaptic transmission is controlled by tuning the response of postsynaptic receptors to glutamate release. This can be achieved by altering both the number and spatial positioning of receptors. The mechanisms governing AMPAR anchoring at postsynaptic sites have been intensely studied for many years, focussing on intracellular interactions with postsynaptic scaffold proteins, however, these interactions do not appear strictly essential to synaptic receptor anchoring. The receptor's N-terminal domain (NTD) comprises 50 % of the protein, and extends into the synaptic cleft, towards the presynapse, offering great potential for subunit-specific receptor control, yet its influence on synaptic transmission remains elusive.

Facilitated by the development of an optimised molecular cloning approach, this study uses a combination of electrophysiological and imaging methods to investigate the role of the AMPAR NTD at synaptic sites. It demonstrates that this domain has a critical role in anchoring the AMPAR at the synapse. Through subunit-specific interactions in the synaptic cleft, the NTD controls the number of receptors present at a synaptic connection. Receptors lacking the NTD are unable to properly anchor at synaptic sites, and are unable to facilitate synaptic plasticity such as long-term potentiation, despite robustly trafficking to the cell surface. When studied in comparison to other AMPAR anchoring interactions, NTD-dependent mechanisms appear to be more influential than classical models involving the intracellular C-terminal of the receptor. Given that NTD-dependent interactions will occur within the synaptic cleft, both pre and postsynaptic neurons have the potential to control and detect the strength of synaptic transmission. Therefore, this mechanism of AMPAR anchoring has profound implications when considering how information is stored at a synaptic connection.

Table of contents

Abbreviations

γ	- single-channel conductance
A-EJ	- alternative end-joining
AAV	- adeno-associated virus
ABDH6	- α/β-hydrolase domain containing 6
ABP	- AMPAR binding protein
aCSF	- artificial cerebrospinal fluid
ADAR	- adenosine deaminases acting on RNA
AMPAR	- α-amino-3-hydroxy-5-methyl-4-isoxazolepropionic acid receptor
ATP	- adenosine 5'-triphosphate
bp	- base pairs
BSA	- bovine serum albumin
C1q	- complement component 1q
CA1	- *cornu ammonis* region 1
CA3	- *cornu ammonis* region 3
CaMKII	- calcium/calmodulin-dependent protein kinase II
CFU	- colony forming units
CMV	- cytomegalovirus
CNIH	- cornichon

CP-AMPAR - calcium-permeable AMPA receptor

CPT1c - carnitine O-palmitoyltransferase 1c

CTZ - cyclothiazide

CUB - C1r/C1s, Uegf, Bmp1

D-APV - D-(-)-2-Amino-5-phosphonopentanoic acid

DAPI - 4',6-diamidino-2-phenylindole

DAT - days after transfection

DG - dentate gyrus

DIV - days *in vitro*

DMEM - Dulbecco's Modified Eagle's medium

DNA - deoxyribonucleic acid

dNTP - deoxyribonucleotide

DTT - dithiothreitol

ECS - extracellular solution

EGFP - enhanced green fluorescent protein

EGTA - Ethylene glycol-bis(2-aminoethylether)-N,N,N',N'-tetraacetic acid

EPSC - excitatory postsynaptic current

FBS - fetal bovine serum

FRAP - fluorescence recovery after photobleaching

FRRS1L - ferric-chelate reductase 1-like

$GABA_AR$ - γ-aminobutyric acid receptor A

GBSS - Gey's Balanced Salt Solution

GFP - green fluorescent protein

GRIP - glutamate receptor interacting protein

HEPES - 4-(2-hydroxyethyl)-1-piperazineethanesulfonic acid

ICD - intracellular domain

ICS - intracellular solution

IgG - immunoglobulin G

iGluR - ionotropic glutamate receptor

ITR - inverted terminal repeat

IV - current/voltage (relationship)

IVA - *In vivo* Assembly

KA - kainic acid/ kainate

LB - lysogeny broth

LBD - ligand-binding domain

LIC - Ligation Independent Cloning

LRRTM - leucine-rich repeat containing transmembrane proteins

MAGUK - membrane associated guanylate kinase

MEM - Minimal Essential Medium

mEPSC - miniature excitatory postsynaptic current

MES - 2-(N-morpholino)ethanesulfonic acid

mGluR - metabotropic glutamate receptor

MOPS - 3-(*N*-morpholino)propanesulfonic acid

mRNA - messenger RNA

NA - numerical aperture

NETO - neuropilin and tolloid like

NHEJ - non-homologous end-joining

NMDAR - N-methyl-D-aspartate receptor

NP - neuronal pentraxin (1/2/R - receptor)

NRAP-1 - NMDAR auxiliary protein 1

NSF - N-ethylmaleimide-sensitive fusion protein

NSFA - Non-stationary fluctuation analysis

NTD - N-terminal domain (also known as amino-terminal domain)

P_o - open probability

P_r - probability of release

PBS - phosphate buffered saline

PCR - Polymerase Chain Reaction

PFA - paraformaldehyde

PICK - protein interacting with C kinase

PIPE - Polymerase Incomplete Primer Extension

PKA - protein kinase A

PMSF - phenylmethylsulfonyl fluoride

PORCN - porcupine

PPD - paired-pulse depression

PPF - paired-pulse facilitation

PPR - paired-pulse ratio

PSD-95 - postsynaptic density protein 95

PSF - point-spread function

Q-dot - quantum-dot

RAIR - *recA*-independent recombination

RI - rectification index

RNA - ribonucleic acid

rtp - room temperature and pressure

SAP - synapse associated protein

SCE - single-cell electroporation

SDS-PAGE - sodium dodecyl sulfate polyacrylamide gel electrophoresis

SEM - standard error of the mean

SEP - super-ecliptic pHluorin

SOC - Super Optimal Broth with Catabolite repression

SOL-1 - suppressor of Lurcher 1

STED - stimulated emission depletion (microscopy)

STORM - stocastic optical reconstruction microscopy

T_m - melting temperature

TARP - Transmembrane AMPAR Regulatory Protein

tCaMKII - truncated CaMKII (constitutively active)

TTX - tetrodotoxin

TWEEN 20 - polyoxyethylene-20

VGCC - voltage-gated calcium channel

Chapter 1

Introduction

1.1 On synaptic transmission

Communication between neurons occurs at specialised connections called synapses (Figure 1.1). At these locations, neurotransmitter is released from one cell (at presynaptic sites) and binds to receptors on the other (the postsynapse) (Lisman et al., 2007). At excitatory synapses, the predominant neurotransmitter, L-glutamate, is released and binds to postsynaptically localised AMPA receptors (Collingridge and Lester, 1989). The strength of the intercellular connection can be altered in a vast number of ways, occurring differently across the diverse synapses in the brain, for example modifying the levels of released neurotransmitter, changing the electrical coupling between the synapse and the rest of the neuron, or as has been intensely studied, it can be controlled by tuning the magnitude of the postsynaptic receptor response. Multiple mechanisms can control the magnitude of this postsynaptic response, such as the channel properties, the number or even spatial positioning of these receptors (Lisman et al., 2007).

Synaptic transmission occurs when the presynaptic cell fires an action potential, which invades the presynaptic terminal causing an influx of calcium ions by activation of voltage-gated calcium channels (VGCC) (Lisman et al., 2007). Glutamate-containing vesicles fill the presynaptic area, a subset of which are associated with the protein machinery required for membrane fusion, primed for fast release of their cargo into the synaptic cleft (Rothman et al., 2017). Glutamate within the synaptic cleft has been estimated to reach approximately 1 mM (Clements et al., 1992) and causes the activation of a wide-range of postsynaptic glutamate receptors, which through either direct or indirect action, introduce a conductance at the postsynaptic membrane, allowing ion flow and depolarisation of the postsynaptic cell.

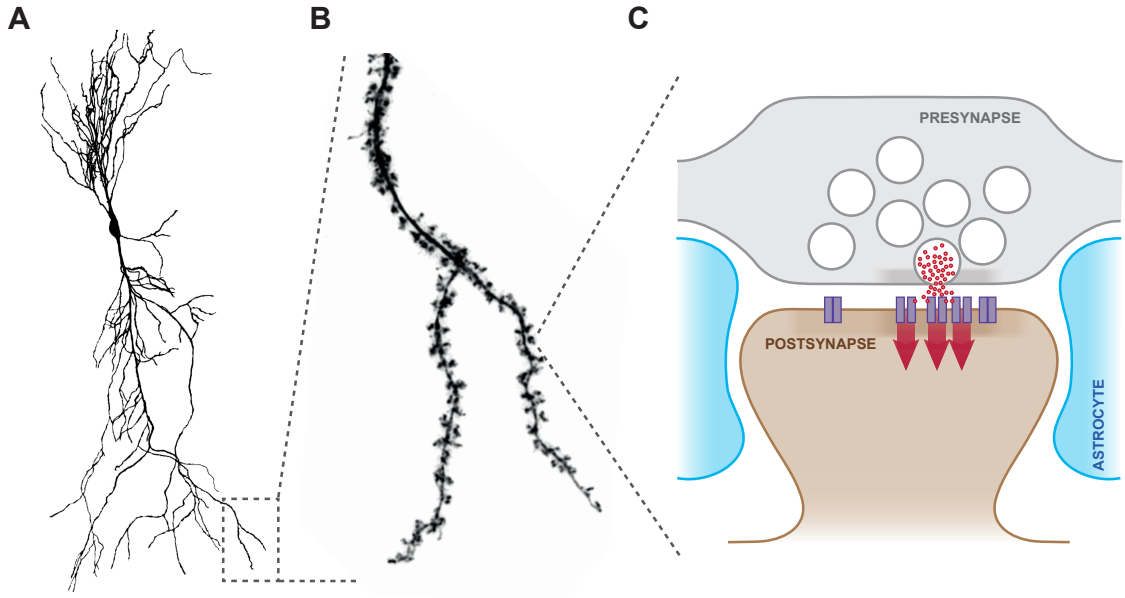

Figure 1.1 ***The synapse.*** *(**A**) CA1 pyramidal neuron outline. (**B**) Magnified view of dendritic section displaying dendritic spines, the location of the postsynapse. (**C**) Schematic of the synapse. Glutamate (red circle) released from the presynaptic vesicles, binds to postsynaptic receptors (purple) to depolarise the postsynaptic membrane allowing ion flow (indicated by red arrow).*

On pyramidal neurons, the postsynaptic site is located on membrane protrusions from the dendrite called spines (Figure 1.1; Spruston, 2008). The synapse is a tripartite structure, with the pre- and postsynaptic connection surrounded by an astrocytic process, which plays a significant role in tuning synaptic transmission, by clearing released glutamate (Diamond and Jahr, 1997), influencing neurotransmitter spillover to adjacent connections (Barbour and Häusser, 1997) and releasing factors which can control the constituents of the synaptic cleft (Eroglu and Barres, 2010).

The influence of synaptic transmission on the postsynaptic cell, is both highly plastic and highly variable between synaptic connections, even within a single cell. A striking example of this occurs at the pyramidal neurons in the CA3 (Cornu Ammonis 3) region of the hippocampus, where the ‘mossy-fibre’ connection from the dentate gyrus (DG) and recurrent CA3 to CA3 connections have very different properties. The mossy-fibre terminals form a so-called ‘detonator synapse’, each with around 20 release sites, which are individually capa-

ble of inducing a postsynaptic action potential (Vyleta et al., 2016). CA3-CA3 connections meanwhile, form more traditional connections, generally with a single release site (Rebola et al., 2017), and therefore the coordinated integration of multiple synaptic inputs is required for postsynaptic cell firing. In such a case, the magnitude of the postsynaptic depolarisation at a single synapse is of critical importance to neuronal signalling.

Particular patterns of synaptic transmission, either at a single synapse or at a subset of synapses on a dendritic branch can induce signalling cascades that increase the strength of transmission, in a phenomenon known as long-term potentiation (LTP). First discovered at the perforant path synapse onto granule cells of the DG (Bliss and Lømo, 1973), this effect has subsequently been discovered at many synapses across the brain (Mayford et al., 2012) and has been shown to last for at least a year (Abraham et al., 2002), providing a candidate mechanism for the molecular basis of long-term memory. Indeed Nabavi et al. (2014) demonstrated control over contextual memory by induction and elimination of LTP. At the hippocampal CA3 to CA1 synapse, LTP expression appears to predominantly occur by increasing the postsynaptic AMPA receptor content (Mainen et al., 1998; Muller et al., 1988), and therefore the mechanisms controlling the trafficking and positioning of AMPARs at the postsynaptic membrane are of great significance to our understanding of information storage.

1.2 Glutamate receptors

Glutamate acts on two classes of receptor after presynaptic release, ionotropic and metabotropic receptors. Ionotropic glutamate receptors (iGluRs) are transmembrane proteins containing a pore which can allow ion flow across the membrane, thus responsible for fast synaptic transmission at the synapse (Traynelis et al., 2010). Despite also being transmembrane proteins, metabotropic glutamate receptors (mGluRs) do not themselves allow ion flow, and act through G-proteins to indirectly modulate synaptic transmission either presynaptically, by altering the probability of vesicle release, or postsynaptically, by initiating signalling cascades influencing ionotropic receptor function and synaptic plasticity (Niswender and Conn, 2010). Given their indirect mechanism, metabotropic glutamate receptors act on a longer time scale than ionotropic receptors, which provide the millisecond timescale signalling required for effective neuronal communication.

Four subfamilies of receptors make up the ionotropic glutamate receptor family (Figure

1.2A), AMPA (α-amino-3-hydroxy-5-methyl-4-isoxazolepropionic acid) receptors (AMPAR), NMDA (*N*-Methyl-D-aspartic acid) receptors (NMDAR), kainate receptors (KAR) and delta receptors, which all have a similar architecture, dictating many functional characteristics of the receptors.

1.2.1 Architecture of the AMPA Receptor

Like all iGluRs, the AMPAR is a tetrameric receptor, and is built into homo- or heterotetramers from four core subunits, GluA1-4 (Traynelis et al., 2010). The receptor consists of four domains, each interconnected by flexible peptide linkers: the extracellular N-terminal domain (NTD, or amino-terminal domain) and ligand-binding domain (LBD), a transmembrane domain (TMD) and an intracellular C-terminal domain (CTD) (Figure 1.2). The LBD and TMD are the most evolutionarily conserved receptor portions, which are highly akin to prokaryotic glutamate receptors (Chen et al., 1999a). The NTD and CTD are the most sequence diverse portions of the receptor, and therefore offer the greatest capacity to confer subunit-specific functions.

The C-terminal domain

The C-terminal domain of the AMPAR does not appear to have a strict structure, instead forming a long flexible polypeptide, which can extend intracellularly to interact with a plethora of proteins. This domain has been implicated in a wide variety of AMPAR functions, from receptor trafficking, to synaptic anchoring and also influencing receptor gating (Kristensen et al., 2011; Shepherd and Huganir, 2007). Both the length and sequence of this receptor portion is highly different between AMPAR subunits, meaning that it has been the subject of intense focus aiming to understand subunit-specific receptor trafficking for a number of years. The CTDs of GluA2 and GluA4 have been shown to exist in two isoforms, produced by differential RNA splicing (Kohler et al., 1994). The less abundant GluA2'long' variant is highest expressed in the juvenile hippocampus, and may have some role in synaptic plasticity (Kolleker et al., 2003). The conformational changes occurring during channel activation have been suggested to drive motions of the CTD, which may have implications for their interactions in the postsynaptic density (Zachariassen et al., 2016). Numerous protein interaction partners have been identified for the CTD, binding subunit-specifically to control receptor function (Shepherd and Huganir, 2007; Shi et al., 2001). The domain is multiply phosphorylated by protein kinases, with roles in receptor trafficking (Shepherd and Huganir, 2007), yet in many cases, the mechanism of this action, beyond initial phosphorylation, re-

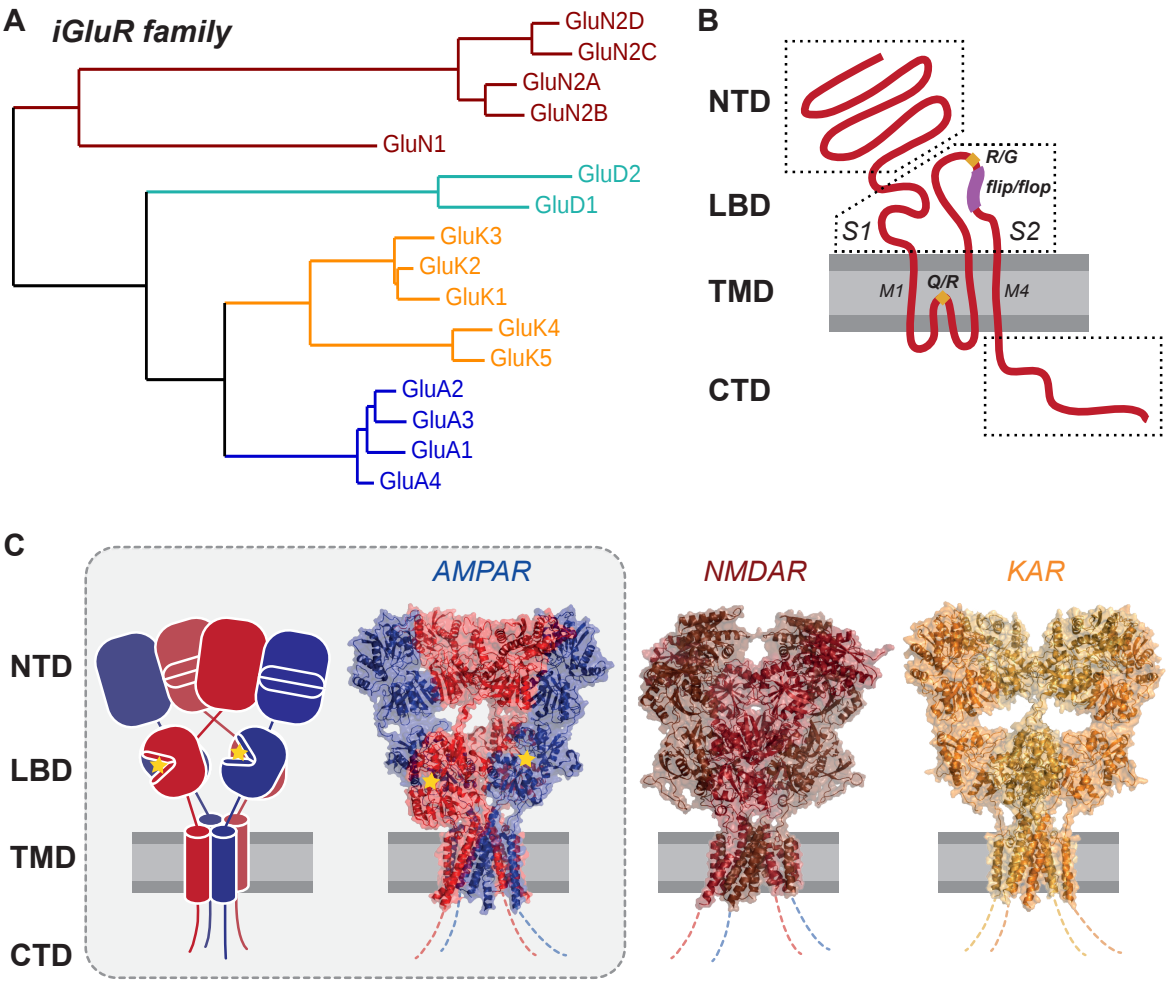

Figure 1.2 *AMPA receptor architecture.* *(**A**) iGluR family phylogeny tree based on protein sequence and coloured by subfamily. Produced using Phylogeny.fr (Dereeper et al., 2008) (**B**) Schematic of AMPA receptor polypeptide depicting topology of domains with respect to the plasma membrane (NTD - N-terminal domain; LBD - Ligand-binding domain; TMD - Transmembrane domain; CTD - C-terminal domain). The extracellular portion of the receptor is formed of the NTD and LBD, the LBD itself being formed of the S1 and S2 loops. The locations of RNA editing and splicing sites are indicated (Q/R and R/G editing sites are yellow diamonds, the flip/flop cassette is depicted in pink). The four transmembrane domains are numbered left to right, with M1 and M4 labelled. (**C**) Cartoon and crystal structure (PDB: 3KG2; Sobolevsky et al., 2009) of AMPAR demonstrating the receptor architecture. Chains are coloured as per the expected positions of subunits within a heteromeric receptor. CTD was not resolved in structure and is represented as a dotted line. Glutamate binding location is indicated with a star. Structures of NMDAR (PDB:4PE5; Karakas and Furukawa, 2014) and KARs (PDB:5KUF; Meyerson et al., 2016) are depicted for comparison.*

mains unclear. The extreme C-terminus of the AMPAR contains a PDZ-domain binding site. Named after three proteins containing this domain (PSD-95, Discs-large, ZO-1; Kennedy, 1995), PDZ domain containing proteins are abundant in the postsynaptic area, with critical roles in assembling the mass of proteins at the postsynaptic density involved in synaptic transmission (Feng and Zhang, 2009). The specific influences of these interactions and phosphorylations on synaptic transmission will be subsequently discussed in greater depth.

The Transmembrane domain

The transmembrane domain forms the pore of the receptor, which conducts ion flow for its primary signalling function. Each monomer of the AMPAR contains three full transmembrane domains (M1, M3 and M4) and one reentrant helix (M2), which dips into the membrane from the intracellular side, forming an ion-selective filter for the channel (Kuner et al., 2001; Sobolevsky et al., 2009). In the full tetrameric receptor, this bundle of 16 helical segments undergoes structural rearrangements on glutamate binding to allow the passage of ions across the membrane (Twomey et al., 2017). The crossing of M3 helices forms the gate of the channel, while the M2 helix exerts unique subunit-specific channel properties. This helix is located centrally within the channel pore, adjacent to the intracellular side of the membrane (Sobolevsky et al., 2009; Figure 1.2B). A conserved glutamine residue (Q) pointing into the receptor pore is encoded in the DNA of all subunits, however RNA (ribonucleic acid) editing of the GluA2 transcript causes a glutamine to arginine (Q to R) single amino-acid transition at this location (Sommer et al., 1991).

Adenosine to Inosine (A to I) editing by ADAR proteins (adenosine deaminases acting on RNA; Nishikura, 2016) causes the CAG ‘Q encoding’ codon to transition to the ‘R encoding’ CIG triplet (Sommer et al., 1991) at GluA2 position 586, with significant implications for channel function. This single-residue substitution controls the permeability of the pore for calcium ions, the conductance of the channel, and the pharmacology of channel block by polyamines. Edited GluA2, incorporated into heteromeric receptors severely limits the permeation of calcium ions, which can pass through channels formed of GluA1, 3 or 4 alone (Burnashev et al., 1992; Hume et al., 1991; Mishina et al., 1991; Verdoorn et al., 1991). Calcium permeability of AMPARs is strictly controlled due to the possible excitotoxic consequences, and prevention of GluA2 editing is lethal (Higuchi et al., 2000). Calcium permeable AMPARs do exist in the brain under strict spatio-temporal control, with functions in specific cell populations and during synaptic plasticity (Isaac et al., 2007). Approximately 100 % of GluA2 transcripts are edited at this position (Egebjerg et al., 1994; Sommer et al.,

1991), meaning that GluA2 'R' likely occurs exclusively throughout the brain. GluA2 'Q' has been suggested to occasionally be produced in disease, with detrimental excitotoxic effects (Wright and Vissel, 2012). Due to their differential ion flux, calcium permeable AMPARs have approximately double the single-channel conductance of GluA2R containing receptors (Swanson et al., 1997).

A second consequence of this editing is its influence on polyamine inhibition of the channel. AMPARs in which all four subunits of the tetramer contain a glutamine residue at this editing position (Q-pore) are blocked by intracellular polyamines at positive membrane potentials (Bowie and Mayer, 1995; Kamboj et al., 1995; Koh et al., 1995), giving rise to a rectifying current-voltage relationship. This phenomenon has been extensively exploited to study AMPAR trafficking, allowing electrophysiological detection of Q-pore receptors among a recorded receptor population (for example Kolleker et al., 2003; Shi et al., 2001). This phenomenon is exploited in the present study and therefore will be subsequently discussed in greater detail.

The Ligand-binding domain

The ligand-binding domain, as can be inferred from its name, binds the receptor agonist 'L-glutamate' and is formed of two separate regions of the receptor polypeptide: S1, which follows the N-terminal domain, and S2, which occurs between the M3 and M4 helices (Figure 1.2B; Stern-Bach et al., 1994). This domain folds into a clamshell shape, which binds glutamate in its cleft (Armstrong and Gouaux, 2000). Channel activation occurs on closure of this cleft, which induces structural arrangements of the pore, transmitted by flexible linkers between the LBD and TMD (Mayer, 2006).

The CTD and TMD are not the only receptor regions which undergo alternative mRNA processing. Alternative splicing at the LBD inserts one of two different sequences termed 'flip' and 'flop', which confer different channel gating properties, pharmacologies (Sommer et al., 1990) and receptor forward trafficking (Figure 1.2B; Coleman et al., 2006). This splicing occurs for all four AMPAR subunits, and has been demonstrated to be activity-regulated, with significant consequences for synaptic signalling (Penn et al., 2012). A to I editing also occurs in the LBD, at the 'RG-site', where either an arginine or glycine can subsequently occur in the protein sequence, influencing receptor gating properties (Lomeli et al., 1994), and being controlled in an activity-dependent manner (Balik et al., 2013).

The N-terminal domain

The N-terminal domain (NTD) of the receptor comprises approximately 50 % of the receptor mass (Figure 1.2C), yet despite this, its function has remained relatively unclear. Similarly to the LBD, it forms a clamshell-like structure, however no known ligand for this domain has been identified (Clayton et al., 2009; Jin et al., 2009; Sukumaran et al., 2011). The tetrameric AMPAR is built from two receptor dimers, and receptor assembly appears to be driven by NTD associations (Rossmann et al., 2011). In particular, associations of the NTD control the heteromeric assembly of tetrameric receptors due to the differential affinities of each subunit NTD with each other (Rossmann et al., 2011; Zhao et al., 2017). Formation of GluA2-containing receptors is strongly favoured by the affinity of other subunits for the GluA2 NTD, which is greater than the affinity for homodimerisation (Rossmann et al., 2011). The greatest example of this is the GluA3 NTD, which has an affinity for the GluA2 NTD which is three orders of magnitude higher than for another GluA3 NTD. This effect contributes to the formation of exclusively GluA2-containing receptors in hippocampal CA1 pyramidal neurons, where GluA1, GluA2 and GluA3 expression forms GluA1/2 and GluA2/3 heteromeric receptors (Lu et al., 2009; Wenthold et al., 1996).

While the NTD of iGluR family members has a strong allosteric influence on channel function (Elegheert et al., 2016; Yuan et al., 2009), no critical role for that of the AMPAR has been shown in channel gating, although the potential of the domain for an allosteric signalling function has been highlighted in multiple reports (Krieger et al., 2015; Sukumaran et al., 2011). Deletion of the NTD affects surface trafficking of the receptor in recombinant cell lines (Möykkynen et al., 2014), but does not have a major impact on channel function, affecting the desensitisation properties of the receptor to some extent (Bedoukian et al., 2006; Pasternack et al., 2002).

This domain has been implicated in synaptic function in sporadic reports. The NTD of GluA4 has been shown to interact with neuronal pentraxins (NPs) which facilitates receptor clustering at synaptic sites in hippocampal interneuron synapses (Chang et al., 2010; Pelkey et al., 2015; Sia et al., 2007), and more recent reports suggest this mechanism may control GluA1-dependent transmission in retinal ganglion cells (Farhy-Tselnicker et al., 2017). Retrograde synaptic signalling through the NTD has been suggested (Ripley et al., 2011; Tracy et al., 2011), but not thoroughly investigated, and the NTD of GluA2 has also been reported to have an incredible synaptogenic function (Passafaro et al., 2003), yet this report has been highly questioned (Biou et al., 2008; Chen et al., 2009; Lu et al., 2009). The potential role of

the NTD in synaptic function is a key focus of the present investigation, and these studies will be subsequently discussed in greater detail.

Rearrangements of the AMPA Receptor

Due to the flexible polypeptide linkers between domains (Figure 1.2C), the AMPAR appears capable of undergoing substantial structural rearrangements, evident from the initial structural analyses of the receptor (Nakagawa et al., 2005). Receptor desensitisation appears to correlate with separation of the NTD layer of the receptor, which can collapse towards the membrane. Further rearrangements of the extracellular portion of the receptor have been predicted by computational modelling (García-Nafría et al., 2016a; Krieger et al., 2015), and confirmed by electron microscopy (Herguedas et al., 2016; Meyerson et al., 2014). The consequence of this flexibility for receptor function are significant. Intrinsic gating of the receptor could be affected by the speed and magnitude of these rearrangements, and may facilitate interaction of the NTD with membrane proximal proteins, as has been demonstrated (Cais et al., 2014). In the crowded location of the synaptic cleft, these motions could potentially either enable or limit the interactions with synaptic proteins, directly controlling the contribution of the receptor to synaptic transmission (García-Nafría et al., 2016a).

1.2.2 The ionotropic glutamate receptor family

Delta receptors

AMPAR, NMDAR and KARs have well characterised ligand-gated ion channel functions, each with their own individual gating characteristics, protein interactions and neuronal expression patterns determining their role in brain function, however delta receptors are classified into the iGluR family by sequence homology, rather than functional alignment (Yamazaki et al., 1992). Despite having a highly similar architecture to their family members, including a pore which can conduct ion flow, no ligand-gated channel function has yet been convincingly described (Yuzaki and Aricescu, 2017).

Two proteins, GluD1 and GluD2 form this subfamily, with the function of GluD2 better characterised. While neither GluD1 nor GluD2 has been reported to have physiological ligand-gated channel function, ion flow has been reported in a well characterised mouse mutant strain. The *lurcher* mouse has an A654T point mutation located in the pore of the receptor, causing ion flow in the absence of any ligand (Zuo et al., 1997). Replacement of the GluD ligand-binding domain with that of AMPARs or KARs permits agonist induced

channel gating demonstrating that the pore of the receptor can gate effectively (Orth et al., 2013; Schmid et al., 2009), however rescue of *Grid2-/-* mice with a ion impermeable GluD2 receptor, can fully rescue the effects of receptor knockout, supporting a purely metabotropic role for the receptor, with little requirement for channel activity (Kakegawa et al., 2007). Physiological ion flow through the receptor has been suggested, initiated by glutamate signalling through metabotropic glutamate receptors (Ady et al., 2014) yet this appears to be a case of mistaken receptor identity, as current flow remains present in GluD2 knockout animals (Kohda et al., 2013). As the channel is able to pass current flow, it is still possible that an endogenous ligand to activate ionotropic function of the receptor is simply yet to be discovered.

GluD2 is expressed predominantly in cerebellar Purkinje cells where it functions metabotropically as part of a transsynaptic complex (Yuzaki and Aricescu, 2017). Cerebellin1 (Cbln1), of the C1q (complement component 1q) protein superfamily, binds to the NTD of GluD2, located postsynaptically (Matsuda et al., 2010), and also to presynaptic neurexin. Two functions of this complex have been identified. GluD2 acts as a postsynaptic organiser at this synapse, stabilising synaptic formation through its transsynaptic interactions (Yuzaki and Aricescu, 2017). D-serine binding at the GluD2 LBD signals postsynaptically, to initiate long-term depression of AMPAR transmission at the parallel fibre synapse (Elegheert et al., 2016; Kakegawa et al., 2011). Synaptic depression induction requires interactions of the GluD2 C-terminal domain with PDZ-domain containing proteins (Kakegawa et al., 2008).

Several interesting points can be inferred from this mechanism which may be of broader importance to iGluR function. Firstly, formation of transsynaptic complexes may be a common mechanism of postsynaptic iGluR anchoring, which has not been observed so far for AMPARs. Secondly, allosteric signalling can be transmitted intracellularly by synaptic protein binding to the extracellular GluD NTD, demonstrating that extracellular iGluR interactions can be detected within the postsynaptic density. Finally, interaction with PDZ domain-containing proteins can be influenced by both agonist and NTD interactions in GluDs. As PDZ interactions exist for all iGluRs, this may be a common theme in their functionality.

Kainate receptors

Five kainate receptor genes, GluK1-5, have been identified, with distinct expression patterns across the brain (Wisden and Seeburg, 1993). Similarly to AMPARs, RNA editing occurs in the transcripts for GluK1 and GluK2, at the position of the M2 helix corresponding to the Q/R

site of GluA2 (Pinheiro and Mulle, 2006). While a subset of KARs are located at postsynaptic sites, a significant population have also been identified at the presynaptic membrane, with signalling roles controlling plasticity of the synaptic connection (Contractor et al., 2011). At the mossy fibre synapse onto CA3 pyramidal neurons, AMPARs mediate the majority of the postsynaptic current, yet due to their differential kinetics, repetitive 'train' stimulation causes a relative increase in the postsynaptic current, dependent on kainate receptor ion flow (Pinheiro and Mulle, 2006), elegantly demonstrating the differential requirements for iGluR family members at a single synapse.

Aside from their distinctly similar architecture, several other characteristics of KARs should be mentioned and considered in the study of AMPAR function. Like other iGluRs, KARs have a PDZ domain interaction site at their extreme C-terminus. This site interacts with a variety of postsynaptic scaffold proteins, such as PSD-95 (postsynaptic density protein 95), GRIP (glutamate receptor interacting protein) and PICK1 (protein interacting with C kinase) (Hirbec et al., 2003). All of these proteins have been demonstrated to bind AMPARs either directly or indirectly to influence their synaptic trafficking, as will be discussed later. The regulation of iGluRs by PDZ-domain containing proteins is complex, as intracellular perfusion of peptides to prevent interactions with these proteins can exhibit differential effects for AMPARs and KARs, demonstrating a differential dependence of the receptors on interactions with the same CTD interacting proteins (Hirbec et al., 2003). It is interesting to note that CTD interacting proteins may even influence iGluR channel gating (Bowie et al., 2003), thereby specifically controlling the activity of synaptic receptor populations only.

KARs do not function alone, but are modulated by auxiliary subunits NETO1/2 (neuropilin and tolloid like), which alter receptor trafficking and channel gating (Straub et al., 2011; Zhang et al., 2009). These proteins contain two CUB (C1r/C1s, Uegf, Bmp1) domains, which interact with the extracellular portion of the receptor. KARs are not alone in having auxiliary subunits, as a wealth of AMPAR auxiliary proteins have been characterised to date (Greger et al., 2017). It is interesting to note that in *Caenorhabditis elegans*, SOL-1 (suppressor of Lurcher), an auxiliary subunit of the AMPAR-like 'GLR-1' (glutamate receptor 1), also utilises CUB domains for its function in modulating glutamatergic transmission (Zheng et al., 2006). Clearly CUB domains are a conserved modulator of iGluR function, however no murine AMPAR auxiliary subunit with this domain has been identified so far.

A further theme running through the iGluR family is transsynaptic complex formation.

In striking similarity to the aforementioned GluDs which are bound by Cbln1, C1ql2/3, also of the C1q superfamily, binds the KAR NTD to form a transsynaptic complex through presynaptic interaction with neurexins (Matsuda et al., 2016). This complex aids the stabilisation of kainate receptors at postsynaptic sites, and is highly suggestive of a common mechanism for iGluR synaptic anchoring.

NMDA receptors

NMDARs are predominantly located at the postsynapse, contributing to the postsynaptic current flow with slower kinetics than AMPARs. These receptors are unique amongst iGluRs for a number of reasons. They require the action of two agonists for channel gating, with glycine binding at the obligatory GluN1 subunit, present in all NMDAR heterotetramers, and GluN3A-B subunits, which are present in triheteromeric complexes with GluN1 and GluN2 subunits (Chatterton et al., 2002; Paoletti et al., 2013). Glutamate sensitivity is conferred by inclusion of GluN2 subunits to the NMDAR (GluN2A-D), the choice of which has strong influences on the kinetics of channel opening (Paoletti et al., 2013).

A critical property of the NMDAR is its inhibition by magnesium. The resting membrane potential of the neuron is highly negative (approx -70 mV) and at these potentials, the pore of the NMDAR is blocked by Mg^{2+} ions. This block is relieved by depolarisation of the membrane (Mayer et al., 1984; Nowak et al., 1984). The discovery of this phenomenon was a revelation for the study of neuronal function, as this receptor could be considered as a molecular 'coincidence detector' for both pre- and postsynaptic activation, which is of great significance to the mechanisms of memory formation. In his book *The Organisation of Behaviour*, Donald Hebb postulated that memory formation could occur at the level of the neuronal connection as follows:

> *When an axon of cell A is near enough to excite cell B or repeatedly or consistently takes part in firing it, some growth or metabolic change takes place in one or both cells such that A's efficiency, as one of the cells firing B, is increased.*
>
> Hebb (1949)

For the NMDA receptor to gate ions, both glutamate, released from the presynapse, and depolarisation of the postsynaptic membrane are required. Therefore temporally coincident activation of both presynaptic and postsynaptic cells is necessary for its activation, so the

receptor can act as the detector of cell A's action and sufficient excitation of cell B.

Activation of the NMDAR subsequently initiates the signalling cascades required for the strengthening of this connection, in NMDA receptor-dependent long-term potentiation (Nicoll, 2017). NMDARs allow the passage of both monovalent cations such as Na^+ and K^+ (as the majority of AMPARs do), and Ca^{2+} ions, which are critical second messengers, activating a variety of protein kinases, such as CaMKII (Calcium/calmodulin dependent protein kinase II), which can modulate the strength of the synapse (Bliss and Collingridge, 1993). Confirmation of the NMDA receptor's role in LTP induction was provided by use of the selective antagonist D-APV (D-(-)-2-Amino-5-phosphonopentanoic acid) (Bliss and Collingridge, 1993; Collingridge et al., 1988, 1983), and the importance of these processes to memory formation has also been inferred from the use of this drug (Bannerman et al., 1995; Bliss et al., 2003). The direct interaction of CaMKII to the CTD of NMDAR subunit GluN2B forms a signalling complex which has been shown to be both necessary and sufficient for synaptic potentiation (Hell, 2014).

Both pharmacological agents (Iacobucci and Popescu, 2017) and synaptic proteins (Lei et al., 2017) cause NTD-dependent modulation of the NMDAR. NRAP-1 (NMDAR auxiliary protein 1) is released from the presynapse to bind NMDARs, and appears essential for channel function in *C. elegans* (Lei et al., 2017). This provides another example of transsynaptic communication through iGluRs, and while physical association of this complex with the presynapse has not been demonstrated, it has been hypothesised (Lei et al., 2017).

NMDARs, like all other iGluRs, also contain a C-terminal PDZ binding motif, which interacts with the abundant postsynaptic protein PSD-95 (Prybylowski et al., 2005), suggested to control postsynaptic receptor localisation. The significance of this interaction is difficult to interpret, as overexpression of PSD-95 does not increase the size of synaptic NMDAR currents (El-Husseini et al., 2000a; Schnell et al., 2002). De-clustering of PSD-95 by limiting palmitoylation has an AMPAR specific effect, with NMDARs unaffected (El-Husseini et al., 2002), and NMDARs are present at the postsynaptic density in PSD-95 knockout animals (Migaud et al., 1998). Most convincingly, disruption of the NMDAR-PSD-95 interaction has little detrimental effect on hippocampal transmission (Lim et al., 2003). It may be that MAGUK interactions facilitate the localisation of synaptic NMDARs, but they are clearly not the primary regulators.

NMDARs have suggested not to be without friends. NETO-1, the KAR auxiliary subunit was proposed to alter NMDAR localisation at synaptic sites, acting as an auxiliary subunit (Ng et al., 2009). It appears that this effect is mediated indirectly, and therefore NMDARs so far have no well characterised partners as yet (Molnár, 2013; Straub et al., 2011).

1.2.3 AMPA Receptor gating

The gating properties of the AMPAR are uniquely fast, which allows extremely high fidelity reproduction of presynaptic firing in the postsynaptic cell (Greger et al., 2017). The receptor activates very rapidly, before closing, either by deactivation or desensitisation, on a timescale that outpaces their iGluR family members the NMDAR, which has far slower kinetics. The speed of AMPAR gating is finely tuned by a number of mechanisms, giving rise to a vast diversity of AMPAR signalling complexes across the brain, with their precise functions differentially required at particular synaptic connections (Greger et al., 2017). Each AMPAR subunit confers unique kinetics to the AMPAR response, which in turn can be modified by RNA splicing at the flip/flop site, and RNA editing at the R/G site (Traynelis et al., 2010). An additional layer of regulation is added by interaction of AMPARs with their auxiliary subunits, which can bidirectionally influence the opening of the channel (Jackson and Nicoll, 2011). The kinetics of the AMPAR complex alone are highly regulated at the gene expression and RNA level, and the diversity produced is beautifully exhibited in the cochlear nucleus, where the time-course of AMPAR signalling varies dramatically between cell-types (Gardner et al., 1999), for example the particularly fast kinetics of GluA4 being employed for the temporal encoding of auditory information at the bushy cell synapse (Gardner et al., 1999).

1.2.4 AMPA Receptor auxiliary subunits

As defined by Jackson and Nicoll, 2011, the characterisation of an AMPAR auxiliary subunit, rather than simply an interacting protein requires the following properties:

> *Our working definition of an iGluR transmembrane auxiliary subunit is that it avidly and selectively binds to mature iGluRs as part of a stable complex at the cell surface, that it can modulate the functional characteristics of iGluRs, and that it may also mediate surface trafficking and/or targeting to specific subcellular compartments, such as synapses.*
>
> Jackson and Nicoll (2011)

The first AMPAR auxiliary protein to be discovered was the transmembrane AMPAR regulatory protein (TARP) γ2, which was identified from the deficit in cerebellar AMPAR transmission in the *stargazer* mutant mouse (Chen et al., 1999b; Hashimoto et al., 1999; Letts et al., 1998). Initially thought to be a calcium channel gene, due to its homology with the voltage-gated calcium channel (VGCC) γ subunits, the striking loss of AMPAR transmission in cerebellar granule cells allowed its identification as a modulator of AMPAR channel gating, receptor trafficking and a mediator of receptor synaptic localisation (Chen et al., 2000; Greger et al., 2017). Initially named stargazin, TARP γ2 was found to be a member of a family of TARPs totalling 6 proteins, TARP γ2, γ3, γ4, γ5, γ7, and γ8 (Figure 1.3A; Jackson and Nicoll, 2011; Tomita et al., 2003), while the homologous γ1 and γ6 proteins do indeed associate with VGCCs (Chu et al., 2001; Letts et al., 1998).

TARPs have been classified into Type Ia (γ2, γ3), Ib (γ4, γ8) and II (γ5, γ7) according to their effects on the receptor (Cho et al., 2007; Kato et al., 2008). They are differentially expressed throughout the brain, in a spatio-temporal manner, and their expression patterns may reflect the requirements of different AMPAR complexes for different synaptic functions. One example is the developmental expression of γ4, which produces a highly sensitive AMPAR complex, which has been suggested to confer a great glutamate sensitivity on the postsynaptic membrane during synapse formation (Milstein et al., 2007). TARP γ2 is the most ubiquitously expressed in the brain, and therefore produces the greatest phenotype on knockout (Fukaya et al., 2005; Menuz et al., 2009, 2008).

More recent proteomic analyses have identified further auxiliary proteins including: cornichon proteins, CNIH-2 and 3 (Schwenk et al., 2009), germ cell-specific gene 1-like protein (GSG1L; Schwenk et al., 2012; Shanks et al., 2012), a family of cysteine knot AMPAR modulating proteins (CKAMP), CKAMP44, 39, 52 and 59, and (Farrow et al., 2015) and a pair of synapse differentiation-induced gene (SynDIG) proteins, SynDIG1 and 4 (Kalashnikova et al., 2010; Matt et al., 2018). The aforementioned SOL-1 is also an AMPAR auxiliary protein, present in *C. elegans*, with no known homologue in *Mus musculus* (see Figure 1.3A).

The influences of TARPs on AMPAR gating

The TARP family generally act to promote AMPAR ion flux, by limiting desensitisation and deactivation, increasing single-channel conductance and channel open probability and altering receptor pharmacology, such as limiting polyamine blockade (Figure 1.3B) (Greger

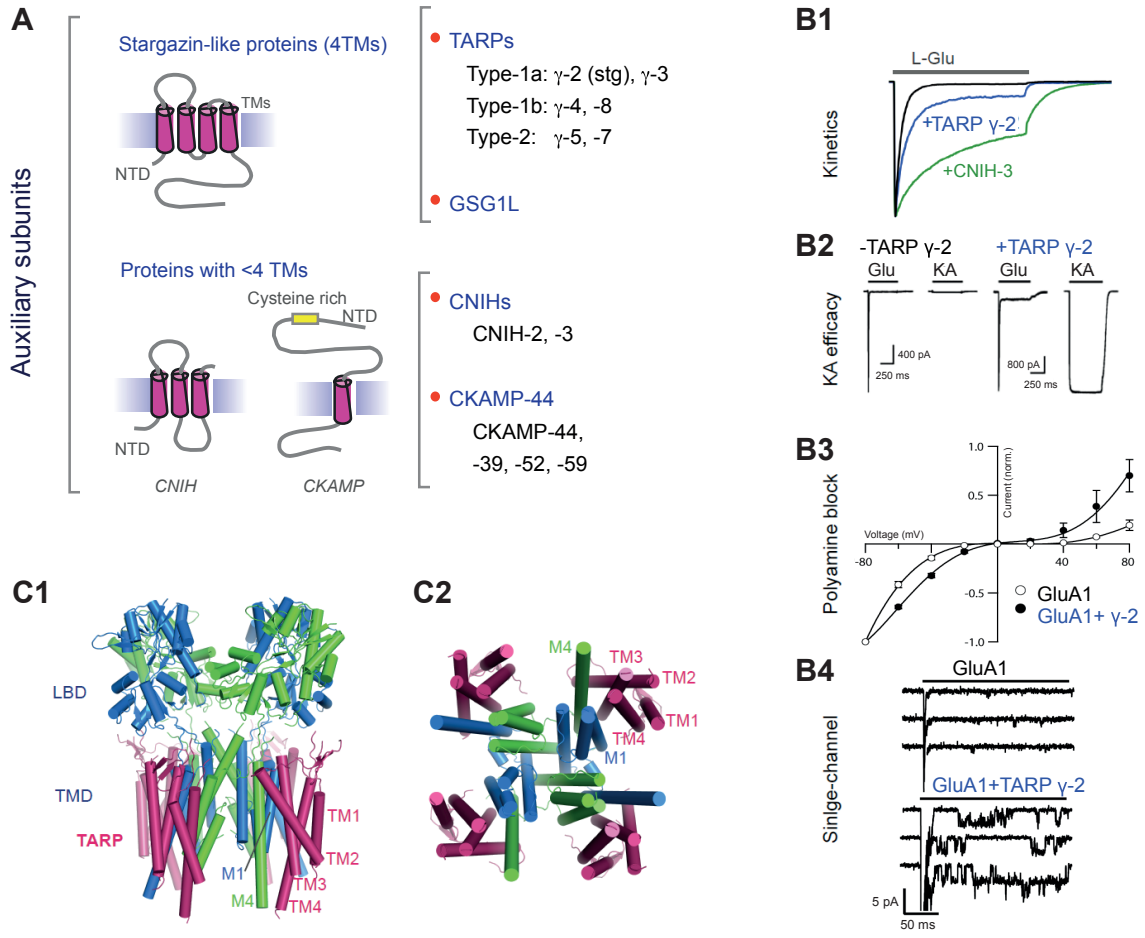

Figure 1.3 ***Main Auxiliary Subunits, and the Structure-Function of the AMPAR-TARP Complex.*** *(**A**) Schematic of AMPAR auxiliary proteins, classified into stargazin-like (containing 4 transmembrane helices) and other auxiliaries, with generalised protein schematics indicated. (**B1**) Both TARP and cornichon association markedly slow desensitisation kinetics of GluA2(Q) in HEK cells (kindly provided by Dr Ondrej Cais). (**B2**) TARP association greatly increases the AMPAR response to kainate converting it from a partial to a full agonist. (**B3**) TARP γ-2 partially alleviates polyamine block, allowing enhanced current flow at depolarised potential (seen as a reduction in the rectification of the I-V relationship). (**B4**) TARP γ-2 increases single-channel conductance. (**C1**) The architecture of the TARP associated AMPAR (PDB: 5KK2, A/C chains indicated green, B/D chains in blue and four TARP molecules in magenta). The NTD was not incorporated in this model. (**C2**) Cytoplasmic view of the AMPAR-TARP complex (PDB: 5KK2). Figure reproduced from Greger et al., 2017, with panels derived from Nicoll et al., 2006, Soto et al., 2007, Turetsky et al., 2005 and Coombs and Cull-Candy, 2009, as detailed in Greger et al., 2017.*

et al., 2017; Priel et al., 2005; Tomita et al., 2005; Yamazaki et al., 2004).

There are of course exceptions to this generalisation, for example TARP γ5 speeds receptor desensitisation (Kato et al., 2008), while TARP γ8 appears to slow the recovery of the AMPAR from a desensitised state in a subunit specific manner (Cais et al., 2014).

The influence of TARPs on AMPAR channel function appears to predominantly be mediated by their extracellular loops, which interact with the LBD and TMD of the receptor (Cho et al., 2007; Hawken et al., 2017; Milstein et al., 2007; Riva et al., 2017). The sequence differences between TARP subtypes in this region likely facilitates their differential effects (Cais et al., 2014; Riva et al., 2017). Structural analysis has been used to identify the regions of AMPAR-TARP association (Figure 1.3C; Chen et al., 2017; Twomey et al., 2016; Zhao et al., 2016), but identification of TARP loop interactions with the AMPAR LBD so far remain elusive.

The significance of AMPAR gating modulation by TARPs cannot be overstated. Through their wide ranging influences on channel properties, auxiliary subunits have the potential to control the fidelity of synaptic transmission and the sensitivity of the postsynaptic membrane, the likelihood of post-synaptic cell activation through synaptic integration, or even the occurrence of synaptic potentiation, by tuning the window for induction of timing-dependent plasticity (Bi and Poo, 1998; Debanne et al., 1997; Jackson and Nicoll, 2011; Jonas and Spruston, 1994).

The AMPAR complex of hippocampal neurons.

Hippocampal CA1 pyramidal neurons express the core subunits GluA1, GluA2 and GluA3, which assemble predominantly into GluA1/2 and GluA2/3 heteromeric receptors (Lu et al., 2009; Schwenk et al., 2014; Wenthold et al., 1996). GluA1-containing receptors comprise almost the entirety of the surface receptor population, while GluA1/2 and GluA2/3 heteromers both contribute to transmission at synaptic sites (Lu et al., 2009).

These cells predominantly express TARP γ8 alongside CNIH-2, with low expression levels of γ2, γ3 and γ4. SynDIG4 and and some CKAMP family members are minimally associated with the AMPAR in the hippocampal region, and may play synapse-specific roles in transmission (Schmitz et al., 2017; Schwenk et al., 2014, 2009; Tomita et al., 2003). Early studies indicated that different TARP subtypes do not associate in the same AMPAR complex

(Tomita et al., 2003), however TARP and CNIH can co-associate (Kato et al., 2010), with CNIH further promoting ion flux in addition to TARP action (Figure 1.3B1; Kato et al., 2010; Schwenk et al., 2009).

TARPs can dramatically increase the efficacy of the partial agonist kainate, which allows identification of TARP associated receptor populations (Shi et al., 2009; Turetsky et al., 2005). This approach has been used to assess the stoichiometry of TARP-AMPAR complexes from neuronal populations, which was described to be 4 TARP γ8 molecules per AMPAR tetramer in CA1 pyramidal neurons, but 2 TARPs in DG neurons (Shi et al., 2009). More in depth analysis of neuronal AMPAR pharmacologies, studying the kainate response in the presence and absence of the AMPAR potentiator cyclothiazide, and measuring AMPAR resensitisation indicates that hippocampal CA1 complexes actually contain two TARP γ8 and two CNIH molecules (Gill et al., 2011; Kato et al., 2010). Correspondingly, when TARP interactions with the PSD are limited by abolishing their interaction with PSD-95, CNIH also decreases its association with the PSD fraction (Sumioka et al., 2011). CNIH appears to have a greater affinity for TARP γ8 containing AMPAR complexes (Kato et al., 2010), and could promote the extrasynaptic expression of TARP γ8 containing AMPARs through their chaperone-like functions (Inamura et al., 2006; Yamasaki et al., 2016). Structural information has demonstrated the interaction site for TARPs on the AMPAR (Figure 1.3C; Zhao et al., 2016). Investigation of whether CNIH associates in the place of, or differentially to TARPs on the AMPAR core is now essential.

A role for CNIH in controlling AMPAR subunit composition at the synapse of CA1 neurons has been suggested. While TARPs appear to show no AMPAR subunit-specific binding (Chen et al., 2000; Tomita et al., 2003), CNIH appears to preferentially associate with GluA1-containing AMPARs to mediate their surface delivery (Herring et al., 2013). As the surface population of AMPARs consists exclusively of GluA1-containing receptors (Lu et al., 2009), CNIH may be the factor contributing to this subunit specific effect. This role has the potential to explain the association of GluA1-containing receptors with synaptic potentiation (Mack et al., 2001; Schmitt et al., 2005; Zamanillo et al., 1999), which relies on recruitment from a surface pool of AMPARs (Granger et al., 2013; Makino and Malinow, 2009; Penn et al., 2017).

Other auxiliary proteins

CKAMP44, expressed in hippocampal DG neurons can associate with 'TARPed' AMPARs to tune the postsynaptic response. Like TARPs, it is a transmembrane protein with a C-terminal PDZ ligand, which helps to accumulate receptors at postsynaptic sites (Khodosevich et al., 2014; Von Engelhardt et al., 2010). Other CKAMP family members are expressed in CA1 pyramidal neurons, and may perform similar roles on AMPAR function in these cells, yet the complement of AMPAR complexes, and the association of multiple auxiliary proteins with the same receptor requires careful study to unravel (Farrow et al., 2015; Klaassen et al., 2016; Schmitz et al., 2017).

GSG1L is a TARP-like auxiliary, which limits the recovery of AMPARs from desensitisation, as CKAMP proteins do, and hence is labelled as a negative regulator of AMPAR gating (Schwenk et al., 2012; Shanks et al., 2012; Twomey et al., 2017). Its role in synaptic transmission still requires investigation.

SynDIG1/4 are also transmembrane proteins associated with the AMPAR complex, yet appear not to be as significant to synaptic transmission as TARPs and CNIH (Kalashnikova et al., 2010; Lovero et al., 2013; Schwenk et al., 2014). Both appear to aid the extrasynaptic localisation of AMPARs (Matt et al., 2018), which may provide the pools of perisynaptic receptors that are required to maintain short and long-term synaptic potentiation (Granger et al., 2013; Heine et al., 2008; Penn et al., 2017).

A number of transmembrane AMPAR interacting proteins which associate with AMPARs in receptor biogenesis have recently been characterised. While not true auxiliary subunits, PORCN (porcupine; Erlenhardt et al., 2016), FRRS1L (ferric-chelate reductase 1-like; Brechet et al., 2017), ABHD6 (alpha/beta-Hydrolase domain containing 6; Erlenhardt et al., 2016) and CPT1c (carnitine O-palmitoyltransferase 1c; Brechet et al., 2017) appear to aid receptor assembly and trafficking, while not playing a role at the cell surface or synapse. AMPAR complexes associated with these proteins are likely the first to form, and once assembled, these primary interactors are shed for association with TARP and CNIH, and delivery to the synapse (Brechet et al., 2017).

TARPs influence the forward trafficking of AMPARs from the endoplasmic reticulum (ER) through its secretory pathway (Bedoukian et al., 2008; Chen et al., 2000; Kessels et al., 2009; Schnell et al., 2002; Shanks et al., 2010; Vandenberghe et al., 2005). This is a prereq-

uisite for receptor surface delivery, and deficits in the surface population of AMPARs are often demonstrated in TARP knockout cells (Chen et al., 2000; Rouach et al., 2005). This 'chaperone-like' function of striking in TARP γ8 knockout mice, which show dramatically reduced AMPAR protein levels (Rouach et al., 2005). Selective interaction of TARPs with transport and golgi-related proteins control this function (Cuadra, 2004; Ives et al., 2004).

1.3 The life of an AMPAR

1.3.1 From biogenesis to the synapse

As a transmembrane protein, the AMPAR begins life in the ER, where it is assembled into tetrameric receptors, glycosylated and trafficked out into the dendrites (Greger and Esteban, 2007). Local translation of AMPAR subunits in the dendrites has been reported, with the potential for branch or even spine specific AMPAR expression (Bowen et al., 2017; Hanus et al., 2016). Receptors are delivered to synaptic sites either via the cell surface, where they can anchor at the synapse by lateral diffusion (Choquet and Triller, 2013), or by direct delivery into dendritic spines, via Rab11 endosomes (Brown et al., 2007; Esteves da Silva et al., 2015). Recycling of AMPARs between intracellular pools within the spine and the extrasynaptic space is a key regulator of AMPAR transmission, providing a pool of receptors for synaptic plasticity (Esteban, 2008). Each step of this life-cycle is intensely regulated by protein interactions and auxiliary subunits, and each of these interactions has the potential to alter the strength of synaptic transmission, despite not occurring itself at synaptic sites. For this reason, the mechanisms of synaptic AMPAR anchoring can be intricate to decipher.

1.3.2 Synaptic potentiation

Intense focus on the interactions controlling AMPAR synaptic anchoring was encouraged by discovery that the AMPAR content of the synapse was plastic, substantially contributing to LTP. The locus of change in LTP was, and still is, hotly debated, with evidence for both pre and postsynaptic effects (Lisman, 2009). In many regards, both conclusions are correct, as the mechanisms for synaptic plasticity appear to be distinct at each synaptic connection (Nicoll and Malenka, 1995). Two synapses in the hippocampus demonstrate this well. At the mossy fibre to CA3 synapse, LTP is expressed presynaptically. An increase in the probability of vesicle release strengthens transmission, as greater levels of glutamate are released to activate the postsynaptic receptors (Nicoll and Malenka, 1995). At the CA3 to CA1 synapse, the strongest

evidence supports a postsynaptic locus (Granger and Nicoll, 2013), however convincing evidence for presynaptic changes have been presented (Emptage et al., 2003; Enoki et al., 2009).

Regardless of the expression locus, CA1 LTP induction begins on NMDAR activation and postsynaptic Ca^{2+} entry (Bliss and Collingridge, 1993; Collingridge et al., 1988, 1983). This initiates intracellular signalling cascades, a critical component being CaMKII, which is both necessary and sufficient for LTP expression (Hell, 2014; Silva et al., 1992). One unequivocally postsynaptic component to LTP is synapse unsilencing. A population of synapses contain NMDARs but lack functional AMPARs. Postsynaptic AMPAR trafficking can 'unsilence' these connections during LTP induction (Isaac et al., 1995; Liao et al., 1995).

In increasing the strength of preexisting connections, a host of postsynaptic rearrangements have been reported. Structural dynamics in the postsynaptic spine, increase its size and electrical coupling to the dendrite (Matsuzaki et al., 2004; Tønnesen et al., 2014). The postsynaptic spine size correlates strongly with AMPAR content (Matsuzaki et al., 2001, 2004), and a major component of LTP is the recruitment of AMPARs to synaptic sites to strengthen the connection (Granger and Nicoll, 2013; Kauer et al., 1988).

During LTP, AMPARs are delivered to synaptic sites by multiple routes. Initial potentiation requires recruitment of surface AMPARs from the extrasynaptic areas (Granger et al., 2013; Makino and Malinow, 2009; Penn et al., 2017), while receptor exocytosis from intracellular stores maintains the potentiated state (Penn et al., 2017; Wu et al., 2017). Once delivered to synaptic sites, the receptors are anchored for transmission, the suggested mechanisms for which will be discussed in greater detail below, but are still unclear.

Some presynaptic components of CA1 LTP have been argued, with evidence for increases in glutamate release (Emptage et al., 2003; Enoki et al., 2009), however strong evidence suggests that presynaptic changes do not occur in all instances of LTP induction. Muller and Lynch (1989) showed that alterations in presynaptic release do not affect the magnitude of LTP. Mainen et al. (1998) demonstrated that the likelihood of AMPAR activation (and hence probability of release, P_r) is unchanged after LTP and transmission changes are AMPAR-specific, with no alterations to NMDAR currents, which would occur with neurotransmitter release. Finally, glutamate transporter currents on astrocytes, which are independent of the postsynapse are unchanged (Diamond et al., 1998). Meta-analysis of the wealth of LTP data suggests that presynaptic components are reported when the magnitude of LTP is particularly

large (Padamsey and Emptage, 2013), and therefore strong induction protocols may trigger major changes in the postsynaptic structure, that are more likely to influence the presynapse. This conclusion is considered plausible by researchers from both sides of the divide (Granger and Nicoll, 2013; Padamsey and Emptage, 2013).

1.3.3 The dynamic AMPAR

Imaging advances have allowed resolution of the AMPARs movements on a single particle level. First, using quantum-dot (Q-dot) conjugated antibodies (Bats et al., 2007; Borgdorff and Choquet, 2002), and more recently, using dye-conjugated antibodies (Nair et al., 2013), individual AMPARs appear to be highly mobile on the dendritic surface, where they can be trapped at the postsynaptic density. This mobility has been confirmed by electrophysiological experiments using photoinactivated AMPARs, where dendritic receptor diffusion occurs on the second timescale (Adesnik et al., 2005). A mobile pool of receptors exchange with synaptic receptors, and are rapidly recruited to the postsynaptic density by lateral diffusion on LTP induction (Granger et al., 2013; Makino and Malinow, 2009; Penn et al., 2017).

The dynamics of synaptic receptor exchange occurs on a much slower timescale than on the dendritic surface, due to their stabilisation by synaptic proteins, reports have suggested that substantial exchange occurs during basal transmission, on the second timescale (Bats et al., 2007; Heine et al., 2008). However, recent technological advances have begun to question the true mobility of the receptor, as Q-dot labelled AMPARs are unable to fit into the synaptic cleft, and therefore their mobility likely represents perisynaptic stabilisation (Lee et al., 2017). Using small molecule labelling techniques, the exchange of synaptic AMPARs appears minimal on the seconds to minutes time-scale (Wakayama et al., 2017), supported by photoinactivation analysis (Adesnik et al., 2005), but contrary to a wealth of previous reports using fluorescent protein, or antibody labelled receptors (Bats et al., 2007; Kerr and Blanpied, 2012; Makino and Malinow, 2009). These discrepancies may reflect the prevention of synaptic cleft interactions by extracellular labelling of the AMPAR, and the continued development of these approaches is important to physiologically quantify the contributions of receptor mobility to synaptic transmission.

1.3.4 The nanoscale synapse

Through the development of superresolution imaging, the synapse has been dissected in finer detail. The postsynaptic site is not a homogeneous assembly of proteins, but contains

subclusters of high density (MacGillavry et al., 2013; Nair et al., 2013). Postsynaptic PSD-95 forms 'nanodomains' of higher density than the rest of the postsynaptic area, at which clusters of AMPARs are located. These nanodomains are localised opposite the sites of glutamate release (Tang et al., 2016) (Figure 1.4A), which greatly enhances the efficiency of synaptic transmission (Raghavachari and Lisman, 2004). The mechanisms for this 'transsynaptic alignment' have not been identified, but a mass of transsynaptic protein complexes form between the synaptic membranes, crossing the cleft (Chamma et al., 2016; Perez de Arce et al., 2015). Consideration of the AMPAR as part of this transsynaptic arrangement is important for understanding the mechanisms of its anchoring.

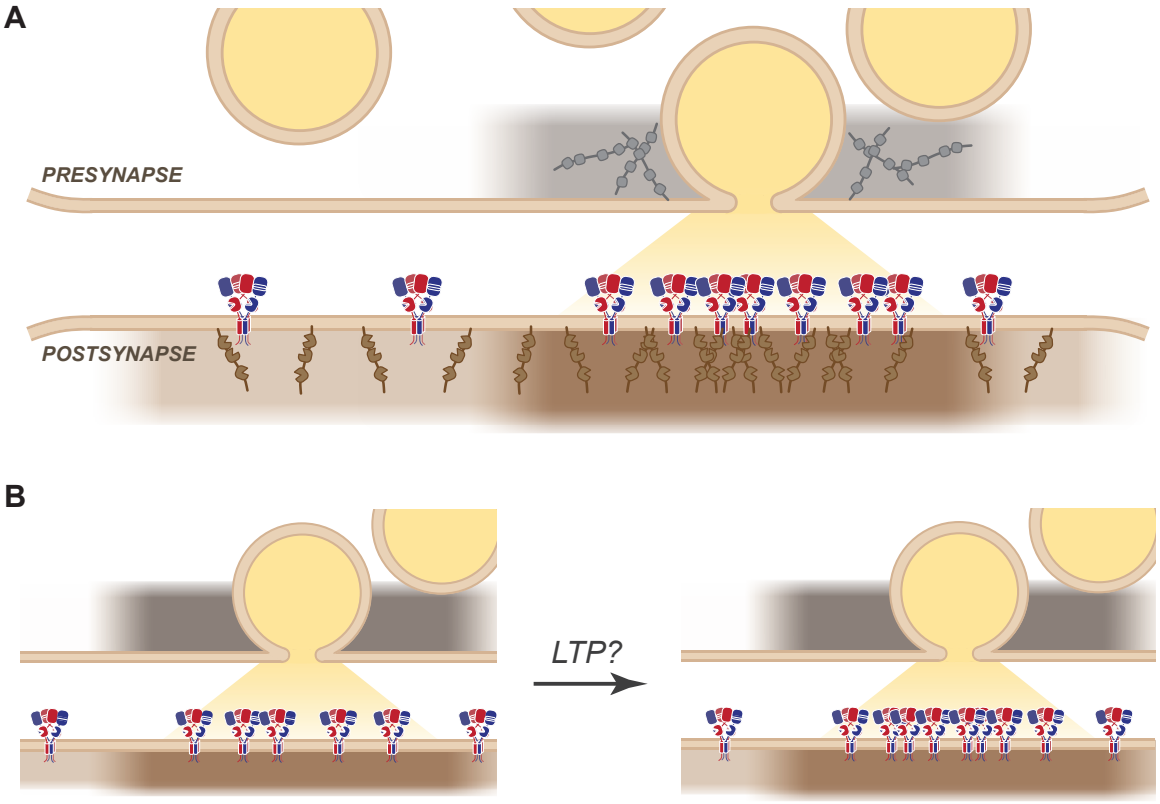

Figure 1.4 ***The nanoscale synapse.*** *(**A**) Postsynaptic scaffold proteins and receptors are clustered within the postsynaptic density (brown) opposite presynaptic release sites (grey) for efficient transmission. (**B**) Synaptic plasticity can involve the recruitment of AMPARs to postsynaptic sites, but may also involve receptor clustering to increase the local density of receptors at glutamate release sites.*

AMPARs at the CA1 synapse are not the only example of transsynaptic alignment of presynaptic signalling and postsynaptic detection. At the rod bipolar cells synapse, postsynaptic mGluRs are aligned with presynaptic release sites through indirect interaction with presynaptic calcium channels, which trigger vesicle release (Kerschensteiner, 2017; Wang et al., 2017). At the neuromuscular junction, superresolution imaging has demonstrated that postsynaptic acetylcholine receptors are highly localised on openings of junctional folds, opposite the sites of vesicle release (York and Zheng, 2017). The advent and application of these imaging techniques to synaptic physiology is facilitating identification of the detailed mechanisms underlying the specificity and efficiency of transmission.

Transsynaptic alignment has consequences for transmission. Not all postsynaptic AMPARs respond to synaptically released glutamate (Liu et al., 1999; McAllister and Stevens, 2000), and many AMPARs are localised in the postsynaptic density, associated with postsynaptic MAGUKs, but are not part of the nanodomain, and likely do not receive presynaptically released glutamate. Synaptic transmission can therefore be tuned, not only by increasing the number of AMPARs at the postsynaptic density, but also through increased clustering of receptors at sites of glutamate release (Lisman and Raghavachari, 2006) (Figure 1.4B).

According to such a model, the critical parameter controlling AMPAR transmission is the *density* of receptors at the postsynaptic site (Raghavachari and Lisman, 2004). Studies of hippocampal CA1 synapses have demonstrated that synapses with perforated postsynaptic densities, show much greater AMPAR densities (approximately 5 times higher; Yamasaki et al., 2016). Perforated synapses are strongly associated with potentiation, and may represent a population of strong synaptic connections, which have undergone LTP (Hering and Sheng, 2001; Jones, 1993). The presence of a high AMPAR density at these connections is in line with the LTP predictions of the alignment model, whereby potentiated synapses contain clustered postsynaptic receptors (Lisman et al., 2007; Raghavachari and Lisman, 2004).

The synapses of the cochlear nucleus, as previously mentioned, represent a heterogeneous population, due to the number of different cell types, and their unique functions in network communication (Rubio et al., 2014). The density of synaptic AMPARs also varies greatly across cell types. Crucially, Rubio et al., 2014 observed that *"synaptic connections with highly plastic properties show large synaptic areas, low AMPAR density, and a mosaic arrangement of AMPARs in the synapse"*. This scenario confers a plastic synapse with the great capacity for potentiation, as the receptor density can be increased to provide stronger

synaptic transmission (Figure 1.4B).

While this model was predicted a number of years ago (Raghavachari and Lisman, 2004), experimental verification is only now emerging (Biederer et al., 2017; Tang et al., 2016). By identifying the synapse not as separate pre and postsynaptic structures, even LTP changes at both pre and postsynaptic loci can be reconciled. If transsynaptic adhesion complexes align both release and postsynaptic receptors (Perez de Arce et al., 2015), then significant cross-commmunication is likely to occur, with the potential for postsynaptic induction and alteration to be detected at the presynapse. Within this nanoscale synapse, understanding the intricate interactions controlling the precise localisation of postsynaptic AMPARs is of great importance to understanding synaptic transmission and plasticity.

1.4 Controllers of the synaptic AMPAR

Multiple interactions of the AMPAR complex have been implicated in its synaptic anchoring. Broadly, these can be considered as intracellular, consisting of AMPAR CTD and TARP CTD interactions, and extracellular, mediated by the NTD.

1.4.1 TARP-MAGUK interactions

The *stargazer* mouse shows almost a complete lack of both surface and synaptic AMPAR currents in cerebellar granule cells, measuring both evoked (Hashimoto et al., 1999) and spontaneous (Chen et al., 2000) synaptic transmission, despite AMPAR transcription and translation levels remaining unchanged (Hashimoto et al., 1999). Immunogold labelling showed that only 15 % of synapses contained AMPARs, and when present, receptor densities were reduced to 60 % of wild-type levels.

Surface AMPAR currents could be rescued by transfection of TARP γ2, however the critical interaction for maintenance of synaptic AMPAR currents is conferred by the TARP PDZ-ligand, which interacts with the MAGUK (membrane associated guanylate kinase) proteins, such as PSD-95 (Chen et al., 2000; Schnell et al., 2002). PDZ-deleted TARP γ2 (Δ4) could rescue surface AMPAR currents, yet was unable to rescue synaptic AMPAR currents, and TARP γ2 Δ4 exhibits a diffuse localisation throughout the neuron (Chen et al., 2000), elegantly demonstrating the bilateral requirement for TARPs in receptor trafficking and synaptic anchoring.

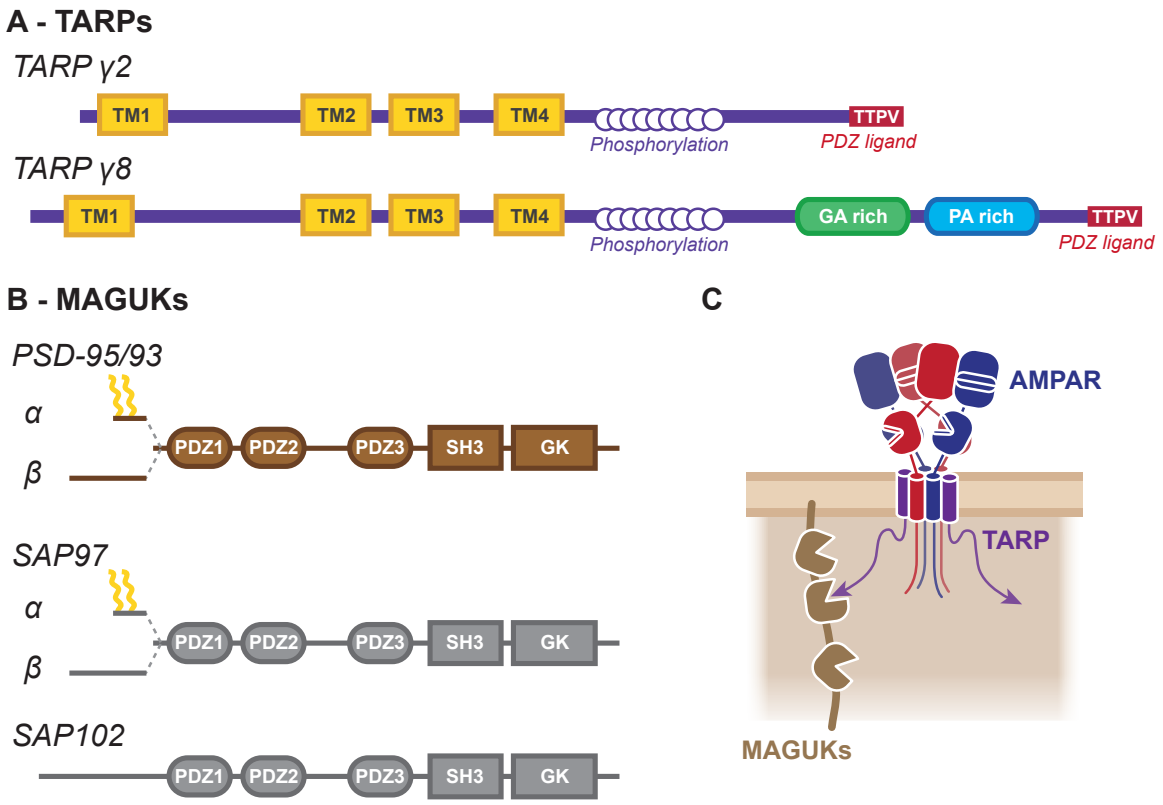

Figure 1.5 ***Schematics of TARP and MAGUK domain organisations.*** *(**A**) Schematic of TARP primary structure with the location of transmembrane domains (TM), phosphorylated regions and PDZ ligands depicted. The unique Gly/Ala (GA) and Pro/Ala (PA) regions of TARP γ8 are also indicated. (**B**) Domain organisation of the predominant MAGUKs of the postsynaptic density, containing PDZ domains, SRC Homology 3 domains (SH3) and catalytically inactive guanylate kinase-like domains (GK). Alternative splicing of PSD-95, PSD-93 and SAP-97 controls palymitoylation, with consequences for synaptic localisation. (**C**) Schematic of AMPAR-TARP anchoring by MAGUKs. PDZ-ligand of TARPs interact with membrane-associated MAGUKs, inserted into the postsynaptic membrane by palmitoylation.*

While the effect is striking in this cell population, is this mechanism the fundamental basis of AMPAR anchoring across all synapses in the brain? Although TARP subtypes are regionally expressed, all TARPs contain a PDZ-ligand of some form (Jackson and Nicoll, 2011), so it has the potential to be a common mechanism underlying AMPAR transmission. In principle, TARP-dependent anchoring is not completely essential for synaptic AMPAR anchoring, as transmission has been observed, albeit at very at low levels, in TARP γ2, γ7 double knockout cerebellar granule cells, which contain no other TARP subtypes (Bats et al., 2012), however in practice, the requirement for this interaction appears almost absolute in these cells.

The role of TARP - PSD-95 interactions in controlling AMPAR anchoring have been applied to the hippocampal CA1 synapse, and are widely recognised as a principle receptor anchoring mechanism (Martenson and Tomita, 2015; Opazo et al., 2012; Figure 1.5C). Overexpression of TARP γ2 ΔPDZ dramatically attenuates AMPAR transmission, reducing AMPAR mEPSC frequency to almost nil (Bats et al., 2007; Chen et al., 2000), and substantially reducing evoked AMPAR transmission (~25 % remaining; Schnell et al., 2002). This attenuation was attributed to its interaction with PSD-95 (Schnell et al., 2002), although interactions with PSD-93 and SAP97 have also be observed (Choi et al., 2002; Dakoji et al., 2003; Ives et al., 2004), and may serve to accumulate receptors at the synapse.

Single-particle tracking has shown that AMPARs are immobilised at synaptic sites and PSD-95 clusters, and that this anchoring is again dependent on the TARP PDZ-ligand (Bats et al., 2007). Interestingly, immobilisation was unaffected by prevention of AMPAR CTD interactions of both GluA2 (Bats et al., 2007) and GluA1 (Opazo et al., 2010). This model could be applied to LTP by the discovery that phosphorylation of the TARP CTD limited its electrostatic interaction with the inner leaflet of the plasma membrane allowing increased interaction with intracellular MAGUKs (Sumioka et al., 2010). The model was developed such that CaMKII-dependent phosphorylation occurs during LTP to increase AMPAR anchoring and to potentiate the synapse (Opazo et al., 2010; Tomita et al., 2005), which coincides well with the fundamental importance of CaMKII in LTP (Silva et al., 1992).

It has been suggested that activation of the AMPAR on glutamate binding dissociates the AMPAR from the TARP (Morimoto-Tomita et al., 2009; Tomita et al., 2004). This appears to increase the mobility of synaptic AMPARs on synaptic activation (Constals et al., 2015), however glutamate-dependent TARP dissociation has been questioned (Nakagawa et al.,

2005; Semenov et al., 2012), and recently explained by other mechanisms (Coombs et al., 2017).

A number of factors raise questions over the completeness of the TARP - PSD-95 interaction explaining AMPAR anchoring in the hippocampus. The predominant TARP in these cells is TARP γ8 (Schwenk et al., 2014), with γ2 only present in 12 % of synapses (Inamura et al., 2006; Yamasaki et al., 2016). TARP γ2 is not present at the extrasynaptic membrane (Fukaya et al., 2006; Inamura et al., 2006) and is therefore highly unlikely to contribute to LTP through lateral diffusion.

TARP γ8 also contains a PDZ-binding 'TTPV' motif, which interacts with synaptic MAGUKs (Figure 1.5A). TARP γ8 knockout reduces AMPAR EPSCs by 35 %, with a complete abolishment of surface receptor currents (Rouach et al., 2005). Synaptic currents could be compensated by other TARPs present in these cells, such as γ2, γ3, or γ4, which are expressed at low levels (Schwenk et al., 2014; Tomita et al., 2003). However, generation of a mouse model where the PDZ-ligand of TARP γ8 is deleted only reduces transmission by 30 %, with LTP unaffected (Sumioka et al., 2011). Disruption of PDZ-interactions using a biomimetic ligand interacting with PDZ1/2 of PSD-95 reduces synaptic transmission, however 45 % of currents remain (Sainlos et al., 2011). This data suggests that other AMPAR anchoring mechanisms are at play at this synapse to control the localisation of receptors for synaptic transmission, although recent data has proposed that PDZ interactions of iGluRs are strictly essential for their contribution to synaptic transmission (Bemben et al., 2018). The CTD of TARP γ8 contains two unique inserts in comparison to γ2 (Figure1.5A). It is possible that other synaptic proteins interact with these regions to contribute to synaptic anchoring, however only a transient interaction with the phosphatase calcineurin has so far been reported for this TARP subtype (Itakura et al., 2014).

All three PDZ domains of PSD-95/93 can interact with the TARP CTD (Dakoji et al., 2003), however in vivo, the interactions of PDZ1 and 2 appears most crucial for its synaptic effect (Schnell et al., 2002). The interaction of TARP γ2 with PSD-95 has been shown to be regulated by protein kinase A (PKA) phosphorylation in PDZ-binding motif (T<u>T</u>PV), which prevents the interaction (Chetkovich et al., 2002; Choi et al., 2002). This has been suggested to have a role in the surface delivery of AMPAR complexes, whereby TARP γ2 phosphorylation would release the subunit from intracellular interactors, for surface delivery (Choi et al., 2002). Given that PKA activation does not alter the synaptic localisation of γ2

(Chetkovich et al., 2002), and PKA activity enhances, rather than limits synaptic AMPAR currents (Carroll et al., 1998; Otmakhova et al., 2000), it seems more likely that this phosphorylation plays a role in trafficking than synaptic receptor anchoring.

Synaptic MAGUKs display great redundancy, and the presence of multiple genes may reflect their essential requirement for maintaining transmission (Elias et al., 2006). Splicing can control the synaptic localisation of these proteins. PSD-93, PSD-95 and SAP97 are all spliced such that they contain residues which can be palmitoylated at their N-terminus (Schlüter et al., 2006; Waites et al., 2009; Figure 1.5B). For PSD-93/95, the palmitoylated version appears to be the major isoform, while the unpalmitoylated SAP97 is predominant (Won et al., 2017). Palmitoylation of PSD-95 and PSD-93 is essential for their synaptic clustering and stability (El-Husseini et al., 2000b,c, 2002; Sturgill et al., 2009), and interestingly the synaptic localisation of PSD-95 at the synapse is also dependent on the lipid composition of synaptic sites (Arendt et al., 2010). The localisation of SAP97 isoforms within the synaptic area has the potential to control AMPAR transmission, as unpalmitoylated (βSAP97) is seen at the edge of the postsynaptic density, while its palmitoylated isoform is found more centrally (Waites et al., 2009). Not only is synaptic transmission influenced by the mobility of the AMPAR, but dynamics of the postsynaptic density have an influential role.

The interest in MAGUKs in the study of AMPAR transmission has been particularly sparked by the specific increases and decreases in AMPAR synaptic currents, with little change in NMDAR currents (Elias et al., 2006; Futai et al., 2007; Levy et al., 2015; Schnell et al., 2002), suggesting they offer a specialised mechanism for controlling AMPAR numbers. However some reports have demonstrated NMDAR current alterations on MAGUK interaction perturbation or RNA knockdown, indicating that these proteins offer a more general role in maintaining transmission. Indeed a multitude of synaptic proteins interact with MAGUKs, including the transsynaptic cell adhesion complex of neurexin and neuroligin, which binds PSD-95 through the neuroligin C-terminus (Chih et al., 2005; Futai et al., 2007; Irie et al., 1997). Interfering with MAGUK interactions therefore has the potential to disrupt transmission through means other than AMPAR anchoring.

1.4.2 CTD interactors

The AMPAR CTD has been extensively studied in the analysis of receptor trafficking. Given its high sequence divergence between AMPAR paralogues and intracellular localisation, the

CTD offers a prime site to mediate subunit-specific trafficking of AMPARs (García-Nafría et al., 2016a), and consequently, multiple interactors and phosphorylation sites on the domain have been identified (Figure 1.6; Shepherd and Huganir, 2007).

Figure 1.6 ***Interactions of the AMPAR CTD.*** *Primary sequence of the GluA1 and GluA2 CTD with identified protein interaction sites labelled. Sites of post-translational modifications such as phosphorylation and palmitoylation are also indicated. After Shepherd and Huganir, 2007.*

The GluA1 CTD

The extreme CTD of GluA1, 2, and 3 contain PDZ-ligands, with differential interactions. GluA1 interacts with SAP97 (Figure 1.6; Leonard et al., 1998), with a most profound effect on transmission during development and likely controls the initial stabilisation of synaptic glutamate receptors in newly formed synapses (Howard et al., 2010). It had been suggested that the interaction between GluA1 and SAP97 was essential for synaptic potentiation (Shi et al., 2001), however LTP remains intact when both the SAP97 interaction site on GluA1 (Kim et al., 2005), and SAP97 itself (Howard et al., 2010), are genetically deleted. The interaction between GluA1 and SAP97 does not appear to strongly regulate synaptic AMPARs (Klöcker et al., 2002; Sans et al., 2001). However it can occur early in GluA1 trafficking, with SAP97 association being described at the ER or Golgi membrane (Inamura et al., 2006; Sans et al., 2003; Waites et al., 2009), and therefore may regulate the trafficking and availability of GluA1-containing AMPARs for synaptic transmission.

Multiple phosphorylation sites are located on the GluA1 CTD, with action by CaMKII phosphorylating reside S831, and PKA acting on S845 (Figure 1.6; Barria et al., 1997a,b; Mammen et al., 1997). Synaptic potentiation involves the activation of multiple protein

kinases, and therefore receptor phosphorylation has the potential to control receptor synaptic delivery to mediate this. While LTP is not prevented in double phosphomutant knock-in mice (Lee et al., 2003), pertubation of phosphorylation at these residues, modulates the level of potentiaton (Esteban et al., 2003; Lee et al., 2003). In particular, S845 phosphorylation facilitates the surface delivery of receptors (Oh et al., 2006), which is a critical step in synaptic potentiation. This phosphorylation site appears to be most significantly as proteomic studies have identified its presence throughout the brain at the highest abundance (Schwenk et al., 2014). While these sites do not completely control receptor delivery in synaptic plasticity, as individual phosphomutant mice do not affect LTP (Lee et al., 2010), the phosphorylation cascades occurring at the synapse on NMDAR activation likely increase the availability of receptors for synaptic localisation.

It should be noted that the level of AMPAR phosphorylation in the brain has been questioned. Careful reports have suggested that only a minimal population of receptors are phosphorylated at any one time (Hosokawa et al., 2015, but see Diering et al., 2016). This report, if validated would question the role of phosphorylation in the maintenance of a synaptic receptor population (Shepherd and Huganir, 2007). As the influence of phosphorylation on synaptic plasticity is evident (Esteban et al., 2003; Lee et al., 2003), it is possible that GluA1 phosphorylation is a transient modification, allowing synapse-specific changes in transmission.

LTP has been observed in the absence of the GluA1 CTD (Granger et al., 2013), questioning the role of this domain in plasticity, however elegant mouse knock-in studies have demonstrated a strict requirement for the domain (Zhou et al., 2018). These results demonstrate that multiple mechanisms control AMPAR anchoring during potentiation. While the exact requirements within the CTD were not dissected by Zhou et al., it is most likely that surface delivery of receptor populations to sustain synaptic potentiation is reliant on the GluA1 CTD, through phosphorylation and protein interactions.

The GluA2 CTD

A greater number of protein interactions have been identified for the GluA2 CTD. The C-terminal PDZ ligand interacts with GRIP (glutamate receptor interacting protein), ABP (AMPAR binding protein) and PICK1 (protein interacting with C kinase 1), with differential roles in receptor trafficking (Osten et al., 2000; Srivastava et al., 1998; Xia et al., 1999). A more membrane proximal region of the CTD interacts with the ATPase NSF

(N-ethylmaleimide-sensitive factor; Nishimune et al., 1998; Osten et al., 1998) at a site overlapping with that which interacts with the adaptor complex protein AP2 (Lee et al., 2002).

The interplay of CTD interactions appears complex. The interaction with PICK1 allows AMPAR endocytosis from the synaptic membrane (Fiuza et al., 2017; Lu and Ziff, 2005; Xia et al., 2000), which is critical for long-term depression of hippocampal transmission (Lüthi et al., 1999). Phosphorylation of S880 (SVKI) can differentiate between PDZ-ligand interactors, preventing the binding to GRIP/ABP and favouring PICK1 association and endocytosis (Braithwaite et al., 2002; Chung et al., 2000; Lüthi et al., 1999). Accordingly, GluA2 CTD knockout mice have impaired LTD, while LTP remains intact (Zhou et al., 2018).

NSF promotes the surface delivery of GluA2-containing AMPARs, by dissociating AMPAR-PICK1 complexes either to release receptors from intracellular receptor pools, or to prevent their internalisation (Hanley et al., 2002; Noel et al., 1999; Passafaro et al., 2001). The majority of studies investigating the NSF interaction have utilised competitive peptides derived from the AMPAR CTD, which cause depression of synaptic AMPAR responses (Lüthi et al., 1999; Nishimune et al., 1998) on a rapid timescale, suggesting that receptor recycling is highly dynamic. The exchange of receptors with intracellular pools does not appear to be as rapid as these studies suggest (Adesnik et al., 2005), and it is likely that peptide wash-in has detrimental effects on transmission through non-AMPAR-specific effects. However, the intracellular pool of receptors, stabilised for synaptic delivery, appears a central mechanism in regulating synaptic strength (Chiu et al., 2017; Penn et al., 2017).

The role of the GluA2 CTD appears to be of primary importance in regulating the surface localisation of AMPARs, rather than in synaptic anchoring, and proteomic analysis of the AMPAR complex demonstrates that they are weaker and less abundant than those between TARP and PSD-95 (Fukata et al., 2005). Bats et al. (2007) showed that synaptic immobilisation of surface diffusing receptors is unaffected by CTD peptide expression, demonstrating that CTD interactions are of less consequence to receptor populations already on the cell surface, supporting an exocytosis/endocytosis function. While clearly playing a crucial role in providing the population of AMPARs required for synaptic transmission, the evidence for a fundamental role for the domain in synaptic anchoring itself is not substantial.

1.4.3 Implicating the NTD

Given that the domain encompasses 50 % of the receptor mass, the influence of the NTD in AMPAR function has been starkly neglected. This domain projects into the synaptic cleft, and potentially provides a docking platform for subunit-specific interactions. Extending approximately 13 nm from the postsynaptic membrane, across the 24 nm synaptic cleft (Greger et al., 2017; Lučić et al., 2005), its proximity to presynaptic sites would allow interactions with presynaptic transmembrane proteins, and could facilitate transsynaptic receptor alignment (Tang et al., 2016).

Two reports have suggested a role for the AMPAR NTD in *presynaptic* function. Tracy et al. (2011) report that AMPAR knockdown decreases the readily releasable pool of vesicles in a manner independent of channel gating, while Ripley et al. (2011) show that presynaptic stability in cultured neurons is increased by interactions of the AMPAR NTD. Both reports suggest that presynaptic sites are able to detect the presence of postsynaptic receptors, implicating the receptor in some transsynaptic communication.

The best characterised AMPAR NTD interaction is that with neuronal pentraxins. Three proteins form this family, NP1, NP2 and NPR (neuronal pentraxin receptor), former two being secreted proteins, while the latter contains a transmembrane domain, allowing localisation on the presynaptic membrane (Dodds et al., 1997). These proteins appear to interact with the AMPAR in a non-subunit-specific manner and can mediate clustering of the receptor, due to the oligomeric state of the pentraxin protein family (Mi et al., 2002; O'Brien et al., 2002, 1999).

This NTD-dependent clustering controls the postsynaptic strength at retinal ganglion cells, where presynaptically released NP1 binds postsynaptic GluA1, strengthening the connection (Farhy-Tselnicker et al., 2017). A similar model has been proposed to occur at glutamatergic input onto hippocampal interneurons, where NP2/NPR double knockout abolishes the postsynaptic localisation of GluA4, resulting in loss of control over network activity in the hippocampus (Pelkey et al., 2015; Sia et al., 2007). The pentraxin-mediated AMPAR clustering provides an interesting mechanism of receptor localisation, as spacial localisation of receptors appears to be controlled by the site of secreted pentraxin release, rather than transsynaptic complex formation. However, given that NPR contains a transmembrane domain, the formation of a transsynaptic complex is plausible.

While elegant, this mechanism of AMPAR anchoring is not universal. Within the hippocampus, pentraxins appear to be exclusively expressed at interneuronal synapses, and therefore cannot be a mechanism of receptor clustering at spine synapses in the region (Chang et al., 2010). Given the similarities between secreted pentraxins, Cbln and C1ql proteins, investigation of these protein families may provide insights into further mechanisms of postsynaptic iGluR control.

Another interaction which has been suggested is that of the AMPAR NTD and neuronal cadherin (N-cadherin), a transsynaptic cell adhesion molecule (Saglietti et al., 2007). The AMPAR NTD was demonstrated to have a spectacular effect on synaptogenesis, which could specifically induce formation of dendritic spines, even on aspiny hippocampal interneurons which do not normally have these structures (Passafaro et al., 2003). GluA2 overexpression also causes an increase in the size of spines (Passafaro et al., 2003), a measure which correlates with the AMPAR content and synaptic strength (Matsuzaki et al., 2004). Several reports have refuted this finding, as knockdown or knockout of GluA2 in dissociated cultures or acute slices fail to show any change in spine density (Biou et al., 2008; Chen et al., 2009; Lu et al., 2009). A more recent study has demonstrated that the interaction between N-cadherin and GluA2 is dependent on glycosylation of the receptor, with a significance in surface trafficking (Takeuchi et al., 2015). As proteomic studies regularly fail to confirm this interaction (Schwenk et al., 2014, 2012; Shanks et al., 2012) and the localisation of N-cadherin within the synaptic cleft appears segregated from that of the AMPAR (Perez de Arce et al., 2015), this interaction appears to be of minimal significance to AMPAR signalling.

Other AMPAR interacting proteins have been suggested. C1ql2/3, while evidently controlling GluK postsynaptic localisation, has also shown binding to GluA1 (Matsuda et al., 2016). Whether this interaction is of functional significance is unknown. AMPAR proteomics has identified a number of other proteins with the potential to interact with the NTD. Noelins, brorins and neuritin are all secreted proteins, which must interact with the extracellular region of the receptor (Schwenk et al., 2014, 2012). The impact of these proteins on AMPAR transmission is unknown, yet neuritin has been implicated in synapse stability in the visual cortex (Fujino et al., 2011), and an AMPAR localising function could participate in this effect.

By studying the synaptic role of the NTD for other members of the iGluR family, some potential influences of the AMPAR NTD can be explored. Interactions of the GluD NTD are required for their metabotropic synaptic function upon agonist binding (Elegheert et al.,

2016). Interactors of the NMDAR NTD in *C. elegans* also now appear essential for ionotropic receptor function on agonist binding (Lei et al., 2017). Given that the AMPAR NTD does not have a major influence on channel gating in a recombinant expression system, it is feasible that NTD-dependent gating control is specifically modulated by the presence of synaptic interacting proteins.

The AMPAR NTD adopts a number of conformations, which could be specifically stabilised by interactions in the synaptic cleft. The N-terminal domain layer of both AMPAR and NMDARs appears to rupture on receptor desensitisation, adopting a 'bent' conformation (Nakagawa et al., 2005; Zhu et al., 2016). Stabilisation of this conformation by protein interactions has the potential to influence the recovery of the receptor from the desensitised state, which can strongly influence the postsynaptic ion flux during trains of presynaptic activation (García-Nafría et al., 2016a). Recent structural insights have strengthened the hypothesis that the AMPAR NTD could influence channel gating. While previous AMPAR structures showed little interaction between NTD and LBD layers (Dürr et al., 2014; Sobolevsky et al., 2009), novel structures of the GluA2/3 heteromeric receptors show close approximation and interactions between the domains (Herguedas et al., 2016). These structures show strong similarities to the domain arrangements of NMDARs, which is controlled by NTD-binding pharmacological agents (Monaghan and Jane, 2009).

A receptor-localising role for NTD interactions has been demonstrated for both GluD and GluK receptors, interestingly, both using indirect interactions with presynaptic neurexin molecules (Elegheert et al., 2016; Matsuda et al., 2016). Given the vast plethora of neurexin genes and splice isoforms which are differentially expressed throughout the brain (Südhof, 2017), neurexin has the potential to provide specific, and spatio-temporal control of postsynaptic receptor localisation.

Another cell-adhesion molecule forming synaptic transsynaptic complexes is the LRRTM (leucine-rich repeat transmembrane protein) family. This protein family has been shown to form nanodomain arrangement within the synapse (Chamma et al., 2016) and therefore association of the AMPAR with these proteins could place the receptor at the sites of glutamate release. Knockdown of LRRTM1 and 2 produces a specific deficit in AMPAR mediated transmission, further suggesting control over synaptic AMPARs (Soler-Llavina et al., 2011). Interactions of LRRTM3 and 4 with the AMPAR have been reported (Schwenk et al., 2012; Shanks et al., 2012), yet these appear particularly weak, and were not observed in hippocam-

pal samples (Schwenk et al., 2014).

The influence of cell adhesion proteins on synaptic potentiation is a growing theme. Both neurexin-neuroligin complexes and neurexin-LRRTM interactions control the strength of transmission, with specific requirements in potentiation (Aoto et al., 2013; Soler-Llavina et al., 2013). It is important to note that the role of such transsynaptic proteins in potentiation could predict both pre and postsynaptic changes occurring in LTP, as has been suggested (Bliss and Collingridge, 2013; Lisman, 2009). Given the interaction-based communication between presynaptic release sites and the postsynaptic density which occurs through cell adhesion molecules, they provide a strong candidate to mediate the transsynaptic alignment of glutamate release and receptor localisation for activation.

A plethora of protein interactions work in combination to control the synaptic localisation of the AMPAR. These dynamic processes control the strength of signal transmission between neurons, and therefore identifying and characterising the interplay of these interactions is of critical importance to understanding the mechanisms of cell-cell communication underlying brain function. Multiple factors suggest the potential for regulation of the AMPAR through its N-terminal domain. Its localisation, in the synaptic cleft, which is rich with potential protein interactions, its high sequence divergence between subunits, allowing control of subunit-specific receptor anchoring, and its proximity to presynaptic release sites, allowing for alignment with the vesicle release machinery. This study aims to understand the role of the AMPAR NTD at synaptic sites, by studying the localisation and contribution to functional synaptic signalling of the receptor in combination with targeted receptor mutagenesis. It aims to understand how sequence divergence of the NTD relates to the different roles of AMPAR subunits in transmission. Finally, during synaptic plasticity, how is the reorganisation of the synaptic connection that occurs during potentiation influenced by this extracellular portion of the receptor. Through investigating these questions, this study aims to further understand the mechanisms of information storage at individual neuronal connections.

Chapter 2

Methods

Statistics and data analysis

All data are presented as Mean ± Standard Error of the Mean (SEM). With two-sample comparisons, paired or unpaired Student's t-tests are applied as appropriate. For multiple sample comparisons, One-way ANOVA with a Tukey's multiple comparisons test was used.

Cloning

All constructs were made by IVA cloning (García-Nafría et al., 2016b) using XL-10 Gold chemically competent *Escherichia coli* (Agilent Technologies, Cat. No. 200315). See Chapter 3 for full method details.

2.1 Recombinant cell use

HEK293 cell culture

HEK293T cells (ATCC; CRL-11268, RRID:CVCL_1926, Lot 58483269: identity authenticated by STR analysis, mycoplasma negative), cultured at 37 °C and 5 % CO_2 in Dulbecco's Modified Eagle's medium (DMEM) (Gibco; 31966-021) supplemented with 10 % fetal bovine serum (FBS) and 100 $\mathrm{U\,ml^{-1}}$ penicillin and 100 $\mu\mathrm{g\,ml^{-1}}$ streptomycin were co-transfected with pN1-EGFP and AMPAR constructs using Effectene (QIAGEN; 301427) according to manufacturer instructions.

Flow cytometry

HEK293T cells (ATCC Cat No. CRL-11268, RRID:CVCL_1926, Lot 58483269: identity authenticated by STR analysis, mycoplasma negative) were co-transfected with pN1-EGFP and AMPAR constructs using Effectene (QIAGEN; Germany). Two days post-transfection, cells were washed in phosphate buffered saline (PBS) containing, in mM: 125 NaCl 16.6 Na_2HPO_4, 9.5 NaH_2PO_4 at pH 7.2, and incubated with AF647 conjugated primary antibody (anti-myc 9E10, Santa Cruz Biotechnology; Dallas TX, RRID:AB_627268) for 30 mins on ice in PBS containing 10 % FBS. Antibody was removed and cells were washed further in PBS before resuspension in PBS containing 10 % FBS and 1:1000 DAPI. Flow cytometry was performed using a LSR II flow cytometer (BD; Franklin Lakes, NJ). AF647 fluorescence was quantified and represents construct surface expression. Cells either positive for DAPI fluorescence or negative for EGFP fluorescence were discarded from analysis as dead or untransfected respectively. AF647 fluorescence of untransfected cells was measured and subtracted during quantifications of surface expression.

Western blotting

Transfected HEK293T cells, grown in 6 well plates, were scraped in PBS containing 1X Protease Inhibitor cocktail (Roche; 5056489001) and 1 mM PMSF (phenylmethylsulfonyl fluoride), pelleted and resuspended in 250 µl lysis buffer, containing (in mM): 25 HEPES, 150 NaCl, 1 EDTA, 1 % Triton X-100, 1 PMSF and 1X Protease Inhibitor cocktail at pH 7.5. Cells were lysed for 30 min on ice before centrifugation at 16,000g for 10 min. Supernatant was retained and 26 µl was combined with 4 µl 1 mM DTT (dithiothreitol; 100 mM final concentration)and 10 µl 4X SDS-PAGE (sodium dodecyl sulfate polyacrylamide gel electrophoresis loading buffer (Invitrogen; NP0007) and proteins were denatured by incubation at 95 °C for 5 min. Samples were run on an Bolt™4-12 % Bis-Tris Plus gel (Invitrogen; NW04122BOX) alongside an Full-Range Rainbow Molecular Weight Marker marker (GE Healthcare; RPN800E) in 1X Bolt MES SDS running buffer (Invitrogen; B0002). Proteins were transferred to a nitrocellulose membrane (Invitrogen; IB301032) using an iBlot™(Invitrogen; IB1001). Equivalent sample loading was confirmed by incubation in Ponceau S solution (Sigma-Aldrich; P7170-1L) for 5 min before blocking in PBS-Tween (PBS plus 0.1 % TWEEN 20 (NBS Biologicals; 17767-B)) plus 5 % milk powder (Marvel; MARVEL198) for 1 h at room temperature with gentle agitation. Primary antibody, anti-GluA2 (Sigma-Aldrich; SAB4501295) was incubated for 1 h at rtp in PBS-Tween plus 5 % milk. Membranes were washed 3 times in PBS-Tween for 10 min before incubation with

secondary antibody, anti-rabbit IgG (Millipore; MAB201P) for 45 min at rtp in PBS-Tween plus 5 % milk. After a further 3 washes in PBS-Tween, Super-signal West Dura substrate (Thermo Scientific; 34076) was added for 5 min to visualise antibody location, with imaging performed using a BioRad ChemiDoc™XRS+ Imaging System (Bio-Rad; 1708265).

2.2 Neuronal tissue preparation

Conditional AMPAR knockout using P0 viral injection

Mice with floxed loci at *Gria1*, *2* and *3* genes [*Gria1*$^{lox/lox}$ (RRID:IMSR_JAX:019012), *Gria2*$^{lox/lox}$ (RRID:IMSR_EM:09212), *Gria3*$^{lox/lox}$ (RRID:IMSR_EM:09215)] were a gift from Rolf Sprengel (MPI - Heidelberg) and were interbred to produce mice homozygous for all floxed alleles (*Gria1*$^{lox/lox}$; *Gria2*$^{lox/lox}$; *Gria3*$^{lox/lox}$, denoted *Gria1-3fl*). 0.5 µl of AAV9-hSyn-Cre-GFP (Penn Vector Core, USA) (titre - 2×10^{12} GC ml^{-1}) was injected into each hippocampus of *Gria1-3fl* mice at postnatal day 0-1 (P0/1) using a borosilicate glass micropipette and a 5 µl syringe (Model 75, Hamilton Company; Reno, NV). Pups were anaesthetised with 4 % Isoflurane in an anaesthetic induction chamber for 3-4 min and subsequently transferred to a stereotactic rig where they were subjected to intracerebral injection, with aesthetic maintained throughout the procedure. Following recovery, pups were returned to their home cage and were used at P6-8 for the preparation of organotypic slices (as detailed below).

Dissociated culture preparation

E18 Sprague Dawley rats were sacrificed and embryonic hippocampi were isolated in Ca^{2+} and Mg^{2+} free Hank's balanced saline solution (HBSS-CMF, Thermo Fisher Scientific; 14170112) supplemented with 10 mM HEPES . Hippocampi were treated with 0.25 % trypsin (Thermo Fisher Scientific; 15090046) at 37 °C for 12 min, washed twice in plating medium (maintenance medium supplemented with 2.5 % FBS) and twice in HBSS-CMF before trituration with a 1 ml Gilson pipette (approx. 8 times). Cells were counted and plated on either 13 mm or 22 mm diameter, #1.5 thickness glass coverslips (Hecht Assistent; Germany) coated overnight with 0.1 % (w/v) poly-L-lysine (Sigma-Aldrich; P8920) or on pre-coated poly-D-lysine and laminin 12 mm diameter coverslips (Corning; 08-774-385). Cells were diluted to 25 - 50,000 cells per ml in plating medium. 100 µl and 400 µl cell suspension were added to 13 mm and 22 mm coverslips respectively. 1-2 hrs after plating, cells were supplemented with 750 µl and 1.5 ml maintenance medium respectively

(containing Neurobasal Medium (21103-049), 1X B27 supplement (0080085SA) and 1X GlutaMax (35050061) (all Thermo Fisher Scientific)) and equilibrated at 37 °C with 5 % CO_2. Cultures were fed at 3-5 days in vitro (DIV) and then once weekly by 50 % replacement with fresh maintenance media.

Dissociated culture transfection

Cultures were transfected at 14-16 DIV using Lipofectamine 2000 (Thermo Fisher Scientific; 11668030). 2 µg plasmid DNA was incubated with 4 µl Lipofectamine in 100 µl Neurobasal medium for 20 minute at room temperature and pressure (rtp). Cells were washed with 50 % old, 50 % fresh (50/50) maintenance medium and DNA-Lipofectamine mix was added. Cells were incubated at 37 °C for 20 minute before replacement of the medium with further 50/50 maintenance medium, before use at 3-6 days after transfection (DAT).

Organotypic slice preparation

Organotypic slice cultures were prepared as per Stoppini et al. (1991). Briefly, hippocampi from P6-8 C57/Bl6 mice were isolated in high-sucrose Gey's balanced salt solution (GBSS containing (in mM): 175 Sucrose, 50 NaCl, 2.5 KCl, 0.85 NaH_2PO_4, 0.66 KH_2PO_4, 2.7 $NaHCO_3$, 0.28 $MgSO_4$, 2 $MgCl_2$, 0.5 $CaCl_2$ and 25 glucose at 7.3 pH. Hippocampi were cut into 300 µm thick slices using a McIlwain tissue chopper and cultured on Millicell cell culture inserts (Millipore Ltd) in equilibrated slice culture medium (37 °C/5 % CO_2). Culture medium contained 78.5 % Minimum Essential Medium (MEM), 15 % heat-inactivated horse serum, 2 % B27 supplement, 2.5 % 1 M HEPES, 1.5 % 0.2 M GlutaMax supplement, 0.5 % 0.05 M ascorbic acid, with additional 1 mM $CaCl_2$ and 1 mM $MgSO_4$ (all from Thermo Fisher Scientific). Medium was refreshed every 3 - 4 days. Cultures were transfected at 4 - 11 DIV by single-cell electroporation (SCE) and recordings were performed 4 - 6 days after transfection.

Single Cell Electroporation

Organotypic slices were transfected using an adapted version of the single-cell electroporation method described in Rathenberg et al. (2003). DNA plasmids were diluted to 33 ng µl^{-1} with potassium-based intracellular solution and the mixture was back-filled into borosilicate microelectrode pipettes (see *Electrophysiology*). Slices were submerged in HEPES-based artificial cerebrospinal fluid (aCSF) containing (in mM): 140 NaCl, 3.5 KCl, 1 $MgCl_2$, 2.5 $CaCl_2$, 10 HEPES, 10 Glucose, 1 sodium pyruvate, 2 $NaHCO_3$, at 7.3 pH. Plasmids were

introduced into individual cells by the application of a short burst of current pulses (60 pulses at 200 Hz) while in cell-attached mode. To visualise transfected cells, pN1-EGFP (Clontech) was routinely mixed with AMPAR-expressing plasmids at a base pair ratio of 1:7. In the CaMKII experiments, the ratio between tCaMKII-EGFP and AMPAR-expressing plasmids was 1:1.

2.3 Electrophysiology

For all experiments, slices were bathed in aCSF containing (in mM) 125 NaCl, 2.5 KCl, 1.25 NaH_2PO_4, 25 $NaHCO_3$, 10 glucose, 1 sodium pyruvate, 4 $CaCl_2$, 4 $MgCl_2$ and 0.001 SR-95531 (Tocris; 1262) at 7.3 pH and saturated with 95 % O_2/5 % CO_2 unless otherwise stated. For rectification index and mEPSC (miniature excitatory postsynaptic current) recordings, 100 µM D-APV (Tocris; 0106) was added to isolate AMPAR currents, and for all recordings using organotypic slices, excluding mEPSC recordings, 2 µM 2-chloroadenosine (Sigma-Aldrich, Cat. No. C5134) was added to minimise epileptiform activity. 3 - 6 MΩ borosilicate pipettes (Science Products; GB150F-8P; dimensions - $0.86 \times 1.5 \times 80$ mm) were pulled using a two-step protocol on a Narishige PC-10 vertical puller, and filled with intracellular solution (ICS) containing (in mM): 135 CH_3SO_3H, 135 CsOH, 4 NaCl, 2 $MgCl_2$, 10 HEPES, 4 Na_2-ATP, 0.4 Na-GTP, 0.15 spermine, 0.6 EGTA, 0.1 $CaCl_2$, at 7.25 pH.

Outside-out patch clamp. Outside-out patches were pulled from GFP positive or negative CA1 cell bodies and patches were subjected to fast-exchange perfusion in HEPES-based aCSF (see SCE) containing 100 µM cyclothiazide, with or without 1 mM L-glutamate. In voltage-clamp mode, a 500 ms holding potential ramp from −100 mV to 100 mV was applied to patches. Recordings in the absence of glutamate were subtracted from those in the presence of glutamate and −60 mV, 0 mV and +40 mV current amplitudes were used to calculate rectification index as described below.

Paired synaptic recordings. Paired recordings involved simultaneous recording from a neighbouring pair of GFP positive and negative cells. EPSCs were evoked by simulation of Schaffer collaterals in the stratum radiatum of CA1 using a monopolar glass electrode, filled with aCSF. Recordings were collected using a Multiclamp™700B amplifier (Molecular Devices). Recordings during which the series resistance varied by more than 20 % or exceeded 20 MΩ were discarded.

Rectification Index. Rectification index was calculated by recording AMPAR currents from cells held at -60 , 0 and +40 mV, using the following equation:

$$\text{Rectification Index (RI)} = \frac{I_{+40\text{ mV}} - I_{0\text{ mV}}}{I_{\text{-60 mV}} - I_{0\text{ mV}}}$$

AMPAR NMDAR ratio. AMPAR/NMDAR EPSCs were compared by recording synaptic currents at -60 mV and +40 mV. AMPAR current amplitudes were quantified as the peak current at -60 mV. NMDAR amplitudes are measured at +40 mV, 100 ms after response initiation.

Paired-pulse ratio. Paired-pulse ratio was calculated from two AMPAR currents, stimulated at an interval of 50 ms.

mEPSC recordings. 1 µM tetrodotoxin (Tocris; 1069) was added to the aCSF for mEPSC recordings to isolate individual spontaneous release events. mEPSC detection was conducted using a template-based search in Clampfit (Molecular Devices). Cumulative frequency plot was produced using equal numbers of events from all cells within each condition to prevent misrepresentation

LTP recordings. Whole-cell LTP recordings were performed in an alternative aCSF containing (in mM) 119 NaCl, 2.5 KCl, 1 Na_2HPO_4, 26 $NaHCO_3$, 4 $CaCl_2$, 4 $MgCl_2$, 11 glucose, 0.002 2-chloroadenosine and 0.01 SR-95531 (based on Shi et al. (2001)) and ICS containing 15 $CsCH_3SO_3$, 20 CsCl, 10 HEPES, 2.5 $MgCl_2$ 4 Na_2-ATP, 0.4 Na-GTP, 10 phosphocreatine, 0.1 spermine at 7.3 pH. Slices were maintained at 25 °C throughout the recordings. LTP was induced by depolarisation of the cell to -10 mV while stimulating the test pathway at 2 Hz for 100 s. The control pathway did not receive input during this period.

Peak-scaled non-stationary fluctuation analysis

Miniature EPSC recordings, digitised at 100 kHz, were subjected to noise analysis using a custom program running in MATLAB (MathWorks) (supplied by Andrew Penn, University of Sussex; available on MATLAB File Exchange, ID: 61567) following Hartveit and Veruki (2007) and Benke et al. (2001). Briefly, events were detected using a template-based search (Pernía-Andrade et al., 2012), aligned by their point of steepest rise and peak scaled to

account for differences in synaptic receptor number. Traces were filtered to those with a 10 - 90 % rise time of less than 0.9 ms and subjected to visual inspection to eliminate obvious artefacts, overlapping mEPSCs or insufficient peak alignment. Correlations between peak amplitude, rise and decay times were analysed to detect and eliminate cells with excessive electrical filtering. Following elimination of suboptimal events, only cells with at least 20 successful events were included for variance analysis. Variance vs amplitude plots were produced for binned decay phase data of mEPSCs (15 bins) and were fitted with a parabolic curve with the equation:

$$\sigma^2(I) = iI - \frac{I^2}{N} + \sigma_b^2$$

from which single-channel current (i) could be calculated, being proportional to the initial gradient of the parabolic curve. Single-channel conductance (γ) is related to current by the equation:

$$\gamma = \frac{i}{(V_m - E_{\text{rev}})}$$

where membrane potential (V_m) and reversal potential (E_{rev}) were -60 mV and 0 mV respectively.

2.4 Imaging

Dissociated culture immunocytochemistry

For surface staining, neurons were incubated with primary antibody, anti-c-myc 9E10 (Sigma-Aldrich; M4439, 1:500 dilution) for 20 min at rtp in culture medium. Cells were washed $\times 3$ in culture medium before fixation in 1X DPBS (Gibco; 14080048) containing 4 % paraformaldehyde (PFA, Electron Microscopy Sciences; 15714S) with 4 % sucrose (w/v) for 10 min at rtp. Cells were washed briefly in 1X DPBS before blocking with 1X DPBS containing 10 % bovine serum albumin (BSA, Fisher Scientific; BP1605-100) for 1 h at rtp. Secondary antibody, goat anti-mouse IgG AF568 conjugate (Thermo Fisher Scientific; A-11004, 1:500 dilution), was applied for 1 h at rtp in 1X DPBS containing 3 % BSA. Cells were washed three times in 1X DPBS for 10 min each before mounting in ProLong™ Diamond Antifade Mountant (Invitrogen; P36961) on glass slides (Thermo Scientific; Menzel-Gläser Superfrost®). Imaging was performed on a Leica SP8 confocal microscope using a 63X objective lens.

STED microscopy

STED microscopy was performed using a commercial Leica SP8 confocal microscope using a 100X objective lens. 660 nm STED beam was used for depletion of AF568 signals allowing STED microscopy. Image analysis was conducted using a custom macro series in Image J (Schneider et al., 2012).

Anatomical Imaging using Lucifer Yellow

To visualise dendritic spines, 1 mg ml^{-1} Lucifer Yellow was added to the intracellular solution. Cells were maintained in a whole-cell configuration for 10 min before live imaging on an inverted Leica SP8 confocal microscope in SCE extracellular solution. Z-stacks of 50 µm regions of secondary dendrite were imaged using a 63X oil-immersion objective, deconvolved using Huygens Professional and segmented using Imaris before manual counting of spines.

Fluorescence recovery after photobleaching

Hippocampal cultures were cotransfected (1:1) with pN1-mCherry (Clontech) and SEP-GluA2 or SEP-GluA2 ΔNTD and imaged in artificial cerebrospinal fluid (aCSF) containing (in mM): 150 NaCl, 2.5 KCl, 2 $MgCl_2$, 2 $CaCl_2$, 20 HEPES, 10 Glucose at pH 7.3 in a heated chamber at 37 °C. Images were acquired on a Leica SP8 confocal microscope using a 63X objective lens at 30 s intervals. Photobleaching was achieved by repetitive xy scanning of the region of interest at high laser intensity. Fluorescence during bleaching was monitored to ensure steady state complete bleaching was achieved and bleaching parameters were constant for all samples and repetitions. Analysis was conducted using Image J (Schneider et al., 2012). Photobleaching due to image acquisition was corrected by normalisation to non-photobleached spines or dendrites, distant to a bleached spine.

Chapter 3

The development of IVA Cloning

3.1 Introduction

Molecular cloning

The field of molecular biology is grounded in molecular cloning, and hence advancements in techniques to manipulate DNA in simpler and more versatile ways are constantly being developed and adopted. This chapter describes the development and optimisation of a molecular cloning approach, which is exploited in the remainder of this study for simplified generation of AMPAR expression constructs.

Historically, and still currently in many labs, molecular cloning would be performed using restriction enzymes, cutting both vector and insert DNA, to be joined by DNA ligase. However, the disadvantages of this method are numerous. Firstly, this approach is entirely reliant on the DNA fragments of interest containing compatible restriction enzyme recognition sequences, allowing little flexibility for custom design of the final product. Many cloning procedures are potentially impossible as the required recognition sites are either not present in template DNA, are not present in the correct location, or are present at multiple locations on the plasmid. Secondly, the final product will inevitably contain the sequence of the restriction enzyme sites used, leaving 'scars' in the DNA. While in some cases this will not matter, in many examples this is either inconvenient or detrimental to future work. For example, if a project required exchange of domains between two proteins, using restriction enzymes would result in a short amino acid sequence being encoded between domains of the final protein due to their inclusion as restriction site DNA. Finally, the process of restriction digestion, DNA purification, and ligation is laborious and requires significant hands-on-time. These

limitations have driven the development of a variety of homology-based cloning methods, which free researchers from the shackles of sequence dependency. This new breed of cloning assembles DNA fragments, generally amplified by PCR, based on homologous sequences introduced at the linear fragment ends. Not only does this facilitate seamless product formation and directional assembly, but also allowed modification at any point on a vector at which a primer could bind and amplify. Many methods have been developed, differing in their assembly mechanisms from *in vitro* enzymatic assembly (Gibson Assembly; Gibson et al., 2009), single-stranded DNA annealing (Ligation independent cloning, LIC; Aslanidis and de Jong, 1990) or *ex vivo* assembly using bacterial extracts (Seamless Ligation Cloning Extract, SLiCE; Motohashi, 2015).

Homologous recombination uses highly similar sequences on DNA fragments to fuse or exchange regions of DNA between them. Given the benefits of homology-based approaches in cloning methodologies and the advantage of a recombination mechanism allowing DNA assembly to be performed 'hands-free' by the host organism, recombination cloning is a powerful approach. 'Recombineering' has been developed in both yeast (Joska et al., 2014; Mashruwala and Boyd, 2016; van Leeuwen et al., 2015) and bacteria (Li and Elledge, 2007; Trehan et al., 2016; Zhang et al., 2000). The disadvantages of a yeast-based approach are numerous, but the primary limit to its widespread adoption is the requirement for yeast handling, before ultimately returning to bacteria for plasmid propagation. Bacterial recombineering traditionally has required *E. coli* strains with high recombinase activity, such as *recA*+ or RedET strains, which come with their own limitations, causing plasmid instability due to their enhanced recombination (Peijnenburg et al., 1987), and therefore they themselves are not widely employed. For this reason, *E. coli* strains used most widely for plasmid propagation are *recA*- and are thought of as recombination deficient.

However, a *recA*-independent recombination pathway *is* present in these widely used *E. coli* strains, and is currently gaining attention for its use in molecular cloning. Such a mechanism has the potential to combine the benefits of homology-based cloning approaches and the simplicity of recombination for DNA assembly, while avoiding the limitations of plasmid instability associated with current recombineering strains. By exploiting a pathway present in *E. coli* strains already used in laboratories worldwide, such a method has the potential for immediate and widespread adoption by the molecular biology community.

Historical cloning using *recA*-independent recombination

The *recA*-independent recombination (RAIR) pathway, and its application to cloning was first reported over 25 years ago (Bi and Liu, 1994; Bubeck et al., 1993; Jones and Howard, 1991), yet it was never widely adopted by the molecular biology community and has only been sporadically developed (Howorka and Bayley, 1998; Klock et al., 2008) and used in specific, high-throughput applications (Parrish et al., 2004; Wang et al., 2015). Recently however, multiple reports are beginning to appreciate its efficiency and potential for simplified molecular cloning.

In the first report showing the potential of the RAIR pathway, Douglas Jones and Bruce Howard described their "recombination PCR" method for plasmid mutagenesis or subcloning. The method required PCR amplification using primers to introduce homologous regions, with DNA assembly occurring by recombination after transformation into DH5α *E. coli*. Despite inclusion in 'Methods in Molecular Biology' on multiple occasions (Jones and Winistorfer, 1993, 1997, 2003), including representation on the cover in 2003, the method never gained widespread popularity. The original report has received just 32 citations since 1991 (Jones and Howard, 1991, PubMed citations). Contrasting this with a more recent and popular cloning method, Gibson Assembly, which has to date received 1156 citations since 2009. (Gibson et al., 2009, PubMed citations) demonstrates that RAIR dependent cloning has made little impact until recent years.

The reasons for its initially poor adoption are interesting to contemplate. The method had several experimental disadvantages when first reported. Firstly, polymerases at the time had poor fidelity and limited amplification lengths (Hultman et al., 1990). Taq was the main polymerase, with an error rate approximately 50-fold higher than current options such as Phusion and Q5 (McInerney et al., 2014). Given that this new technique required amplification of the entire plasmid vector, the frequency of random mutagenesis by PCR amplification was high. As the technique aimed to engineer a desired mutation, this could end up being a case of one step forward, two or three steps back. Not only the fidelity, but also the processivity of polymerases was limited. The amplification length limit of Taq would have prevented large vectors from being amplified, further reducing the usefulness of the technique. While this could be overcome by using multiple PCRs to amplify the vector in separate parts (Yao et al., 1992), the substantial effort required for this approach likely deterred potential users. Multiple reports cite the cost of oligonucleotides as the major caveat of this method (Lai et al., 1993; Schulga et al., 1994; Zaret et al., 1990).

Subcloning using RAIR was separately characterised by Bubeck et al. (1993). This report was quickly followed by Oliner et al. (1993), which characterised recombination dependent cloning using the JC8679 *E. coli* strain, making comparisons with the work of Bubeck et al. (1993) and demonstrating far greater cloning efficiency. However, while Bubeck et al. used the DH5α strain, and *recA*-independent recombination, the specialised JC8679 strain has enhanced recombination, through activation of the RecE pathway. The close temporal publication of these reports and non-equivalent comparisons between recombination pathways likely meant that these reports caused great confusion for potential recombination cloning users.

In recent years, polymerase fidelity, processivity and the cost of oligonucleotide synthesis have improved dramatically; as prices of 9 pence per base for oligonucleotides of up to 110 bp are now available, considerably sized modifications can be made to plasmids simply through incorporation into PCR primers. Due to these factors, a host of recent reports highlight the usefulness of the RAIR pathway for molecular cloning (Beyer et al., 2015; García-Nafría et al., 2016b; Huang et al., 2017; Jacobus and Gross, 2015; Kostylev et al., 2015; Li et al., 2011).

The *recA*-independent recombination pathway

The mechanism of the *recA*-independent recombination pathway is still not fully appreciated, despite multiple recent reports of its use as a cloning tool (Beyer et al., 2015; García-Nafría et al., 2016b; Huang et al., 2017; Jacobus and Gross, 2015; Kostylev et al., 2015; Li et al., 2011). It was initially appreciated that the pathway allowed recombination of short homologous regions, whereas the *recA*-dependent pathway required long homologous regions (Lovett et al., 2002). This attribute lends itself to use as a cloning tool, where homology must be introduced in primer sequences, and therefore cannot be extensive. Required homology lengths have been reported as > 10 bp (Bubeck et al., 1993), 6 bp (Nakano and Kuramitsu, 1992) or even just 4 bp (Jones and Howard, 1991), with multiple reports describing that recombination efficiency is dependent on the length of homologous region (Jacobus and Gross, 2015; Li et al., 2011) producing both a greater number of bacterial colonies on transformation, and a greater percentage of correct clones when longer homology is used.

Bubeck et al. (1993) performed an insightful characterisation of the requirements for source DNA, which provides insights into the mechanism of action. For recombination between two

separate DNA fragments, if either, or both pieces are circular, recombination cannot occur, demonstrating a clear requirement for linear ends to DNA fragments. Additionally, while the pathway requires linear ends for successful recombination, homologous regions need not be at the termini of the fragments, and there are reports of successful recombination of sequences at least 180 bp from fragment termini (Jacobus and Gross, 2015). In such cases, the non-homologous sequence is lost from the final product (Bubeck et al., 1993; Jones and Howard, 1991). These observations provide insights into the recombination mechanism. In an earlier study, Conley et al. (1986) studied plasmid recombination in both recA+ and recA- *E. coli* strains by linearising plasmid DNA and studying the deletions which occur on re-circularisation, after transformation. Recombination occurred at sites of limited homology, with preference to those closer to linear DNA ends, which has since been confirmed by Bi and Liu (1994). Conley et al. (1986) postulate a RAIR mechanism based on single-strand annealing, whereby 3' to 5' exonuclease activity would produce single-stranded DNA at linear ends, which can anneal through short regions of homology to be subsequently repaired by polymerases and ligases. This explains the apparent bias for recombination at sites of homology close to linear ends, as those more distant require greater exonuclease activity, and therefore are less likely to be converted to single-stranded DNA. Interestingly, this mechanism is in principle equivalent to that of Gibson Assembly, which uses *in vitro* action of an exonuclease, polymerase and ligase enzyme for DNA assembly, however simply proceeding *in vivo* rather than *in vitro*.

As recombination is facilitated in DNA with free termini (Bubeck et al., 1993), and does not rely use of an intact DNA sequence as a template, as other recombination pathways such as RecA dependent recombination do (Bell and Kowalczykowski, 2016), it is likely that the endogenous function of the RAIR pathway is emergency repair of double-stranded DNA breaks. Given the reliance on repeated small homologies for this repair, the pathway will be highly error prone when utilised by bacteria. Small regions of homology which are recombined on double-strand break will originally be separate in the original sequence and therefore the intervening base-pairs will be deleted on repair. However, for its use in cloning, homologous sequences can be introduced at the termini of linear fragments by PCR, thus circumventing any error introduction by recombination.

Further data supports the single-strand annealing hypothesis. Dutra et al. (2007) demonstrate that RAIR efficiency is increased by almost two orders of magnitude in bacterial strains deficient for single-stranded DNA exonucleases. Such proteins could potentially degrade

the single-stranded homologous regions which are required for annealing, thus limiting its effectiveness. Strains lacking single-stranded exonucleases cause DNA instabilities, with increased DNA replication errors, such as frameshift introductions at repeated sequences (Dutra and Lovett, 2006; Viswanathan and Lovett, 1998), which could either result from lack of exonuclease activity or enhanced RAIR activity. However, such observations could be used as an interesting starting point for the development of bacterial strains with improved RAIR cloning efficiency. The discovery of enhanced RAIR in *yjiP* expressing bacteria could be similarly used for bacterial development (Kingston et al., 2015), although the reason for the effect in this strain seems less clear. Enhanced-RAIR strains offer the potential to revolutionise cloning, for example by development of 'PCR-less' mutagenesis, by co-transformation of plasmids with mutagenic oligonucleotides which recombine to produce the desired plasmid. This approach has been attempted previously (Dutra et al., 2007; Swingle et al., 2010), however the efficiency of recombination was not high enough for use as a viable cloning procedure. Initial attempts in the direction of bacterial improvement have been made (Murphy and Marinus, 2010), but are yet to gain widespread use.

Lovett et al. (2002) suggest that RAIR is dependent on RecBCD, proteins which bind DNA double strand breaks. RecBCD carries exonuclease activity from linear DNA ends, however on encountering homologous DNA regions exonuclease activity is limited, and recombination is promoted. While RAIR between circular plasmids has been described at very low levels by Lovett et al. (2002), a RecBCD dependent mechanism, requiring protein binding to DNA linear ends would be greatly enhanced by transformation of linear DNA, and therefore is likely to explain unsuccessful RAIR cloning using circular input sequences (Bubeck et al., 1993). Further evidence for the involvement of RecBCD in RAIR is the identification of a *recA*-independent single-strand annealing mechanism for double strand break repair in *Mycobacterium smegmatis* (Gupta et al., 2011, 2013). Similar single-strand annealing based RAIR has been identified in other bacteria such as *Deinococcus radiodurans* (Xu et al., 2010). An 'Alternative End-Joining' pathway (A-EJ) has been described in *E. coli* by studying non-homologous end-joining (NHEJ) mechanisms. Chayot et al. (2010) studied how double strand breaks in transformed plasmid DNA are repaired and found that short regions of homology (microhomologies) at DNA termini can be joined through RecBCD exonuclease activity revealing regions of homology. The authors implicate LigA as the DNA ligase responsible for DNA repair after single-strand annealing. Given the strikingly similar mechanism and suggested protein requirements, it is likely that A-EJ and RAIR are in fact the same process.

Interestingly, a single-strand annealing mechanism raises interesting parallels with suggestions in previous cloning studies utilising RAIR. Li et al. (2011) proposed that 3' to 5' exonuclease activity of proofreading DNA polymerases in the final cycles of PCR, occurring due to depletion of nucleotides in the reaction, would leave single-stranded DNA available for annealing *in vitro* and was essential for successful cloning. Similarly, Klock et al. (2008) suggested that incomplete action of DNA polymerases during PCR would produce single-stranded termini for annealing, naming the method Polymerase Incomplete Primer Extension (PIPE) because of this. Both cloning protocols have highly similar requirements to RAIR cloning reports, needing short regions of homology (15 bp) at linear DNA termini, which are repaired upon transformation. However, substantial evidence demonstrates that initially single-stranded DNA termini is not an essential requirement for successful cloning. Firstly, the 'polymerase incomplete' notion which is the basis of PIPE is based on a historic observation utilising *Taq* polymerase (Olsen and Eckstein, 1989), while PIPE, among other studies (Jacobus and Gross, 2015; Klock et al., 2008; Kostylev et al., 2015; Li et al., 2011) use newly engineered polymerases with greater processivity, which are unlikely to leave incomplete termini. Secondly, Li et al. (2011) suggest polymerase proofreading activity is required for producing single-stranded DNA termini, while Klock et al. (2008) mention that both *Taq* (non-proofreading) and Phusion (proof-reading) enzymes are sufficient for successful cloning. Finally, cloning can be performed if the vector is linearised using restriction enzymes, which will not leave single-stranded termini (Bubeck et al., 1993; Jacobus and Gross, 2015). Therefore, the single-strand exposure mechanism performed *in vivo* by the bacteria, is clearly sufficient alone for exploitation of the pathway as a cloning tool.

The implications of RAIR for *in vitro* assembly cloning

In vivo assembly methods are not the only cloning techniques which utilise the RAIR pathway. The SLiCE (Seamless Ligation Cloning Extract) method uses the recombinatorial activity of bacterial lysates for *ex vivo* assembly of PCR amplified DNA fragments (Motohashi, 2015; Zhang et al., 2012, 2014b). Interestingly, extracts from RecA expressing and RecA lacking strains (Motohashi, 2015; Zhang et al., 2014b) have been successfully used for this technique, with the latter example most likely utilising the RAIR pathway discussed here. It is interesting to note that the efficiency of homology based methods which use *in vitro* assembly, such as Gibson Assembly, In-Fusion or SLiCE, are likely enhanced by *in vivo* RAIR, which can assemble remaining linear DNA in the same manner as RAIR cloning, given that the homology requirements are strikingly similar. In fact this phenomenon has

been recognised and quantified in one *ex vivo* cloning method characterisation (Fisher et al., 2013), who recognised that this is '*a process that is often overlooked when characterizing in vitro DNA assembly methods*'.

Development of a universal cloning method

While the possibility of cloning using RAIR is clear and well documented, the method is far from fully optimised. Different reports use DNA purification by PCR-clean up (Verheijen et al., 1997) or gel extraction (Beyer et al., 2015; Jacobus and Gross, 2015; Martin et al., 1995), and some protocols lack PCR clean-up altogether (Li et al., 2011). The power of RAIR to assemble multiple DNA fragments has also not been investigated or appreciated. For these reasons, *recA*-independent recombination can be exploited to develop a rapid, cheap cloning method, capable of performing a multitude of plasmid modifications.

This study describes the development of a complete cloning system: *In Vivo Assembly* (IVA) cloning, based on the RAIR mechanism present in common laboratory *E. coli* strains. All cloning procedures (insertions, deletions, mutagenesis and sub-cloning) can be performed and combined at will, using a single universal protocol consisting exclusively of a single-tube PCR followed by *Dpn*I digestion and transformation. IVA cloning utilises fully optimised primer design and is applied to examples of DNA modifications for plasmids encoding AMPA receptor subunits or auxiliary proteins in a variety of mammalian expression vectors.

3.2 Methods

E. coli strains and reagents

E. coli XL10-Gold ultracompetent cells (Agilent; 200314) were used throughout, unless otherwise stated, from either commercial stocks, or prepared by the Rudibidum Chloride method (transformation efficiency $> 5 \times 10^9$ and $\simeq 3 \times 10^6$ respectively).

Rubidium Chloride method for competent cell production

Buffers RF1 and RF2 were used for this process (both filter sterilised). RF1 contained (in mM): 100 RbCl (Sigma-Aldrich; R2252), 50 $MnCl_2 \cdot 4H_2O$ (Sigma-Aldrich; M3643), 30 potassium acetate, 10 $CaCl_2 \cdot 2H_2O$ and 15 % (w/v) glycerol, adjusted to pH 5.8 using 0.2 M glacial acetic acid. RF2 contained (in mM): 10 MOPS (3-(*N*-morpholino)propanesulfonic acid, Sigma; M1254), 10 RbCl, 75 $CaCl_2 \cdot 2H_2O$ and 5 % (w/v) glycerol, adjusted to pH 6.8 using 1 M NaOH.

XL-10 Gold ultracompetent bacteria (Agilent; 200314) were spread on LB-agar (for recipe see below) containing 30 µg ml^{-1} chloramphenicol and grown overnight at 37 °C. An individual colony was grown overnight in 3 ml LB containing 30 µg ml^{-1} chloramphenicol at 37 °C. 1 ml of overnight culture was added to 100 ml of LB and grown at 37 °C until OD_{600} reached 0.44 - 0.55. Culture was chilled on ice for 15 min before centrifugation to pellet bacteria (2700 g for 10 min at 4 °C). Supernatant was discarded and bacterial pellet was gently resuspended in 33 ml chilled RF1 buffer. Cells were incubated on ice for 15 min before centrifugation at 580 g for 15 min at 4 °C. Supernatant was again discarded and bacterial pellet was resuspended in 4 ml RF2 buffer. Cell suspension was incubated on ice for 15 min before dispensing into 100 µl aliquots in chilled 1.5 ml eppendorf tubes on dry ice. Cells were stored at −80 °C.

Primers

Primers were designed using OligoCalc (Kibbe, 2007) or Oligo Calculator (Krantz Lab and University of California; Berkley, 2002) and DNA sequences were handled using SnapGene®. Primers were obtained from Integrated DNA Technologies (IDT) (sequences $\leq$ 60 bp) or Sigma-Aldrich (sequences > 60 bp). Primers were designed with a template DNA binding T_m of 60 °C. All primer sequences used in this study are presented in Appendix A.

PCR

Unless otherwise stated, PCRs were performed using Phusion® High-Fidelity DNA Polymerase (NEB; M0530L) in 25 µl reactions and run in a PTC-200 Thermocycler (MJ Research) using the following recipe and cycling protocol:

Table 3.1 *PCR components*

	Final Conc. (mM)	µl of Stock	Stock Conc.
Reaction buffer	1X	5	5X
Phusion	0.5 units	0.25	50 units/µl
Betaine	1 M	5	5 M
DMSO	3 %	0.75	100 %
dNTPs	200 µM	2	2.5 mM
Each Primer	0.2 µM	1	5 µM
Template DNA	1 ng	1	1 ng/µl
distilled H_2O	to 25 µl		

Table 3.2 *PCR conditions*

Temp. (°C)	Time	
95	30”	
95	10”	
60	30”	18 cycles
72	4’	
72	5’	
4	hold	

PCR extension time was reduced to 3 minutes for multi-site or multi-fragment procedures, as the longest individual fragment was significantly shorter in such cases than in the majority of standard procedures. After PCR, all samples were separated by gel electrophoresis on a 1 % agarose gel, stained with SYBR®Safe in a Mini-Sub® Cell GT Cell tank (Bio-Rad; 1704406) coupled to a PowerPac™ power supply (Bio-Rad; 1645050). DNA products were visualised and quantified using a ChemiDoc™ XRS+ Imaging System (Bio-Rad; 1708265)

and fragment molecular weights were measured by comparison to a 1 kb Plus DNA Ladder (Invitrogen; 10787018). FastDigest Green Buffer (ThermoFisher Scientific; B72) was used as loading dye for all samples. After gel analysis to confirm successful PCR amplification, 1 µl of FastDigest *Dpn*I (ThermoFisher Scientific; FD1703) was added to PCR reactions (without PCR purification) and samples were incubated at 37 °C for 15 min. QIAquick PCR Purification kit (QIAGEN; 28106) or QIAquick Gel Extraction kit (QIAGEN; 28706) were used for DNA isolation from PCR reactions or agarose gels (only when stated), according to manufacturer instructions. PCRs using alternative DNA polymerases, KOD Hot Start Polymerase® (Merck Millipore; 71086), *Pfu Turbo* DNA Polymerase (Agilent; 600250) or Taq DNA Polymerase (Invitrogen; 10342020) were run in manufacturer buffers, using template, nucleotide and primer concentrations described previously, and according to the previously described cycling protocol.

Transformation

Transformation was performed by heat-shock as follows: 15 min incubation of DNA with bacteria on ice (< 4 °C), 30 s at 42 °C in a water bath, 2 min incubation on ice, before addition of 200 µl Super Optimal Broth with Catabolite repression medium (SOC, VWR; 100894-916) and recovery at 37 °C for 45 min. The entire volume was spread on Lysogeny Broth (LB)-agar plates with appropriate antibiotics (Kanamycin or Ampicillin at 50 or 100 $\mu g\,ml^{-1}$ respectively) overnight at 37 °C. Colonies were counted manually when appropriate and are reported throughout as the number of Colony-Forming Units per plate (CFU/plate). For propagation of plasmid DNA, individual colonies were picked using a pipette tip and grown overnight in LB at 37 °C with appropriate antibiotics. QIAspin Miniprep kit (QIAGEN; 27106) was used for plasmid isolation from bacteria. LB consists of (all w/v); 1 % tryptone, 0.5 % yeast extract, 1 % NaCl at pH 7.5. LB-agar consists of LB with 1.5 % (w/v) agar.

Transformation efficiency of homemade competent cells was assessed as follows. pUC18 plasmid was diluted to 1 $ng\,\mu l^{-1}$ and 1 µl was transformed into 100 µl cells by heat shock (as above). After heat shock, 900 µl SOC was added to cells before 45 min incubation at 37 °C. 100 µl of a 1:1, 1:10 and 1:100 dilution of transformant were spread on LB-agar plates with ampicillin (resistance gene conferred by pUC18 plasmid) and incubated overnight at 37 °C. Transformation efficiency was calculated from the number of colonies formed.

Plasmid Screening: Restriction analysis and Sanger Sequencing

Where appropriate, new DNA constructs were screened by restriction digestion. Appropriate restriction enzyme combinations were selected using SnapGene® to produce unique DNA fragment patterns between template and desired product plasmids. 10 µl digestions were performed using 1 µg plasmid DNA in 1X FastDigest Green buffer with appropriate FastDigest enzymes (ThermoFisher Scientific) at 37 °C. DNA samples were separated by agarose gel electrophoresis for analysis, and 'correct' plasmids were subject to Sanger sequencing before use. Sanger sequencing was performed by GENEWIZ (formerly Beckman Coulter Genomics).

Mutagenesis time-courses

Mutagenesis time courses were performed in multiple 50 µl reactions with 5 ng of DNA template for improved signal at early time points. Whole reactions were removed from the thermocycler every 2 cycles.

3.3 Results

3.3.1 Method Overview

IVA cloning uses *in vivo* assembly of PCR amplified DNA fragments, guided by short homologous flanking regions that are fused together by recombination. All cloning procedures for single or multi-site modifications proceed through a single-step PCR, template DNA digestion with *Dpn*I (an endonuclease specific for methylated DNA) and transformation (Figure 3.1). As outlined in Figure 1, all DNA modifications and homologous regions are introduced at the 5' end of the primers. Insertions (of short sequences that can be included within the primers), deletions and site-directed mutagenesis proceed through inverted PCR with primers binding astride the modification site (Figure 3.1). For insertions, it is cost-optimal to include the extra sequence in the overlapping regions of both Forward (Fw, 5'-3') and Reverse (Rv, 3'-5') primers, acting as the homologous region (Figure 3.1A). Deletions require inverted primers flanking the undesired region, amplifying outwardly, with the Fw primer containing a region homologous to the Rv primer. Similarly, mutation primers flank the undesired codon, with the new sequence encoded in the Fw primer. Sub-cloning uses PCR of the vector at the location for insertion, while the insert is amplified independently in the same tube, with homologous regions at both linear ends (Figure 3.1B). These regions may be included in either the vector or the insert primers. Due to the inverted nature of the primer design, multiple modifications can be performed, simply by combining primers for single modifications in the same PCR tube (described in detail below). Hence, any combination of plasmid modifications may be performed using the same protocol and primers as for single-site protocols.

3.3.2 Optimisation of PCR conditions

The efficiency of a cloning method can be quantified by two parameters: a) the number of colonies produced on transformation, and b) the percentage of those colonies that contain the desired DNA product. While greater amounts of template DNA in the PCR will produce exponentially more of the desired product, this will also lead to a greater likelihood of 'false positive' colony formation, from undigested template DNA. To determine the maximum amount of template DNA that can be used while producing minimal false positive colonies, PCR was performed using primers designed with no homologous overlaps. In this way, no 'true positive' CFUs could be formed and all colones produced represent false positives. Independent PCRs were set up, containing increasing levels of template DNA (0 - 50 ng)

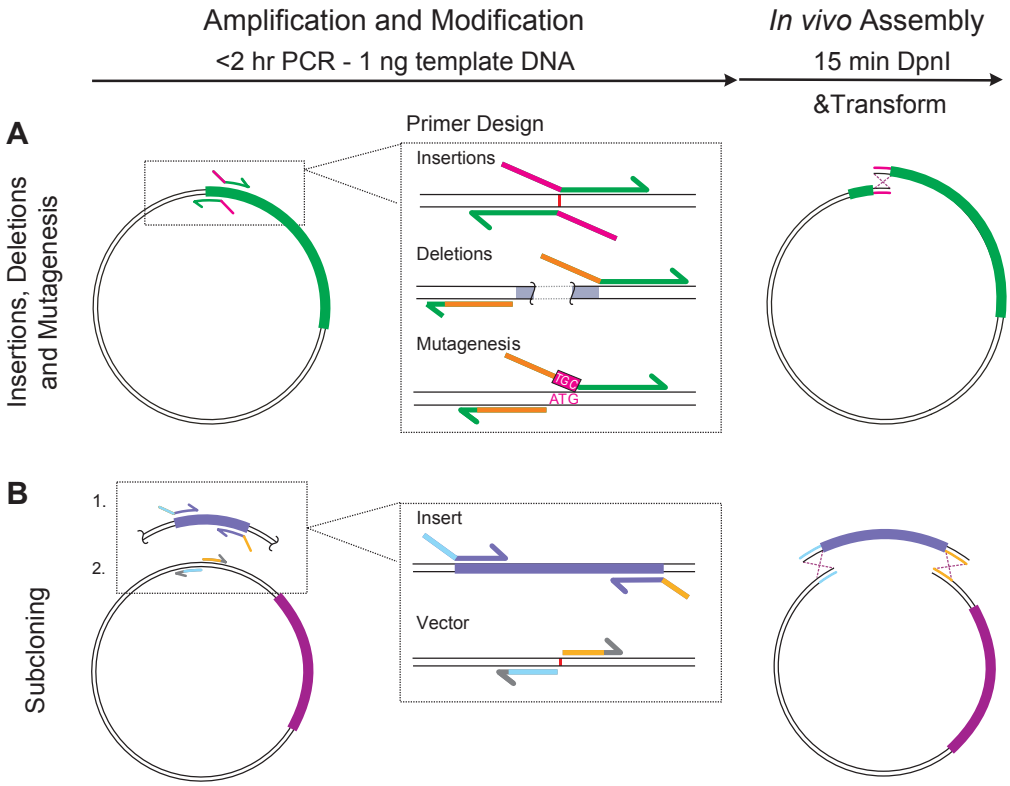

Figure 3.1 *IVA Cloning Method Overview.*
*Schematic of the universal IVA cloning protocol consisting of a single PCR reaction, producing homologous linear ends, followed by DpnI digestion and transformation, where amplified DNA is assembled in vivo by recombination. Primer design is shown for each type of basic modification: insertion, deletions, site-directed mutagenesis and sub-cloning. (**A**) For insertions, the new sequence is best included in Fw and Rv primers, acting as the homologous region (magenta). For deletions, the overlap can be incorporated in any one primer, homologous to the other primer (orange) with primers straddling the undesired region (grey). Mutagenesis is similarly performed, inversely amplifying outside the undesired codon (ATG), with the replacement encoded in the forward primer (TGC). (**B**) Sub-cloning involves the amplification of both vector and insert in a single tube with homologous regions to directionally control assembly (blue and yellow).*

and run using a standard 18 cycle PCR protocol (Figure 3.2A1). After PCR, reactions were digested for 15 min at 37 °C before transformation into commercial XL-10 bacteria and plating on ampicillin resistant LB-agar plates. The number of CFUs per plate correlated with the amount of template DNA, but not with the level of amplification (see 50 ng point), indicating that colonies are produced from template DNA and not the PCR product (Figure 3.2A2). This was confirmed by restriction analysis and Sanger sequencing of plasmid DNA from a subset of colonies. Multiple colonies were produced from PCRs containing 10 and 50 ng of template DNA, while none were observed when using 1 ng. For this reason, all subsequent PCRs were performed using 1 ng template DNA.

3.3.3 Optimisation of primer properties for RAIR

The future potential of the *recA*-independent recombination (RAIR) pathway for use as a cloning method is strongly dependent on the efficiency of recombination. Aside from an apparent correlation between the length of the homologous overlap between linear DNA ends (Beyer et al., 2015; Jacobus and Gross, 2015), there is little known about the mechanism or requirements for RAIR. To maximise the level of recombination, the effect of both the length and melting temperature (T_m) of homologous regions on RAIR efficiency was investigated.

For both assessments, cloning procedures were performed using primers designed for deletion of the GluA3 NTD coding region in the pRK5 vector. To assess the length dependence of recombination, homologous regions were engineered to range from 10 to 25 bp, all with an equal T_m of 40 °C. This was achieved by varying the GC-content, as guanine/ cytosine pairing confers a higher T_m on the DNA region than adenine/ thymine pairing. For example, the sequence of 10 bp homologous regions was 'CGCCCGGCGG', while that of 25 bp sequences was 'ATTATAATATTTACTATATATTATT'. In every case, the template binding region of the primers remained unchanged. The homologous region had no effect on PCR amplification, as all primers gave similar amounts of PCR product (Figure 3.2B1). The number of colonies produced increased to 15 bp, but plateaued at greater lengths (Figure 3.2B2). A subset of colonies was analysed by restriction analysis and Sanger sequencing and 100 % contained the correctly assembled product.

Analysis of the effect of binding strength was achieved using homologous regions of a constant 15 bp length, and T_m of 20 to 53 °C. Variations were similarly achieved by alterating GC content (sequence of 20 °C homologous region was 'ATTATTAATTATTTA' and

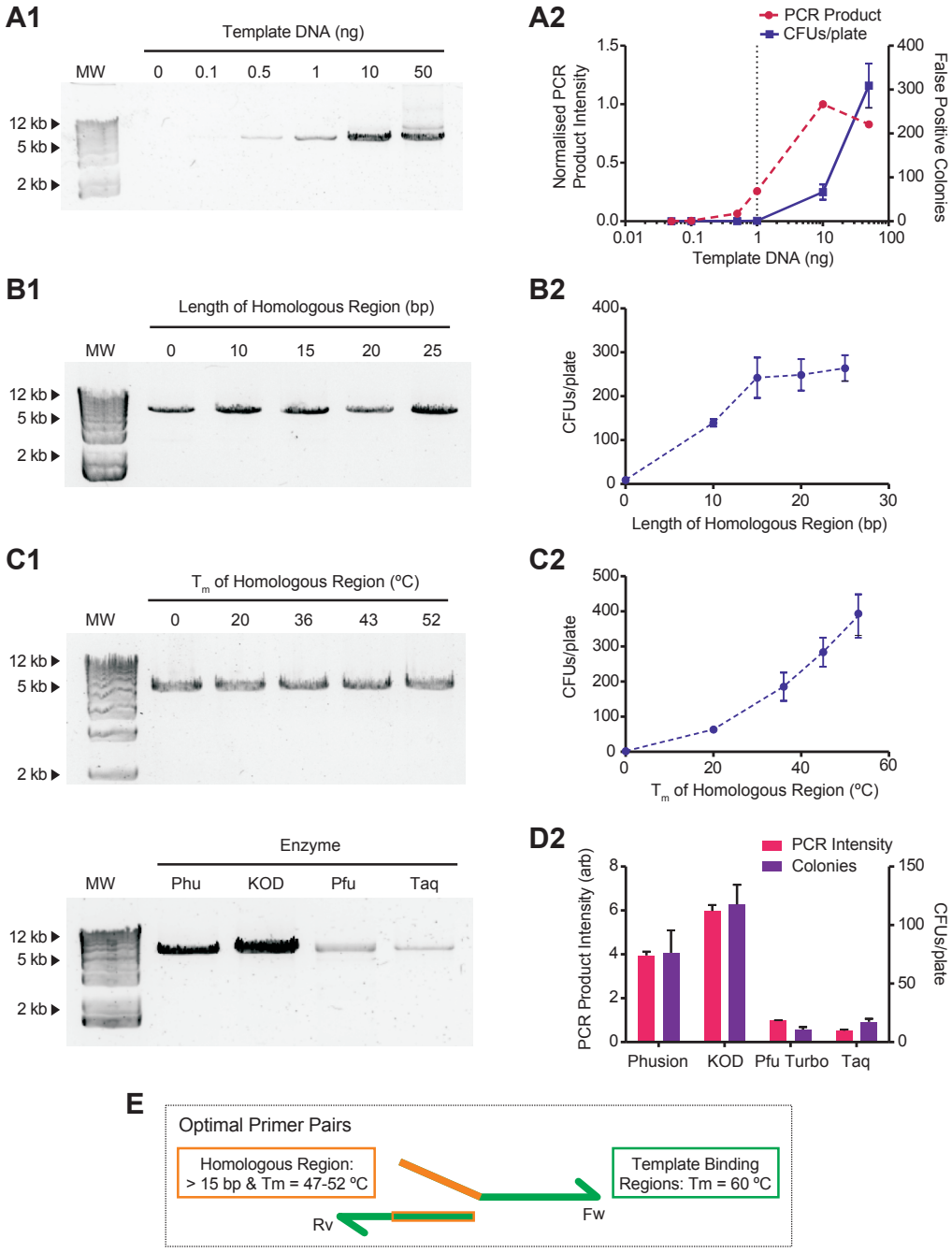

Figure 3.2 *IVA Cloning Optimisation.*

Figure 3.2 *(**A**) Performing PCR with no homologous regions (agarose gel displaying amplification - **A1**) highlights potential false positives arising from template DNA. Increasing template DNA increases the number of colonies produced on transformation (**A2**) (■ purple), independent of PCR amplification (● magenta). 1 ng regularly produces 0 colonies, yet gives substantial PCR amplification (dashed line). (**B**) Relationship between increasing length of homologous regions (constant Tm) and colony yield shows little length dependence of recombination above 15 bp (**B2**). Agarose gel displaying amplification - **B1**. (**C**) Increasing the Tm of homologous regions increases the colony yield and hence recombination efficiency (**C2**) despite no effect on PCR amplification efficiency (**C1**). (**D**) Bar chart indicates that IVA cloning colony yield (purple) is reliant on amount of PCR product (magenta) independent of the type of PCR polymerase (**D2**). Agarose gel depicting PCR amplification is displayed in **D1**. (**E**) Properties of optimum primer design to maximise recombination efficiency. Homologous regions are included in 5'-end of primers, homologous to a region (orange) of the partner primer. Template binding regions are shown in green.*

53 °C region was 'GGCGTCAGCGCGGTC'). Increasing binding strength correlated with greater levels of recombination (more CFUs/ plate) (Figure 3.2C2), while no differences in amplification level were observed (Figure 3.2C1). Together this data demonstrates that RAIR efficiency is dependent on the strength of homologous region DNA dimerisation, when lengths of at least 15 bp are used. Similarly to the previous analysis, 100 % of analysed colonies contained the desired product.

Previous reports have suggested that the RAIR pathway requires PCR amplification using polymerases with proofreading capabilities (Klock et al., 2008; Li et al., 2011). Enzymes with such proofreading capability have 3' to 5' exonuclease ability, which in the presence of dNTPs, allows removal and replacement of incorrectly paired bases (Ganai and Johansson, 2016). It has been suggested that during the final cycles of PCR, when dNTP concentrations are low, enzymatic activity favours base pair removal by 3' to 5' activity, leaving single-stranded linear 'sticky ends' to DNA products (Jacobus and Gross, 2015; Klock et al., 2008). DNA assembly apparently occurs through annealing of the engineered homologous regions, producing a double stranded plasmid which is repaired *in vivo* after transformation. In order to test this model and investigate the mechanism of RAIR, the polymerase requirements for recombination were studied. GluA3 NTD deletion was again performed, according to manufacturers instructions, using four commercial DNA polymerases: Phusion (NEB), KOD

(Merck), *Pfu Turbo* (Agilent) and *Taq* (Invitrogen). Phusion, KOD and *Pfu Turbo* are all proofreading enzymes, while *Taq* does not possess the 3' to 5' exonuclease activity that is essential for proofreading capabilities. All enzymes successfully produced the 6.2 kbp product, however to vastly different levels due to their differing processivities (Figure 3.2D1). All reactions were subject to *Dpn*I digestion and transformed as usual. Despite lacking 3' to 5' exonuclease activity, *Taq* amplified DNA still successfully produced colonies, of which a subset were screened with 100 % confirmed as the desired product. While PCR efficiency differed between enzymes, the number of colonies produced correlated well with the level of amplification (Figure 3.2D2). Coupled with the successful cloning using *Taq* polymerase, this evidence suggests that cloning efficiency is independent of specific enzyme activity, and is mainly dependent on the amount of DNA produced by the PCR. An important factor to consider when selecting a polymerase for this method is its fidelity. Despite the greatest level of PCR amplification being achieved using KOD polymerase, the fidelity of Phusion is approximately 7.5 times greater (McInerney et al., 2014). For this reason, Phusion polymerase was used for all future experiments during the development of IVA cloning. As a result of this optimisation, the recommended primer properties for IVA Cloning are template binding strengths of 60 °C, and homologous region strength of 47-52 °C (Figure 3.2E).

3.3.4 Basic cloning procedures

Insertions and Deletions

Insertion or deletion of DNA sequences is a regularly required cloning procedure, and an essential component of the molecular cloning toolkit. Currently the most widespread method for such procedures uses PCR amplification with phosphorylated primers. Using such an approach, primers are designed to be 'inverted' such that they bind in close proximity on the DNA sequence, yet direct amplification away from each other, such that the majority of the vector sequence undergoes PCR amplification (in a similar manner to Figure 3.1A). Small sequences of DNA can be inserted into a plasmid by inverted amplification using primers binding at the site of desired modification, and including the new sequence at the 5' end of the primers. A large PCR product is formed, consisting of the desired final plasmid in linear form. As primer sequences may be purchased with 5' phosphorylations, the linear product will contain these phosphorylations, so can be ligated back to a circular product using T4 ligase, after purification of the PCR product. Deletion of DNA sequences can be produced in a similar manner by designing inverted primers to anneal to the template DNA flanking the region that requires removal. In such an approach, the entire plasmid

will be amplified to produce a linear product that can be ligated to circular DNA, excluding the deleted region. While this method is efficient and widespread, it requires multiple *in vitro* steps, PCR purification and ligation, prior to transformation and also the use of costly phosphorylated primers.

IVA cloning can be applied to insertions and deletions using an inverted primer design, as per the previously described method, however by encoding a homologous region in primer 5' ends. The requirement for phosphorylated primers, PCR purification and DNA ligation can be all be avoided, as the linear product of PCR can be assembled *in vivo*. For insertions, the homologous region can be incorporated by inclusion of the desired insert into both forward and reverse primers, while deletions can be achieved by including a short sequence in the forward primer which corresponds to the template binding region of the reverse primer (Figure: 3.1). Currently, primers can be cheaply synthesised up to around 110 bp in length. This approach facilitates insertion of up to 120-140 bp of new DNA sequence (using two 100 bp primers, and accounting for 20-30 bp of template binding region per primer and 20 bp overlapping homology). For deletions, as the length of the deleted region is independent of primer length, instead relying on primer annealing position, any length of DNA sequence can be deleted. In many cases, small DNA sequences require replacement, for example replacement of one epitope tag with another, or an interdomain linker with a cleavage site. In such cases the primer design for insertions and deletions can be combined to perform a replacement in one action (Figure 3.3A).

The feasibility of performing such modifications was demonstrated using the following examples: 1) insertion of a c-myc tag in the pRK5-GluA3 plasmid (30 bp) (INS1 primers), 2) deletion of a c-myc tag in the pIRES2-EGFP-GluA2 plasmid (30 bp) (DEL1 primers), 3) deletion of the N-terminal domain coding region of GluA3 in the pRK5-GluA3 vector (1140 bp) (DEL2 primers) and 4) replacement of the IRES cassette (587 bp) with a linker sequence (15 bp) in the pIRES2-EGFP-GluA2 plasmid, which would then produce a fusion protein, rather than coexpressed products (DELINS1 primers) (Figure 3.3A). As a comparison, phosphorylated primer design was also used for amplification of example 1) (c-myc insertion in GluA3). No difference in PCR amplification efficiency was seen between phosphorylated primer and IVA cloning primer designs for this example (Figure 3.3B), indicating that inclusion of the homologous region in IVA primers does not interfere with primer-template binding, as anticipated by designing the homologous region to anneal at a lower T_m than the template binding region. All IVA cloning procedures were subject

to DpnI digestion before transformation into XL10 Gold *E. coli* produced in house, which have a transformation efficiency of 10^6 CFU/μg of pUC18. Significant numbers of colonies were produced for in all cases, indicating successful recombination *in vivo*. 5-10 colonies per plate were grown up overnight in 3 ml of LB, mini-prepped using the Qiagen Miniprep kit, and Sanger sequenced to confirm successful modification. 100 % of colonies in every case contained the correctly modified product (Figure 3.3B).

Site-directed Mutagenesis

Mutagenesis involves the replacement of a few base pairs with desired alternatives, with widespread use in molecular biology to study protein function. The ability to selectively alter individual amino-acid residues allows fine study of protein function. While there are a variety of current methods (Mccullum et al., 2002), the commercial QuikChange™ Mutagenesis kit is the most widely used. This approach involves amplifying the whole plasmid from the site of modification, using fully overlapping primers which encode the desired modification (Figure 3.3C). According to the manufacturers information, QuikChange™ mutagenesis proceeds through linear PCR amplification, as the overlapping primer design does not give rise to a DNA product that can be used for future amplification rounds. Thus all products are amplified directly from the original DNA template. PCR amplification produces 'nicked circular products', which can be repaired upon transformation, after *Dpn*I digestion.

Due to the nature of primer design, the formation of primer-dimers is more favourable than primer-template binding, thus limiting the efficiency of PCR amplification, and producing a population of incorrect clones (80 % correct clones, Bommarius and Riebel, 2004). These incorrect clones consist of template DNA, as 5-50 ng parent DNA is required for PCR due to poor amplification efficiency, or undesired plasmid modifications due to primer-dimer formation, such as introduction of base-pair repeats. Several studies have now demonstrated that the efficiency of amplification can be improved substantially by displacing the primer binding sites on the template DNA, thus decreasing the primer-primer binding strength, while maintaining primer-template binding (Xia et al., 2015; Zheng et al., 2004). As previously described, IVA cloning primer design eliminates primer-dimers by designing the melting temperature of template binding regions to be 8-13 °C greater than that of homologous regions for recombination. In comparison to QuikChange™ IVA cloning primers can be considered to be 'fully displaced', with the modified base pairs outside the template binding region (Figure 3.3C). Using this approach, both primer-dimers and mispriming can be fully avoided.

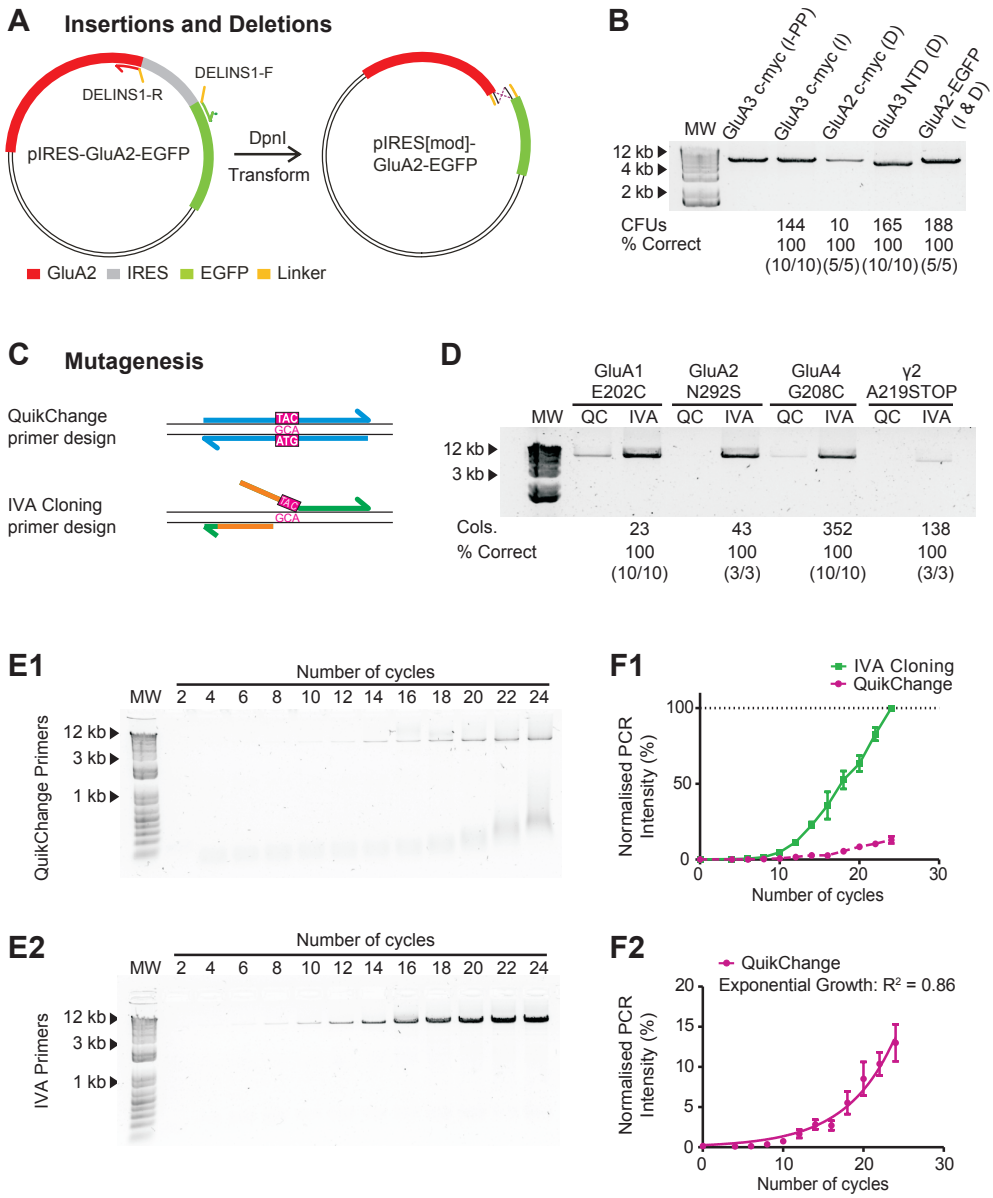

Figure 3.3 *Simple Modifications using IVA Cloning*

Figure 3.3 *(**A**) Schematic depicting the simultaneous deletion of an IRES cassette (grey) and insertion of a linker sequence (yellow) in the GluA2-pIRES-EGFP vector. (**B**) Agarose gel showing the resulting amplification of insertions (I) and deletions (D). These include (Lane 2) insertion of a myc-tag at the N-terminus of GluA3 using phosphorylated primers (PP), and (Lane 3) IVA primers, (Lane 4) deletion of an N-terminal myc-tag in GluA2, (Lane 5) deletion of the N-terminal domain of GluA3 and (Lane 6) construction of a fusion GluA2-EGFP tandem construct by replacing the IRES cassette with a linker. Number of colonies produced on transformation, and the percentage of colonies tested that contain the correct plasmid are shown below. (**C**) A comparison of primer design for mutagenesis using QuikChange™ (upper - blue) and IVA (lower - green). (**D**) Agarose gel of PCR products providing a comparison between IVA and QuikChange™ mutagenesis primers. An enhancement of the intensity is seen for IVA primers in all cases. Number of colonies and percentage of correct clones for IVA cloning are shown below. (**E**) Comparison of IVA (**E2**) and QuikChange™ (**E1**) amplification rates by examining band intensity every two PCR cycles for the GluA4 G208C mutation over 24 cycles . Higher intensity and no low molecular weight smearing are seen using IVA primers. (MW = 1 kb Plus Ladder). (**F1**) Cycle-by-cycle comparison of the PCR product formation from E (IVA - ■ green; QuikChange™ - ● magenta; normalised to maximum value as 100 %, n = 3). The increased PCR yield of IVA is appreciable. (**F2**) When plotting intensity against cycle number, an exponential curve can be fitted (R^2 = 0.86) when using QuikChange™ mutagenesis primers (normalised to IVA cloning).*

To demonstrate the utility of IVA cloning for site-directed mutagenesis, four modifications were performed using both QuikChange™ and IVA primer design approaches. Protein coding genes were mutated as follows: pIRES2-mCherry-GluA1; GluA1 E202C, pIRES2-EGFP-GluA2; GluA2 N292S, pRK5-GluA4; GluA4 G208C, pGW1-TARP γ2; TARP γ2 A219Stop (Primers MUT1-4 for IVA and MUT5-9 for QuikChange™). Both IVA and QuikChange™ PCRs used 1 ng of template DNA, and samples were simultaneously separated by agarose gel electrophoresis to allow comparisons of amplification efficiency after PCR. IVA primer design consistently yielded greater product DNA (Figure 3.3D), seen for all mutagenesis primer pairs. Upon transformation, all IVA mutations produced substantial numbers of colonies, and all of those sampled (5 per mutation) contained the desired product DNA (Figure 3.3D).

As it has been suggested that QuikChange™ DNA amplification is linear, simultaneous PCRs were run using QuikChange™ and IVA primers (GluA4 E208C mutation) for increasing numbers of amplification cycles (4-24) to quantify the increase in product formation. QuikChange™ primers clearly show smearing at low molecular weights, indicative of mispriming or abhorrent DNA product formation due to primer-dimer formation (Figure 3.3E1). This smearing is absent when using IVA primer design (Figure 3.3E2). Interestingly, quantification of product formation shows that while QuikChange™ amplification is substantially lower than IVA (Figure 3.3F1), amplification proceeds exponentially (Figure 3.3F2), raising questions over the true mechanism of the method as suggested by the manufacturer.

Subcloning

Subcloning is one of the most widely required plasmid modifications. While this would historically have been performed using restriction enzymes, the current most favourable methods are homology based, such as Gibson Assembly (Gibson et al., 2009) or In-Fusion cloning (Sleight et al., 2010). The common procedure for these approaches is as follows: separate PCR amplifications of insert and vector, DNA purification, *in vitro* enzymatic assembly and finally transformation. While primer design requirements for such methods are almost identical to IVA cloning, using the IVA approach can substantially reduce the procedure duration. Both vector and insert are amplified in a single PCR tube, and both DNA purification and *in vitro* enzymatic assembly are eliminated.

Subcloning using IVA was demonstrated using two examples: subcloning the GSG1L

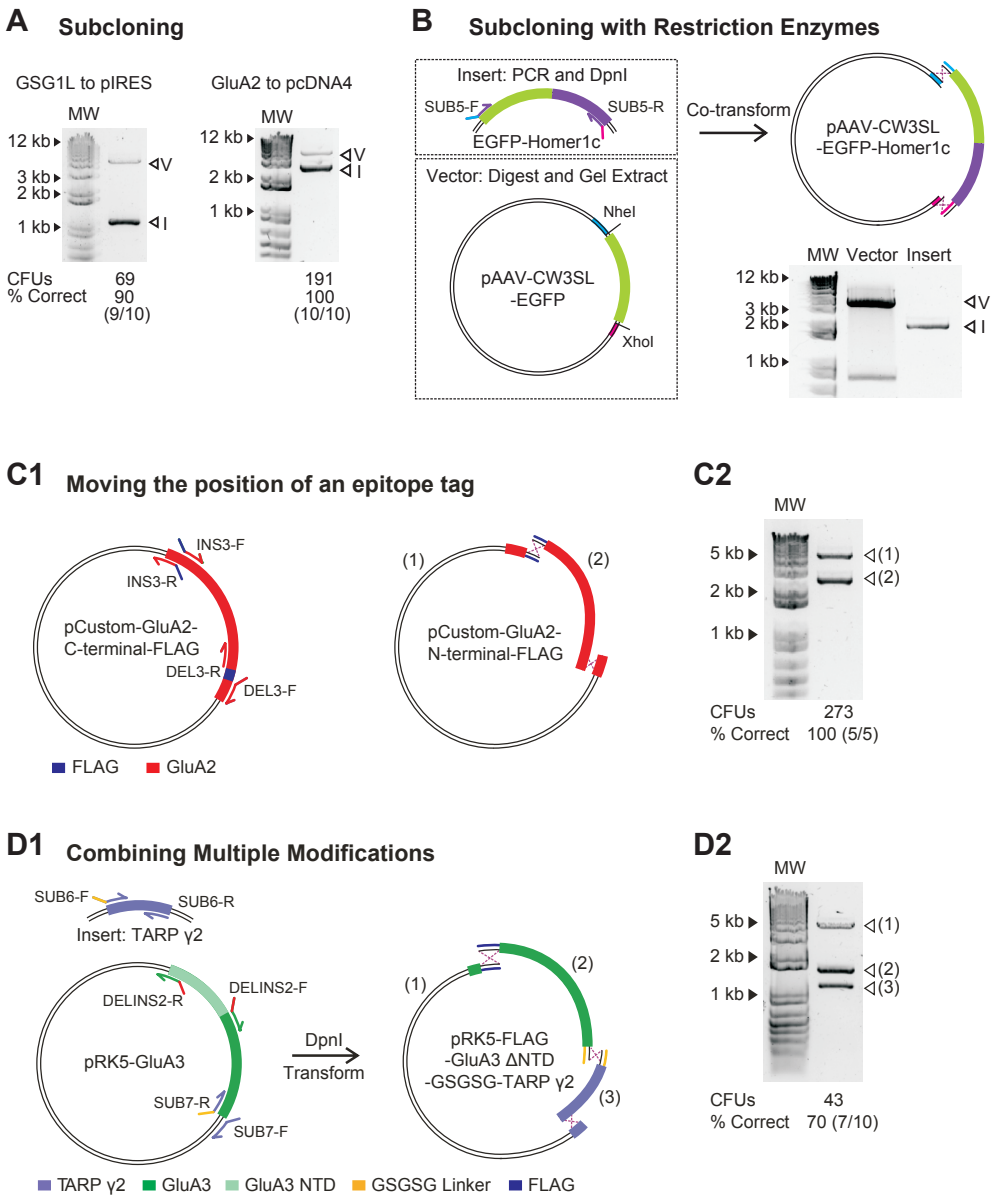

Figure 3.4 *Subcloning and Multi-site Modifications*

Figure 3.4 *(**A**) Agarose gel electrophoresis visualisation of PCR products for sub-cloning examples (GSG1L coding region into pIRES-mCherry and GluA2 coding region into pcDNA4.1/TO) each showing two independent amplifications (Vector: V, Insert: I). Colony yields and percentage correct are shown below. (**B**) Alternative strategy for vectors not amenable to amplification, shown with the cloning of EGFP-Homer1c (Insert), subject to PCR, DpnI treatment and PCR purification, into the adeno-associated virus vector pAAV-CW3SL-EGFP (cut with NheI and XhoI, and gel purified. Agarose gel visualisation of vector post-digestion identifies gel purified fragment (V) alongside PCR amplified Insert (I). (**C1**) Schematic for multi-site modification whereby the position of a FLAG-tag (purple) is exchanged from the C- to the N-terminus of GluA2 (red) coding region in a CMV-based custom plasmid. The combination of deletion and insertion primers produces two amplification products after PCR. (**C2**) The corresponding fragments (1 and 2) are visualised by agarose gel electrophoresis. (**D1**) Schematic detailing multiple plasmid modification of GluA3-pRK5 vector in one tube. One set of primers a) deleted the N-terminal domain of GluA3 and b) inserted a FLAG-tag, while a second set of primers a) sub-cloned the TARP γ2 coding region (from a second vector) at the end of GluA3 and b) inserted a GSGSG linker to create a fusion construct. Together, these primers amplify three independent fragments, which are shown on an agarose gel (**D2**).*

coding region into the pIRES2-mCherry vector, and subcloning the GluA2 coding region from the pIRES2 vector into the pcDNA4/TO vector (SUB1/2 and 3/4 primers respectively). Designing primers such that the homologous regions are included in the insert primers, vector primers or both is of no consequence to the final assembly, on the condition that the final linear DNA products have a homologous region of 47-52 °C T_m. In both examples, homologous regions were added to the insert primers (SUB1-2). Both PCR amplifications showed two distinct products (Figure 3.4A), corresponding to the desired insert and vector, and 90-100 % of colonies produced contained the desired product. This example not only demonstrates the applicability of IVA cloning for subcloning, but also first demonstrates that the recombination pathway utilised by this method is able to recombine not only linear ends of a single DNA fragment, but homologous ends of two separate fragments in a specific and directional manner.

One pitfall of IVA cloning arises when the template DNA required for subcloning cannot be amplified by PCR. Very large destination vectors, such as Bacterial Artificial Chromosomes, which can be greater than 100 kb in size (Monaco and Larin, 1994), are beyond the amplification limit of current polymerases, while vectors containing regions of high GC content or multiple repetitions, such as adeno-associated virus (AAV) vectors, cannot be be processed by polymerases and so also cannot be amplified by PCR. While in many instances high GC content can be overcome by PCR additives such as DMSO, betaine, 1,2-propanediol or ethylene glycol (Chen et al., 2002; Henke et al., 1997; Sabzghabaee et al., 2014), there will be instances when the standard IVA approach of vector amplification is unusable. In such instances, an alternative approach utilising restriction enzymes for vector linearisation can be employed.

To subclone a gene from one vector to an unamplifiable destination vector, the destination vector can be linearised at the desired insertion point by either one, or two restriction digestions. By introducing regions homologous to the linear ends of the destination vector, post-restriction, the two fragments can be assembled *in vivo* as per previous examples. To test this approach, EGFP-Homer1c (kindly provided by Dr Andrew Penn, U. Sussex) was subcloned into the pAAV-CW3SL-EGFP vector (kindly provided by Professor Bong-Kiun Kaang, Seoul), which cannot be amplified by PCR due to the AAV ITRs (inverted terminal repeats) (Figure 3.4B). The vector was digested using *Nhe*I and *Xho*I, separated by gel electrophoresis, purified and co-transformed with the insert, which was amplified by PCR to introduce regions homologous to the linear ends of the destination vector (SUB5 primers). 55

colonies were produced, with 60 % containing the desired product (12/20 colonies) (Figure 3.4B). Interestingly, transformation of the vector alone produced 25 colonies. As two ITRs are present in the vector, which have a high GC content, and therefore a high binding strength, recombination between these sites can occur to product a false positive circular product, lacking the insert. This is most likely the cause of the decreased method efficiency when compared to the standard PCR-based IVA cloning strategy previously described.

3.3.5 Multi-site modifications

Often the final plasmid required from a cloning strategy does not simply require a single modification from the original template, but multiple modifications. Therefore a universal cloning strategy requires the ability to easily combine and perform modifications simultaneously. The current best methods for insertion, deletion and mutagenesis are not compatible with simultaneous use: a QuikChange™ mutagenesis cannot be combined with an insertion using phosphorylated primers due to their different assembly mechanisms. While all modifications can in theory be performed by homology-based methods such as Gibson Assembly or LIC, the use of such methods for single modifications such as mutations is more expensive and complicated than the alternatives. Current strategies for performing multiple modifications are laborious and time consuming, involving multiple rounds of individual modifications. Mainly, protocols for multi-mutagenesis have been reported (Kim and Maas, 2000; Luo et al., 2012; Mitchell et al., 2013; Sawano and Miyawaki, 2000; Wei et al., 2012), which involve multiple steps, expensive primers, or both.

A common feature of primer design for all modifications using IVA cloning is their inverted nature. The significance of this is that pairs of primers used to perform different modifications can be used either individually, or in the same PCR reaction to simultaneously perform multiple different modifications. For example, when performing both an insertion and a mutation, the forward primer of one modification will amplify a DNA fragment with the reverse of the second modification, with the corresponding reverse and forward primers working similarly. Two fragments would be produced from the PCR, with overlapping homologous linear ends, which can drive assembly upon transformation. In this manner, and primer pair designed for a single modification can be reused in combination with another.

Given that insert DNA can be cloned from one vector to another (subcloning), the RAIR pathway is able recombine two separate DNA fragments. Combining two simple modifica-

tions, such as an insertion and a deletion, is theoretically equally simple. To demonstrate this possibility, the position of a c-myc epitope tag was moved within the GluA2 gene in a custom vector (pCustom). Originally encoded at the C-terminus of GluA2, primers to delete it from this position were simultaneously used in one PCR with those to insert the tag at the N-terminus of the coding region (INS3 and DEL3 primers) (Figure 3.4C1). Two fragments were produced from the PCR, through inverse primers amplifying with each other (Figure 3.4C2). On transformation, 273 colonies were produced, and 100 % of those sampled (5/5) contained the correctly assembled product.

More complex combinations can similarly be attempted, requiring a greater number of recombination events. To explore these possibilities the construction of a pRK5-FLAG-GluA3 ΔNTD-GSGSG-TARP γ2 was attempted from a single PCR, using pRK5-GluA3 and pGW1-TARP γ2 as template plasmids. The primers included in the reaction mix were designed as follows: 1) to delete the N-terminal domain coding region of GluA3 and simultaneously replace it with a FLAG-tag (DELINS2 primers), 2) to subclone the TARP γ2 coding region after the GluA3 encoding gene, from the pGW1 vector, and inserting a GSGSG linker at the fusion site (SUB6 and 7 primers) (Figure 3.4D1). Three DNA fragments are produced from this PCR, requiring recombination of three homologous regions to produce the intact circular plasmid. Agarose gel electrophoresis after PCR shows the successful production of three DNA fragments, which were co-transformed after *Dpn*I digestion and produced 43 colonies. 10 colonies were analysed by Sanger sequencing and 70 % (7/10) contained the successfully assembled product, demonstrating the effectiveness of the recombination pathway for assembly of more than two DNA fragments (Figure 3.4D2).

The limiting factor controlling the number of possible simultaneous modifications is the efficiency of recombination for multiple linear fragments. To assess the potential of IVA cloning for performing more complex plasmid modifications, recombination efficiency was assessed by combining increasing numbers of mutations on a single plasmid. Primers were designed to incorporate *Xho*I restriction sites in the pRK5-GluA3 vector, which originally does not contain any *Xho*I sites. This modification was chosen, as correct plasmid mutation can easily be assessed by restriction digestion and agarose gel electrophoresis, rather than Sanger sequencing (primers MUT9-13). PCRs were set-up using increasing numbers of primer pairs from 1 to 5 (Figure 3.5A). PCR amplification was unaffected by the number of primers (Figure 3.5B1) with the number of DNA fragments produced corresponding to the number of included primer pairs. All samples were treated with *Dpn*I and transformed

into commercial XL10-Gold bacteria. All reactions were performed 3 times, and averaged data is presented in Figure 3.5B2. All reactions successfully produced colonies and a subset of colonies were mini-prepped and subject to *Xho*I restriction digestion. The number of colonies produced and the percentage of correct colonies both decreased as more mutations were performed, however even 5 simultaneous mutations could be successfully incorporated into the plasmid with 13 % correct colonies. The incorrect clones generally consisted of circular plasmids which have recombined without at least one of the desired fragments. Such assembly must occur independently of the specific homologous sequences at the DNA fragment linear ends. Analysis of the DNA sequences reveals that such 'non-specific' assembly occurs at endogenous regions of lower homology downstream of linear DNA ends.

As 5 mutations could still be successfully combined, a 6th primer pair was incorporated and IVA cloning was performed as previously described. While the number of colonies produced decreased further, following previous trends, the percentage of correct clones increased (63 %). Interestingly, the binding site for the final primer pair was between the ampicillin resistance gene and the origin of replication; both essential for plasmid propagation (Figure 3.5C1). It was hypothesised that the increased % of correct colonies could be due to a 'selection' for highly recombinant bacteria. In cases without this unique primer pair (see Figure 3.5A), non-specific recombination of weakly homologous sequences could produce an undesired, yet circular plasmid which can propagate and provide ampicillin resistance to the host bacteria, this producing a colony. However, when the origin of replication and the ampicillin resistance gene are separated, such non-specific recombination events are less likely to produce a functional plasmid, and therefore correctly assembled plasmids will form a greater proportion of the bacterial colonies. To test this hypothesis, previous mutations were repeated, exchanging one of the primer pairs with the 'sixth pair' (MUT14 primers) (Figure 3.5C1). On transformation, the percentage of correct clones was increased for all combinations (3 mutations: 87 % rose to 92 % correct, 4 mutations: 33 % to 67 %, 5 mutations: 13 % to 75 %) (Figure 3.5C2). Inclusion of such a primer pair in future cloning strategies could be used to decrease the required screening of colonies, and is therefore a useful tool for consideration in protocol design. It is of interest to note that inclusion of a non-mutagenising primer within the AmpR gene has previously been reported to aid cloning efficiency (Howorka and Bayley, 1998; Pasieka et al., 2003).

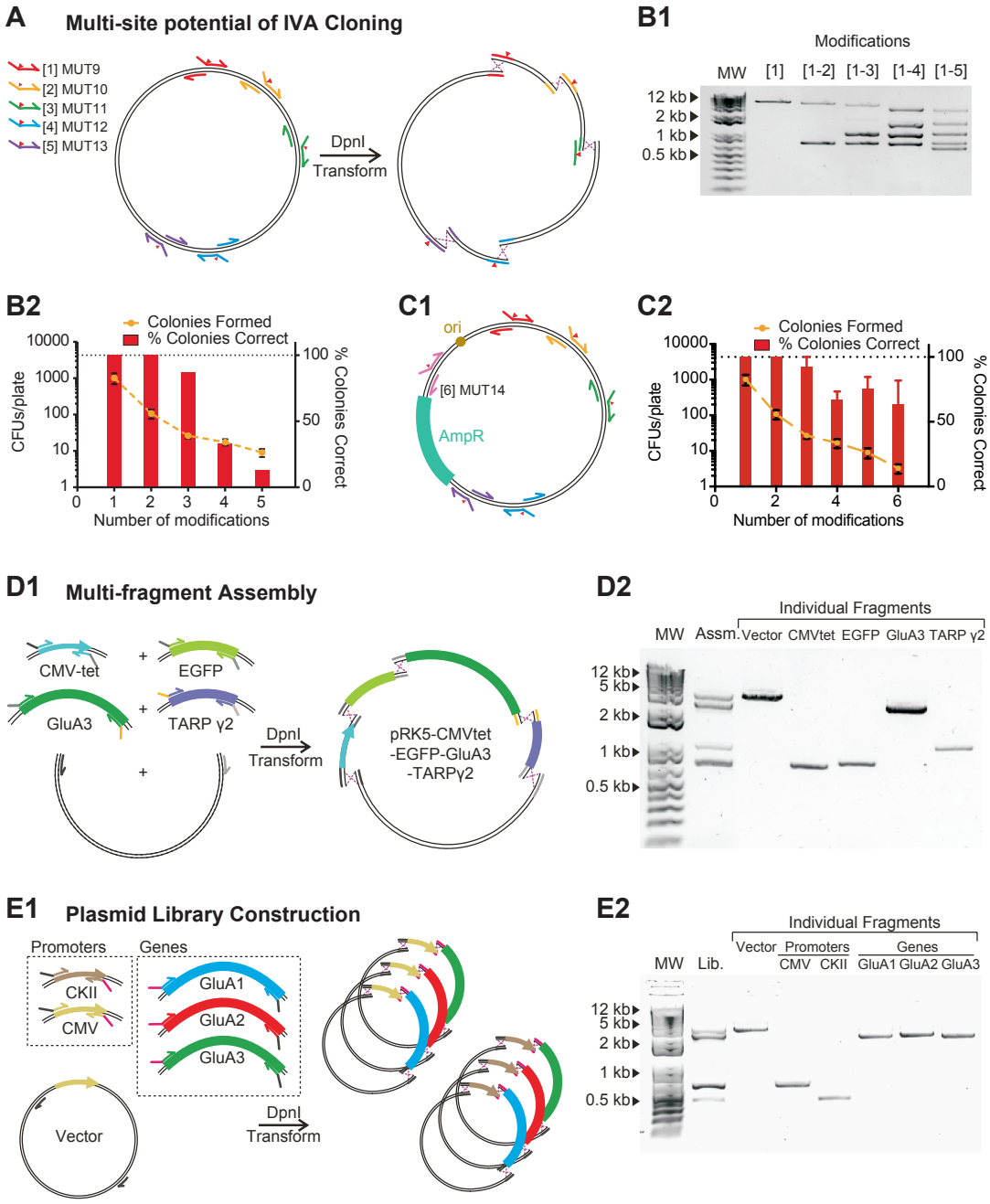

Figure 3.5 *The multi-site potential of IVA Cloning*

Figure 3.5 *(**A**) Testing the number of multiple modifications that IVA cloning can perform simultaneously. Increasing number of XhoI restriction sites were created in the pRK5 plasmid using mutagenesis primers. Site of mutation is indicated by ▼. (**B1**) PCR produced increasing numbers of bands corresponding to the number of modifications (1 to 1-5). (**B2**) The number of colonies produced (yellow) and the percentage of correct clones (red) decreased with more modifications (n = 3-5). (**C1**) Location of sixth mutagenesis primer between origin of replication (ori) and ampicillin resistance gene (AmpR). (**C2**) The number of colonies produced (yellow) and the percentage of correct clones (red) from multi-mutagenesis utilising the sixth primer pair from C1. (**D1**) Schematic of a multi-fragment assembly where five independent fragments (CaMKII, EGFP, GluA3 and TARP γ2 coding regions together with the pRK5 vector) were amplified in one PCR and assembled in vivo. (**D2**) The amplification result is shown by agarose electrophoresis (Lane 2). Individual fragments were independently amplified to facilitate identification (Lanes 3-7). (**E1**) Schematic of mammalian expression library construction. Two promotors (CaMKII and CMV) and three genes (GluA1, GluA2 and GluA3 coding regions) where amplified in a single tube alongside the pRK5 vector. Assembly is guided by specific homologous regions that are shared within promotors and within genes. (**E2**) Agarose electrophoresis resulting from the amplification in a single tube (Lane 2) with individual fragments shown (Lanes 3-8) to aid in the identification.*

3.3.6 Multi-fragment assembly

Given that at least 5 homologous regions can be recombined into a single plasmid, IVA cloning can be used to assemble complex plasmids from multiple templates. To demonstrate this, a new plasmid was assembled to express GFP-tagged GluA3 fused to TARP γ2 under a tetracycline-inducible CMV promoter (CMVtet), in the pRK5 vector backbone (Figure 3.5D1). Five fragments were amplified from separate vectors in one PCR tube, with homologous regions designed to specifically drive the directional assembly of the planned plasmid: CMVtet from pcDNA4/TO, EGFP from pIRES-EGFP, GluA3 from pRK5-GluA3, TARP γ2 from pGW1-TARP γ2 and the vector backbone from pRK5-GluA4 (ASS1-5 primers) (Figure 3.5D2). PCR amplification of individual fragments were performed and separated by agarose gel electrophoresis alongside the assembly to confirm correct PCR amplification (Figure 3.5D2). On transformation and Sanger sequencing, 14 % of colonies (2/14) contained the complete plasmid, in line with efficiencies previously seen for 5 mutations (Figure 3.5B2).

3.3.7 Plasmid library construction

IVA cloning can not only be applied to production of individual custom plasmid, but also for construction of DNA libraries. DNA libraries with randomised sequences are important tools for protein evolution or selection of nucleotide aptamers. The ability to combine multiple different fragments with high efficiency permits construction of plasmid libraries, where many alternative DNA fragments are incorporated. One example of such an application is for optimisation of mammalian protein expression, as currently a case-by-case optimisation of constructs with different vector properties seems to be the most popular strategy to overcome the problem (Almo and Love, 2014; Aricescu et al., 2006a,b; Backliwal et al., 2008). However, the ease of IVA cloning allows simultaneous production of multiple plasmid options, simplifying what could be the limiting factor in such an optimisation.

As a proof of principle for such an application, a small mammalian expression library was constructed by shuffling two promoters (CMV and CaMKII) and three genes (GluA1, 2 and 3) to form 6 product plasmids from a single PCR. Homologous regions were designed to drive assembly of one promoter and one gene with the vector through unique sequences. Both promoters were amplified to introduce the same homologous regions as each other at each end, such that they are equally likely to be incorporated into the final product. The DNA sequence upstream of the promoter was homologous to the linear end of the amplified vector sequence (pRK5) and the downstream region was homologous to that of gene containing

fragments, which in turn contained similar assembly regions to each other (Figure 3.5E1). Amplification of 6 fragments, the pRK5 vector, CMV promoter (both from pRK5-GluA4), CaMKII promoter (from pCaMKII-Homer1c-EGFP), GluA1, 2 and 3 (from pIRES-GluA1, pIRES-GluA2 and pIRES-GluA3 respectively) was performed in a single PCR tube (Figure 3.5E2), subject to *Dpn*I digestion and transformed (LIB1-6 primers). For clarity, individual fragments were amplified separately to aid identification after gel electrophoresis (Figure 3.5E2).

Theoretically, the number of colonies which require screening in order to identify all plasmids from the library, with 95 % confidence, can be calculated as follows:

$$0.95 = 1 - (1 - f)^n$$

where 'f' is the frequency of the least occurring construct and n is the number of colonies required. In this instance, given that 87 % of colonies contain a desired product for three modifications (see Figure 3.5B2) and assuming all six constructs will be equally likely to be formed (1/6 chance), the number of required colonies for screening was 20. In the example described, all six plasmids were identified by screening 15 colonies, highlighting the efficiency and versatility of IVA cloning for a multitude of cloning procedures.

3.4 Discussion

A comparison of methods

The *In Vivo* Assembly cloning method developed and described here is a powerful and universal system, which offers multiple advantages over current alternative methods. By using a single-tube, single-step PCR protocol and elimination of *in vitro* enzymatic assembly and purification steps, IVA offers a streamlined protocol which is substantially faster than alternative methods, with greatly reduced hands-on time. The protocol we describe not only offers time advantages, but also, as there is no reliance on special kits, enzymes or bacteria, is more cost-effective than other widespread cloning methods. To summarise these advantages, the current optimal protocols for each cloning procedure have been compared to IVA cloning in Figure 3.6. The protocol for all individual procedures presented is reduced by at least 45 min, and all purification and assembly kit requirements, except for *Dpn*I are eradicated. For insertions and deletions of small numbers of base pairs, currently using a phosphorylated primer approach would be cheapest and simplest. While the length of IVA primers is slightly increased, by inclusion of a homologous region, overall the cost of primers is substantially reduced by elimination of the requirement for costly 5' phosphorylation modification. As other procedures, such as In-Fusion or Gibson Assembly, also rely on incorporation of homologous regions, primer design is essentially equivalent.

The improvement in protocol duration is particularly significant for complex procedures (Figure 3.6), where lengths are almost halved (IVA: 1h45, Gibson Assembly: 3h15) and hands on time is reduced by approximately 70 %. It is of interest to note that by combining increased number of modifications (for complex procedures), the protocol duration for IVA cloning is actually decreased rather than increased. The major rate-determining-step of PCR is the required extension time, which is proportional to the length in base-pairs of the longest fragment being amplified. By introducing a greater number of modifications, and thus amplifying a greater number of smaller fragments, the PCR duration can be shortened.

Another important asset of the IVA cloning system is its universality. As it is advantageous for all plasmid modifications, IVA cloning can be used for the vast majority of molecular cloning procedures, without the need for other methods. The inverted primer design, which allows primer pairs for single modifications to be combined and used in unison to perform multiple modifications, further favours the use of IVA for both simple and complex procedures, as all primers can be repurposed in multiple combinations, if and when required. This modular and

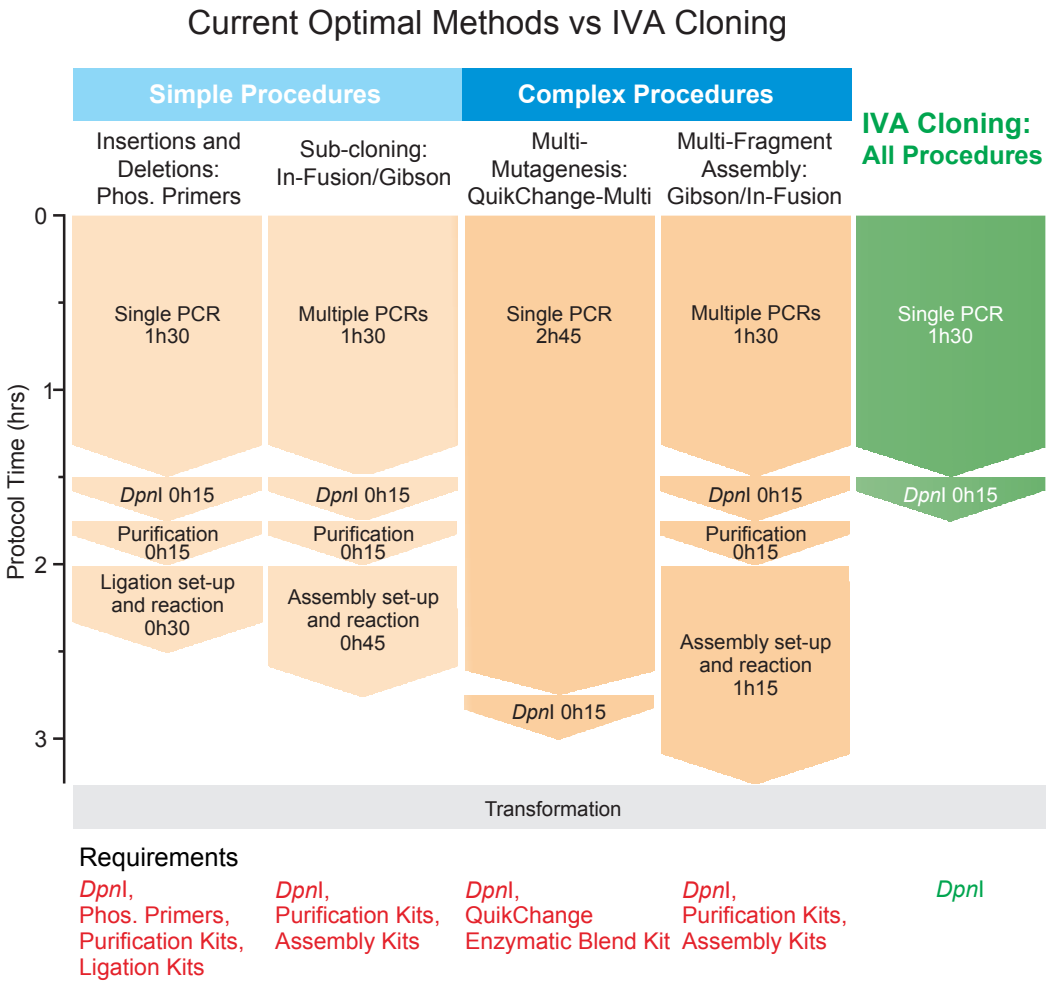

Figure 3.6 ***A Comparison of current cloning methods.*** *Optimal methods for each type of cloning procedure have been selected (orange) for comparison with IVA (green). Labour time and requirements are shown for each example, with the universal IVA protocol significantly outperforming all methods, becoming the best option for all procedures. Of special importance are multisite applications (Complex Procedures), where IVA halves the time required by the next best method and eliminates costs associated with enzymatic assembly and DNA. Furthermore, the IVA multi-site protocol surpasses optimal methods for performing single modifications (Simple Procedures). All protocols require transformation into E. coli (grey). Contrasting with other methods, IVA only requires DpnI (Requirements). (Phos. = phosphorylated).*

versatile nature is unique to IVA, as primer pairs for alternative optimal methods for each procedure are incompatible in combinations. Phosphorylated primers for insertions cannot be used in conjunction with QuikChange™ primers for mutagenesis, or homology-based primers for subcloning. While enzymatic assembly methods such as In-Fusion or Gibson Assembly are also able to perform simple procedures such as insertions or mutagenesis, protocols are substantially longer and more complex than required. Thus by improving protocols for all modifications, IVA offers the first example of a universal method for molecular cloning.

The potential usage of IVA for plasmid library creation has been explored. While a library of just 6 plasmids does not require a simplified approach, the example presented acts a proof of concept. Golden Gate cloning offers a particularly powerful alternative for library formation (Engler et al., 2009, 2008). This approach utilises type II restriction enzymes which cut outside of the recognition site, such as *Bsa*I. Using such enzymes allows the use of restriction enzymes to create a product which lacks the original restriction site, and therefore both restriction and ligation can be performed in a single-step, giving rise to a one-directional reaction (product DNA cannot be restricted and reassembled to the original template). The power of this method is highly dependent on template DNA containing the desired restriction sites in the correct location, and therefore is not advantageous for the majority of everyday cloning procedures, examples of which have been described throughout this IVA method development. However, for plasmid library construction, where high efficiency of multi-fragment assembly is required, Golden Gate cloning is a viable and advantageous technique, and has been used for one-pot construction of shuffled libraries of large pools of plasmid variants (Weber et al., 2011; Werner et al., 2012). A considerable disadvantage of the method is that template DNA fragments for shuffling must be individually cloned into a standardised origin vector prior to library creation. Unless the number of fragments that require assembly is very large, at which point RAIR becomes poorly efficient, producing few colonies (> 4 fragments), IVA cloning offers a simple alternative to be considered for such projects.

Method requirements

For simplicity and speed of the cloning procedure, elimination of all unnecessary DNA purification steps is highly desirable. Purification of PCR products by gel electrophoresis and extraction, prior to transformation has been described in some RAIR cloning protocols (Beyer et al., 2015; Jacobus and Gross, 2015; Martin et al., 1995). While historically this was essential for the separation of PCR products from template DNA, *Dpn*I can now be used to prevent template DNA false positive colonies arising. However, whether the purification

of DNA aids transformation or recombination is unclear, as PCR-clean up (Verheijen et al., 1997), gel extraction (Beyer et al., 2015; Jacobus and Gross, 2015; Martin et al., 1995) and purification-free approaches (García-Nafría et al., 2016b; Li et al., 2011) have all been successfully used but not compared. As the efficiency of IVA cloning demonstrates, purification is not essential, and unlikely to be of significance for simple procedures. Purification may allow more complex procedures through improved transformation efficiency, or better recombination, however the protocol time-course of such techniques (e.g. AQUA cloning, Beyer et al. (2015)) approaches that of enzymatic assembly methods. Because of this, using RAIR protocols with PCR clean-up offers only cost advantages over Gibson Assembly (Gibson et al., 2009), yet with the disadvantage of lower method efficiency. Consequently, they are unlikely to be of widespread usefulness.

The choice of DNA Polymerase for RAIR cloning does not appear to be of consequence for successful recombination, as has been previously suggested (Jacobus and Gross, 2015), however, given that amplification efficiency differs between enzymes, amount of product DNA transformed will be dependent on the selected polymerase. The increased colony yields presented above when using Phusion rather than *Pfu Turbo* have also previously be confirmed by other studies (Li et al., 2011). It is of interest that Li et al. (2011) report that transforming a greater PCR volume, and therefore greater amount of DNA, produced a lower number of colony forming units, conversely to what would be expected. This most likely occurs due to addition of excess solution volume, which lowers the transformation efficiency of the cells.

Interestingly, both Oliner et al. (1993) and Bubeck et al. (1993) claim that RAIR cannot occur with electroporated bacteria, and only with DNA transformed by chemical competency. Martin et al. (1995) report successful RAIR cloning using electrocompetent DH5α, yet only one recombination event within a single fragment was required for plasmid circularisation, whereas the studies of Bubeck et al. and Oliner et al. both required recombination of two separate fragments. It is possible therefore that electroporation does not effectively transform two separate DNA fragments into the same bacteria at a high enough frequency for successful cloning.

Using restriction enzymes for vector linearisation

For unamplifiable vectors, restriction enzymes are an alternative approach for vector linearisation, as described above. However, there are a number of disadvantages of this method that limit its use a primary cloning approach when compared to the standard IVA procedure.

Firstly, the possible insertion locations are reliant on suitable restriction sites being present in the destination vector, whereas a PCR-based linearisation facilitates insertion at any location. Secondly, if two enzymes are used for restriction digestion, the linear vector must be purified from the excised DNA. This requires agarose gel electrophoresis for DNA separation and gel extraction of the vector DNA, a lengthly, hands-on procedure. Finally, in order to transform an equivalent amount of vector and insert, insert DNA will require PCR purification and measurement of DNA concentration. These factors limit the versatility and simplicity of the IVA protocol, however offer a viable alternative when strictly required.

When linearising the destination vector with restriction enzymes, unless a region of the template plasmid requires removal (as in the example experiment described above), either one or two restriction enzymes can be employed. If a single site is cut, and leaves 'sticky-ends' as many type II restriction enzymes do, the vector will be able form a nicked circular product by re-annealing at the restriction site. This will likely lead to an increased number of false positive colonies, as this circular product can be repaired *in vivo* to produce a plasmid lacking the desired insertion. While it has not been assessed, it is possible that such re-annealing may also prevent the desired insertion by homologous recombination. For this reason, use of either two distinct restriction enzymes which do not produce compatible sticky-ends, or a single enzyme which leaves blunt ended linear DNA is likely to be a more advantageous strategy.

As discussed earlier, homologous recombination is most efficient when homologous regions are at the termini of linear DNA fragments (Conley et al., 1986). Therefore the location of IVA homologous regions at the termini of DNA fragments is optimal for efficient recombination. It is interesting to note that because homology regions which are downstream of linear ends can be used for successful recombination (Bubeck et al., 1993), some improvements to IVA when linearising the vector using restriction enzymes to create a seamless product can be made. If restriction enzyme recognition sequences are not located at the desired modification location, homologous regions can be designed for assembly at these desired locations, as long as the vector can be linearised between the regions of homology at any restriction site.

Mutagenesis

Together with previous reports (Xia et al., 2015), the data presented above question the suggested mechanism of QuikChange™ mutagenesis, as both studies demonstrate exponential rather than linear amplification using QuikChange™ primer design. QuikChange™ most likely proceeds through RAIR on transformation, after inefficient PCR amplification. IVA

primer design lies at the optimal theoretical point, with the mutation lying fully outside the primer annealing region, giving greatest control over the primer-template T_m and fully avoiding primer-dimer formation, while optimally using the recombination pathway. Given that offset primer design was used originally by both Jones and Howard (1991) and Howorka and Bayley (1998), how the inefficient approach of QuikChange™ gained such widespread popularity is as fascinating as it is perplexing.

Future perspectives

Using IVA primer design and the one-tube strategy, highly complex cloning protocols can be performed rapidly and effortlessly, with minimal hands-on time. Therefore this system has the potential to have an immediate impact on many different fields, from fundamental biochemical research to protein engineering and synthetic biology. IVA cloning provides a platform for simplified randomisation, while the minimal hands-on time is of critical importance for high-throughput studies. This will greatly benefit protein engineering projects, for example allowing the simultaneous randomisation of a loop length and a saturation site-directed mutagenesis. Synthetic biology is now facilitated by developments such as BioBricks (Shetty et al., 2008), where DNA blocks can be purchased to be assembled at the user's preference. Advances in directional assembly of DNA fragments are key to progress.

Molecular cloning is a core technique in biomedical research and IVA cloning will simplify construct preparation for all molecular biologists. Fundamental research is gearing towards the study of more technically challenging protein systems, such as protein complexes, membrane proteins and unstable proteins. Bottlenecks are regularly found during protein expression, purification and stability, and construct design has become a key tool to overcome these barriers. IVA cloning provides a platform where multiple plasmid modifications can be performed and combined as desired, eliminating a significant barrier to ideal experimental design and unifying molecular cloning to a single protocol. For the present study, IVA cloning will prevent a major limitation in molecular biological research, by facilitating the rapid and flexible generation of optimal AMPAR expression constructs, allowing a more complete investigation of receptor physiology to be achieved.

Chapter 4

The role of the AMPAR N-terminal Domain in Synaptic Anchoring

4.1 Introduction

AMPA receptors are localised at the postsynaptic membrane and mediate the majority of fast excitatory synaptic transmission (Greger et al., 2017; Traynelis et al., 2010). Firing of the presynaptic cell causes release of glutamate into the synaptic cleft, which activates the AMPAR, causing depolarisation of the postsynaptic membrane. This depolarisation plays two important roles. Firstly, in synaptic signalling, the depolarisation propagates the signal from the presynapse, and through synchronous signalling with other synapses can cause activation of the postsynaptic cell. Secondly, depolarisation of the postsynaptic membrane allows activation of NMDA receptors, which are blocked by Mg^{2+} ions at resting membrane potentials (Mayer et al., 1984; Nowak et al., 1984). NMDAR activation allows calcium flow into the postsynapse that triggers signalling cascades which regulate the strength of the postsynapse (Bliss and Collingridge, 1993; Huganir and Nicoll, 2013; Kessels and Malinow, 2009).

The mechanisms involved in trafficking AMPARs to synaptic sites have been extensively studied (Shepherd and Huganir, 2007), primarily because the AMPAR content of the postsynapse controls the strength of synaptic transmission, and modulation of the synaptic AMPAR content is a major mechanism of synaptic plasticity (Huganir and Nicoll, 2013; Malinow et al., 2000). Simply recruiting AMPARs to the postsynapse does not appear to be the only requirement for their involvement in transmission. It has been predicted that receptors need to be clustered opposite presynaptic release sites (Lisman et al., 2007; Raghavachari and Lisman,

2004), which is consistent with data showing that postsynaptic AMPARs are not saturated with agonist during synaptic transmission (Liu et al., 1999; McAllister and Stevens, 2000). Initial evidence for this model has recently emerged through use of super-resolution imaging. The postsynaptic density is not homogenous, and postsynaptic proteins such as PSD-95 form regions of higher density, termed 'nanodomains' (Fukata et al., 2013; MacGillavry et al., 2013). AMPARs are enriched at these sites (MacGillavry et al., 2013; Nair et al., 2013), which are aligned with the sites of vesicle release (Tang et al., 2016). Synaptic anchoring of AMPARs therefore requires precise receptor positioning within the postsynaptic area.

Two regions of the receptor have been the focus of attention in studying synaptic anchoring of the receptor. The AMPAR CTD, a polypeptide (of 50 - 80 amino acids) which is able to interact intracellularly with postsynaptic proteins (Shepherd and Huganir, 2007), and the CTD of the AMPAR-binding TARPs, which is also intracellular, and interacts with MAGUKs such as PSD-93 and PSD-95 in the postsynaptic density (Schnell et al., 2002). The TARP CTD is currently the best described anchoring mechanism, and is almost entirely responsible for maintaining synaptic AMPARs in cerebellar granule cells (Chen et al., 2000). The interaction between the extreme C-terminus of TARPs and PSD-95 limits the lateral diffusion of the AMPAR, serving to anchor the receptor at the postsynapse (Bats et al., 2007; Opazo et al., 2012; Schnell et al., 2002), however a mouse model lacking the PSD-95 binding ligand of TARP γ8, the major TARP in the hippocampus (Rouach et al., 2005), does not prevent AMPAR transmission (Sumioka et al., 2011). In fact AMPAR currents are reduced by a modest 30 %, suggesting that TARPs are not the only anchor regulating AMPAR localisation.

The AMPAR CTD has been shown to interact with a plethora of intracellular proteins, such as GRIP/ABP (Dong et al., 1997; Srivastava et al., 1998) and SAP97 (Leonard et al., 1998) scaffolding proteins at the postsynaptic density, NSF for receptor recycling (Nishimune et al., 1998; Osten et al., 1998; Song et al., 1998) and PICK for endocytosis and association with intracellular pools (Braithwaite et al., 2002; Dev et al., 1999; Hanley et al., 2002; Xia et al., 1999) among others (Shen et al., 2000). The CTD is also extensively phosphorylated by various protein kinases, which appear to modulate synaptic anchoring of the receptor (Barria et al., 1997a; Oh et al., 2006; Seidenman et al., 2003, but see Hosokawa et al., 2015 and Diering et al., 2016). However, deletion of the AMPAR CTD is not a prerequisite for receptor clustering (Bats et al., 2007; MacGillavry et al., 2013) and how essential each of these interactions are in synaptic plasticity remains unclear (Boehm et al., 2006; Granger et al., 2013; Kim et al., 2005).

The AMPAR NTD has been remarkably overlooked in the study of synaptic function. While having a strong influence on receptor assembly (Ayalon and Stern-Bach, 2001; Leuschner and Hoch, 1999; Rossmann et al., 2011), and subtly modifying receptor gating in heterologous cells (Cais et al., 2014; Möykkynen et al., 2014), its effect on synaptic transmission has been understudied. The NTD has been implicated in receptor clustering, having been shown to interact with neuronal pentraxins (NPs) (O'Brien et al., 1999), which can cluster GluA4 at synaptic sites in a neuron/heterologous cell co-culture system (Sia et al., 2007). This interaction has been demonstrated to control the synaptic AMPAR content at interneuronal synapses in the hippocampus (Chang et al., 2010), with an essential role in controlling network activity (Pelkey et al., 2015). At spine synapses, the AMPAR NTD has been implicated in stability of presynaptic sites (Ripley et al., 2011; Tracy et al., 2011), indicating a transsynaptic signalling function, and has even been suggested to cause synaptogenesis (Passafaro et al., 2003), however this effect remains highly questionable (Biou et al., 2008; Lu et al., 2009).

The domain comprises 50 % of the AMPAR polypeptide, and protrudes approximately halfway across the 24 nm synaptic cleft (Greger et al., 2017; Lučić et al., 2005). This volume is not simply a space between cells, but is filled with a high density of cell adhesion molecules spanning the cleft (Perez de Arce et al., 2015), providing numerous opportunities for interactions with the NTD. As the AMPAR extracellular domain is highly mobile (Krieger et al., 2015), it provides a large, structurally dynamic docking platform, with the potential to control synaptic anchoring (García-Nafría et al., 2016a). The NTD of other members of the iGluR family, delta receptors (GluD) and kainate receptors (GluK) have recently been demonstrated to form transsynaptic bridges as part of protein complexes, with roles in receptor localisation and signalling (Elegheert et al., 2016; Matsuda et al., 2016), therefore such a role for the AMPAR NTD could be expected.

As recent imaging studies have shown (MacGillavry et al., 2013; Nair et al., 2013), AMPARs are specifically clustered within the postsynaptic density, and these clusters are aligned with the sites of presynaptic glutamate release (Tang et al., 2016). Given the size and location of the AMPAR NTD within the synaptic cleft, it provides a strong candidate to mediate such receptor alignment. This study aims to investigate the role of the AMPAR NTD in synaptic function at the CA1 hippocampal synapse.

4.2 Results

4.2.1 GluA2 ΔNTD Construct Optimisation

The GluA2 subunit is present in a heteromeric complex with either GluA1 or GluA3 in the vast majority of CA1 pyramidal AMPARs (Lu et al., 2009; Wenthold et al., 1996), and therefore its NTD was first studied for a role in synaptic transmission. In order to study the role of the AMPAR N-terminal domain, a construct expressing GluA2 lacking its NTD was optimised. Previous reports demonstrate that AMPARs lacking the NTD (ΔNTD) traffic poorly to the cell surface (Möykkynen et al., 2014), which could potentially complicate assessing their effect on synaptic transmission. In this study, GluA2 was truncated such that D385 was the first residue of the ΔNTD construct, by deletion of the entire NTD coding region and a portion of the NTD-LBD linker coding region. However, NTD deletion constructs have not been fully optimised for surface trafficking capabilities.

The NTD-LBD linker consists of a flexible 18 amino-acid peptide between structured domains (for primary amino-acid sequence see Figure 4.1A). To avoid excessive perturbation of protein folding or LBD function, ΔNTD constructs were designed such that the first residue occurs in this flexible linker. In order to identify the optimal GluA2 ΔNTD construct, plasmids were cloned to express GluA2Q from the pRK5 vector initiating the protein sequence at each difference amino-acid residue of the NTD-LBD linker. 18 constructs were created each containing the GluA2 signal-sequence, followed by a c-myc epitope tag (Evan et al., 1985) for antibody detection, before the remaining GluA2 protein. GluA2Q was selected for this screening due to its superior trafficking over GluA2R (Greger et al., 2002).

The surface trafficking capacity of ΔNTD constructs was quantified using a flow cytometry based assay. HEK293 cells were transfected with plasmids expressing EGFP and AMPAR constructs and stained for surface receptors by detection of the c-myc tag using an AF647 conjugated antibody and DAPI for identification of dead cells, due to their greater membrane permeability, allowing dye access (Figure 4.1B). A single-cell suspension was generated from cells expressing each AMPAR construct, which were individually imaged by flow cytometry, measuring individual cell fluorescence intensities for DAPI, EGFP and AF647. Two cell populations could be separated by DAPI fluorescence to select for live cells (Figure 4.1C1, D1), which were subsequently separated into untransfected and transfected cells by analysis of EGFP expression (Figure 4.1C2, D2). The extent of AF647 staining was far greater in transfected than untransfected cells (Figure 4.1C3 vs C4 and D3 vs D4) and the

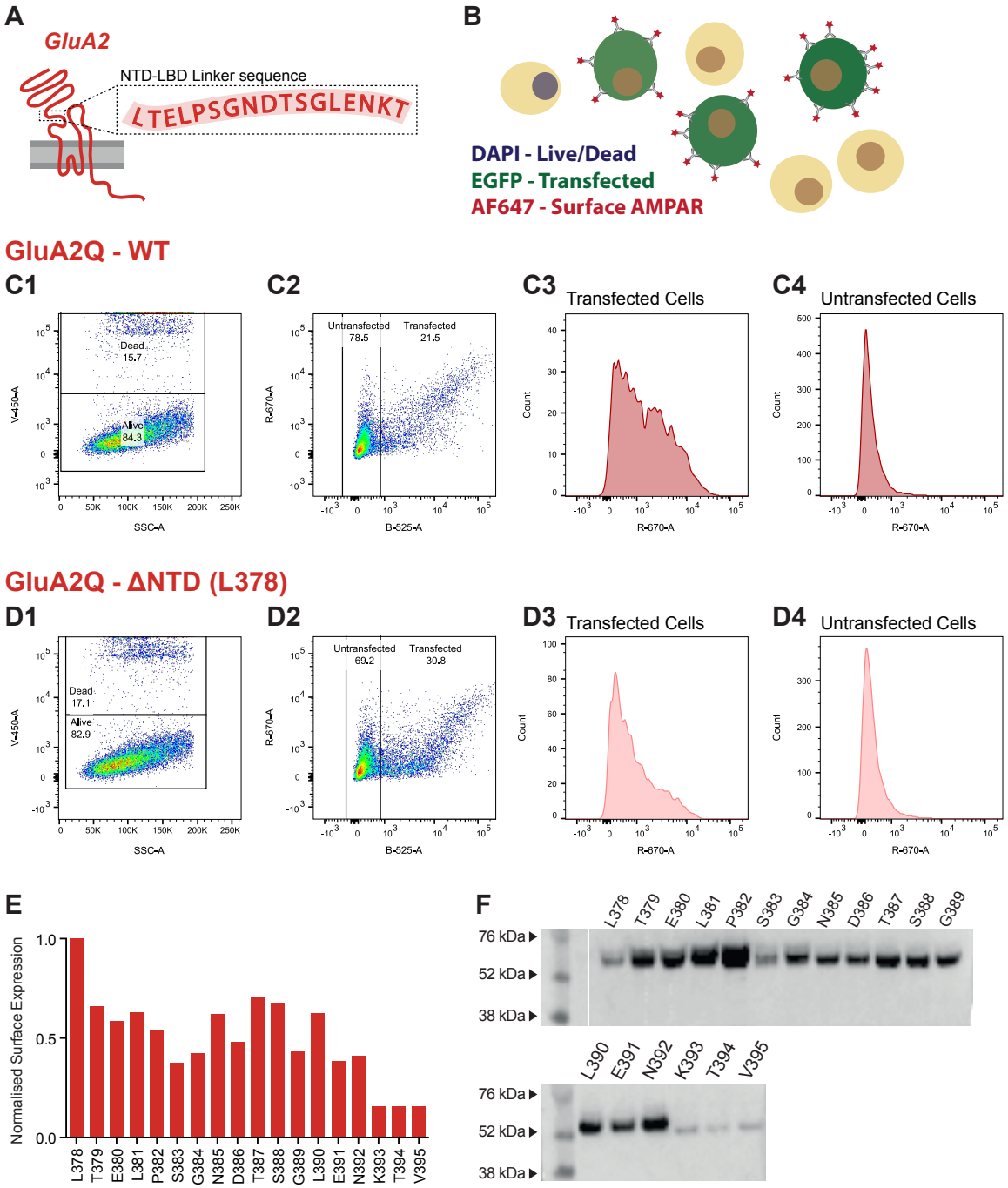

Figure 4.1 ***Optimisation of GluA2 ΔNTD Construct surface expression.***

Figure 4.1 ***Optimisation of GluA2 ΔNTD Construct surface expression.*** *(**A**) The amino-acid sequence of the GluA2 NTD-LBD linker. (**B**) Flow cytometry HEK293 cell-staining procedure distinguishes live from dead cells by uptake of DAPI dye, transfected from untransfected cells by EGFP plasmid expression, and measurement of surface AMPAR expression using an AF647 conjugated antibody against an AMPAR extracellular c-myc tag. (**C**) GluA2Q WT flow cytometry data examples. (**C1**) Flow cytometry data plotting cell side-scatter (x-axis) vs DAPI fluorescence (y-axis) to selectively analyse live cells. (**C2**) Plotting EGFP fluorescence (x-axis) vs AF647 fluorescence (y-axis) allows selection of transfected cells and shows correlation between AMPAR and EGFP expression for those cells, due to varying transfection levels. Histograms of AF647 staining levels for transfected (**C3**), and untransfected (**C4**) cells are shown. (**D1-4**) Equivalent plots for GluA2 ΔNTD construct initiating at residue L378. (**E**) Surface expression of GluA2 ΔNTD constructs initiating at each NTD-LBD linker residue, normalised to maximally expressing construct. Average of two repeats. (**F**) Western blot analysis of total GluA2 ΔNTD construct expression in HEK293 cells.*

surface AMPAR expression could be quantified as the median AF647 intensity.

GluA2Q ΔNTD constructs showed markedly different surface trafficking capabilities (Figure 4.1E), with maximal trafficking observed with the full NTD-LBD linker sequence present (L378 first linker residue). Two post-translational N-glycosylations are added to the protein in the linker sequence (at N385, N392). Interestingly, removal of the second glycosylation site (N392) reduced surface trafficking almost completely (see constructs beginning K393, T392, V395) (Figure 4.1E). The total protein expression level was quantified by lysis of a subset of transfected cells, before detection by Western blot analysis (Figure 4.1F). Removal of N392 glycosylation resulted in minimal protein production, most likely causing the reduced surface detection seen in Figure 4.1E, indicating a role for this site in protein expression and stability. As the L378 ΔNTD construct showed the strongest surface trafficking capability (Figure 4.1E), which did not appear to be due to increased protein production (Figure 4.1F) it was selected for all future experiments, henceforth denoted as GluA2Q ΔNTD.

4.2.2 Studying AMPAR synaptic trafficking

In order to study the synaptic localisation of exogenously expressed AMPARs on overexpression, such as GluA2 ΔNTD, the contribution of endogenous and exogenous receptors to transmission requires separation. The channel properties of AMPAR subunits can be utilised for this purpose. RNA editing of GluA2 causes a single-amino acid point mutation at residue 586 from glutamine (Q) to arginine (R) (Sommer et al., 1991). As this residue is at the heart of the channel pore, it has serious consequences for channel function. GluA2'R' is impermeable to calcium (Burnashev et al., 1992; Hume et al., 1991; Mishina et al., 1991), while GluA2'Q' can conduct calcium ions. Importantly, GluA2Q is also susceptible to block by polyamines, such as spermine from the intracellular side at positive membrane potentials (Bowie and Mayer, 1995) (Figure 4.2A), whereas GluA2R is not. This RNA editing property does not affect GluA1 or GluA3, which always contain a Q at the equivalent pore position (Figure 4.2B). When incorporated into heteromeric receptors, GluA2R confers its properties of calcium impermeability and resistance to polyamine block (Figure 4.2C). GluA2Q does not exist is substantial quantities in the brain, and in CA1 pyramidal neurons, the vast majority of receptors are GluA1/2 or GluA2/3 heteromers (Lu et al., 2009; Wenthold et al., 1996). Therefore, endogenous AMPAR subunits in these cells have a linear current voltage (IV) relationship (Figure 4.2C). On overexpression of exogenous GluA2Q, the presence of these exogenous receptors contributing to a measured AMPAR current can be assessed by the ratio

of current response at +40 mV and -60 mV membrane potentials; the rectification index (RI). The equation for RI calculation used throughout this study is as follows:

$$\text{Rectification Index (RI)} = \frac{I_{+40\text{ mV}} - I_{0\text{ mV}}}{I_{\text{-60 mV}} - I_{0\text{ mV}}}$$

The contribution of exogenous receptors in an AMPAR population is detected by a decrease in the RI relative to untransfected cells, caused by increased polyamine block at positive membrane potentials.

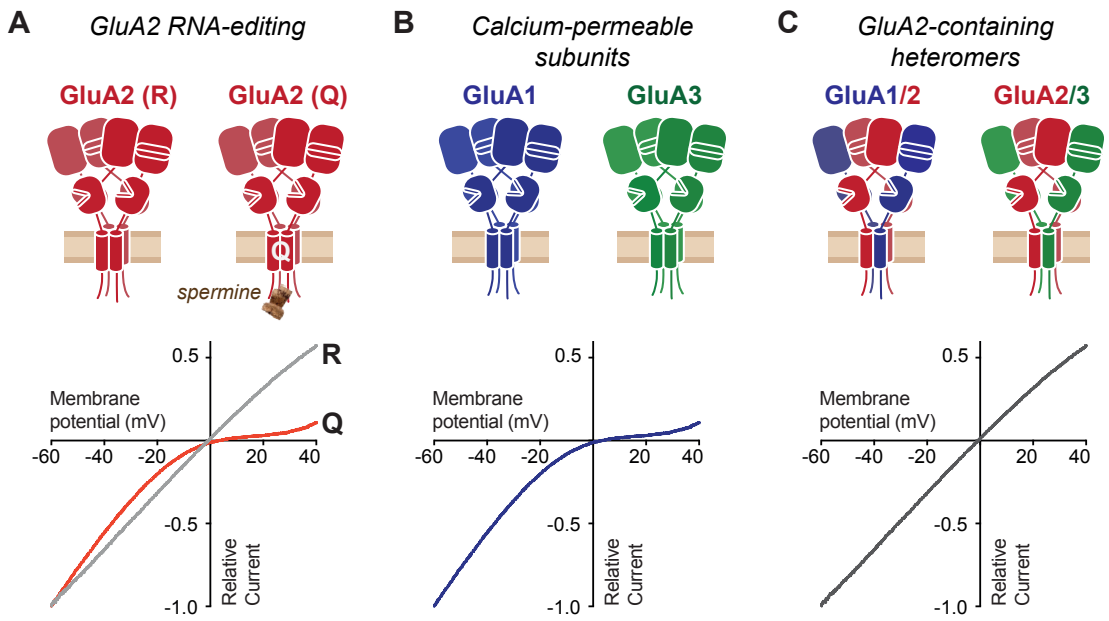

Figure 4.2 ***AMPAR rectification properties*** *(**A**) RNA editing of GluA2 induces a glutamine (Q) to arginine (R) transition at residue 586 changes receptor pore properties to prevent spermine-dependent block at positive membrane potentials which gives rise to a 'rectifying' IV relationship. (**B**) GluA1 and GluA3 subunits alone give rise to rectifying responses, however (**C**) incorporation of GluA2(R) in heteromeric subunits renders receptors insensitive to spermine inhibition and therefore have linear IV curves.*

As CA1 pyramidal cells almost exclusively express GluA2R containing heteromeric receptors, exogenous expression of GluA2Q or GluA1 homomers can therefore be detected by comparison of current amplitudes at -60 mV and +40 mV: the rectification index.

To study the effect of NTD deletion on AMPAR function at the synapse, plasmids encoding AMPAR subunits can be transfected into hippocampal organotypic slices by single-cell electroporation (SCE, Figure 4.3A). While low-throughput, requiring individual electroporation in the cell-attached configuration using a glass microelectrode, the advantage of SCE is that only a subset of neurons are modified, so pairs of untransfected and transfected cells can be directly compared. Also, cell transfection requires only plasmid DNA, and therefore construct modifications can be performed swiftly and easily in comparison to the alternative of viral DNA delivery.

Simply delivering DNA encoding AMPAR constructs does not confirm that the protein is produced, trafficked correctly, or functional, all of which are essential for studying synaptic function. For this reason, expression of exogenous receptors can be studied by recording receptors present on the cell surface of transfected neurons. Outside-out patches of neuronal membrane can be pulled by retraction of the patch pipette after achieving a whole-cell configuration (Figure 4.3B1). Surface receptors can be characterised by isolation of the AMPAR current using inhibitors for other ion channels (such as APV for NMDAR and SR-95531 for $GABA_AR$). A fast-solution exchange setup was used for surface receptor analysis, consisting of a piezo-driven theta-glass, allowing simultaneous perfusion of glutamate containing and lacking extracellular solution. By piezo actuation, the membrane patch can be immersed in glutamate containing solutions to record AMPAR currents, with a time resolution of approximately 300 µs (Figure 4.3B2).

As previously stated, the sparse transfection of neurons using SCE allows paired recording of both untransfected and transfected cells simultaneously. Synaptic receptor currents can be induced using a single glass stimulation electrode in stratum radiatum, which, by activation of a subset of Schaffer collateral axons, will induce synaptic glutamate release on both cells (Figure 4.3C). The paired recording configuration gives greater statistical power for comparison of cells, facilitating the most robust and reliable analysis of the effect of AMPAR construct expression. The RI of both surface and synaptic currents can be measured using these approaches to detect the contribution, and therefore trafficking of GluA2Q or GluA2Q ΔNTD receptor to surface or synaptic compartments.

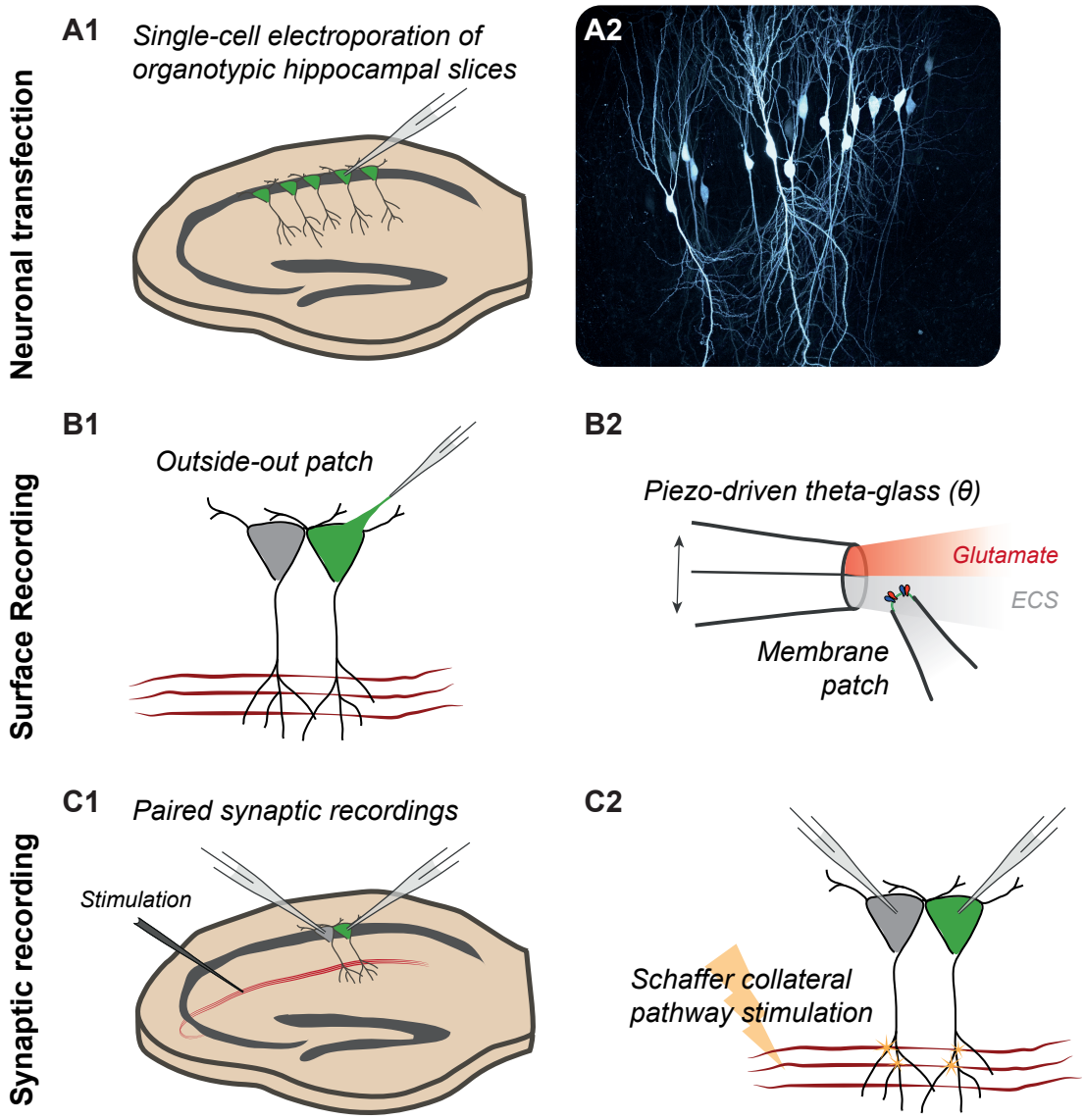

Figure 4.3 ***Patch-clamp methodology*** *(**A1**) Hippocampal organotypic slice cultures are transfected by single-cell electroporation (SCE) with plasmid DNA to allow sparse expression. (**A2**) Example image of CA1 subfield after SCE of EGFP expressing plasmid DNA in a subset of cells. (**B1**) Outside-out patch recording allows surface receptor response analysis. Small membrane patches are excised by pipette retraction in the whole-cell configuration. (**B2**) glutamate is applied to membrane patches using a piezo-driven theta glass perfusing extracellular solution (ECS with or without glutamate addition, which allows rapid solution exchange. (**C1**) Synaptic recordings are performed by simultaneous whole-cell patch clamp of neighbouring transfected and untransfected CA1 pyramidal neurons, with stimulation of CA3-CA1 Schaffer collateral axons in stratum radiatum using a glass electrode (**C2**).*

4.2.3 Surface trafficking of GluA2 ΔNTD

To quantify the level of surface expression of GluA2 constructs, outside-out patches of transfected CA1 pyramidal neurons were excised and subjected to a membrane ramp protocol for RI measurement (Figure 4.4A1). Patches were immersed in extracellular solution containing APV and SR-95531 for AMPAR current isolation, and 100 µM cyclothiazide (CTZ), an AMPAR modulator which blocks receptor desensitisation (Trussell et al., 1993) to provide robust responses for analysis. Patches were stepped into 1 mM glutamate while the membrane potential was increased from -100 mV to +100 mV (Figure 4.4A1). An example of the current response from an untransfected cell is depicted in (Figure 4.4A2), showing a highly linear relationship between current and membrane potential.

While the IV of untransfected cells was linear, cells expressing either GluA2Q or GluA2Q ΔNTD exhibited strong inward rectification (Figure 4.4B1). Quantification of RI (Figure 4.4B2) showed similar, strong surface trafficking of both GluA2Q and GluA2Q ΔNTD. The amplitude of currents at -60 mV also showed an apparent increase on exogenous receptor expression (Figure 4.4B3), which is most likely due to the increased single-channel conductance of Q-pore containing receptors in comparison to the endogenous GluA2R containing heteromers (Swanson et al., 1997).

AMPARs are associated on the cell surface and in synapses with auxiliary proteins such as TARPs (Jackson and Nicoll, 2011), which are important mediators of AMPAR anchoring at the post-synaptic density (Chen et al., 2000; Opazo et al., 2012). Regions of the AMPAR NTD have been shown to associate with extracellular loops of TARPs (Cais et al., 2014), and while this is thought to influence channel properties, rather than the stability of the AMPAR-TARP complex, it is nevertheless possible that NTD deletion could impact TARP association, and as a consequence, AMPAR synaptic anchoring.

The partial agonist kainate (KA) has a dramatically increased efficacy at TARP-bound AMPARs (Shi et al., 2009; Turetsky et al., 2005). This property allows quantification of AMPAR-TARP association, by measuring the ratio of response to glutamate and kainate (KA/Glu ratio). Shi et al. (2009) describe that, in the presence of CTZ, this ratio is approximately 0.5 for receptors associated with four TARP proteins, falling to under 0.1 when no TARPs are present. They also report a dose-dependence to this effect, whereby receptors associated with two TARPs have a KA/Glu ratio of approximately 0.3. To study the TARP-association level of overexpressed AMPAR subunits on SCE, the KA/Glu response ratio was

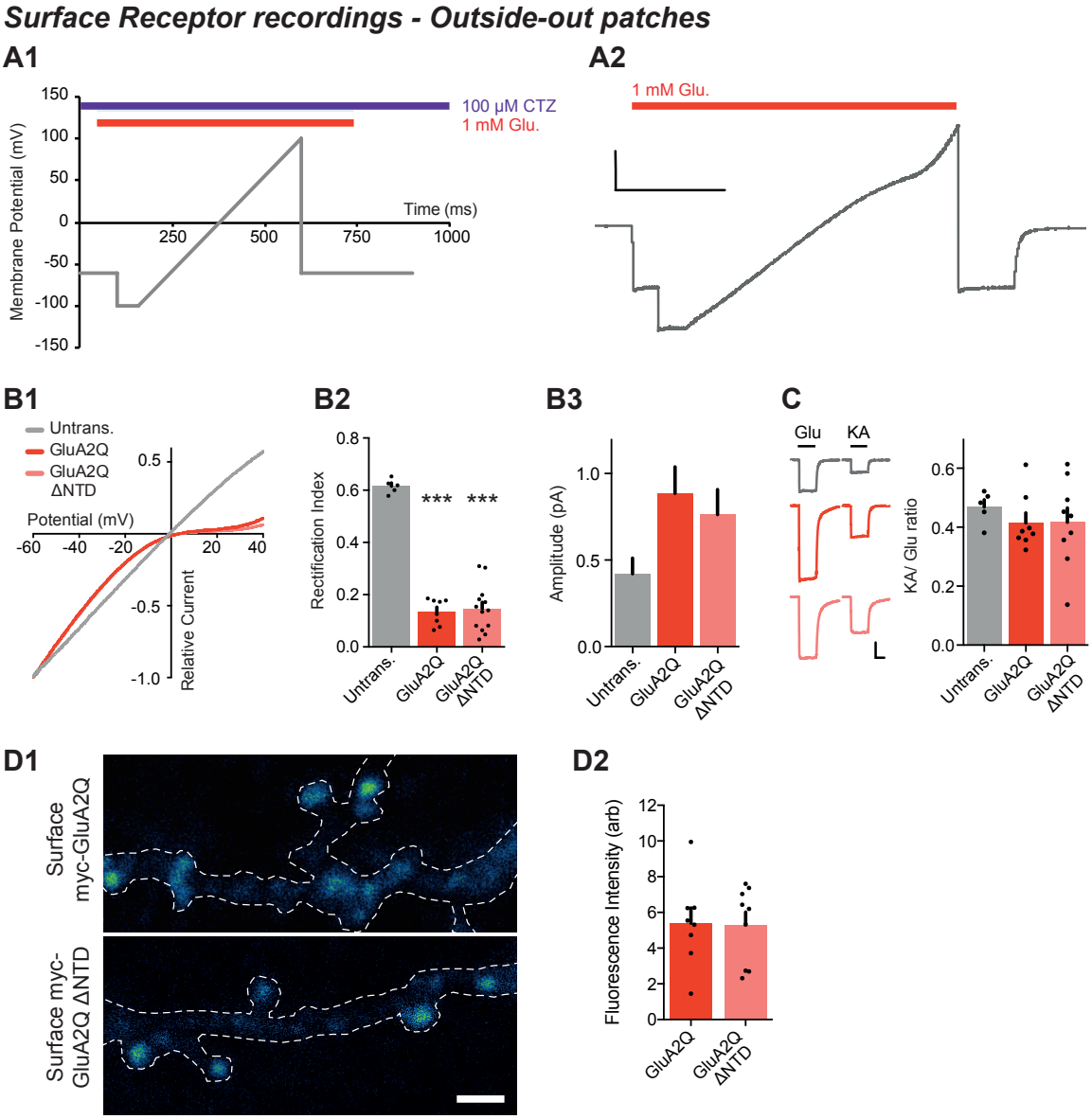

Figure 4.4 ***GluA2 ± NTD construct surface expression.***

Figure 4.4 ***GluA2 ± NTD construct surface expression.*** *(**A1**) Experimental protocol for rectification analysis of AMPARs from outside-out patches. 1 mM glutamate is perfused onto patches in the constant presence of 100 µM cyclothiazide (CTZ) while a membrane potential ramp (grey) is applied to patches. (**A2**) Full example trace of surface AMPAR current from an untransfected cell. Scale bar = 250 ms and 200 pA. (**B1**) I/V curves of glutamate-evoked AMPAR currents recorded from outside-out patches of untransfected, GluA2Q and GluA2Q ΔNTD-expressing cells. (**B2**) AMPAR currents from transfected neurons show strong inward-rectification on GluA2 construct expression (Rectification index (RI): untrans.: 0.62 ± 0.03 (n = 5); GluA2Q: 0.13 ± 0.02 (n = 8); GluA2Q ΔNTD: 0.15 ± 0.02 (n = 13); One-way ANOVA, p<0.0001). Significance (*) indicates difference to untransfected cells. (**B3**) Amplitudes of surface patch AMPAR glutamate responses (-60 mV membrane potential) are apparently elevated on GluA2Q or GluA2Q ΔNTD overexpression (untrans.: 398 ± 50 pA; GluA2Q: 886 ± 153 pA; GluA2Q ΔNTD: 763 ± 145 pA). (**C**) Ratio of response amplitude to kainic acid and glutamate, indicative of auxiliary subunit association, from somatic patches is unchanged on receptor overexpression (KA/Glu: untrans.: 0.48 ± 0.03 (n = 5); GluA2Q: 0.41 ± 0.03 (n = 8); GluA2Q ΔNTD: 0.42 ± 0.05 (n = 9); One-way ANOVA, p=0.51). Example traces showing glutamate (Glu) and kainic acid (KA) application are shown left. Scale bar = 50 ms and 100 pA. (**D1**) Example images of dendritic regions from GluA2 ± NTD overexpressing dissociated hippocampal neurons stained for exogenous surface receptors via an N-terminal c-myc tag. Approximate dendrite location is indicated (white). Scale bar = 1 µm. (**D2**) Average surface stain intensity from **D1** shows equivalent surface expression of GluA2 constructs (GluA2Q: 5.40 ± 0.86, GluA2 ΔNTD: 5.30 ± 0.72, unpaired t-test: p=0.93).*

measured from outside-out patches of CA1 pyramidal neurons overexpressing GluA2Q or GluA2Q ΔNTD (Figure 4.4C). This ratio was no different between untransfected or cells transfected with either construct, indicating that indeed all exogenous AMPARs are TARP associated.

As a final confirmation that surface trafficking was unaffected by NTD removal, dissociated hippocampal cultures were transfected with GluA2 ± NTD expressing constructs containing an extracellular c-myc epitope. Cells were stained under non-permeabilising conditions with an antibody recognising the myc tag and the fluorescence intensity was quantified to measure surface GluA2Q levels (Figure 4.4D). Using this approach, surface trafficking appeared equivalent between conditions (Figure 4.4D2).

Taking together surface RI, patch amplitude and KA/Glu data, it appears that overexpression of AMPARs predominantly replaces the endogenous heteromeric receptor population with fully TARP-associated exogenous subunits, and that NTD deletion has little detrimental effect on surface trafficking.

4.2.4 Contribution of GluA2Q to synaptic currents

To study the contribution of exogenous subunits to synaptic transmission, paired whole-cell recordings of untransfected and transfected cells were performed, as per Figure 4.3C, by recording AMPAR EPSCs at -60, +40 and 0 mV holding potentials. As previously described (Shi et al., 2001), GluA2Q expression produced strongly rectifying responses (Figure 4.5A1). GluA2Q ΔNTD expression produced a similarly strong change in synaptic RI (Figure 4.5A2), indicating that both receptors contribute to synaptic transmission.

By correlating the AMPAR EPSC amplitudes within recorded pairs, the average change in EPSC amplitude can be assessed. Expression of GluA2Q caused a significant increase in EPSC amplitude of around 50 % (Figure 4.5B1-2). By recording evoked currents at positive holding potentials, in the absence of APV, NMDAR currents can also be elicited. Due to the kinetics of channel opening/closing, while the AMPAR current rapidly decays, a prolonged NMDAR current exists for a few hundred ms after receptor activation (depicted in Kauer and Malenka, 2007). Therefore, the change in NMDAR EPSC amplitude can be compared between conditions by recording at +40 mV membrane potentials and quantifying current amplitude 100 ms after stimulation, when AMPARs will no longer contribute to

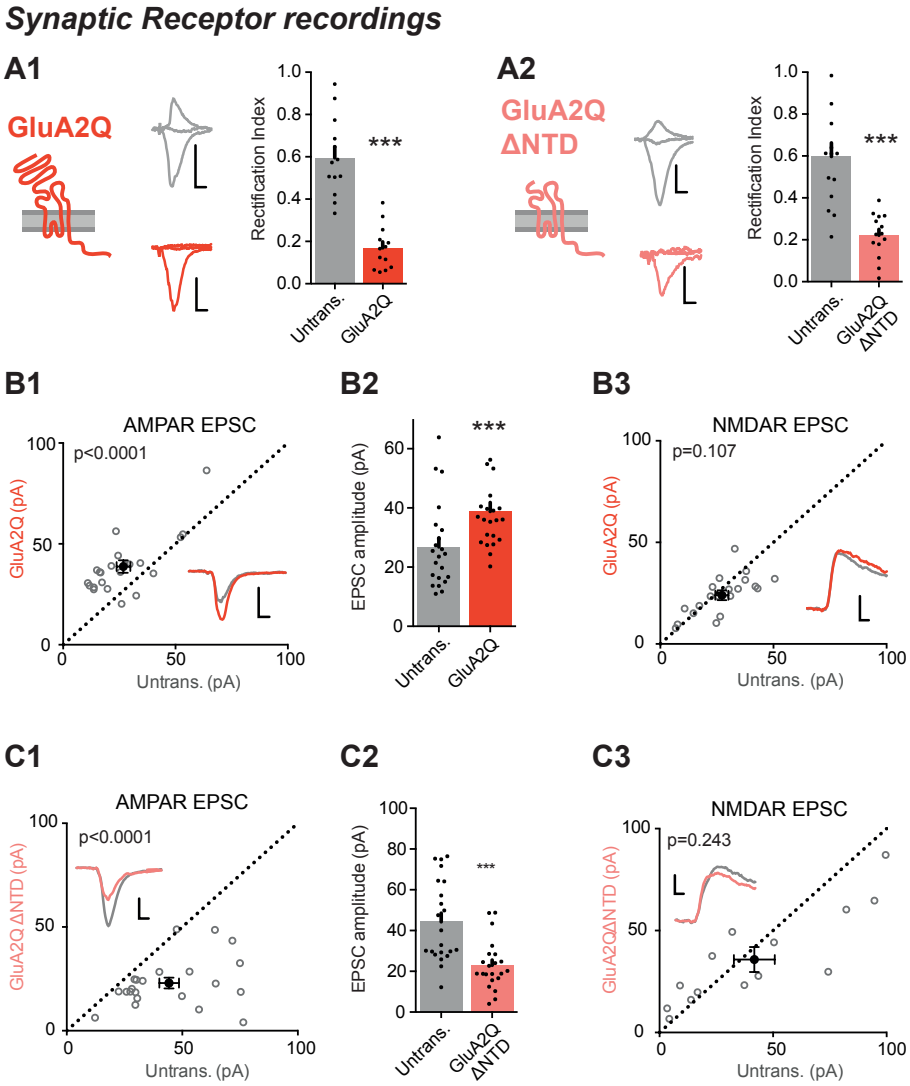

Figure 4.5 *Expression of NTD-deleted GluA2 causes large reduction in synaptic currents.*

Figure 4.5 ***Expression of NTD-deleted GluA2 causes large reduction in synaptic currents.*** *(**A**) Synaptic RI measured from pairs of untransfected and transfected cells indicate both homomeric GluA2Q and GluA2Q ΔNTD are inserted into synapses. (**A1**) Untrans., 0.60 ± 0.19; GluA2Q, 0.17 ± 0.10; n = 13 pairs; paired t-test, p=0.001. (**A2**) Untrans., 0.60 ± 0.25; GluA2Q ΔNTD, 0.22 ± 0.11; n = 16 pairs; paired t-test, p<0.0001. Sample traces and construct schematics are shown on the left. Scale bar = 10 ms, 50 pA (grey and GluA2Q) or 20 pA (GluA2Q ΔNTD). (**B - C**) Scatter plots and bar charts of EPSC amplitudes from pairs of cells, showing single pairs (open circles) and mean values ± SEM (filled circles). Sample traces inset. Scale bar = 10 ms, 30 pA. (**B1**) GluA2Q-expressing cells have increased AMPAR EPSCs relative to untransfected cells (untrans.: 26.8 ± 3.1 pA; GluA2Q: 38.8 ± 3.0 pA; n = 22 pairs; paired t-test, p<0.0001). (**B2**) Bar chart of AMPAR EPSCs from **B1**. (**B3**) NMDAR-mediated EPSCs remain unchanged (untrans.: 27.2 ± 2.7 pA; GluA2Q: 24.0 ± 2.2 pA; n = 20; paired t-test, p=0.107). (**C1**) GluA2Q ΔNTD-expressing cells show AMPAR EPSC amplitude depression (untrans.: 44.3 ± 4.3 pA; GluA2Q ΔNTD: 23.0 ± 2.5 pA; n = 22; paired t-test, p<0.0001). (**C2**) Bar chart of AMPAR EPSCs from **C1**. (**C3**) NMDAR EPSCs show no amplitude change (untrans.: 41.8 ± 9.0 pA; GluA2Q ΔNTD: 35.8 ± 6.1 pA; n = 14; paired t-test, p=0.243).*

the postsynaptic current. The amplitude of NMDAR EPSCs was unchanged on GluA2Q overexpression, indicating that no major perturbations were caused to the number or size of synaptic connections (Figure 4.5B3).

Interestingly, while GluA2Q ΔNTD caused a similar RI change to GluA2Q, EPSC amplitude was decreased by approximately 50 % on expression of NTD-deleted receptors (Figure 4.5C1-2). NMDAR currents were again unchanged, indicating that the effect was specific to the AMPAR component of synaptic transmission (Figure 4.5C3). The altered RI but decreased AMPAR EPSCs is suggestive that exogenous GluA2Q ΔNTD is contributing to transmission, but far less receptors are receiving glutamate for activation.

4.2.5 Characterising GluA2-induced changes in AMPAR EPSCs

The are a number of possible explanations for the observed changes in AMPAR EPSC amplitude between GluA2Q and GluA2Q ΔNTD expression, given that both receptors are contributing to the majority of the AMPAR postsynaptic current in each case, as seen by synaptic RI measurements. Firstly, the number of synapses contributing to transmission may be altered. Secondly, changes in the probability of glutamate release from the presynapse may be induced. Thirdly, the single-channel conductance (γ) may be dramatically different on NTD deletion. Finally, a difference in the number of receptors contributing to transmission in each case could give rise to the effect.

Studying spine density

GluA2 NTD-dependent changes in the number of synapses has been reported in the past, and therefore would not be an unexpected explanation for the result described above. Passafaro et al. (2003) reported that overexpression of GluA2 increased both the number and volume of dendritic spines (postsynaptic structures) in dissociated hippocampal neurons, yet overexpression of NTD-deleted GluA2 had the opposite effect, decreasing spine density, a result strikingly similar to EPSC recordings described here. However, a number of reports have failed to reproduce or support this finding (Biou et al., 2008; Chen et al., 2009; Lu et al., 2009; Medvedev et al., 2008; Sans et al., 2003; Tracy et al., 2011).

As Passafaro et al. (2003) used dissociated cultures for their study, a similar approach was adopted to study the role of GluA2 in spine density changes. GluA2Q ± NTD were co-transfected into dissociated hippocampal cultures with an EGFP expressing plasmid to

allow visualisation of cell morphology (Figure 4.6A1). The spine density was manually counted in a blinded fashion, and no difference was observed between conditions (Figure 4.6A1). To more objectively identify postsynaptic structures, this experiment was repeated, using coexpression of GluA2Q ± NTD with Homer1c-EGFP. As Homer1c is a postsynaptic protein, expression of an EGFP-tagged variant allows fluorescent labelling of the postsynapse in an approach that has previously been shown not to affect AMPAR synaptic trafficking (Nair et al., 2013). Using this protocol, the density of fluorescent postsynaptic puncta was quantified, and again, cells transfected with GluA2Q and GluA2Q Δ NTD showed no difference in synaptic density (Figure 4.6A2).

As EPSC recordings were performed in organotypic slice cultures, a spine density analysis was repeated in this system. Cells transfected with GluA2Q ± NTD by SCE were held in the whole-cell patch-clamp configuration using an intracellular solution containing the membrane-impermeable dye Lucifer Yellow for approximately 10 min. Cytosolic dye-filling was followed by slice fixation and confocal imaging for spine density measurement (Figure 4.6B). Similarly to experiments performed in dissociated cultures, neither GluA2Q nor GluA2Q Δ NTD expression significantly altered the spine density when compared to untransfected counterparts (Figure 4.6B). It should also be noted, that had either construct altered the number of synaptic connections, the NMDAR EPSC amplitude would likely have changed in unison. Therefore, this accumulated evidence suggests that the GluA2 NTD has little effect on synapse formation, and spine number cannot explain the NTD-dependent changes in synaptic transmission that have been observed.

Studying presynaptic changes

An increase in the probability of presynaptic vesicle release would result in elevated postsynaptic EPSC amplitude either by increasing the concentration or frequency of glutamate presence in the synaptic cleft. It is feasible that NTD-dependent interactions could regulate the presynapse, as retrograde signalling has been described (Tao and Poo, 2001) and even suggested to involve the AMPAR NTD (Ripley et al., 2011; Tracy et al., 2011). The paired-pulse ratio (PPR) is a well established measure of presynaptic release probability (Lu et al., 2009). On action potential invasion of the presynaptic terminal, voltage-gated calcium channels (VGCC) are activated, increasing intracellular calcium concentrations, which trigger the calcium-dependent exocytosis of synaptic vesicles (Lisman et al., 2007). By evoking presynaptic axon action potentials twice in quick succession, the elevated calcium from stimulation 1 does not have enough time to clear, and therefore maximal calcium con-

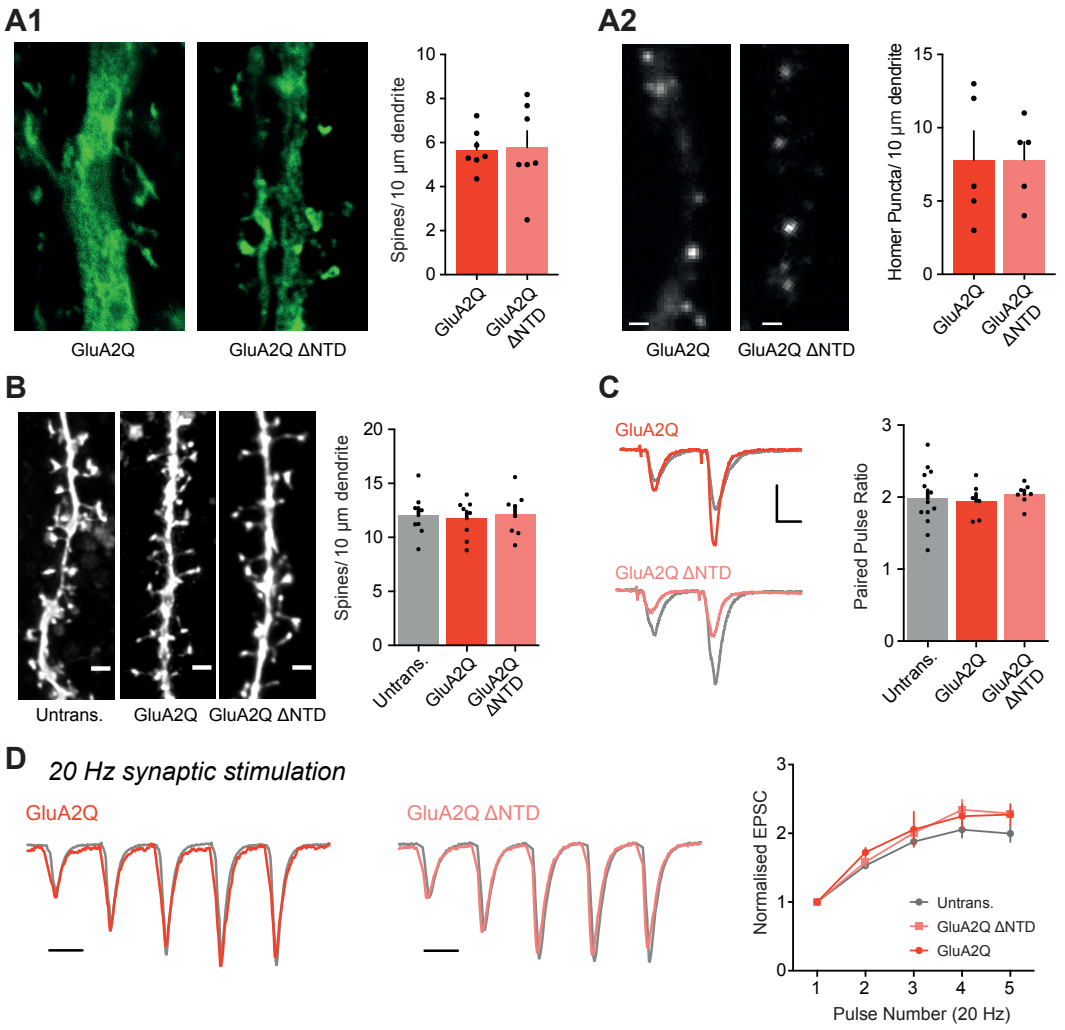

Figure 4.6 ***Characterising GluA2-dependent changes in EPSC amplitude*** *(**A1**) Dissociated culture spine density is unchanged between GluA2 construct expressions (GluA2Q: 5.68 ± 0.35 spines/* 10 µm*, GluA2Q ΔNTD: 5.78 ± 0.75 spines/* 10 µm*, unpaired t-test: p=0.899). (**A2**) Homer1c puncta density is unchanged between GluA2 construct expressions (GluA2Q: 7.8 ± 2.0 puncta/* 10 µm*, GluA2Q ΔNTD: 7.8 ± 1.2 puncta/* 10 µm*, unpaired t-test: p>0.999). (**B**) Bar chart of dendritic spine density on untransfected and transfected cells (untrans.: 12.0 ± 0.7 (n = 8 cells); GluA2Q: 11.8 ± 0.6 (n = 8); GluA2Q ΔNTD: 12.2 ± 0.7 (n = 8); One-way ANOVA: p=0.916). Sample images are shown on the left. Scale bar = 2.5 µm. (**C**) Average paired-pulse ratio of neighbouring untransfected and transfected cells (untrans.: 1.98 ± 0.11 (n = 13); GluA2Q: 1.95 ± 0.10 (n = 6); GluA2Q ΔNTD: 2.04 ± 0.06 (n = 7); One-way ANOVA: p=0.876), with example traces from pairs of cells shown on the left. Scale bars = 20 ms and 30 pA. (**D**) AMPAR EPSC responses to* 20 Hz *train stimulation (5 pulses) normalised to amplitude of peak 1. Scale bar = 30 ms. Averaged data demonstrates no difference between GluA2 construct expressions (Pulse 5/1 ratio - GluA2Q: 2.27 ± 0.15 (n = 4), GluA2QΔNTD: 2.29 ± 0.05 (n = 3), untrans.: 2.00 ± 0.124 (n = 8)).*

centrations after stimulation 2 exceed those during stimulation 1 (Jackman and Regehr, 2017). Because of this, the probability of vesicle release is higher during the second stimulation, causing an increase in the measured postsynaptic current: paired-pulse facilitation (PPF). PPF is balanced in the presynaptic terminal by paired-pulse depression (PPD), a decrease in postsynaptic EPSC amplitude between two successive events. This is caused by a decrease in the availability of docked vesicles at the presynaptic membrane which can be released, due to recent exocytosis events. Two temporally close presynaptic action potentials could cause this effect (Jackman and Regehr, 2017). These processes are highly influential on the levels of short-term plasticity during rapid synaptic transmission.

To determine if any changes in presynaptic release probability occurred on postsynaptic GluA2 construct expression, two axonal simulations were delivered 50 ms apart (20 Hz) and postsynaptic EPSCs were recorded. No difference was observed in PPR between untransfected, GluA2Q or GluA2Q ΔNTD expressing cells (Figure 4.6C). To extend this experiment further, 5 pulse trains of postsynaptic EPSCs were induced at 20 Hz. Again, no significant difference was seen in postsynaptic amplitudes across the stimulations (Figure 4.6D). This data suggests that EPSC amplitude changes occur by a postsynaptic mechanism.

Studying spontaneous postsynaptic events

To characterise the postsynaptic changes in greater detail, mEPSCs were recorded from the GluA2 construct overexpressing cells (Figure 4.7A), by patch-clamp recording in the presence of tetrodotoxin (TTX) to block action potential induced release and APV and SR-95531 to inhibit NMDAR and $GABA_AR$ currents respectively, as used above.

In line with evoked EPSC data, spontaneous transmission was also dramatically impaired on NTD deletion. The average amplitude of mEPSC events was significantly reduced by GluA2Q ΔNTD expression when compared to either untransfected, or GluA2Q expressing cells (Figure 4.7B). The frequency of mEPSC events was also dramatically reduced in GluA2Q ΔNTD expressing cells when compared to full-length GluA2Q cells (Figure 4.7C1).

It is of interest to note that the amplitude of mEPSC events did not appear to increase on GluA2Q expression, as was recorded for evoked EPSC amplitudes (Figure 4.5B). While this observation could result from an interesting disparity between receptor populations activated by evoked and spontaneous transmission (Kavalali, 2015; Tang et al., 2016), mEPSC data requires careful analysis. Historically, changes in mEPSC frequency were ascribed

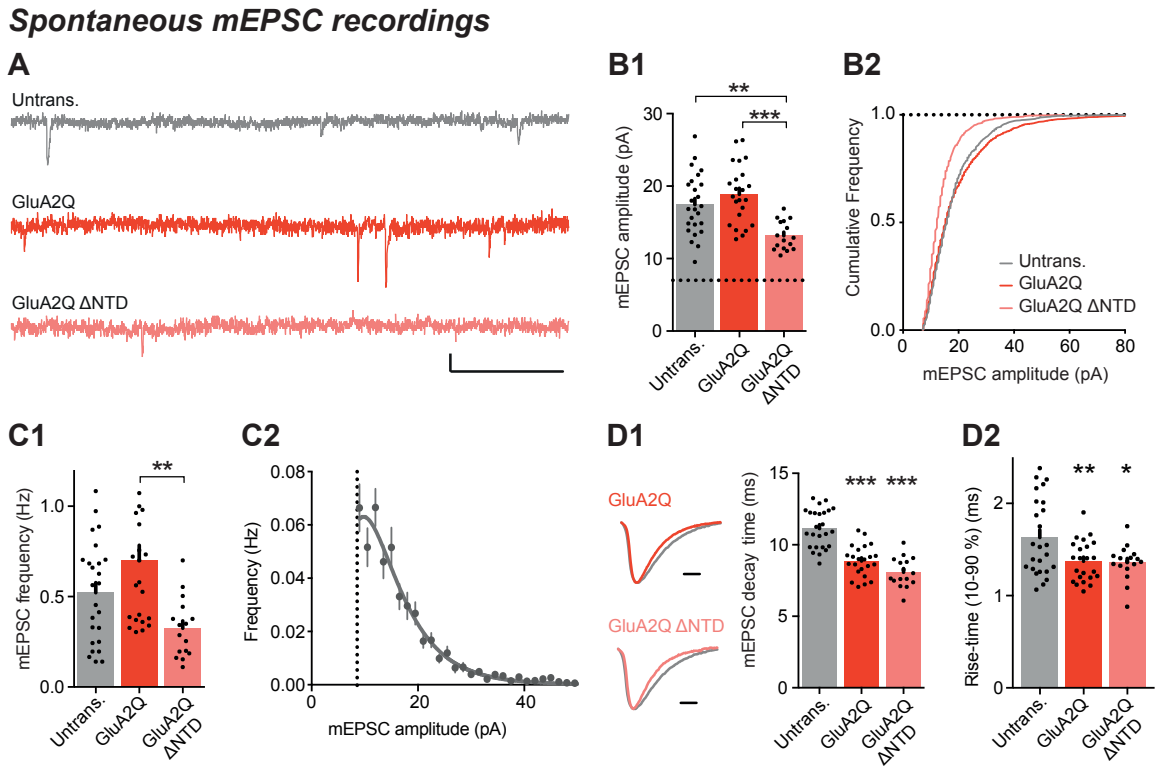

Figure 4.7 ***NTD-deleted GluA2 is detrimental to spontaneous transmission.*** *(**A**) Example traces of mEPSCs recorded from untransfected, GluA2Q and GluA2Q ΔNTD-expressing cells. Scale bar = 0.5 s, 5 pA. (**B1**) Bar chart of mEPSC amplitude with event detection limit indicated (dotted line) (untransfected: 17.5 ± 0.8 pA (n = 25 cells); GluA2Q: 18.9 ± 0.8 pA (n = 23); GluA2Q ΔNTD: 13.2 ± 0.5 pA (n = 16); One-way ANOVA, p<0.0001). (**B2**) Cumulative frequency distribution of mEPSC amplitude data from **B1**. (**C1**) Bar chart of mEPSC frequency (untransfected: 0.52 ± 0.06 Hz; GluA2Q: 0.70 ± 0.08 Hz; GluA2Q ΔNTD: 0.32 ± 0.04 Hz; One-way ANOVA, p=0.002). (**C2**) Frequency histogram of binned mEPSC amplitudes for untransfected cells showing that a substantial population of events occur below the detection limit. (**D1**) Example traces of scaled mEPSCs from untransfected (grey) and GluA2 construct-expressing cells. Scale bar = 3 ms. Bar chart shows cell averaged mEPSC decay times (untrans.: 11.14 ± 0.27 ms (n = 25); GluA2Q: 8.86 ± 0.23 ms (n = 23); GluA2Q ΔNTD: 8.08 ± 0.26 ms (n = 16); One-way ANOVA, p<0.0001). (**D2**) Bar chart of cell averaged mEPSC rise-time (untrans.: 1.63 ± 0.08 ms (n = 25); GluA2Q: 1.37 ± 0.05 ms (n = 23); GluA2Q ΔNTD: 1.36 ± 0.05 ms (n = 17); One-way ANOVA, p<0.0001).*

to presynaptic changes, caused by increased vesicle release probabilities, while changes mEPSC amplitude were explained by postsynaptic effects, such as increased postsynaptic receptor content. This model however, is oversimplified and changes in mEPSC amplitude and frequency require careful interpretation due to the event detection limit. Many mEPSC events can occur at amplitudes below the level of noise in a recording, and thus cannot be detected or analysed. This effect is demonstrated by plotting mEPSC amplitudes as a histogram (Figure 4.7C2), which shows that a large population of the skewed Gaussian distribution of events are hidden below the detection limit (7 pA in this example). A postsynaptic increase in event amplitude will cause previously sub-threshold events to be detected, and therefore, while the average event amplitude may not change, this would instead be represented as an increase in mEPSC frequency. Such postsynaptic effects on mEPSCs have been noted in previous studies (Gutierrez-Castellanos et al., 2017b; Lu et al., 2009; Rumbaugh et al., 2006). As expression of GluA2Q shows an apparent increase in mEPSC frequency (Figure 4.7C1), and the proportion of large mEPSC events appears selectively increased (Figure 4.7B2), an increase in mEPSC amplitdue most likely explains the difference between evoked and spontaneous amplitude changes on GluA2Q expression.

mEPSC decay kinetics were unaffected by NTD deletion (Figure 4.7D), however overexpression of either GluA2Q construct altered the kinetics of responses similarly when compared to untransfected cell responses. This can be explained by the difference in kinetics between homomeric GluA2Q channels, and the endogenous GluA1/2 heteromeric receptors, which has been observed previously for mEPSC events after GluA1 deletion (Lu et al., 2009).

Non-stationary fluctuation analysis of mEPSCs

As suggested earlier, one possible explanation for the impact of GluA2Q ΔNTD expression on synaptic current amplitudes is that such channels have a very low single-channel conductance due to NTD deletion. Single-channel conductance (γ) can be calculated from mEPSC data by analysis of variance between individual events (Benke et al., 2001; Hartveit and Veruki, 2007; Robinson et al., 1991). The profile of an AMPAR EPSC is a product of multiple single-channel conductances (Benke et al., 2001; Smith and Howe, 2000). At the peak current, the maximum number of receptors are open. The decay phase of the response is caused not by gradual closing of all receptors, but non-synchronised deactivation of a subset of receptors. As receptor deactivation is probabilistic, each mEPSC event will have a subtly different shape, varying from the average mEPSC to a different degree in each individual case. If the event is composed of fewer receptors each with a greater single-channel conduc-

tance, the variability will be increased. Thus, variance analysis or non-stationary fluctuation analysis (NSFA) of mEPSC event decay allows calculation of receptor conductance.

NSFA was conducted on mEPSC recordings from cell populations, following Hartveit and Veruki (2007), using a custom Matlab script written by Dr Andrew Penn (U. Sussex). mEPSCs were identified using a template-based search and were visually screened before inclusion in analysis. All recordings were subject to stability analysis to confirm that no temporal changes occurred during the recordings, which could skew or falsify future calculations. Event amplitude, rise-time and decay time were plotted as a function of event number; the chronological order of event occurrence (Figure 4.8A). Spearman Rank Correlation Coefficient was calculated in each case, and cells with significant correlations in any parameter were discarded.

The morphology of neuronal projections has a detrimental impact on patch-clamp recordings. Long, thin dendritic projections act as a resistor in series between the synaptic event and the recording electrode, located at the cell body. This can cause distance-dependent filtering of synaptic events, misrepresenting their true kinetics on detection (Hartveit and Veruki, 2007). Given that NSFA utilises the variation in the decay phase of mEPSC events, filtering would have serious consequences for the validity of the analysis. For this reason, the extent of dendritic filtering was assessed. Such filtering would result in a decrease in mEPSC amplitude, and slowing of both rise and decay kinetics (Hartveit and Veruki, 2007; Jonas et al., 1993). Therefore, the amplitude vs rise-time (Figure 4.8B1), rise-time vs decay slope (Figure 4.8B2) and amplitude vs decay time (Figure 4.8B3) were plotted for each cell recorded. A positive correlation between amplitude and rise-time or rise-time and decay slope would be indicative of electrotonic filtering of a subset of mEPSCs and therefore any cells in which this was observed were discarded. Figures 4.8A and B depict these plots for one example of a GluA2Q expressing cell. Figure 4.8B3 shows a significant positive correlation between mEPSC amplitude and decay time, however such a correlation is the *opposite* of what would be expected due to filtering, and most likely results from channel or synaptic properties.

Usually variance of peak amplitude at a single synapse would allow calculation of the receptor open probability (P_o). However, mEPSCs cannot feasibly be recorded from the same synapse, due to the lack of control over their induction, and therefore instead the population of mEPSCs from all synapses is analysed. In such a case however, a great deal of variance is introduced by differences between synapses, for example because of different receptor

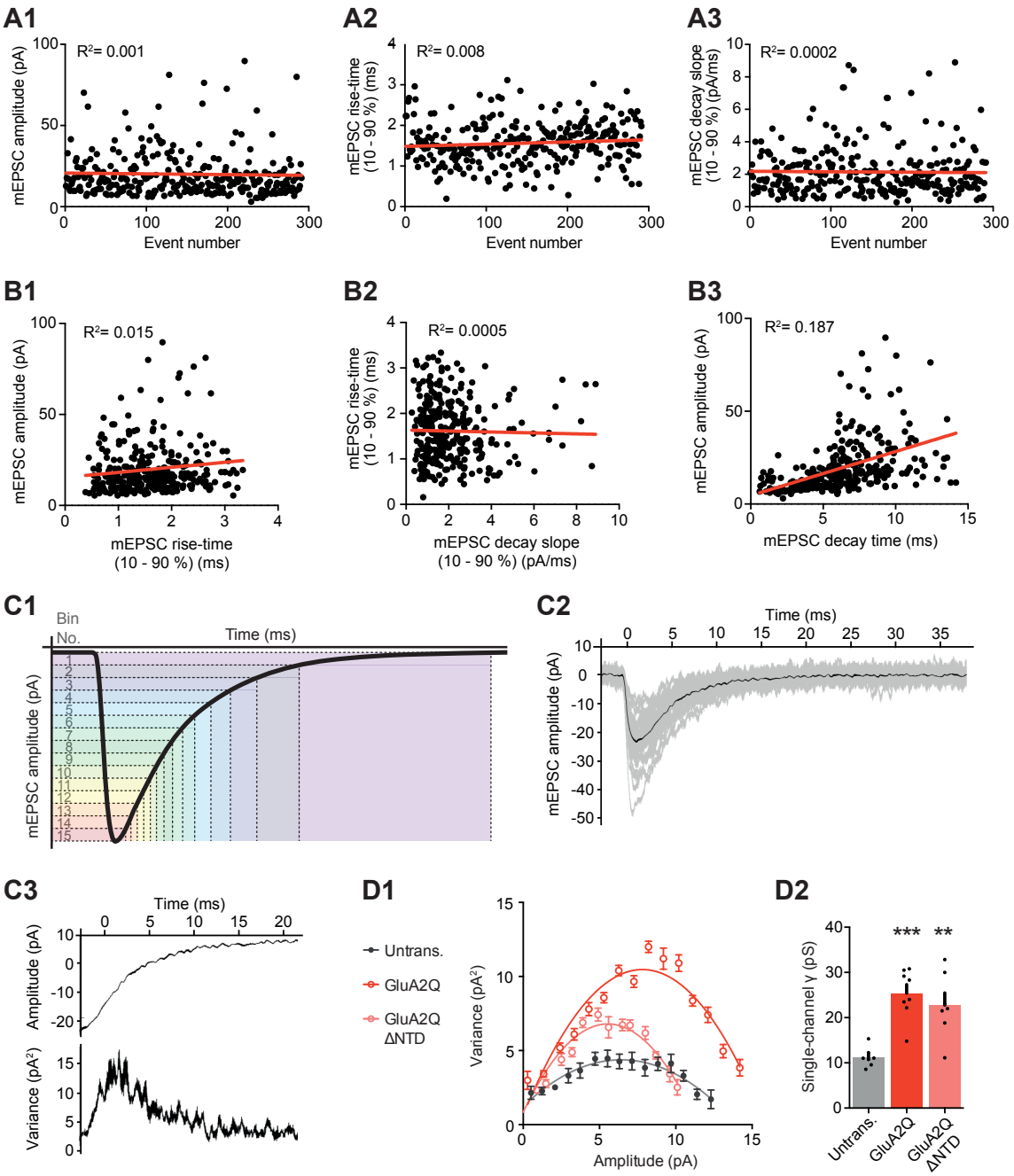

Figure 4.8 ***Non-stationary fluctuation analysis from mEPSC data for single-channel conductance calculation.***

Figure 4.8 ***Non-stationary fluctuation analysis (NSFA) from mEPSC data for single-channel conductance calculation.*** *(**A**) Plot of mEPSC event amplitudes (**A1**), rise-times (**A2**), and decay slopes (**A3**), in order of event occurrence demonstrates recording stability. Lack of correlation between mEPSC amplitude and rise-time (**B1**) and mEPSC rise-time and decay-slope (**B2**) confirm that data is unaffected by electrotonic filtering. Slight positive correlation between mEPSC amplitude and decay time (**B3**) is the opposite of what would be expected due to filtering. (**C1**) Decay-phase data from peak-scaled mEPSC data are binned in 15 bins with equal amplitude, corresponding to variable sized time bins. (**C2**) Example data prior to peak-scaling depicting average mEPSC (black) and individual mEPSC events (grey). (**C3**) Variance between individual mEPSCs and average mEPSC prior to binning shows greatest variance during the steepest phase of decay. (**D1**) Averaged amplitude - variance plot post-binning has a parabolic distribution. Single channel conductance (γ) is proportional to the initial gradient of parabolic fit. Example data from representative GluA2Q, GluA2Q ΔNTD and untransfected cells. (**D2**) Synaptic AMPAR single-channel current is increased on GluA2Q construct expression independent of the NTD (untransfected: 11.2 $\pm$ 0.82 pS (n = 7); GluA2Q: 25.4 $\pm$ 1.92 pS (n = 8); GluA2Q ΔNTD: 22.8 $\pm$ 2.70 pS (n = 7); One-way ANOVA, p=0.0002).*

contents, thus preventing accurate single-channel conductance calculation (Figure 4.8C2). To circumvent this, mEPSC events must be scaled to the same peak amplitude (that of the average mEPSC). While this allows single-channel conductance calculation, the P_o can no longer be obtained.

For a single synapse, the greatest variance between mEPSCs occurs during the steepest phase of decay, due to the maximal variation in the number of channels open (Figure 4.8C3). Therefore higher sampling of such regions provides more accurate quantification of channel conductance (Hartveit and Veruki, 2007). For this reason, variance data is binned by dividing the amplitude into equally sized segments, corresponding to different temporal segments (Figure 4.8C1). For the present study, 15 bins were used. The variance vs amplitude relationship was plotted for each cell, which was fitted with a parabolic curve of the equation:

$$\sigma^2(I) = iI - \frac{I^2}{N} + \sigma_b^2$$

Increased single-channel conductance would cause greater variation across the same event amplitude, and thus affects the initial gradient of the fitted parabola. The single channel current (i) is proportional to the initial parabolic gradient. Single-channel conductance can be calculated from i according to the equation:

$$\gamma = \frac{i}{(V_m - E_{\text{rev}})}$$

where membrane potential (V_m) and reversal potential (E_{rev}) were -60 mV and 0 mV respectively.

Example parabolas are presented in Figure 4.8D1. The average single-channel current was doubled on expression of GluA2Q, as would be expected from previous studies (Swanson et al., 1997), yet was no different between GluA2Q constructs (Figure 4.8D2). Therefore, deletion of the GluA2 NTD does not appear to affect channel conductance, and cannot explain the dramatically reduced synaptic currents observed on GluA2 ΔNTD expression.

From the accumulated evidence presented above, the most likely explanation for the difference in synaptic transmission between NTD containing and NTD lacking AMPARs is a differential accumulation of receptors at the postsynapse. The AMPAR NTD therefore likely plays a critical role in synaptic receptor anchoring.

4.2.6 Imaging the role of the NTD in synaptic anchoring

FRAP of SEP-tagged receptors

A body of accumulating evidence demonstrates that AMPAR trafficking is not a static system and instead receptors dynamically exchange between synaptic and extrasynaptic sites (Ashby et al., 2006; Choquet and Triller, 2013; Makino and Malinow, 2009). A combination of specific and non-specific (Li et al., 2016) protein interactions appear to maintain a stable population of receptors opposite vesicle release sites, which contribute to transmission (Tang et al., 2016). This lateral diffusion has been demonstrated to be of consequence for both short-term (Heine et al., 2008) and long-term plasticity (Makino and Malinow, 2009; Penn et al., 2017). The AMPAR NTD appears to have a role in controlling receptor anchoring at synaptic sites. Its removal could prevent protein interactions and therefore limit trapping of diffusing receptors.

To study the effect of NTD removal on receptor mobility, a fluorescence recovery after photobleaching (FRAP) assay was employed. Super-ecliptic pHluorin (SEP) is a derivative of GFP which is sensitive to the pH of the local environment (Miesenböck et al., 1998; DNA kindly provided by Dr Jonathan Hanley, Bristol). At neutral pH, SEP is fluorescent, however at low pH the protein is poorly fluorescent. Therefore, SEP-conjugation to a protein of interest allows selective visualisation of a subset of proteins in particular cellular compartments (Figure 4.9A). By conjugating SEP to the N-terminus of the AMPAR, surface receptors will fluoresce, while intracellular receptors contained in recycling endosomes will be quenched by the low pH. By bleaching the AMPAR fluorescence in a spine head and monitoring the fluorescence recovery over time, the relative mobility of surface receptors on NTD deletion can be monitored (Figure 4.9B). This approach has been successfully used to study AMPAR trafficking on multiple occasions (Ashby et al., 2006; Kerr and Blanpied, 2012; Makino and Malinow, 2009).

While imaging of SEP-tagged AMPARs in organotypic slices has been performed previously (Makino and Malinow, 2009), imaging deep in tissue requires two-photon imaging to overcome light scattering effects. As such a setup was not available for this experiment, FRAP was performed in dissociated hippocampal cultures, which are more amenable to confocal imaging. Expression of both N-terminally tagged GluA2Q and GluA2Q ΔNTD in dissociated hippocampal cultures showed dendritic localisation, with enrichment in dendritic spines (Figure 4.9C). Spine heads or equivalently sized areas of dendritic branch were

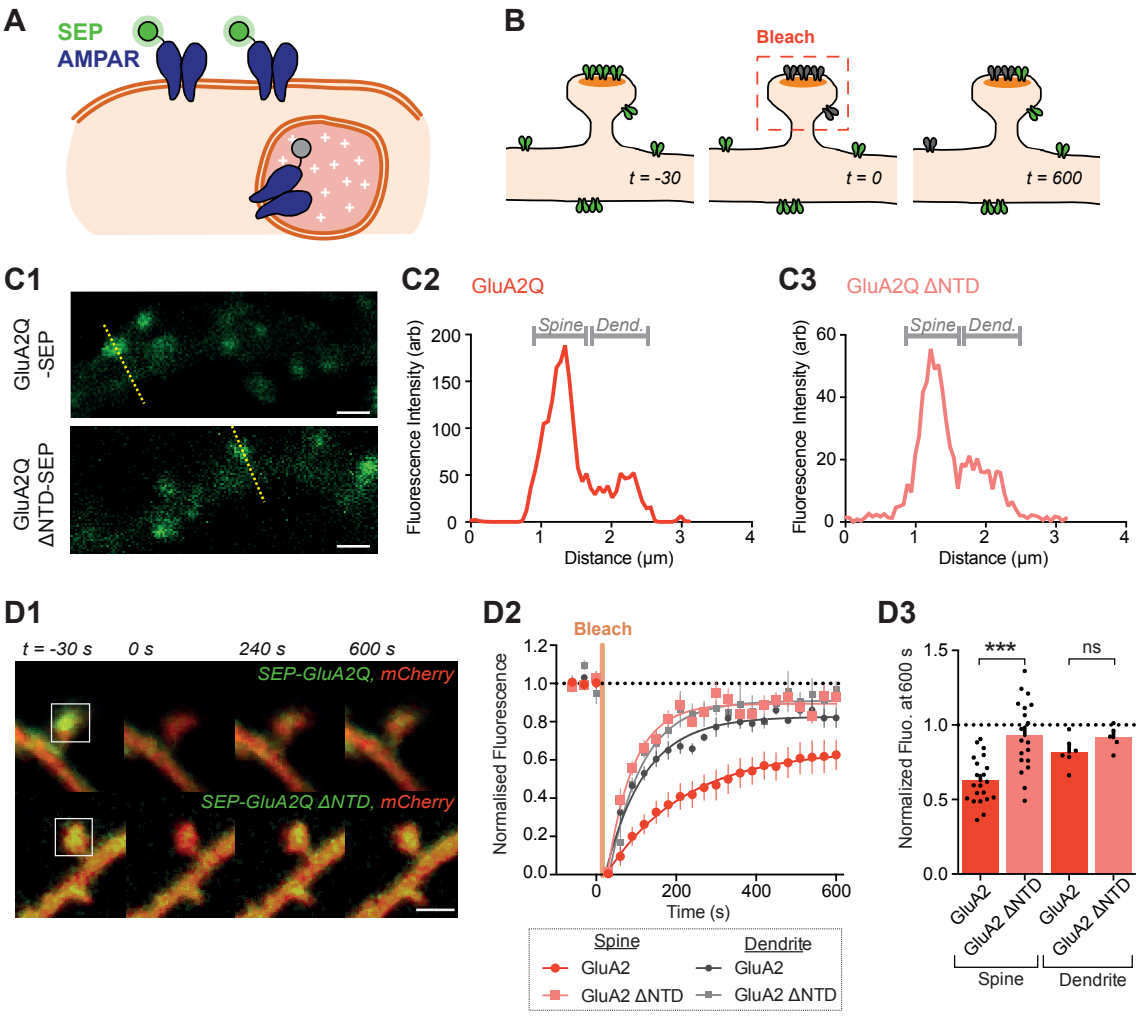

Figure 4.9 ***FRAP analysis of AMPAR mobility.*** *(**A**) Super-ecliptic pHluorin (SEP) protein fluorescence is quenched in intracellular compartments with low pH, allowing selective surface-localised protein visualisation. (**B**) FRAP procedure: AMPAR-SEP fluorescence is bleached in a spine head and recovery is monitored over time (t). Increased receptor mobility and dendrite to spine exchange is measured by increased fluorescence recovery. (**C1**) Example images of cells expressing SEP-GluA2Q ± NTD. Scale bar = 1 μm. (**C2-3**) Line profiles (yellow line in **C1**) show spine enrichment of both constructs. (**D1**) Spine FRAP example images where t = 0 indicates time and square indicates location of photobleaching. Red: cytosolic mCherry; green: SEP fluorescence. Scale bar = 1 μm. (**D2**) SEP fluorescence over time in bleached regions of dendrite or spine, normalised to pre-bleaching fluorescence. Orange vertical line indicates onset of photobleaching (time constant of fit τ: spine GluA2 = 197.3, spine GluA2 ΔNTD = 65.4, dendritic GluA2 = 98.1, dendritic GluA2 ΔNTD = 83.1). (**D3**) Fluorescence at 600 s averaged by cell shows greater recovery for GluA2Q ΔNTD than full-length GluA2Q (spine GluA2Q: 0.63 ± 0.03 (n = 22 cells); spine GluA2Q ΔNTD: 0.93 ± 0.05 (n = 19); dendrite GluA2Q: 0.80 ± 0.04 (n = 6); dendritic GluA2Q ΔNTD: 0.92 ± 0.04 (n = 5); One-way ANOVA, p<0.0001).*

bleached by repetitive imaging and the recovery was monitored over 600 s. Coexpression of AMPAR constructs with a cytosolic mCherry expressing plasmid allowed visualisation of cell morphology throughout the experiment.

SEP-GluA2Q spine fluorescence recovered partially over the course of imaging (Figure 4.9D1), demonstrating that a subset of receptors (~40 %) were immobile over the imaging time period (Figure 4.9D2-3). This observation is in line with previous studies (Kerr and Blanpied, 2012; Makino and Malinow, 2009; Zhang et al., 2013). Conversely, SEP-GluA2Q ΔNTD fluorescence recovered rapidly (τ_{rec}= 65 s cf. 197 s for GluA2Q) and almost completely (7 % immobile) (Figure 4.9D2-3). Receptor mobility could increase on NTD deletion due to smaller protein bulk having lower steric hindrance. To investigate this effect, regions of dendrite were bleached and FRAP was monitored. For dendritic regions, both receptors exhibited rapid and complete recovery, which was not significantly different. Moreover, diffusion in dendrites of SEP-GluA2Q resembled the behaviour of spine localised SEP-GluA2 ΔNTD (Figure 4.9D3). Thus, NTD-deleted receptors are poorly confined in spines, supporting the hypothesis that the NTD plays a role in specifically stabilising AMPARs at postsynaptic sites.

Super-resolution imaging of receptor clusters

The advent of super-resolution imaging has allows unprecedented study of synapses (Dani et al., 2010). Conventional confocal microscopy is limited by diffraction of light. This diffraction limit is calculated as:

$$\textit{Diffraction limit} = \frac{\lambda}{2.NA}$$

where λ denotes the wavelength of light and NA is the numerical aperture of the microscope objective. In practice, this means that objects smaller than the diffraction limit cannot be imaged accurately, and separate objects closer than this limit cannot be resolved separately. For example, imaging EGFP on a confocal microscope using a standard 63X oil-immersion objective (NA $\approx$ 1.4):

$$\textit{Diffraction limit} = \frac{480\,\text{nm}}{2 \times 1.4} = 171\,\text{nm}$$

AMPAR nanodomains have been reported as around 80 - 100 nm in diameter (MacGillavry et al., 2013; Nair et al., 2013), and therefore cannot be properly investigated using conventional light microscopy.

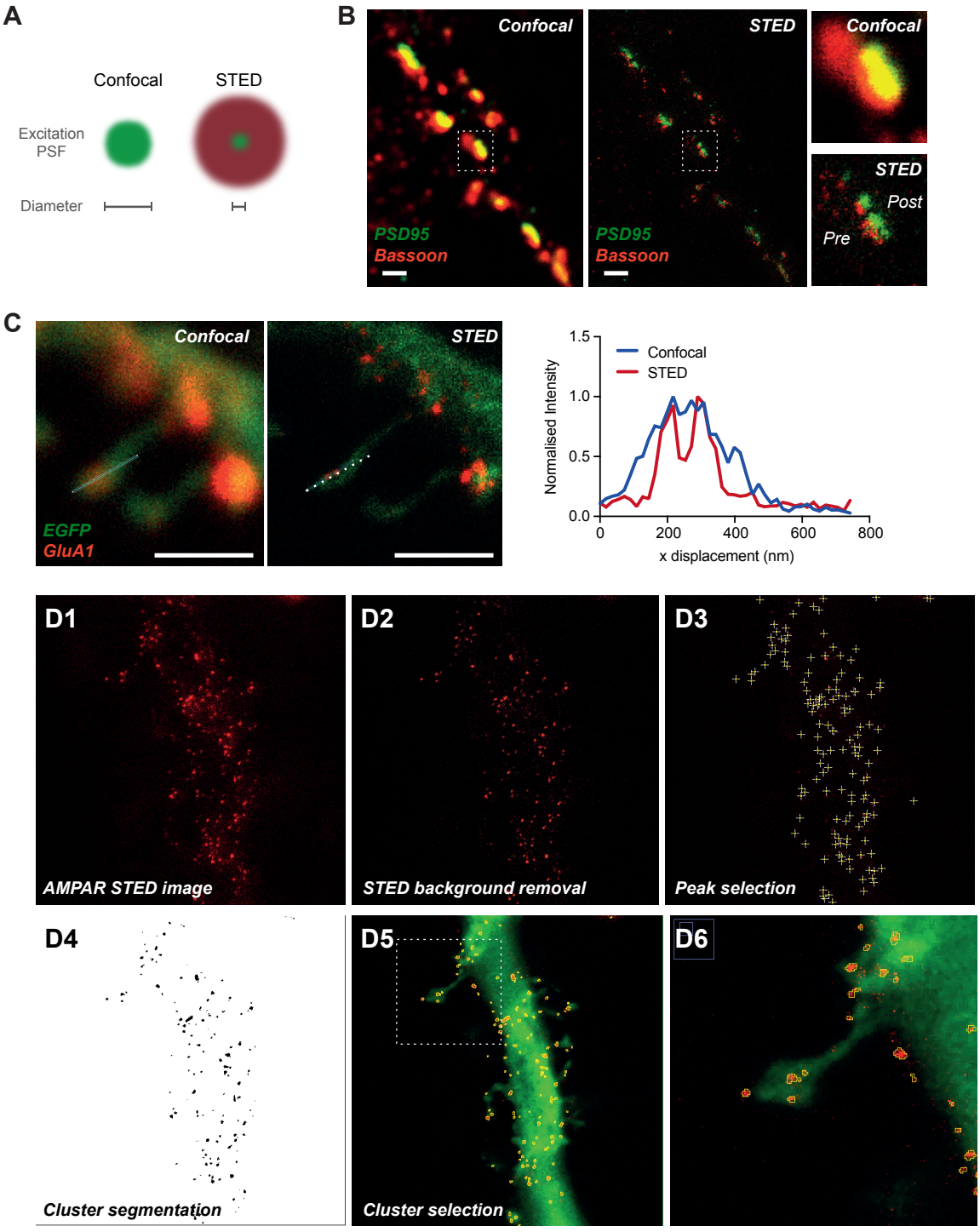

Figure 4.10 ***STED microscopy experimental procedure and example images.***

Figure 4.10 ***STED microscopy experimental procedure and example images.*** *(**A**) Confocal imaging excitation spot has a diffraction limited point-spread function (PSF, green). STED can overcome this limitation by using a torus shaped depletion laser (red) to allow excitation of a smaller volume. (**B**) Example images of two-colour synaptic STED imaging. Postsynaptic PSD95 (green) and presynaptic Bassoon (red) are seen as spatially separated using STED but not diffraction-limited confocal imaging. Box indicates location of magnified image (right). Scale bar = 1 µm. (**C**) STED microscopy can resolve separate AMPAR (GluA1) nanoclusters spatially separated by* 300 nm *which are seen as a single spot by confocal imaging (green: cytosolic EGFP for cell visualisation, red: surface GluA1 staining). Line indicated line-profile location. Scale bar = 1 µm. (**D**) Procedure for selection and analysis of AMPAR clusters in STED microscopy images. 2D images (**D1**) are background corrected by subtraction of image acquired with STED beam only (no excitation laser) (**D2**), before local peak intensity selection (**D3**) and intensity threshold based image segmentation (**D4**). Individual clusters are isolated and quantified for size and fluorescence intensity (**D5**). White box indicates location of enlarged image (**D6**).*

One approach to overcome the diffraction limit is STED (Stimulated Emission Depletion) microscopy. Fluorescence excitation provides energy to excite the electrons of a fluorophore to a high energy state. The relaxation of this fluorophore releases that energy as a photon, which is the detected fluorescence of a microscopy image. STED microscopy uses a second laser at a specific wavelength to deplete the high energy state, thereby preventing fluorescence. By shaping this STED laser as a torus or 'doughnut' in line with the excitation beam, the actual diameter of excitation can be reduced to below the diffraction limit (Figure 4.10A).

Applying this approach to synaptic imaging allows resolution of pre and postsynaptic proteins (Figure 4.10B), which are separated by just 80 nm (Dani et al., 2010). By transfecting c-myc tagged AMPAR subunits into dissociated hippocampal neurons, STED imaging can reveal their subsynaptic localisation within a dendritic spine (Figure 4.10C). In Figure 4.10C, two AMPAR clusters, spatially separated by 100 nm are seen as a single object using conventional confocal imaging, however are clearly separate when imaged using STED.

As the AMPAR NTD is required for ensuring receptor contribution to synaptic transmission, it is possible that the domain has a role in either clustering receptors at the postsynapse, or, given that it protrudes into the synaptic cleft, could facilitate alignment with presynaptic release sites. STED microscopy was employed to image the synaptic localisation of GluA2 upon NTD deletion.

Plasmids encoding GluA2Q and GluA2Q ΔNTD containing extracellular c-myc epitopes were transfected into dissociated hippocampal cultures alongside a Homer1c-EGFP expressing plasmid to visualise synaptic sites. Cells were stained live with an anti-myc antibody to label only surface receptors, of which synaptic receptors will be a sub-population. After fixation an AF568 conjugated secondary antibody was applied to visualise receptors. The procedure for analysis of STED images is depicted in Figure 4.10D. Unexpectedly, imaging cultures with the STED beam but no excitation laser active produced a weak but detectable image of the AF568 dye. For this reason, images with and without excitation laser were acquired, and this 'background' signal was subtracted (Figure 4.10D2). Peaks in fluorescence intensity were detected (Figure 4.10D3), and a threshold based segmentation approach was used to detect local areas of strong fluorescence around peaks (Figure 4.10D4).

AMPAR clusters were clearly observed both within spine heads and along the dendritic

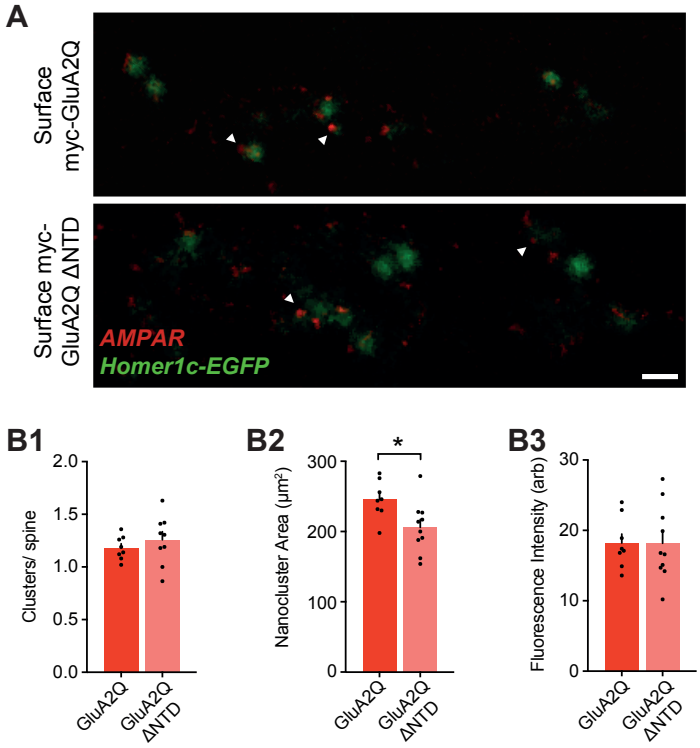

Figure 4.11 ***STED imaging of GluA2 construct expressing dissociated hippocampal neurons.*** *(**A**) Example images of cells expressing Homer1c-EGFP (green) and stained for surface overexpressed GluA2Q or GluA2Q ΔNTD receptors. Arrows indicate synaptic AMPAR clusters. Scale bar = 1 µm. (**B1**) No difference in the number of AMPAR clusters per spine (GluA2Q: 1.18 ± 0.04 (n = 8 cells), GluA2Q ΔNTD: 1.25 ± 0.07 (n = 10), unpaired t-test: p=0.445) or fluorescence intensity per cluster (GluA2Q: 18.2 ± 1.3 (n = 8), GluA2Q ΔNTD: 18.2 ± 1.7 (n = 10), unpaired t-test: p=0.992) were observed, however a GluA2Q ΔNTD receptor clusters appeared slightly smaller (GluA2Q: 246.0 ± 1.0 µm^2 (n = 8), GluA2Q ΔNTD: 206.0 ± 1.1 µm^2 (n = 10), unpaired t-test: p=0.020).*

surface (Figure 4.10D5-6). Both GluA2 constructs showed a punctuate, clustered distribution throughout the cell (Figure 4.11A). Quantification of the number of receptor clusters within spine heads showed no difference between conditions, both constructs giving an average of approximately 1.2 clusters (GluA2Q: 1.18, GluA2Q ΔNTD: 1.25) (Figure 4.11B1). Similarly, the fluorescence intensity of clusters, which is proportional to the receptor content, was also unaffected by NTD deletion (Figure 4.11B3). However, the size of synaptic clusters on NTD removal was decreased by a statistically significant amount (Figure 4.11B2). The data presented here is the result of one dissociated culture preparation and therefore requires further investigation to confirm the validity of this finding, yet is indicative that the increased mobility of NTD-deleted GluA2 may result in fewer clustered receptors at synaptic sites.

4.3 Discussion

Despite their initial characterisation almost 30 years ago (Keinänen et al., 1990), the function of the AMPAR's N-terminal domain has remained largely elusive. The domain has a well described role in receptor assembly (Ayalon and Stern-Bach, 2001; Herguedas et al., 2013; Jin et al., 2009; Rossmann et al., 2011), yet no major effects on channel operation have been reported (Möykkynen et al., 2014) despite a hypothesised allosteric potential to influence receptor gating (Krieger et al., 2015). The fact that the domain represents almost 50 % of receptor mass and projects into the synaptic cleft raises interesting questions as to why its function has not been investigated sooner.

The mechanisms controlling AMPAR anchoring at the synapse have been studied for many years, with a great focus on the intracellular CTDs (Shepherd and Huganir, 2007). This focus was likely a result of their localisation in the postsynaptic density, interactions with which would logically facilitate synaptic anchoring. The interaction of TARPs with PSD-95 is the best characterised anchor (Schnell et al., 2002), however TARPs can also interact with other postsynaptic proteins via their C-terminal 'TTPV' motif (Dakoji et al., 2003; Deng et al., 2006). Cais et al. (2014) reported that interactions between the NTD and the extracellular loops of TARPs influence the TARP's modulation of channel gating, and therefore theoretically, deletion of the AMPAR NTD could negatively affect the affinity for complex formation, and as a result of this, impair AMPAR synaptic anchoring by significant disruption of its interactions with the postsynaptic density. However, the strongest associations between the receptor and TARPs occurs in through their transmembrane domains (Twomey et al., 2016; Zhao et al., 2016) and NTD interactions wit TARPs are likely to be possible only when the receptor samples a 'bent' conformation (García-Nafría et al., 2016a; Krieger et al., 2015; Nakagawa et al., 2005). By assessing the response ratio to agonists glutamate and kainate, it is clear that NTD deletion has little to no impact on complex stability, and therefore the impaired synaptic anchoring observed on NTD removal most likely occurs through direct interactions with this domain.

The surface recordings presented above offer interesting insights into the effect of receptor overexpression. The amplitude of surface patches, while not a statistically significant effect due to the variability in such data, was apparently doubled. The surface RI is extremely rectifying upon GluA2Q overexpression, indicating that the vast majority of surface receptors are exogenous channels. Therefore, the amplitude 'doubling' could be explained by the

increased channel conductance of GluA2Q receptors, as previously described (Swanson et al., 1997) and confirmed by NSFA in this study. Both of these results suggest that exogenous receptors predominantly *replace* endogenous ones on the cell surface, rather than add to them. Does this result infer that endogenous receptors outcompete endogenous ones in the trafficking pathway?

Kessels et al. (2009) performed an in-depth analysis of the effect of receptor overexpression. They suggest that overexpressed AMPARs, while increasing the somatic cytosolic and dendritic intracellular receptor pools substantially, it did not affect the amount of receptors either on the surface of the soma or dendrite to as great an extent. The exogenous receptor exchange observed in this study supports their findings. Overexpression of TARPs increases the surface AMPAR responses to bath applied glutamate, which has been suggested to result from increased receptor trafficking. Such a model would indicate that TARPs are the limiting factor in AMPAR surface trafficking and would explain the exogenous/endogenous receptor exchange observed here for GluA2Q expression. However, Kessels et al. (2009) demonstrate that the increase in AMPAR currents on TARP overexpression is due to alleviation of surface AMPAR desensitisation, rather than increased receptor trafficking. This result has significant consequences. Firstly, it indicates that surface AMPARs are not fully saturated with TARPs under normal conditions, as has been more recently suggested (Shi et al., 2009). Secondly, it means that AMPAR surface trafficking is not limited by TARPs. If AMPAR surface levels are not increased by either TARP or AMPAR overexpression, it can be concluded that other factors, for example cornichon proteins (Schwenk et al., 2009) or CTD interactors such as NSF (Hanley et al., 2002; Kessels et al., 2009) may control this trafficking. The significance of control over surface AMPAR levels cannot be overstated, given the apparently essential requirement for a diffusible surface receptor pool in synaptic potentiation (Granger et al., 2013; Penn et al., 2017).

The increase in AMPAR EPSCs on GluA2Q overexpression is most likely a result of the increased conductance of Q-pore receptors, as seen by NSFA and described above for surface AMPAR currents. However, this increase is not the doubling which is observed for surface currents, suggesting that despite first impressions of the phenomenon, the actual number of receptor channels responding at the synapse is lower in GluA2Q transfected than untransfected cells. Strikingly, GluA2Q ΔNTD transfection, whereby currents appear 3 times lower than GluA2Q transfected cells, must result in dramatically greater reductions in the number of responding channels.

The increased mobility of GluA2 on NTD removal, as seen by FRAP analysis is in line with the increased mobility of AMPARs caused by altered synaptic anchoring in other studies (Bats et al., 2007). While non-specific interactions also appear to facilitate the retention of proteins at the postsynaptic density (Li et al., 2016), the mobility of GluA2 receptors were no different in dendritic regions, suggesting that the altered mobility is not a result of reduced protein mass, but more likely is explained by specific interactions of the NTD. Receptor diffusion has been shown to affect short term plasticity of AMPAR responses (Heine et al., 2008). One could expect that NTD deletion would also represent changes in such assays, however no difference in response amplitudes was seen on train stimulation between GluA2 expressing cells. While this result does not apparently fit with the 'increased mobility' model of GluA2 ΔNTD action, there are many competing factors with affect the synaptic response to train stimulation, such as paired-pulse facilitation, depression, AMPAR desensitisation and deactivation and cleft glutamate clearance. Therefore, given that the majority of these factors will be unchanged between GluA2Q and GluA2Q ΔNTD expression, the effect of mobility on train responses may have only a minor influence, and therefore was undetected in this study.

Imaging of receptor localisation showed no gross differences on NTD deletion. Both GluA2Q and GluA2Q ΔNTD were present on the surface of both dendrites and spines in equal levels, indicating that the effect on synaptic transmission is not simply due to impaired dendritic trafficking. In fact, given that receptor clusters appeared only slightly affected on NTD deletion, it is possible that NTD dependent interactions are most important for alignment of the receptor with presynaptic release sites, rather than postsynaptic localisation, or intrinsic receptor clustering. A more in depth super-resolution imaging study would be required to investigate such a hypothesis.

The GluA2 NTD was suggested to have a spectacular effect on synaptogenesis in dissociated hippocampal cultures (Passafaro et al., 2003). Passafaro and colleagues reported that overexpression of GluA2 dramatically increased both spine density and spine size, in a mechanism entirely dependent on the NTD and independent of channel function. GluA1 with the GluA2 NTD replacing its own, GluA2Q or GluA2R all increased spine density, and even a single-pass transmembrane domain presenting the GluA2 NTD alone produces the same effect (Saglietti et al., 2007). Expression of GluA2 ΔNTD or siRNA knockdown of GluA2 produced the opposite effect, reducing spine density, while surprisingly, transfection of

GluA2 into aspiny interneurons, which do not normally express GluA2 or produce dendritic spines, caused spine production (Passafaro et al., 2003). This finding is of great significance to understanding spine formation, and therefore has subsequently gained further attention. If the GluA2 NTD harbours synaptogenic function, one would expect that knockout of GluA2 would decrease synapse density, however this is not the case (Lu et al., 2009; Medvedev et al., 2008; Sans et al., 2003). Overexpression of GluA2 in cortical cultures had no effect on spine density (Chen et al., 2009) and separate studies in hippocampal cultures using GluA2 knockdown (Tracy et al., 2011) or knockout (Biou et al., 2008) saw no effect on spine density in hippocampal cultures. As detailed in the present study, overexpression of either full-length GluA2 or GluA2 ΔNTD had no effect on spine density, and therefore given the accumulated evidence, it appears prudent to conclude that the NTD of GluA2 has either minimal or no synaptogenic function.

Despite the lack of reproducibility surrounding Passafaro et al. (2003), there are interesting parallels between their results and this study. Passafaro et al. (2003) report not only spine density changes, but also an increase and decrease in spine size (length and width) on expression of GluA2 or GluA2 ΔNTD respectively. The effect of GluA2 on changes in spine dimensions are not as well studied as those in spine density. However, Medvedev et al. (2008) report that spines in GluA2 knockout animals are smaller in volume, post-synaptic densities are less complex and 'mature' mushroom spines are lower in abundance. Such a result is best explained by the reduction in AMPAR transmission caused by GluA2 knockout (Jia et al., 1996), as the correlation between spine size and AMPAR content is well established (Matsuzaki et al., 2004). However, this does not exclude an NTD-dependent role in spine size regulation, as Passafaro et al. (2003) suggest. The effects of GluA2 and GluA2 ΔNTD overexpression on organotypic EPSCs presented in this study are most likely a result of altered synaptic receptor content, yet mirror the changes in spine size reported by Passafaro et al. (2003), and therefore assessing whether these manipulations affect spine volume in organotypic slices would be an interesting experiment. A mechanism whereby reduced receptor anchoring through NTD removal causes a reduction in spine volume by reduced receptor activation could be envisaged, but would be opposite to the expected result of homeostatic plasticity, which would upscale the AMPAR content of weakly transmitting synapses (Turrigiano, 2012). Homeostatic plasticity may also be impaired on GluA2 NTD removal, by limiting receptor synaptic anchoring, especially given the importance of this subunit in such mechanisms (Ancona Esselmann et al., 2017). Further study into the interplay of receptor anchoring, homeostatic scaling and spine volume would certainly be required to

unravel these observations.

Reports have suggested a synapse-stabilising role for the AMPAR NTD. Ripley et al. (2011) demonstrated that the GluA2 NTD increases the stability of presynaptic connections to dendritic spines, and also increases the formation of presynaptic areas in contact with GluA2-NTD presenting HEK293 cells. Their data supports a structural role for the domain, through protein interaction, rather than a role involving signalling through GluA2 receptor channel activation. Tracy et al. (2011) also suggest a role in synaptic organisation for the AMPAR NTD, independent of channel activity. Presynaptic termini maturation appeared to be triggered by the AMPAR NTD, which hypothetically involve a transsynaptic interaction. No obvious effect of the GluA2 NTD on presynaptic function was observed in the present study, however this was not studied in great detail, although interactions between the NTD an synaptic cleft proteins would be well placed to alter presynaptic function.

The requirement for NTD-dependent interactions in AMPAR synaptic anchoring is evident from the data presented above, however the details of the protein interactions are as yet unknown. One key question to address will be the origin of the NTD binding partner involved. This interactor could be physically attached to either the pre or postsynaptic membrane (acting in *cis* or *trans*), could already form a transsynaptic connection to which the AMPAR associates, or could be a soluble, secreted factor.

Comparison with other iGluR family members may offer clues to this mechanism. GluRδ, a non-conducting receptor forms a transsynaptic connection between pre and postsynapse by binding of the secreted factor cerebellin to its NTD, which in turn interacts with presynaptic neurexin (Elegheert et al., 2016; Matsuda et al., 2010). This complex has significant signalling function, whereby D-serine binding to GluRδ induces an intracellular signalling cascade to induce AMPAR endocytosis. Importantly, this function only occurs with an intact transsynaptic interaction, demonstrating transsynaptic signalling through NTD interactions (Elegheert et al., 2016). A surprisingly similar complex appears to control kainate receptor function (Matsuda et al., 2016). Binding of C1ql2/3 to the postsynaptic GluK2 NTD and to presynaptic neurexin anchors the receptor at postsynaptic sites, in a manner highly reminiscent of the GluD complex. Given that such an arrangement has now been described for two of the four iGluR family members, it is tempting to suggest that such a transsynaptic arrangement could exist to maintain synaptic AMPARs in an NTD-dependent manner (Figure 4.12).

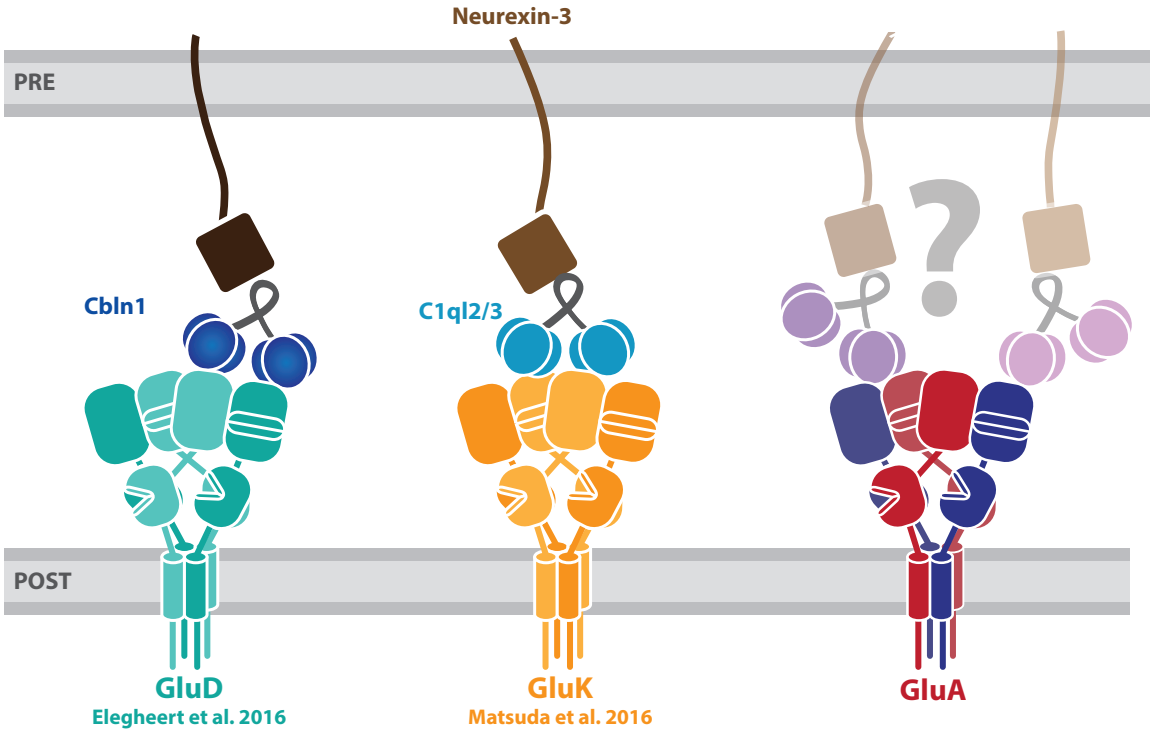

Figure 4.12 ***iGluR transsynaptic anchoring.*** *δ receptors (GluD) and kainate receptors (GluK) have recently been demonstrated to form transsynaptic complexes with presynaptic neurexins through mutual binding to secreted proteins, in manners essential to their function. A similar, but as yet undescribed role for the AMPAR (GluA) could be inferred from family traits.*

A secreted factor model has already been described for neuronal pentraxins, the best characterised NTD interactors. These multimeric proteins have been shown to cluster AMPARs (O'Brien et al., 1999), and are essential for maintaining a normal synaptic AMPAR complement at hippocampal interneuronal synapses, at which the GluA4 NTD appears to mediate this interaction (Pelkey et al., 2015; Sia et al., 2007). At retinal ganglion cells, an elegant signalling cascade controls the postsynaptic AMPAR content (Farhy-Tselnicker et al., 2017). An astrocyte secreted factor, glypican-4, stimulates presynaptic release of neuronal pentraxin 1 (NP1), which clusters postsynaptic GluA1 to enable its contribution to transmission (Allen et al., 2012). This study highlights the interplay between pre and postsynapse. So far, a presynaptic partner for pentraxin has not been reported (see Figure 4.12), however it may function in the absence of such an interactor, with spacial specificity opposite presynaptic release sites simply controlled by the location of protein release. Despite the strong evidence for the influence of pentraxins on AMPAR synaptic transmission, acting in an NTD-dependent manner, these proteins are unlikely to mediate the effect observed in the present study. In the hippocampus, their expression appears to be specific for interneuronal synapses (Chang et al., 2010), rather than those on pyramidal cells as were recorded here.

A model of transsynaptic NTD interactions in line with the suggestions of Ripley et al. (2011) and Tracy et al. (2011) is an attractive hypothesis. A transsynaptic 'nanocolumn' of pre-postsynaptic alignment has been revealed using super-resolution imaging. STORM imaging has demonstrated that not only are postsynaptic proteins PSD-95 clustered into AMPAR containing nanodomains (MacGillavry et al., 2013), but these clusters are aligned with presynaptic release sites, illuminated by imaging both presynaptic proteins, and functional glutamate release (Tang et al., 2016). The mechanism for this alignment is yet to be discovered, and could be mediated by the plethora of transsynaptic cell adhesion complexes which bridge the synaptic cleft, such as presynaptic neurexin with postsynaptic neuroligin or LRRTMs or homophilic interactions of N-cadherins (Perez de Arce et al., 2015). However, a mechanism of transsynaptic alignment through interaction with the AMPAR NTD would explain both the arrangement of the nanocolumn, and the requirement of the AMPAR NTD in synaptic transmission. On this front, both N-cadherin (Saglietti et al., 2007) and LRRTM (Schwenk et al., 2012) have been reported to interact with the AMPAR, with the latter involved in controlling the synaptic AMPAR content during LTP (Soler-Llavina et al., 2013) and also forming nanodomain like arrangement in the synapse (Chamma et al., 2016).

For many years synaptic studies have studied effects on transmission as ‘postsynaptic’ or ‘presynaptic’. Given the emerging themes of transsynaptic communication (Tang et al., 2016), it is very likely that postsynaptic changes would be felt by the presynapse, and vice versa. Understanding how both sides of the synaptic cleft influence each other now emerges an important avenue for research, and it is clear that the AMPAR NTD is not simply a large ornament.

Chapter 5

Subunit-specific AMPAR synaptic anchoring via the N-terminal Domain

5.1 Introduction

At CA1 pyramidal cell synapses, AMPARs consist predominantly of GluA1/2 and GluA2/3 heteromeric receptors, with a subpopulation of GluA2 lacking receptors (Lu et al., 2009; Rozov et al., 2012; Wenthold et al., 1996). These subsets of receptors have different kinetics (Traynelis et al., 2010), ion permeabilities (Burnashev et al., 1992; Mishina et al., 1991) and possibly even plasticity mechanisms (Gutierrez-Castellanos et al., 2017b), and therefore precisely controlling the receptor subtypes at a synapse is of great importance for tuning synaptic transmission.

Of the AMPAR synaptic anchoring mechanisms, TARP interactions are unlikely to control subunit-specific receptor anchoring, given that the majority AMPARs appear to be associated with TARPs in these cells (Shi et al., 2009), and TARP interactions do not appear to show any subunit-specific binding (Chen et al., 2000; Vandenberghe et al., 2005). This is unsurprising given that the primary TARP interaction site is with the AMPAR TMD, which is highly conserved between subunits (Figure 5.1A). Analysis of sequence conservation among AMPAR orthologs and paralogs shows the strongest sequence conservation throughout the LBD and TMD regions, which are the most evolutionarily ancient receptor regions (Chen et al., 1999a; Greger et al., 2017). The most sequence diverse receptor portions are the CTD, which has been reported as a controller of subunit-specific interactions (Shepherd and Huganir, 2007; Shi et al., 2001), and the NTD, which has been shown to control synaptic anchoring of GluA2 (see Chapter 4). Given that around 56 % of NTD residues are conserved

between AMPAR NTDs (compared to ~90 % for the LBD and TMD, García-Nafría et al., 2016a, Figure 5.1A), the NTD-dependent interactions controlling synaptic transmission could provide subunit specificity, or even subunit selectivity. However, a subunit-selective NTD anchoring mechanism via GluA2, would not provide subunit-specificity in CA1 hippocampal neurons, given that GluA2 is present in both GluA1/2 and GluA2/3 heteromeric channels. Therefore specific interactions with GluA1 and GluA3 could be expected to provide such control.

GluA1 containing receptors appear to contribute the majority of synaptic transmission at CA1 hippocampal synapses (Lu et al., 2009), and heteromeric GluA1/2 receptors appear to comprise the entirety of the surface receptor pool (Lu et al., 2009). GluA1 subunit has long been linked to hippocampal plasticity (Lee et al., 2003; Mack et al., 2001; Schmitt et al., 2005; Shi et al., 2001), with an apparent activity requirement for synaptic delivery (Shi et al., 2001) and key role in the expression of LTP (Zamanillo et al., 1999; Zhou et al., 2018). However, given that the majority of receptors contain GluA1, that the subunit is required for surface delivery of AMPARs (Lu et al., 2009), and the need for an extrasynaptic pool of receptors for synaptic plasticity (Granger et al., 2013; Makino and Malinow, 2009; Penn et al., 2017), this association may be caused more by its role in AMPAR distribution within the cell, than with intrinsic properties of the subunit.

In fact, GluA1 containing receptors may even comprise the population of 'generally active' receptors, while GluA2/3 heteromers remain inactive until a signalling stimulus occurs (Gutierrez-Castellanos et al., 2017b). GluA2/3 heteromers appear to reside in a low conductance state until cAMP signalling allows them to gate conventionally sized currents (Gutierrez-Castellanos et al., 2017b). This effect provides a second layer of synaptic plasticity, aside from changing the number of synaptic receptors and such properties would demand a definitive subunit-specific AMPAR anchoring mechanism to control the properties of the receptors which are responding to transmission.

Another channel property which demands close control over subunit-specific anchoring is calcium permeability. Calcium-permeable, GluA2-lacking AMPARs comprise a small minority in these cells (approximately 10 % of AMPARs are calcium-permeable in CA1 pyramidal neurons, see Mattison et al., 2014; Rozov et al., 2012; Wenthold et al., 1996), but have strong influences on the induction of synaptic plasticity under certain developmental and induction conditions (Park et al., 2016b; Plant et al., 2006; Sanderson et al., 2016). As

excess calcium influx can be toxic (Mahajan and Ziff, 2007), spatio-temporal control over the contribution of these subunits to transmission must be highly regulated, and AMPAR anchoring is presumably geared to promote recruitment of GluA2 containing receptors under the majority of conditions.

These calcium-permeable receptors appear to most likely comprise GluA1 homomeric channels, although GluA1/3 heteromeric receptors are also a possible option. GluA3, while being calcium-permeable (Hollmann et al., 1991) does not appear to readily form homomeric channels, and such channels very poorly traffic to synaptic sites, even in the absence of all other AMPAR subunits (Lu et al., 2009; Shi et al., 2001). This effect appears to be caused in part by certain LBD residues, which prevent homomeric receptor trafficking (Coleman et al., 2016, 2010) and also by the GluA3 NTD, which has a uniquely low affinity for homodimer formation, driving the almost obligatory formation of heteromeric channels (Rossmann et al., 2011).

Rules for AMPAR subunit-specific receptor anchoring have been described previously. Shi et al. (2001) propose that GluA1/2 heteromeric channels require an activity stimulus for synaptic anchoring, while GluA2/3 receptors constitutively traffic to synaptic sites. In fact, the authors demonstrate that GluA1 is unable to alter synaptic RI or even enter dendritic spines without a plasticity inducing stimulus, however this result has been questioned. GluA1 overexpression has been shown to contribute to synaptic transmission under basal conditions in both acute and organotypic slices (Granger et al., 2013). The difference between the studies of Shi et al. (2001) and Granger et al. (2013) appears to be an N-terminal GFP-tag used in the original study, which limits synaptic anchoring under basal conditions (Granger et al., 2013). While this suggestion has been questioned (Nabavi et al., 2013), such a result would be supportive of a role for the GluA1 NTD in synaptic anchoring, as has been demonstrated for GluA2 (see Chapter 4).

Subunit-specific AMPAR anchoring is fundamental to tuning of the postsynaptic signalling which occurs downstream from presynaptic glutamate release. Controlling the subunit composition and AMPAR content of the synapse is critical to synaptic information storage and the sequence divergence of the AMPAR NTD is a strong candidate to control this. This study will investigate the requirement for NTD-dependent interactions in GluA1 and GluA3 synaptic anchoring, and by comparison to the effects so far reported for GluA2, will establish the role of this domain in controlling AMPAR transmission.

5.2 Results

5.2.1 Synaptic anchoring of GluA1 is dependent on its NTD.

Given that overexpression of GluA1 gives rise to predominantly homomeric GluA1 receptors (Shi et al., 2001), a similar analysis of the role of the GluA1 NTD could be performed as that of GluA2Q (see Chapter 4). To study the effect of the GluA1 NTD in synaptic transmission, GluA1 ΔNTD constructs were screened and optimised for surface expression in the same manner as GluA2Q, using a flow cytometry assay (Figure 5.1B). Interestingly the length of remaining NTD-LBD linker on ΔNTD constructs showed a similar trend to GluA2Q (Chapter 4), whereby the best surface expression was achieved with the complete linker intact (Figure 5.1B2). The NTD deletion construct starting at residue A374 was selected for all further analyses, and is henceforth referred to as GluA1 ΔNTD.

Expression of GluA1 and GluA1 ΔNTD on the surface of organotypic neurons was confirmed using outside-out patch recordings, which showed strong rectification on receptor overexpression in comparison to untransfected cells (Figure 5.1C1), demonstrating that overexpressed GluA1 does indeed form homomeric receptors. Rectification was equivalent on expression of GluA1 and GluA1 ΔNTD expression confirming that surface trafficking of NTD-deleted receptors is unaffected as was seen for GluA2 (Figure 5.1C2). Analysis of the KA/Glu ratio for cells expressing GluA1 constructs confirmed that TARP association was no different between surface AMPARs of untransfected and transfected cells (Figure 5.1D1). Any effects on synaptic anchoring that may be observed are therefore unlikely to occur indirectly, by reducing the interaction of receptors and the postsynaptic density through TARP association with PSD-95/93 (Bats et al., 2007; Chen et al., 2000; Dakoji et al., 2003; Schnell et al., 2002). The amplitude of surface patches was apparently doubled on receptor overexpression, which, as has been discussed for GluA2Q overexpression, likely reflects the exchange of endogenous surface receptors with a population of exogenous receptors with a doubled mean single-channel conductance (Swanson et al., 1997; Figure 5.1D2). The accumulated data here shows no gross differences between full-length and NTD-deleted GluA1 in surface receptor populations upon overexpression.

The influence of the GluA1 NTD on synaptic anchoring was assessed by recording the RI of synaptic currents on GluA1 or GluA1 ΔNTD overexpression at the Schaffer collateral synapse onto CA1 pyramidal cells in the same manner as GluA2Q (Chapter 4). The synaptic RI of cells expressing GluA1 was significantly different to untransfected cells, showing that

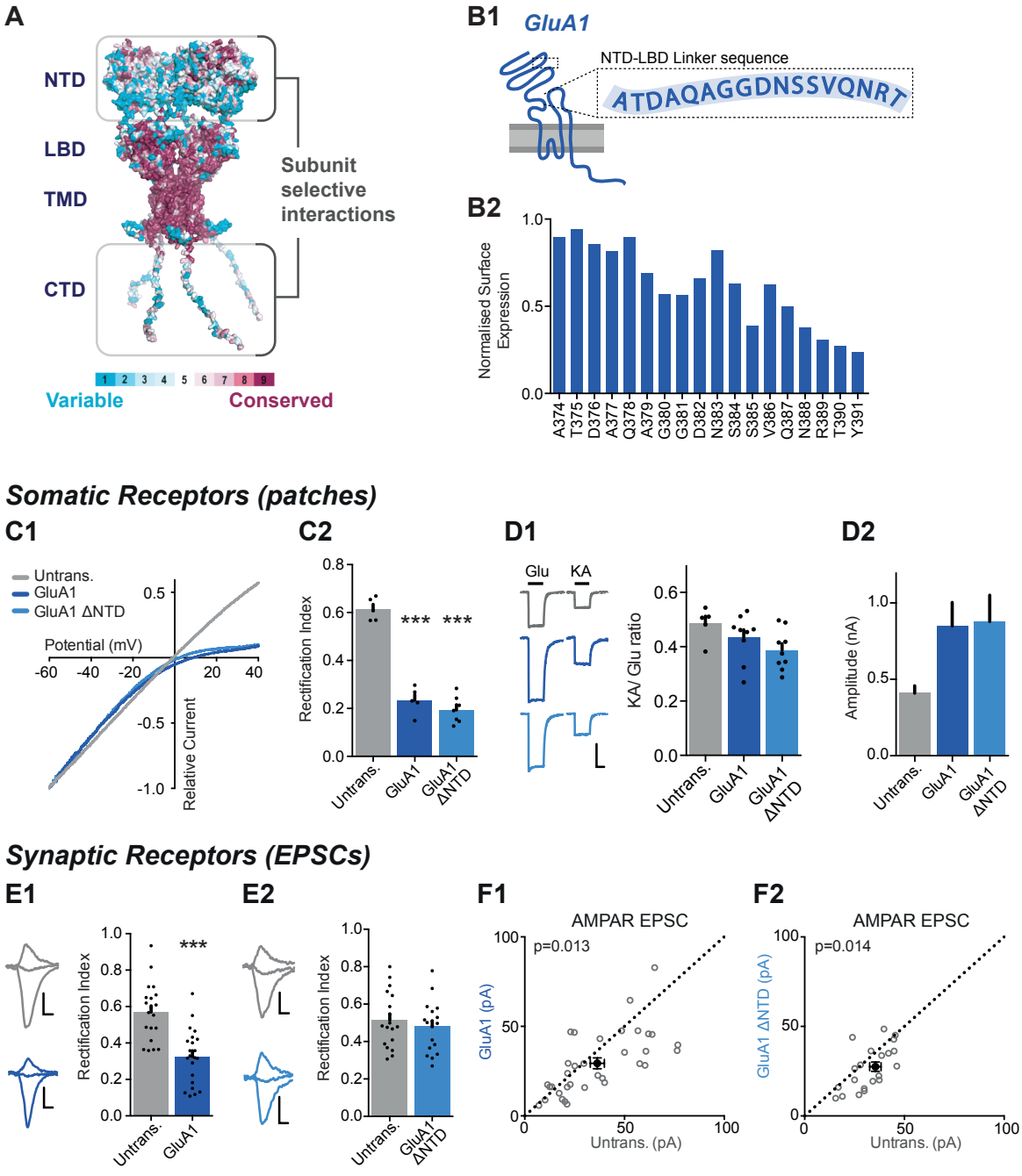

Figure 5.1 ***Surface and synaptic trafficking of GluA1 ± NTD.***

Figure 5.1 ***Surface and synaptic trafficking of GluA1 ± NTD.*** *(**A**) AMPAR structural model colored by sequence conservation across AMPAR paralogs and orthologs highlighting the potential of the NTD and CTD for subunit-specific interactions (Ashkenazy et al., 2016), while the channel core (LBD and TMD) is highly conserved (Conservation map produced by Dr James Krieger). (**B1**) GluA1 NTD-LBD linker sequence. (**B2**) Surface expression of GluA1 ΔNTD constructs initiating at each NTD-LBD linker residue, quantified by flow cytometry, normalised to maximally expressing construct. Average of two repeats. (**C1**) I/V relationships of glutamate-evoked AMPAR-mediated current from outside-out patches of untransfected, GluA1 and GluA1 ΔNTD expressing cells. (**C2**) Average RI of surface currents from above neurons (untrans.: 0.61 ± 0.05 (n = 5); GluA1: 0.23 ± 0.03 (n = 5); GluA1 ΔNTD: 0.19 ± 0.02 (n = 7); One-way ANOVA, p<0.0001). (**D1**) KA/Glu ratio from somatic patches is unchanged on GluA1 construct overexpression (KA/Glu: untrans.: 0.47 ± 0.02 (n = 5); GluA1: 0.43 ± 0.03 (n = 9); GluA1 ΔNTD: 0.39 ± 0.02 (n = 9); One-way ANOVA, p=0.16). Example traces showing glutamate (Glu) and kainic acid (KA) application are shown left. Scale bar = 50 ms and 300 pA. (**D2**) AMPAR surface patch amplitudes are similarly elevated on GluA1 or GluA1 ΔNTD overexpression (untrans.: 421 ± 90 pA; GluA1: 849 ± 154 pA; GluA1 ΔNTD: 878 ± 173 pA). (**E1**) Synaptic RI from pairs of untransfected and GluA1-expressing cells (untransfected: 0.57 ± 0.04; GluA1: 0.33 ± 0.03; n = 20; paired t-test, p=0.0001), with example traces and construct schematic shown on the left. Scale bars for panel D = 10 ms and 15 pA. (**E2**) Synaptic RI from pairs of untransfected and GluA1 ΔNTD-expressing cells (untransfected: 0.51 ± 0.04; GluA1 ΔNTD: 0.48 ± 0.03; n = 18; paired t-test, p=0.072), with example traces shown on the left. (**F1**) Scatter plot of AMPAR EPSC amplitudes from pairs of untransfected and GluA1-expressing cells (untransfected: 36.4 ± 3.5 pA; GluA1: 29.4 ± 3.0 pA; n = 34; paired t-test, p=0.013). (**F2**) Scatter plot of AMPAR EPSC amplitudes from pairs of untransfected and GluA1 ΔNTD-expressing cells (untransfected: 32.6 ± 2.1 pA; GluA1 ΔNTD: 26.9 ± 2.7 pA; n = 21; paired t-test, p=0.014).*

homomeric GluA1 is able to contribute to synaptic transmission (Figure 5.1E1). Strikingly, despite robust surface trafficking, GluA1 ΔNTD overexpression did not affect the synaptic RI, indicating that the NTD of GluA1 is essential for synaptic anchoring of this receptor subunit (Figure 5.1E2). In both cases, the amplitude of synaptic AMPAR currents was subtly decreased (Figure 5.1F). While the NTD of GluA2 appeared to promote synaptic anchoring, the GluA1 NTD seems essential for contribution of GluA1 to synaptic transmission.

Previous reports have demonstrated both a change (Granger et al., 2013) and no change (Shi et al., 2001) to synaptic RI on GluA1 overexpression. The difference between the observed effects has been suggested to result from the use of GFP-tagged receptors, which may not successfully incorporate into the synapse (Granger et al., 2013), yet there is some disagreement in the field over this effect (Nabavi et al., 2013). As the synaptic targeting of GluA1 is apparently activity dependent (Hayashi et al., 2000; Shi et al., 2001), with GFP-tagged GluA1 producing rectifying synaptic responses after potentiating or activity stimuli (Hayashi et al., 2000), reports of RI changes on GluA1 overexpression could theoretically result from basal activity which occurs in organotypic slice cultures (Otmakhov et al., 2004) causing activity-dependent receptor trafficking. This mechanism was suggested by Nabavi et al. (2013) to explain the results of Granger et al., 2013.

To clarify these discrepancies and to understand the requirements for GluA1 synaptic anchoring, GluA1-dependent RI changes were compared on both GFP-tagging and in the absence of synaptic activity. In previous studies, GFP-GluA1 was designed such that the GFP coding sequence was inserted between the third and fourth amino acids of the mature GluA1 protein, flanked by two amino-acid linker sequences (Hayashi et al., 2000). GFP-GluA1, designed as per this study showed robust surface trafficking by recording the RI of surface neuronal patches (Figure 5.2A1), however synaptic responses did not show rectification (Figure 5.2A2). Synaptic EPSC amplitudes were not significantly altered, but appeared subtly decreased in a similar manner to wild-type GluA1 overexpression (Figure 5.2A3).

This result indicates that GFP-tagging the N-terminus of GluA1 affects its successful incorporation into the synapse for functional transmission, and as activity-dependent trafficking of GluA1 can drive incorporation of GFP-tagged receptors into the synapse (Hayashi et al., 2000), it is unlikely that excessive activity in slice cultures is the reason for the change in RI observed on untagged-GluA1 expression in this study (Figure 5.1E1). Nevertheless, spontaneous activity in slice cultures was prevented from the beginning of the culture period

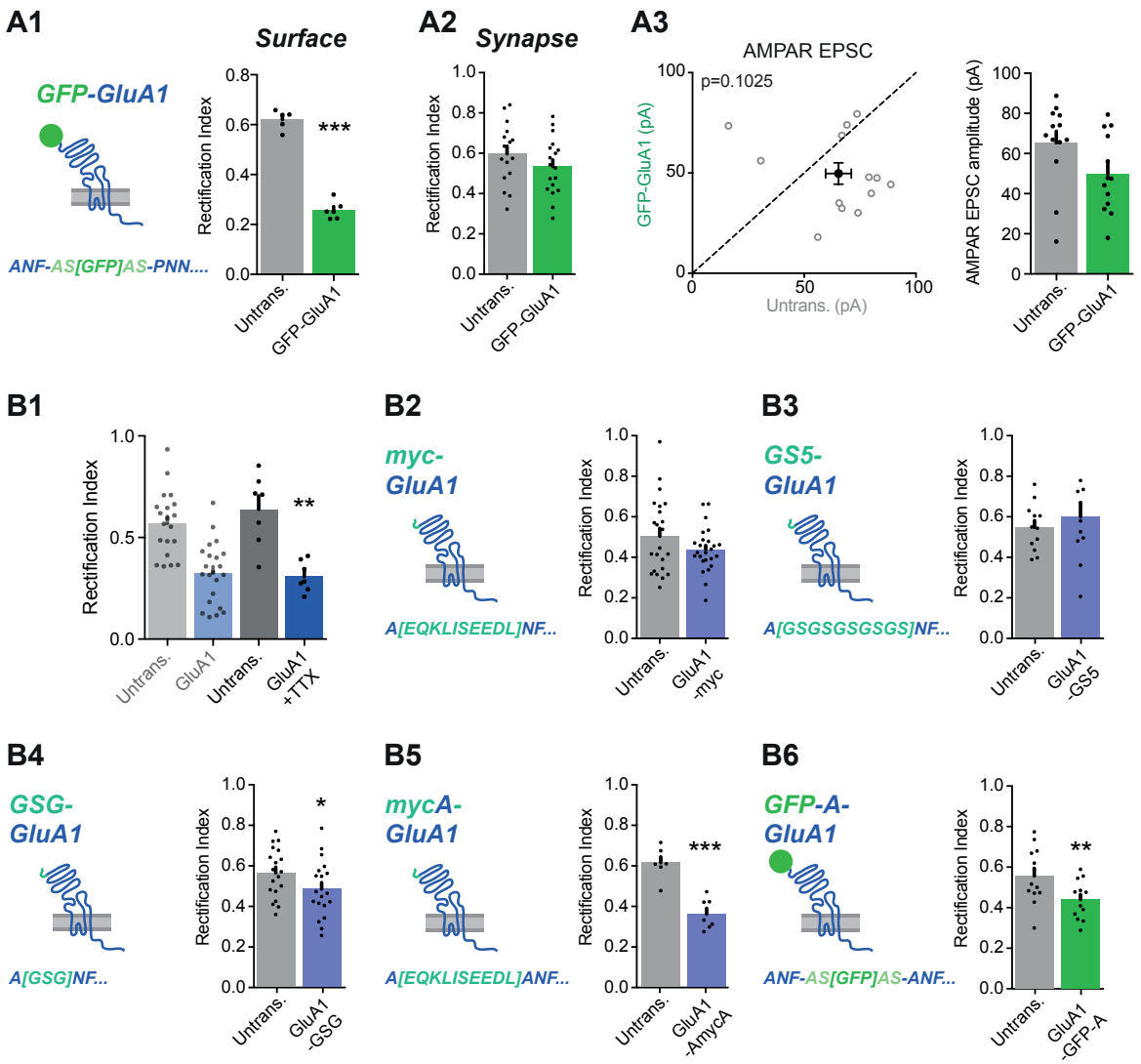

Figure 5.2 ***NTD-tagging prevents GluA1 synaptic targeting***

Figure 5.2 ***NTD-tagging prevents GluA1 synaptic targeting*** *(**A1**) Surface RI demonstrates that GFP-GluA1 traffics to the cell surface (untransfected: 0.62 ± 0.02, n = 5; GFP-GluA1: 0.26 ± 0.01 n = 6; unpaired t-test, p<0.0001). Schematic and primary amino-acid sequence of protein N-terminus are provided. [GFP] indicates location of GFP insertion. (**A2**) Synaptic RI from pairs of untransfected and GFP-GluA1-expressing cells (untransfected: 0.60 ± 0.04; GFP-GluA1: 0.53 ± 0.04; n = 16; paired t-test, p=0.086). (**A3**) Scatter plot of AMPAR EPSC amplitudes from pairs of untransfected and GFP-GluA1-expressing cells (untransfected: 65.34 ± 5.73 pA; GluA1: 29.4 ± 3.0 pA; n = 13; paired t-test, p=0.103). (**B1**) Synaptic RI from pairs of untransfected and GluA1-expressing cells with or without TTX pretreatment (GluA1 data reproduced from Figure 5.1) (untransfected: 0.64 ± 0.18; GluA1+TTX: 0.31 ± 0.08; n = 7; paired t-test, p=0.008). (**B2**) Synaptic RI from pairs of untransfected and myc-GluA1 expressing cells (untransfected: 0.50 ± 0.04; GluA1+TTX: 0.44 ± 0.02; n = 7; paired t-test, p=0.138). (**B3**) Synaptic RI from pairs of untransfected cells and those expressing GluA1 with an N-terminal $(GS)_5$ insertion (untransfected: 0.56 ± 0.03; GS5-GluA1: 0.59 ± 0.07; n = 11; paired t-test, p=0.570). (**B4**) Synaptic RI from pairs of untransfected cells and those expressing GluA1 with an N-terminal GSG insertion (untransfected: 0.56 ± 0.03; GSG-GluA1: 0.48 ± 0.03; n = 19; paired t-test, p=0.034). (**B5**) Synaptic RI from pairs of untransfected cells and those expressing GluA1 with a myc-tag inserted as to not disrupt endogenous N-terminal sequence (untransfected: 0.62 ± 0.03; mycA-GluA1: 0.36 ± 0.03; n = 7; paired t-test, p=0.0003). (**B6**) Synaptic RI from pairs of untransfected cells and those expressing GluA1 with GFP inserted as per mycA (untransfected: 0.55 ± 0.04; GFP-A-GluA1: 0.44 ± 0.03; n = 13; paired t-test, p=0.008).*

by inclusion of 1 μM tetrodotoxin (TTX), a sodium channel blocker which will prevent action potential firing in all neurons. In a similar manner to Figure 5.1E1, the synaptic RI on GluA1 overexpression was assessed in these slices, and the successful synaptic incorporation of GluA1 was again observed by a change in the RI (Figure 5.2B1), clearly demonstrating that GluA1 is able to anchor at synaptic sites in an activity-independent manner.

Given that the NTD of GluA1 appears to play a critical role in synaptic anchoring, it is unsurprising that inserting a GFP-tag at the N-terminus of the receptor also affects its synaptic anchoring. The GFP protein is approximately 30 kDa, so constitutes a large modification to the receptor, which could cause steric hindrance for binding of N-terminally interacting proteins.

To investigate the effect of N-terminal modifications further, a much smaller modification was employed. A c-myc tag was inserted into the N-terminus of GluA1 between the first and second residues of the mature protein, such that the new N-terminal sequence was AEQKLISEEDLNF... (from ANF...; see Figure 5.2B2). The synaptic RI on overexpression of this construct was measured, and surprisingly, despite this modification consisting of just 10 amino-acids, receptor synaptic anchoring was prevented (Figure 5.2B2). As the c-myc tag contains a number of charged residues, which could affect protein interactions in the local area, this sequence was replaced by an uncharged sequence (AGSGSGSGSGSNF...), which should provide less interference, but produces a similar sized modification. Overexpression of this construct similarly had no effect on synaptic RI, indicating no synaptic incorporation (Figure 5.2B3). Reducing the length of the sequence to just 3 amino-acids (AGSGNF...) resulted in a small change to synaptic RI (Figure 5.2B4), however the magnitude of the change to RI was far less than that caused by wild-type GluA1 expression.

As the insertion of all these modifications caused disruption of the GluA1 N-terminus, a myc-tag insertion was designed to maintain the endogenous N-terminal sequence of GluA1 (AEQKLISEEDLANF...). Surprisingly, despite this construct differing from the previous myc-tagged construct just by the insertion of one alanine residue after the tag sequence (Figure 5.2B2), robust rectification was observed (Figure 5.2B5), which appeared similar in magnitude to that of GluA1 overexpression (Figure 5.1E1). This phenomenon indicates that N-terminal modification of GluA1 disrupts the interaction site of a potential synaptic anchoring protein. Following this thought process to its conclusion, a GFP-tagged GluA1 construct was designed to maintain the endogenous N-terminal sequence of GluA1 (ANF-

AS[GFP insertion]AS-ANF...). While previously, GFP-tagged GluA1 did not change the synaptic RI, this modified version did show significant rectification (Figure 5.2B6), albeit not to the same extent as wild-type GluA1 (Figure 5.1E1). These accumulated results suggest that synaptic anchoring of GluA1 requires N-terminal interactions, which likely occur in close proximity to the extreme N-terminus of the protein, and modification of this region can limit contribution of this subunit to synaptic transmission.

5.2.2 Spine localisation of GluA1 is independent of the NTD.

While the expression of GluA1 ΔNTD has been confirmed on the somatic surface of the neurons (Figure 5.1C), it cannot be inferred from this data that the receptor is present in dendrites, or in the extrasynaptic space. In order to investigate the localisation of the receptor, dissociated hippocampal cultures were transfected with GluA1 or GluA1 ΔNTD with an N-terminal c-myc tag. Experiments were performed in dissociated hippocampal cultures, so that live staining of neurons could be performed, allowing detection by immunofluorescence of only surface receptors. Such an approach cannot be performed in slices, due to the requirement for tissue fixation and permeabilisation for antibody access. By isolating only the surface receptor populations, which will include synaptic receptors, the confounding fluorescence of intracellular receptor pools in dendrites and spine heads can be excluded.

Receptor staining could be observed in dendritic regions for both constructs, with both showing a distinctly clustered appearance when imaging using STED microscopy (Figure 5.3A). The receptor clustering present on dendritic spines, the location of postsynaptic sites, was quantified and no difference in the number of clusters per spine (Figure 5.3B1), the fluorescence intensity of clusters (Figure 5.3B2), which is proportional to the number of receptors present, or the area of clusters was observed (Figure 5.3B3). The intensity of fluorescence which displayed either a clustered or diffuse distribution was not different either, indicating that the receptor localisation was largely unchanged on NTD deletion, and that surface receptor expression is equivalent (Figure 5.3B4). Given that NTD-deleted GluA1 does not contribute to functional transmission, as seen by synaptic RI recordings, the subsynaptic receptor arrangement must be different between conditions, which cannot be seen in this imaging analysis. This data is suggestive of a role for the AMPAR NTD in transsynaptic alignment with presynaptic glutamate release sites, rather than simply an essential role in postsynaptic accumulation.

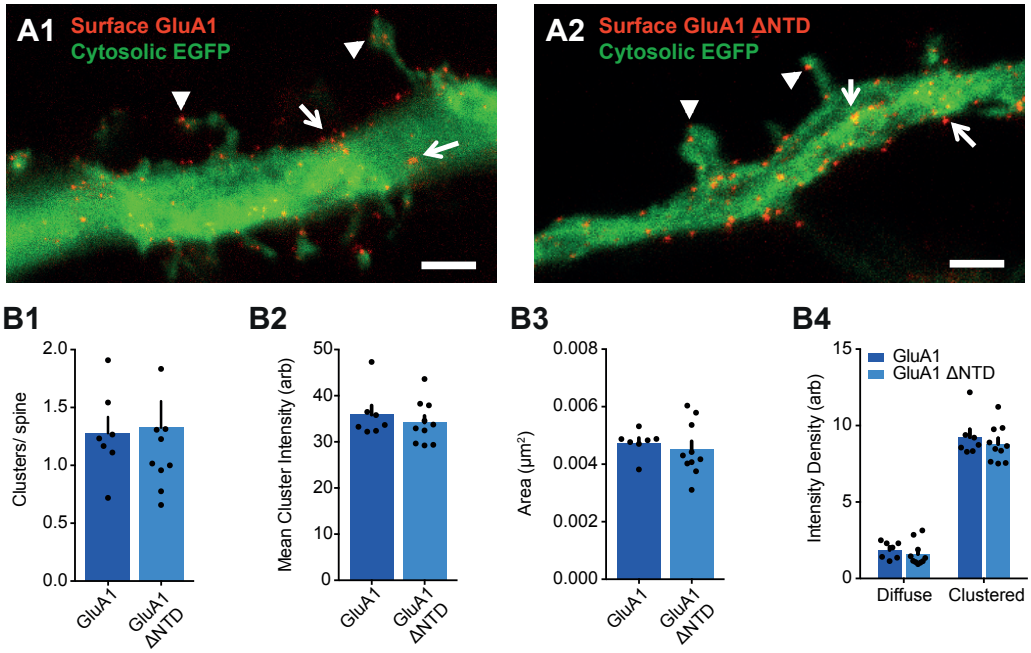

Figure 5.3 ***STED imaging of synaptic GluA1 shows no difference on NTD removal*** *(**A**) Example images of dissociated hippocampal neurons transfected with myc-GluA1 (**A1**) or myc-GluA1 ΔNTD (**A2**) with pN1-EGFP to express cytosolic EGFP. Surface receptors are antibody labelled and imaged using STED microscopy. Both Synaptic (▲) and dendritic (arrow) clusters are evident in both conditions. Scale bar = 5* μm.*(**B**) Quantification of receptor clusters shows no difference in cluster number per spine (**B1**, GluA1: 1.28 ± 0.14 (n=7 cells), GluA1 ΔNTD: 1.33 ± 0.23 (n=10 cells), unpaired t-test: p=0.115), mean fluorescence intensity of synaptic clusters (**B2** GluA1: 35.9 ± 2.0 (n=7 cells), GluA1 ΔNTD: 34.2 ± 1.5 (n=10 cells), unpaired t-test: p=0.506), or the area of synaptic clusters (**B3** GluA1: 0.0047 ± 0.0002* μm^2 *(n=7 cells), GluA1 ΔNTD: 0.0045 ± 0.0003* μm^2 *(n=10 cells), unpaired t-test: p=0.499), and the fluorescence intensity of neither clustered nor diffuse receptor staining was different (**B4** Diffuse GluA1: 1.86 ± 0.21 (n=7 cells), Diffuse GluA1 ΔNTD: 1.60 ± 0.25 (n=10 cells), Clustered GluA1: 9.24 ± 0.51 (n=7 cells), Clustered GluA1 ΔNTD: 8.79 ± 0.38 (n=10 cells)).*

5.2.3 NTD-dependent synaptic anchoring is subunit-specific.

The effects on synaptic transmission observed on overexpression of GluA1 and GluA2Q are notably different (see GluA1 - Figure 5.1 and GluA2Q - Chapter 4). GluA2Q overexpression increases the amplitude of AMPAR EPSCs, whereas GluA1 decreases them slightly, and the rectification change caused by GluA2Q overexpression is more substantial than GluA1 (approximately 0.2 vs 0.35, cf. 0.55 for untransfected cells). These differences indicate that GluA2Q has a greater propensity to anchor at the synapse and replace endogenous receptors than GluA1.

This data is suggestive of subunit-specific NTD interactions controlling synaptic anchoring, which would be facilitated by the substantial differences between subunit NTD sequences (Figure 5.1A). To investigate this, two constructs were expressed, the first where the NTD of GluA1 was replaced by that of GluA2 (including NTD-LBD linker sequence), and the second in which the NTD of GluA2Q was replaced by that of GluA1 (Figure 5.4A1). Both constructs trafficked well to the cell surface, causing strong rectification of surface responses (Figure 5.4A2), indicating that they have no deficits in either channel gating or forward trafficking.

The synaptic responses of cells overexpressing these constructs was subsequently assayed. Consistent with a subunit-specific NTD anchoring model, GluA1 with the GluA2 NTD showed stronger rectification than that of wild-type GluA1 (Figure 5.4B1). Although AMPAR EPSCs within each pair were not significantly increased in comparison to untransfected cells (Figure 5.4B2), analysing the relative AMPAR EPSC ratio within each pair between conditions showed a significant elevation in EPSC amplitudes (Figure 5.4B3; GluA1 data reproduced from Figure 5.1). Both stronger rectification and increased EPSC amplitudes are representative of the effects of GluA2Q, and therefore the strong synaptic anchoring of GluA2 can be conferred on GluA1 by NTD replacement.

When studying the reverse NTD swap construct, GluA2Q with the GluA1 NTD, strong synaptic rectification was observed, which was highly reminiscent of GluA2Q (Figure 5.4C1). Despite the clear subunit-specific anchoring observed by transplanting the GluA2 NTD onto GluA1, the fact that removing the GluA2 NTD and replacing it with that of GluA1 does not affect the synaptic RI is not surprising, as that GluA2Q lacking any NTD also causes a strong change in synaptic RI. An indication of subunit-specific NTD-dependent control of receptor anchoring by the GluA2 NTD was observed when comparing AMPAR EPSC

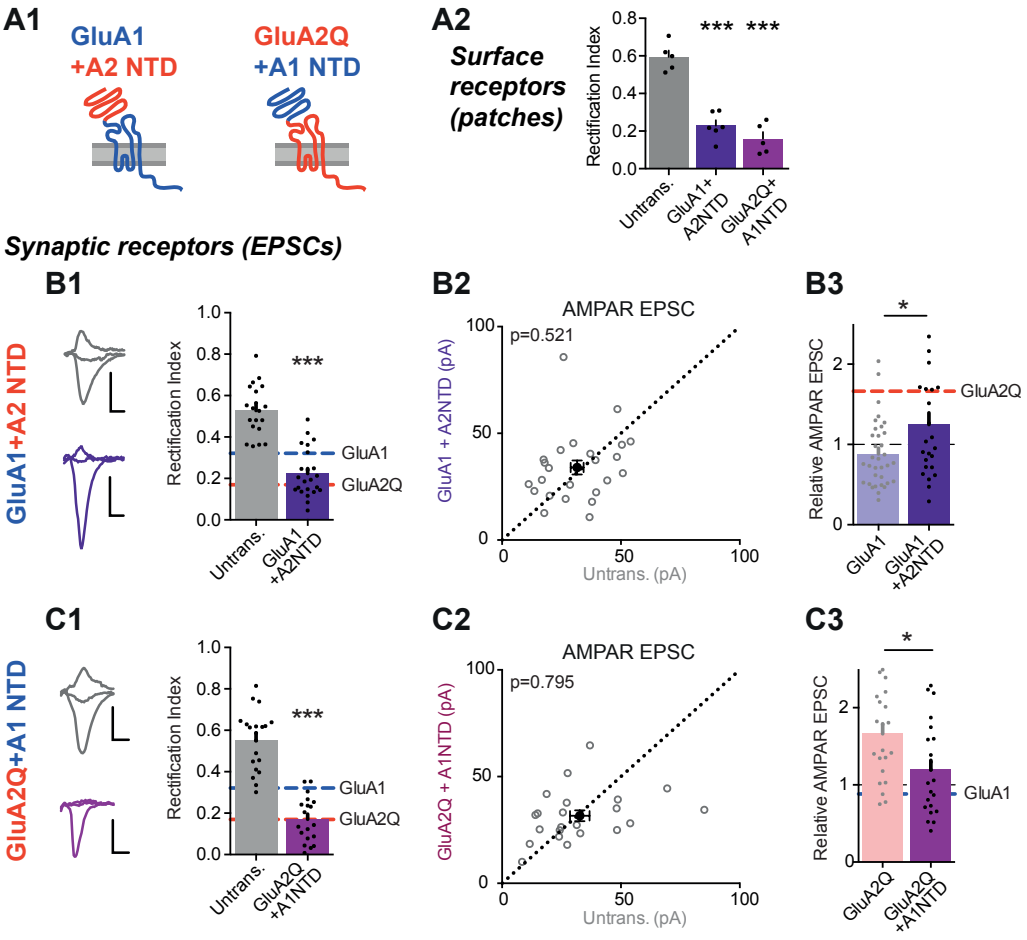

Figure 5.4 ***GluA1 and GluA2 NTDs control subunit-specific synaptic anchoring.*** *(**A1**) AMPAR NTD swap construct schematics. (**A2**) Surface RI for chimeric construct expression (untrans.: 0.60 ± 0.08 (n = 5), GluA1+A2NTD: 0.23 ± 0.07 (n = 6), GluA2Q+A1NTD: 0.16 ± 0.08 (n = 5), One-way ANOVA: p<0.0001). (**B1**) Synaptic RI on GluA1+A2NTD expression (untransfected: 0.56 ± 0.04; GluA1+A2NTD: 0.22 ± 0.02; n = 23; paired t-test, p<0.0001). GluA1 and GluA2Q RI values are indicated for reference. Scale bars = 10 ms and 20 pA. (**B2**) AMPAR EPSCs from pairs of untransfected and GluA1+A2NTD expressing cells (untrans.: 31.6 ± 2.7 pA; GluA1+A2NTD: 34.0 ± 3.3 pA; n = 24; paired t-test, p=0.521). (**B3**) AMPAR EPSC amplitudes of transfected cells normalised to untransfected cells within pairs (GluA1: 0.88 ± 0.07 (n = 34); GluA1+A2NTD: 1.25 ± 0.15 (n = 24); unpaired t-test, p=0.017). Value for GluA2Q is indicated by red line for reference. (**C1**) Synaptic RI on GluA2Q+A1NTD expression (untransfected: 0.55 ± 0.03; GluA2Q+A1NTD: 0.17 ± 0.03; n = 19; paired t-test, p<0.0001). (**C2**) AMPAR EPSCs from pairs of untransfected and GluA2Q+A1NTD expressing cells (untrans.: 32.7 ± 4.1 pA; GluA2Q+A1NTD: 31.6 ± 2.6 pA; n = 22; paired t-test, p=0.795). (**C3**) AMPAR EPSCs amplitudes normalised to untransfected cells within pairs (GluA2Q: 1.66 ± 0.13 (n = 22); GluA2Q+A1NTD: 1.19 ± 0.13 (n = 22); unpaired t-test, p=0.013). GluA1 value indicated by blue line.*

amplitudes. GluA2Q+A1NTD did not change the amplitude of AMPAR EPSCs relative to untransfected cells (Figure 5.4C2), which indicates that the synaptic receptor content is not as great as that on GluA2Q overexpression (Figure 5.4C3). While this domain does not completely define the phenotype of the receptor, these accumulated results demonstrate that the AMPAR NTDs have subunit-specific interactions which control receptor anchoring at synaptic sites. Alongside NTD interactions, the strong rectification observed with all GluA2Q constructs tested thus far must be aided by other interactions, which are able to promote synaptic accumulation of GluA2.

5.2.4 NTD-dependent anchoring on an AMPAR-null background.

To corroborate the observations presented so far demonstrating the role of the NTD in synaptic anchoring, the effect of NTD deletion was studied on an AMPAR-null background. This approach provides complementary evidence to that so far observed using overexpression.

Overexpression data can be difficult to interpret due to the contribution of endogenous subunits to transmission, however the effect of subtle receptor mutations can be more easily identified due to the competition between exogenous and endogenous receptor populations. The advantage of an AMPAR-null background is that it allows analysis of the effect of mutations without interference of endogenous receptor populations. However, in the absence of other receptor subunits, there is a strong possibility of compensatory effects, where important observations of detrimental receptor mutagenesis could be missed. This disadvantage is likely the causes for recent differences in studies investigating the role of the GluA1 CTD in LTP (Granger et al., 2013; Zhou et al., 2018), where little detrimental effect of domain deletion are observed in an AMPAR-null background. These approaches can be employed together to produce a more complete picture of the requirements for synaptic transmission.

Introduction of *loxP* sequences can allow simple modification of genomic DNA. Cre recombinase is able to recognise the sequences, and excise DNA between repeated pairs of sites. This approach has widely been used to generate mouse lines which are 'conditional knockouts' for a particular gene: protein expression is effectively as per wild-type unless Cre recombinase is present to cause gene inactivation by genomic DNA excision.

Mice containing *loxP* sites in each of the genes encoding GluA1, 2 and 3 (*Gria1, Gria2, Gria3*; kindly provided by Dr Rolf Sprengel, Heidelberg) were interbred to produce con-

ditional knockout mice for all AMPAR subunits present in CA1 pyramidal neurons (Lu et al., 2009). Cells from these mice, denoted *Gria1-3fl*, would express all AMPAR subunits, unless Cre recombinase was expressed in those cells, which would cause genomic DNA recombination to prevent transcription and translation of GluA1, 2 and 3. It has previously been shown that Cre recombinase expressed in these cells causes a complete knockout of both surface and synaptic AMPAR currents (Lu et al., 2009).

To study the effect of NTD-deletion in these mice, animals were subject to intracerebral injection of AAV expressing Cre recombinase fused to EGFP (AAV-Cre-GFP) at P0 (day of birth). Organotypic slices prepared from these animals at P7 showed robust Cre expression in a subset of CA1 cells, visualised by imaging EGFP fluorescence, which was confined to the nucleus. Single-cell electroporation of EGFP expressing neurons was performed to rescue AMPAR currents, and transfected cells were identified by cotransfection with a plasmid expressing EGFP throughout the cytosol, rather than just in the nucleus (Cre-GFP only). This procedure is illustrated in Figure 5.5A. As expected, recording from pairs of Cre-GFP expressing, and uninfected neurons showed an absence of AMPAR synaptic currents at 16 days after infection (Figure 5.5B). As AMPAR currents were absent from Cre-GFP infected cells, to confirm that synaptic transmission was intact on these cells, NMDAR currents were recorded and the AMPAR/NMDAR current ratio is presented throughout these analyses.

Rescue of AMPAR transmission by expression of exogenous GluA2Q resulted in an AMPAR/NMDAR ratio which was no different to untransfected and uninfected cells of the paired recordings (Figure 5.5C1). Rescue with GluA2Q ΔNTD however, did not produce such robust AMPAR synaptic currents (Figure 5.5C2), and the AMPAR/NMDAR ratio was less than 50 % of uninfected cells (Figure 5.5C3) (Relative AMPAR/NMDAR - GluA2Q: 0.99 $\pm$ 0.10, GluA2Q ΔNTD: 0.44 $\pm$ 0.05). Thus, role of the GluA2 NTD in anchoring AMPARs for synaptic transmission can be observed in a knockout and rescue scenario, and even in the absence of other receptor subunits, NTD-lacking receptors cannot maintain normal levels of synaptic transmission.

AMPAR rescue using a GluA1 expressing plasmid did not produce the complete recovery of AMPAR/NMDAR ratio seen using GluA2Q. GluA1 rescue produced a ratio approximately 50 % that of uninfected cells (Figure 5.5D1), which recapitulates the subunit-specific anchoring seen upon overexpression, where GluA2Q produces a stronger change to RI than GluA1. GluA1 ΔNTD gave even smaller AMPAR EPSCs, resulting in just 28 % of the uninfected

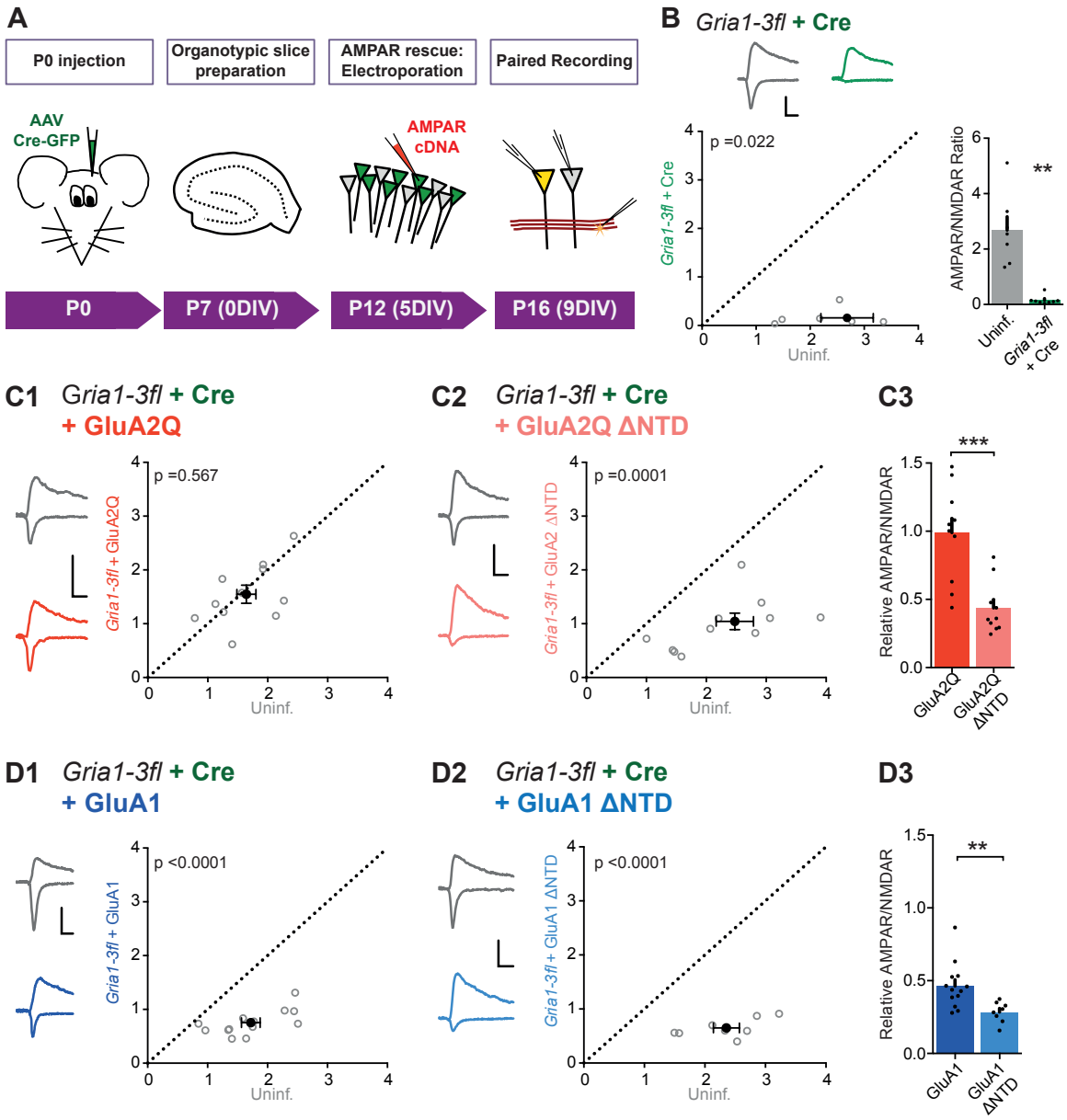

Figure 5.5 ***NTD-dependent trafficking on an AMAR null background***

Figure 5.5 ***NTD-dependent trafficking on an AMAR null background*** *Paired recordings from Gria1-3fl neurons infected with AAV-Cre and rescued with AMPAR subunits, or uninfected and untransfected (uninf.). Example traces show current responses at -60 mV (AMPAR) and +40 mV (NMDAR) holding potentials. Scale bars = 30 ms and 50 pA. (**A**) Protocol schematic for AMPAR knockout and rescue in Gria1-3fl neurons, with timings shown as mouse postnatal age (P) and days in vitro (DIV). (**B**) Paired recordings from AAV-Cre and uninfected (Uninf.) neurons from Gria1-3fl slices shows almost complete loss of AMPAR EPSCs (normalised to NMDAR current amplitude) (AMPAR/NMDAR, (n = 7 pairs): uninf.: 2.68 ± 0.48; Cre: 0.16 ± 0.06; paired t-test, p=0.022) as seen by scatter (left) and bar charts (right). Example traces show currents at -60 mV and +40 mV holding potentials for each condition. Scale bar = 30 ms and 50 pA. (**C1**) Rescue with GluA2Q restores the ratio of AMPAR to NMDAR currents to levels of uninfected neurons (AMPAR/NMDAR, (n = 11 pairs): uninf.: 1.64 ± 0.16; GluA2Q: 1.55 ± 0.17; paired t-test, p=0.567). (**C2**) Rescue with GluA2Q ΔNTD cannot fully restore AMPAR currents relative to NMDAR (AMPAR/NMDAR, (n = 11 pairs): uninf.: 2.28 ± 0.26; GluA2Q ΔNTD 0.97 ± 0.15; paired t-test, p=0.0001). (**C3**) Normalization of synaptic currents to uninfected cells reveals that GluA2Q NTD deletion reduces synaptic AMPAR rescue (Relative AMPAR/NMDAR ratio: GluA2Q: 0.99 ± 0.10; GluA2Q ΔNTD: 0.44 ± 0.05; unpaired t-test, p=0.0001). (**D1**) Rescue of synaptic currents by GluA1 transfection (AMPAR/NMDAR, (n = 13 pairs): uninf.: 1.72 ± 0.15; GluA1: 0.75 ± 0.06; paired t-test, p<0.0001). (**D2**) Rescue of synaptic currents with GluA1 ΔNTD (AMPAR/NMDAR, (n = 9 pairs): uninf.: 2.48 ± 0.23; GluA1 ΔNTD: 0.83 ± 0.19; paired t-test, p<0.0001). (**D3**) GluA1 rescues synaptic currents to a greater extent than GluA1 ΔNTD (Relative AMPAR/NMDAR ratio: GluA1: 0.46 ± 0.04; GluA1 ΔNTD: 0.28 ± 0.03; unpaired t-test, p=0.007).*

cell AMPAR/NMDAR ratio (Figure 5.5D2). A significant difference in the level of rescue by GluA1 is seen on NTD deletion (Figure 5.5D3), further reiterating the requirement for the GluA1 NTD in anchoring this subunit at synaptic sites.

5.2.5 The role of the GluA1 NTD in synaptic potentiation.

The role of GluA1 in synaptic potentiation has been extensively studied (Mack et al., 2001; Plant et al., 2006; Shi et al., 2001; Zamanillo et al., 1999). However, the strict activity-dependence of its trafficking, which was previously postulated (Hayashi et al., 2000; Shi et al., 2001) appears not to be such a clear-cut rule (see Figure 5.1, Granger et al. (2013)). In this study, the requirement for the GluA1 NTD in synaptic anchoring has been clearly demonstrated, however it is the C-terminal domain of GluA1 which has been most extensively studied and implicated in LTP dependent receptor trafficking (Hayashi et al., 2000; Shi et al., 2001). It was therefore investigated whether a potentiating stimulus would be sufficient to drive incorporation of overexpressed GluA1 ΔNTD receptors into the synapse.

CaMKII, a postsynaptic protein kinase, is a key player in the induction of LTP (Hell, 2014). Overexpression of a constitutively active version of the kinase, denoted tCaMKII (truncated CaMKII) has been used as a simple model of synaptic potentiation in the past (Hayashi et al., 2000), and was demonstrated to drive the synaptic incorporation of GFP-GluA1. For this reason, it was utilised to study the synaptic anchoring of NTD deleted GluA1. Expression of tCaMKII (kindly provided by Dr José A. Esteban, Madrid) in CA1 pyramidal neurons elevated the amplitude of AMPAR EPSCs relative to untransfected cells (Figure 5.6A1), with no effect on the synaptic RI (Figure 5.6A2). This result is in line with previous studies (Hayashi et al., 2000), and suggests that the protein increases the postsynaptic AMPAR current by increasing the number of endogenous heteromeric receptors which contribute to synaptic transmission.

Coexpression of GluA1 with tCaMKII produced a robust potentiation, similar to expression of tCaMKII alone (Figure 5.6B1), and synaptic currents were rectifying, as previously seen (Figure 5.6B2), indicating that exogenous GluA1 receptors were contributing to the potentiated currents. Coexpression of GluA1 ΔNTD with tCaMKII did not produce any synaptic potentiation (Figure 5.6C1), in fact AMPAR EPSCs were subtly depressed, as they had been on expression of GluA1 ΔNTD alone. Interestingly, the RI of synaptic currents was significantly affected by this manipulation (Figure 5.6C2). This data indicates that while

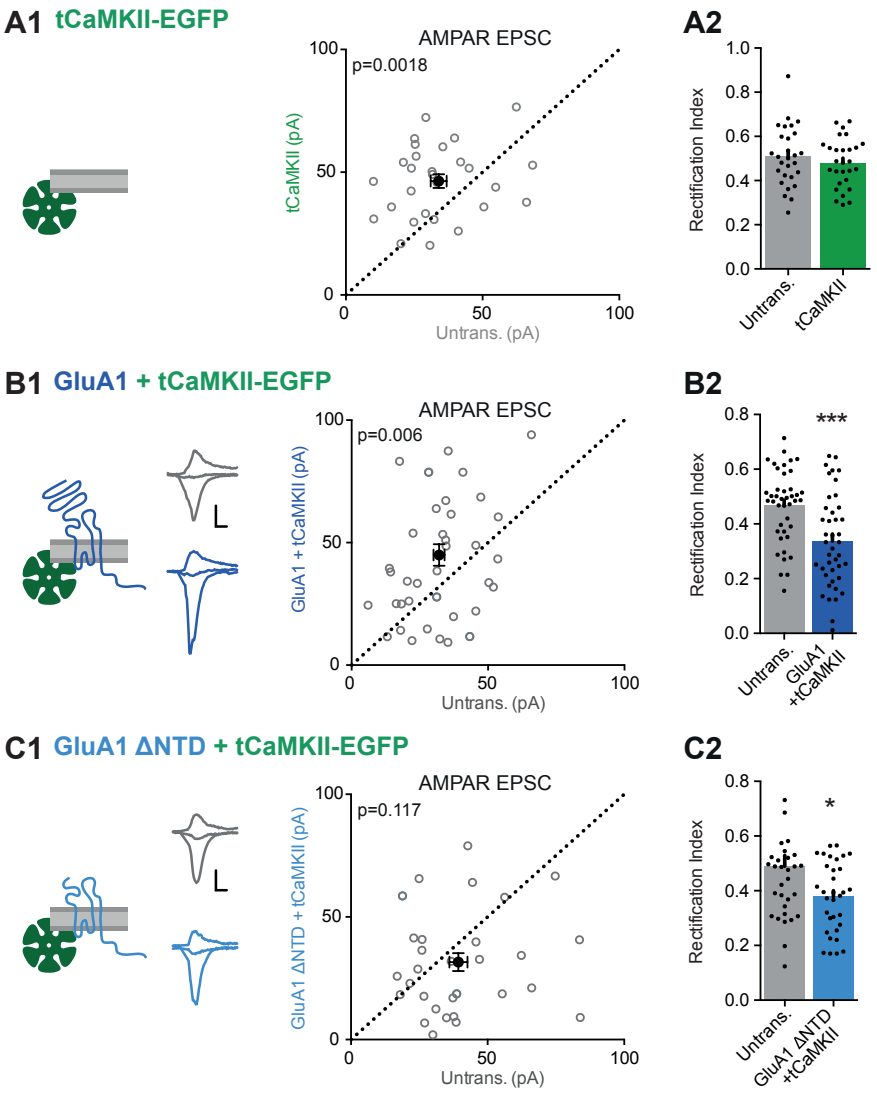

Figure 5.6 ***Synaptic potentiation by tCaMKII requires NTD-dependent anchoring*** *(**A1**) Scatter plot of AMPAR EPSCs from tCaMKII-EGFP and untransfected cells showing successful potentiation (untrans.: 33.9 ± 2.9 pA, tCaMKII: 46.4 ± 2.8 pA; n = 28; paired t-test, p=0.0018). (**A2**) RI is unchanged on tCaMKII expression (untrans.: 0.51 ± 0.03, tCaMKII: 0.48 ± 0.02; n = 28; paired t-test, p=0.369). (**B1**) Co-expression of GluA1 and tCaMKII increases AMPAR EPSC amplitude (untransfected: 32.1 ± 2.0 pA; GluA1 + tCaMKII: 44.9 ± 4.4 pA; n = 42; paired t-test, p=0.006). Scale bar = 10 ms and 20 pA. (**B2**) RI from above cells (untransfected: 0.47 ± 0.02; GluA1 + tCaMKII: 0.34 ± 0.03; n = 42; paired t-test, p=0.0003). (**C1**) Potentiation mediated by tCaMKII is impaired in GluA1 ΔNTD expressing cells (untransfected: 39.3 ± 3.3 pA; GluA1 ΔNTD + tCaMKII: 31.6 ± 3.7 pA; n = 32; paired t-test, p=0.117). Scale bar = 10 ms and 20 pA. (**C2**) RI from above cells (untransfected: 0.49 ± 0.04; GluA1 ΔNTD + tCaMKII: 0.38 ± 0.02; n = 33; paired t-test, p=0.019).*

GluA1 ΔNTD is unable to maintain a potentiated synapse, further implicating the GluA1 NTD in synaptic anchoring, a subset of these receptors were contributing to transmission. This result is supportive of some role for other portions of the receptor, such as the CTD in activity-dependent receptor anchoring. To study synaptic potentiation in a more physiological manner than overexpression of CaMKII, an electrical stimulation potentiation protocol was employed. A plethora of LTP induction protocols have been reported, but the most reliably reported method for single-cell recording in organotypic slice cultures involves a paired depolarisation. Individual CA1 pyramidal neurons were recorded by whole-cell patch clamp in the voltage-clamp configuration. Two stimulation electrodes were placed in the stratum radiatum either side of the recorded cell and displaced in the longitudinal axis of the neuronal dendritic tree, such that different populations of CA3 axons would be stimulated (Figure 5.7A1). LTP was induced by pairing postsynaptic depolarisation to -10 mV with presynaptic stimulation at 2 Hz for 100 s using one of the two stimulating electrodes (test pathway). As a test of LTP induction efficiency, a set of recordings were performed using untransfected neurons, and induction of LTP was successful, producing potentiation that lasted at least 45 mins, the entire duration of recording (Figure 5.7A2).

LTP recordings were performed on cells overexpressing either GluA1 or GluA1 ΔNTD (unbinned data is presented in Figure 5.7B1). Cells expressing GluA1 showed robust potentiation in the test pathway (Figure 5.7B2,C1), with AMPAR EPSCs elevated for the duration of recording. By plotting the level of potentiation on a cell-by-cell basis, all GluA1 cells could be seen to have an AMPAR EPSC amplitude which was greater at the end of the recording than during the baseline (Figure 5.7C2). GluA1 ΔNTD expressing cells, on the other hand, did not show LTP, with AMPAR EPSCs increasing after the pairing protocol, but returning to baseline levels after 30 - 35 mins (Figure 5.7B-C).

To demonstrate the stability of recordings, a subset of recordings in which stimulation using the second pathway was performed and is presented in Figure 5.7D. While the control pathway in both GluA1 and GluA1 ΔNTD expressing cells showed transient potentiation (Figure 5.7D1), LTP was not observed in either case, and the return of AMPAR EPSC amplitudes to baseline in GluA1 ΔNTD expressing cells is evident. Such a transient potentiation in the control pathway has been observed previously in LTP recordings from organotypic slices (Hayashi et al., 2000) and is likely caused by the increased connectivity of this preparation, meaning that stimulating two sets of entirely distinct axons is difficult to achieve. Nevertheless, the specific potentiation of GluA1 expressing cells in the test pathway is clear (Figure

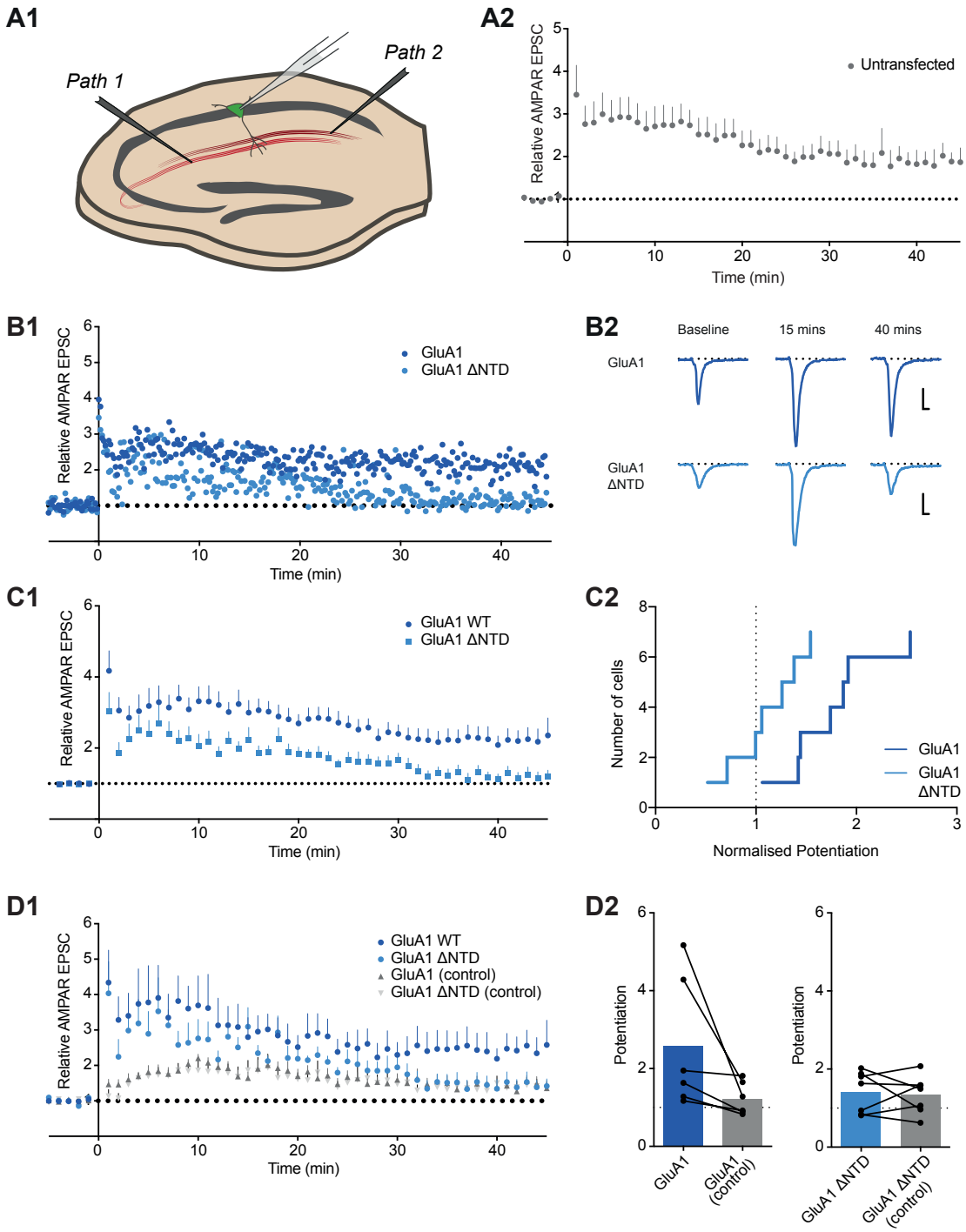

Figure 5.7 ***LTP requires GluA1 NTD-dependent interactions***

Figure 5.7 ***LTP requires GluA1 NTD-dependent interactions*** *(**A1**) Schematic of LTP arrangement, where one CA1 pyramidal cell is recorded in a whole-cell configuration, with two pathways of Schaffer collateral axons stimulated independently, one of which receives LTP stimulus (test-pathway) and the other does not (control pathway). (**A2**) Pairing of 2 Hz stimulation for 100 s with postsynaptic depolarisation to -10 mV holding potential produces robust LTP in untransfected cells, lasting over 45 min. (**B1**) Un-binned example data for test-pathway LTP recording of GluA1 and GluA1 ΔNTD expressing cells, showing robust LTP lasting 45 min only in GluA1 cells. (**B2**) Representative AMPAR EPSC traces from cells expressing GluA1 or GluA1 ΔNTD. Traces show EPSCs before induction (baseline) and 15 and 40 min after induction. Scale bar = 10 ms and 20 pA. (**C1**) AMPAR EPSC amplitudes from cells expressing GluA1 or GluA1 ΔNTD over time, averaged in one-minute bins. At time = 0 LTP was induced. EPSC amplitudes are normalised to pre-induction amplitude. LTP is maintained past 35 min in cells expressing GluA1, but not GluA1 ΔNTD. Normalised amplitude at 45 mins: GluA1: 2.35 ± 0.49 (n = 16); GluA1 ΔNTD: 1.20 ± 0.17 (n = 14). (**C2**) Plot of individual cell potentiation at 45 mins. (**D1**) AMPAR EPSCs from a subset of GluA1 and GluA1 ΔNTD-expressing cells with intact control pathway recordings. Control pathways from both conditions remained comparable and stable over recording duration. Only test pathway of GluA1 remained potentiated at 45 mins (GluA1: n = 7; GluA1 ΔNTD: n = 7) (**D2**) Pairing of LTP test and control pathways on a cell-by-cell basis.*

5.7D2). This data shows that NTD-dependent anchoring of the GluA1 subunit is required for stable synaptic potentiation.

5.2.6 The role of the GluA3 NTD in surface trafficking.

The third AMPAR subunit present in CA1 pyramidal neurons is GluA3, which forms heteromeric receptors with GluA2, likely in an obligatory manner (Rossmann et al., 2011), unlike GluA1 which can form homomeric channels. GluA3 has been demonstrated to have two residues in its LBD (Y432 and R439) which are non-conserved among AMPAR subunits, and control the surface delivery in a cell-line assay (Coleman et al., 2016, 2010). To confirm this effect also occurs in a neuronal setting, where auxiliary proteins such as cornichons or TARPs are present and could aid receptor forward trafficking, GluA3 and GluA3 R439G were transfected in subsets of dissociated hippocampal cultures, and the presence of surface receptors was detected by immunofluorescence against N-terminal c-myc tags (Figure 5.8A). The single R439G point mutation doubled the levels of exogenous GluA3 on the surface of neurons, bringing the surface trafficking capability of the subunit to at least the levels of GluA2Q (Figure 5.8A2).

This surface trafficking difference between GluA2Q and GluA3 was further confirmed by measuring the RI of surface neuronal patches in organotypic slice cultures, as previously described. While both GluA1 and GluA2Q showed strong surface delivery, GluA3 only modestly changed the surface RI (Figure 5.8B). In order to study the synaptic anchoring role of the GluA3 NTD whilst avoiding the potential caveats of reduced receptor surface expression, the GluA3 NTD was placed on either GluA1 or GluA2Q. Surprisingly, these receptors showed poorer surface delivery, both producing surface RIs which were substantially higher than the receptors containing their respective NTDs (Figure 5.8B). Due to incomparable surface receptor populations, the role of the GluA3 NTD in synaptic anchoring cannot be unbiasedly studied, but this data indicates that not only the LBD, but also the NTD of GluA3 limits surface delivery of the receptor.

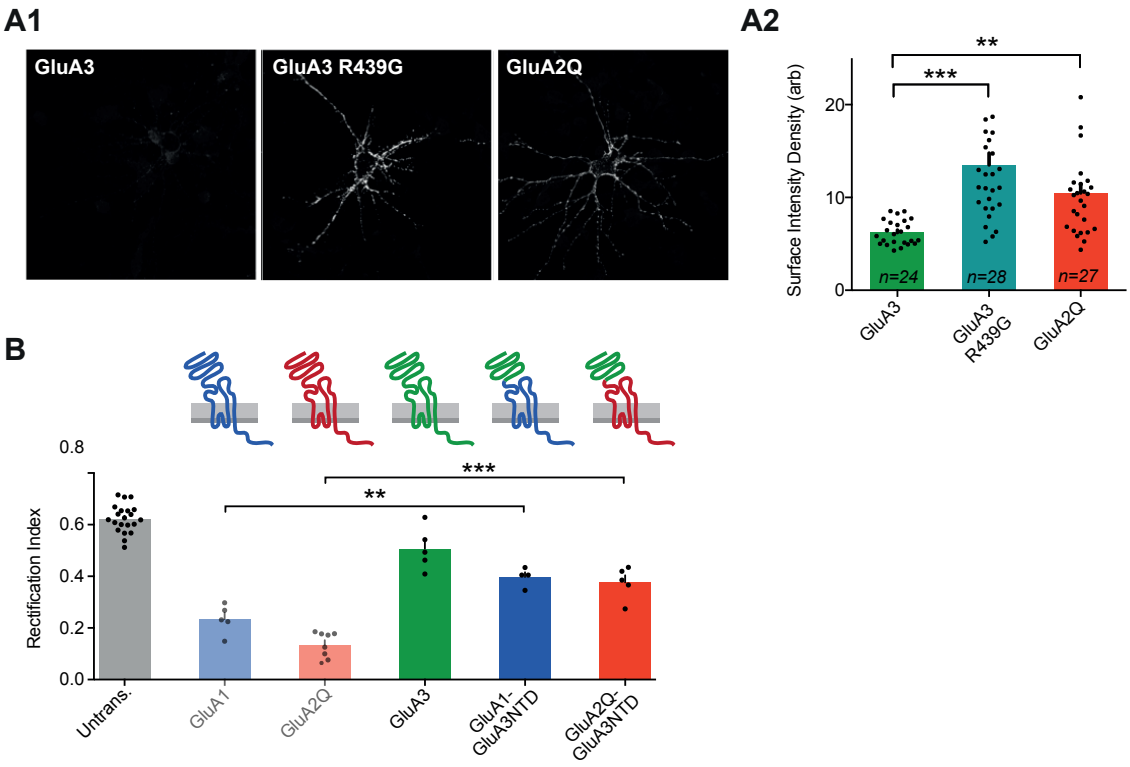

Figure 5.8 ***Surface trafficking of GluA3 is impaired by both the LBD and NTD*** *(**A**) Surface trafficking of GluA3 is increased by R439G mutatgenesis, which aligns surface expression with GluA2Q Example images (**A1**) and surface expression quantification (**A2**) of overexpressed GluA3, GluA3 R439G and GluA2Q in dissociated hippocampal cultures. (GluA3: 6.21 ± 0.27, GluA3 R439G: 13.51 ± 1.27, GluA2Q: 10.49 ± 0.95, One-way ANOVA: p<0.0001). (**B**) Surface rectification from outside-out patches of organotypic cultures demonstrate that the GluA3 NTD impairs surface trafficking of both GluA1 and GluA2Q (GluA1: 0.23 ± 0.03, GluA2Q: 0.13 ± 0.02, GluA1+GluA3 NTD: 0.40 ± 0.02, GluA2Q 0.38 ± 0.03, One-way ANOVA: p<0.0001).*

5.3 Discussion

The sequence divergence of the AMPAR NTD was appreciated even from the initial cloning of the AMPARs, with Keinänen et al. (1990) stating: *This region contained the highest number of substitutions in the four receptors*. However, the significance of this divergence has long been underappreciated. These sequence differences are present not only on the surface of the domain, but also in the interface of NTD dimers, producing dramatic effects on the affinity of NTD monomers for each other (Rossmann et al., 2011; Zhao et al., 2017).

Trafficking of GluA3 containing receptors.

The differences in NTD dimer affinities alluded to earlier mean that GluA3 NTD dimers form around an order of magnitude less strongly than GluA2-GluA3 dimers, strongly driving GluA3 towards heteromeric assembly. It is possible that the poor surface trafficking of GluA3 which is dependent on the NTD in this study is caused by the poor assembly of receptors. However, while GluA1 and GluA1 ΔNTD both surface traffic similarly well, the latter in the absence of any NTD, the poor surface trafficking of GluA1+A3NTD means that the GluA3 NTD has a detrimental effect on receptor surface trafficking.

While the investigation of GluA3 was not continued due to the impaired surface trafficking of the subunit, it can be inferred from previous data that GluA3 containing receptors are targeted to the synapse through a route that does not involve somatic surface delivery. Both conditional (Lu et al., 2009) and genomic (Andrásfalvy et al., 2003; Zamanillo et al., 1999) GluA1 knockout mice show dramatically reduced surface AMPAR currents, with more modest effects on synaptic currents, indicating GluA2/3 heteromeric receptors contribute predominantly to synaptic currents rather than surface currents. Recent proteomic analysis of subunit abundance within sub-cellular fractions confirmed the mostly synaptic localisation of GluA3, compared to the more widespread GluA1 (Pandya et al., 2017). By looking at the location of GluA1 and GluA3 within the postsynaptic density (indicative of the location of GluA1/2 and 2/3 heteromeric receptors respectively) suggests that GluA2/3 complexes are arranged more centrally within the synapse than GluA1/2 heteromers (Jacob and Weinberg, 2015).

Taking into account the current diffusive model of AMPAR synaptic anchoring (Choquet and Triller, 2013; Opazo and Choquet, 2011) where synaptic and extrasynaptic receptors are constantly exchanging, and that the surface population of receptors is predominantly

GluA1/2 heteromers, could explain this organisation, whereby the surface pool of GluA1/2 receptors comprise the exchanging pool of subunits at the synaptic periphery, and GluA2/3 receptors comprise a relatively more stable population of centrally anchored subunits. Such a model could account for the strong association between GluA1 containing receptors and LTP (Hayashi et al., 2000; Lee et al., 2003; Mack et al., 2001; Schmitt et al., 2005), and the apparent need for an extrasynaptic population of receptors for LTP expression (Granger et al., 2013; Penn et al., 2017). Similarly, the stability of GluA3 containing receptors at the centre of the synapse could be maintained by their low channel activity, if, as has been suggested, AMPAR activation promotes receptor diffusion from synaptic sites (Constals et al., 2015; Gutierrez-Castellanos et al., 2017b). However, a significantly greater level of investigation would be required to answer this hypothesis.

The requirements for GluA1 synaptic anchoring

The present study utilises exogenous receptor overexpression, the effects of which are interesting to contemplate. Overexpression of GluA1 produces homomeric receptors (see surface currents and Hayashi et al., 2000; Shi et al., 2001, 1999). Given that the endoplasmic reticulum contains a reserve pool of GluA2 (Greger et al., 2002) which likely drives the formation of heteromeric GluA2 containing receptors, why does exogenous GluA1 not assemble predominantly as heteromeric channels? While this is an interesting question, the fact that GluA1 forms predominantly homomeric channels conveniently allows comparative analysis with expression of GluA2Q in this study.

The requirement for an activity stimulus in delivery of exogenous GluA1 to the synapse had been described as essential (Hayashi et al., 2000; Shi et al., 2001, 1999). These studies were the basis of a model for subunit-specific AMPAR trafficking, whereby GluA1/2 heteromers contribute to activity-dependent synaptic scaling, whereas GluA2/3 receptors constitutively traffic to synapses to replace GluA1-containing receptors over time (Shi et al., 2001), however this model was built on data obtained using N-terminally tagged AMPAR subunits. The present study, confirmed by others (Díaz-Alonso et al., 2017) demonstrates that GluA1 trafficking is not so strictly dependent on activity, and can even cause rectification when spontaneous activity in cultured slices is dampened with TTX. It appears that N-terminal GFP tagging limited the constitutive trafficking of this subunit, yet a comparison of these results shows that activity dependent trafficking of GluA1 can overcome the inhibitive effect of the GFP. This result indicates that other receptor interactions can contribute to GluA1

trafficking in synaptic potentiation, most likely those of the CTD (Shi et al., 2001; Zhou et al., 2018).

Subunit-specific AMPAR roles.

The evidence presented here demonstrates a subunit-specific role for AMPAR NTD interactions in controlling synaptic transmission. The GluA1 NTD appears essential for anchoring of this subunit in synaptic transmission, a result that has more recently been confirmed by others (Díaz-Alonso et al., 2017). The GluA2 NTD appears not to have such an essential role, but strongly promotes contribution of the subunit to transmission, which, while not stated or commented on, can also be seen in the results of Díaz-Alonso et al. (2017), who also rescued currents of *Gria1-3fl* neurons with exogenous AMPAR expression, demonstrating around 50 % less rescue on GluA2 NTD removal. The results presented above demonstrate that the interactors for GluA1 and GluA2 have unique properties, suggesting that the NTDs either have different interactors in the synaptic cleft, or their NTDs have different affinities for a single interactor which promotes anchoring. Given that the NTD of GluA2 can promote increased anchoring of GluA1 yet does not appear strictly necessary for receptor anchoring (given that GluA2 ΔNTD causes synaptic rectification) other parts of the receptor are likely to influence synaptic anchoring, for example the C-terminus, which has previously been implicated in basal receptor trafficking (Shi et al., 2001).

Despite the incredible amount of interest the CA3-CA1 synapse has attracted, the role of individual AMPAR subunits here is still relatively uncertain. The first model of subunit-specific requirements by Shi et al. now seems slightly unclear. The relative contribution of GluA1/2 and GluA2/3 heteromers to synaptic currents has been debated (Cheng et al., 2006; Geiger et al., 1995; Sans et al., 2003; Wenthold et al., 1996), until the contribution of each subunit to synaptic transmission was elegantly dissected by conditional subunit knockout. Lu et al. (2009) showed that GluA1/2 complexes contribute the majority of the postsynaptic AMPAR current (81 %), while GluA2/3 heteromers contribute a more modest 16 %. This data is supported by immunogold labelling of AMPAR subunits (Yamasaki et al., 2016) which showed a greater labelling density for GluA1 than GluA3 at this synapse, and proteomic analysis of AMPAR complexes (Schwenk et al., 2014).

It is interesting to note that a novel plasticity mechanism has been reported for GluA3 containing receptors (Gutierrez-Castellanos et al., 2017b), being inherently dormant, with a very low single-channel conductance that can be increased to normal AMPAR levels in

a cAMP-dependent manner. This data would suggest that while the results of Lu et al. (2009) are true for contributions to transmission under basal conditions, the actual synaptic receptor populations contain a greater percentage of GluA3-containing AMPARs, which can contribute to transmission after culmination of a signalling cascade. This intriguing hypothesis has also been demonstrated for GluA3-containing heteromers in the cerebellum (Gutierrez-Castellanos et al., 2017a) and offers a completely novel mechanism to alter the strength of synaptic transmission, aside from simply changing the synaptic receptor content. Confirmation and demonstration of the function of this mechanism can be eagerly awaited.

Another subunit-specific AMPAR role is that of calcium-permeable receptors, which have been shown to contribute to synaptic plasticity (Plant et al., 2006). Given that the vast majority of GluA2 is RNA edited to prevent calcium permeability (Geiger et al., 1995; Wenthold et al., 1996) in the CA3-CA1 synapse, these receptors most likely represent a population of GluA1 homomers or GluA1/3 heteromers. It has been proposed that these subunits are specifically inserted upon LTP, and their calcium-flow is important for producing long-term synaptic potentiation (Plant et al., 2006). This hypothesis is meaningful, as insertion of calcium-permeable subunits in an NMDAR-dependent manner would allow subsequent low frequency stimulation at the same synapse to allow continual calcium flow, in the absence of sufficient depolarisation for NMDAR activation, potentially allowing correlation between a particular activity stimulus (LTP induction) and subsequent low level activity at the synapse. The insertion of CP-AMPARs in LTP however has been the subject of intense debate (Adesnik and Nicoll, 2007; Gray et al., 2007), yet the difference between observations appears now to have been clarified, and their involvement in LTP appears to be both developmentally regulated (Sanderson et al., 2016) and induction-protocol dependent (Park et al., 2016b).

The strong synaptic anchoring conferred by the GluA2 NTD which is observed in this study could be a mechanism to control the contribution of CP-AMPARs at this synapse, by biasing for GluA2 containing receptor anchoring, and preventing the potentially toxic effects of excess calcium signalling, unless required for LTP induction (Liu and Zukin, 2007; Pellegrini-Giampietro et al., 1997).

On overexpression, the stronger anchoring of GluA2 compared to GluA1 could be explained by the higher affinity of GluA2 for synaptic sites, favouring GluA2 homomers (4 GluA2 NTDs) over the endogenous GluA1/2 heteromers (2 GluA2 NTDs), whereby GluA1 homomers would be not so advantaged, resulting in a weaker change to synaptic RI. However,

GluA1 is not able to fully rescue AMPAR currents in the absence of other subunits, as seen by knockout/rescue experiments. The poor anchoring of GluA1 in a knockout scenario is not an unprecedented finding, as conditional GluA2 knockout reduces synaptic AMPAR currents by approximately 50 % without significantly affecting the surface receptor pool (Lu et al., 2009). Together these results are suggestive that N-terminal AMPAR anchors for GluA1 are either lower affinity or less abundant than those of GluA2. It would be interesting to speculate that such anchors may increase on LTP induction to allow either CP-AMPAR incorporation or increased GluA1 containing receptor mediated transmission, yet so far there is no evidence for such an effect.

An obvious extension to this investigation would be to identify the interactors of the NTD which meditate the observed effects. Given the sensitivity of the extreme N-terminus to modification (Figure 5.2) it is likely that this site is the location for GluA1 dependent synaptic anchoring, and crosslinking of protein interactions at this position may allow identification of this binding partner.

The role of AMPAR subunits in synaptic potentiation.

The present study offers no indications of subunit requirements in LTP, given that the GluA2 and its NTD have not been studied, however it confirms that GluA1-dependent interactions are important, implicating this subunit in LTP expression.

While the GluA1 NTD appears essential for synaptic anchoring during basal transmission, leaving little apparent role for CTD interactions of the subunit, the mechanisms involved in LTP are not as clear. Both tCaMKII and electrical stimulation induced potentiation are blocked by GluA1 ΔNTD expression, indicating that 1) the GluA1 NTD is required for synaptic anchoring of the receptor under potentiated conditions, and 2) that this construct acts as a dominant negative, preventing LTP expression by endogenous AMPARs. To act as a dominant negative, other interactions of GluA1 must be involved in synaptic potentiation. The GluA1 CTD had previously been described as both essential (Hayashi et al., 2000; Shi et al., 2001) and dispensible (Granger et al., 2013), yet a recent elegant study using CTD knock-in mice unequivocally showed that the GluA1 CTD is required for receptor trafficking in synaptic potentiation (Zhou et al., 2018). As CTD interactors appear to be required for GluA1 trafficking in LTP, it is most likely that sequestration of CTD interactors by GluA1 ΔNTD is what inhibits LTP, especially given that TARP association of the receptor is unchanged.

While the trafficking rules suggested by Shi et al. (2001) do not appear so absolute, the results presented above draw interesting parallels with this study. Synaptic anchoring of GluA2 can occur strongly under basal conditions, while that of GluA1 is not as robust. GluA2 ΔNTD can act as a dominant negative under basal conditions, indicating a role for the CTD in constitutive receptor trafficking, while GluA1 ΔNTD does not. However, GluA1 ΔNTD does act as a dominant negative under potentiating conditions, implicating its CTD in such scenarios, as clearly shown by Shi et al. (2001). Therefore, while the authors were unfortunate to limit the influence of NTD-dependent interactions on AMPAR function, thus exaggerating the role of the CTD in their study, the elegant mechanisms of subunit-specific targeting appear to hold trends of truth.

A transient short-term synaptic potentiation is observed in GluA1 ΔNTD expressing cells in LTP recordings. As AMPAR trafficking is the major component of LTP on this time-scale (Penn et al., 2017), this effect could be mediated by two mechanisms. One possibility is that endogenous receptors could contribute to this transient potentiation, with the dominant negative effect of GluA1 ΔNTD only acting at later stages. This would be consistent with a role for the CTD in late LTP maintainance, through GluA1 receptor surface trafficking, especially given that AMPAR exocytosis has been demonstrated as responsible for these stages of potentiation maintainance (Makino and Malinow, 2009; Penn et al., 2017).

The second possible explanation for this potentiation is that TARP interactions with the postsynaptic density cause the accumulation of postsynaptic AMPARs during this period. Phosphorylation of TARPs by CaMKII, which is activated on LTP induction, has been demonstrated to facilitate AMPAR anchoring (Opazo et al., 2010). If this is indeed the case, it would suggest that these interactions are inadequate for long term maintenance of potentiation. Clearly the interplay of AMPAR interactions in synaptic transmission and plasticity requires further more detailed analysis.

A nanoscale dissection of synaptic function.

As has been described previously for GluA2 (Chapter 4), the difference in synaptic transmission on GluA1 NTD removal does not appear to be caused by any trafficking deficits, either by reduced surface trafficking or spine enrichment. With no difference observed in receptor clustering, the best explanation of why GluA1 ΔNTD does not contribute to transmission while GluA1 does, is the relative position of the subunits in relation to presynaptic release

sites. To dissect out such nanoscale arrangement of postsynaptic receptors would require either multicolour superresolution imaging, to visualise both pre and postsynaptic structures, or to use glutamate uncaging to study the rectification properties of *perisynaptic* receptors. From the imaging data presented, it could be expected that GluA1 ΔNTD would give strong rectification in glutamate uncaging responses at dendritic spines, yet the receptors which are functionally aligned for transmission are endogenous subunits, which preferentially anchor at release sites through NTD-dependent interactions. As NTD-deleted receptors still associate with auxiliary subunits, and will have unaffected CTD-dependent interactions, it is clear that these interactions with the postsynaptic density are alone insufficient to maintain proper AMPAR synaptic anchoring. For this reason, clarification of the distinct roles of each of these interactions remains a major challenge in understanding AMPAR function.

Chapter 6

The interplay of interactions controlling AMPAR synaptic anchoring

6.1 Introduction

Since the revelation that AMPAR trafficking provides a significant contribution to synaptic potentiation (Kauer et al., 1988; Muller et al., 1988; Nicoll, 2017), the mechanisms controlling the AMPAR content of a synapse have been the subject of intense investigation. As has been previously discussed, a host of intracellular AMPAR interactions have been identified each with differing roles in synaptic transmission, yet how these interactions work in combination has not been the subject of great attention, and therefore the relative contribution or importance of each is not understood.

TARPs in AMPAR synaptic anchoring

The best characterised interaction of the AMPAR with the postsynaptic density occurs indirectly, through the association of the receptor with the auxiliary subunits TARPs (Transmembrane AMPAR regulatory proteins). These transmembrane proteins associate with the transmembrane domain of the AMPAR and cause substantial modulation of receptor gating and conductance (Jackson and Nicoll, 2011). TARPs are part of a family of 8 proteins which were originally characterised as calcium channel subunits, two of which, γ1 and γ6 function as calcium channel associated genes (Chu et al., 2001). γ2, 3, 4, 5, 7 and 8 form a family of AMPAR modulating transmembrane proteins with distinct effects on channel gating and unique expression patterns throughout the brain (Jackson and Nicoll, 2011; Tomita et al., 2003). TARP γ2, 3, 4 and 8 all show some level of expression in CA1 pyramidal neurons,

with TARP γ8 the most abundant and influential TARP in these cells (Rouach et al., 2005; Tomita et al., 2003; Yamasaki et al., 2016).

The intracellular C-terminus of TARPs γ2, 3, 4 and 8 all end with a PDZ ligand 'TTPV' motif, which interacts with the PDZ domain of MAGUKs such as PSD-95 and PSD-93 (Dakoji et al., 2003; Schnell et al., 2002). These MAGUKs (membrane-associated guanylate kinases) both contain three PDZ domains, all of which can interact with the TARP CTD (Dakoji et al., 2003), however it has been suggested that the two most N-terminal domains (PDZ1 and PDZ2) mediate the majority of synaptic interactions with TARPs (Schnell et al., 2002; Xu et al., 2008). Given that PSD-95 is such an abundant protein in the postsynaptic density (Chen et al., 2015), this interaction has the potential to strongly accumulate synaptic AMPARs, and indeed, overexpression of PSD-95 increases the postsynaptic AMPAR response (Ehrlich and Malinow, 2004; Stein et al., 2003). Further to this, PSD-95 has been demonstrated to form subclusters within the postsynaptic density (Fukata et al., 2013; MacGillavry et al., 2013), which are aligned with presynaptic release sites (Tang et al., 2016) and therefore the TARP to PSD-95 interaction could mediate receptor clustering.

The importance of this TARP interaction cannot be more dramatic than in cerebellar granule cells, where *stargazer* (TARP γ2 knockout) cells almost completely lack synaptic AMPAR currents that cannot be rescued by stargazin expression unless the PSD-95 interacting region is intact (Chen et al., 2000). In hippocampal neurons however, the importance of this interaction does not appear so clear cut. Overexpression of TARP γ2 lacking the TTPV PDZ ligand, causes almost complete loss of spontaneous transmission (Bats et al., 2007; Chen et al., 2000) indicating a strict requirement for this interaction, however generation of a mouse line with the PDZ ligand removed from TARP γ8 (TARP γ8 Δ4), the predominant TARP in CA1 hippocampal cells (Rouach et al., 2005), causes only a modest 30 % reduction in basal transmission while LTP in these cells was intact (Sumioka et al., 2011). Use of biomimetic ligands to disrupt the TARP PSD-95 interaction acutely reduces currents to a greater extent (55 %) (Sainlos et al., 2011), however this approach has the potential to affect other interactions of PSD-95, thus overstating the influence of this interaction on transmission. Together, while this data demonstrates that TARP-PDZ interactions, while certainly contributing to synaptic receptor accumulation, are not the sole requirement for AMPAR transmission. TARPs are not the only auxiliary subunits with PDZ domain interactions. The CKAMP (or shisa) family of auxiliary subunits also interact with PSD-95, allowing AMPAR anchoring (Klaassen et al., 2016).

A current model of AMPAR incorporation in LTP involves phosphorylation of TARP CTDs (Opazo et al., 2010; Tomita et al., 2005), which allows greater interaction with PSD-95 by limiting the association of the TARP CTD with the plasma membrane (Hafner et al., 2015). In this model, diffusing surface extrasynaptic AMPARs are specifically trapped at synaptic sites by TARP-PSD interactions on CaMKII phosphorylation (Bats et al., 2007; Opazo et al., 2012). However, the TARP interaction may not be the sole mediator of synaptic anchoring in potentiation, as the initial influx of receptors in LTP temporally coincides with a transient *loss* of PSD-95 from the spine (Zhang et al., 2014a). Additionally, this model has been constructed by studying overexpressed TARP γ2, which is neither the predominant TARP in hippocampal CA1 pyramidal neurons (Rouach et al., 2005; Schwenk et al., 2014; Yamasaki et al., 2016) nor present in extrasynaptic areas (Inamura et al., 2006; Yamasaki et al., 2016), questioning the models significance and validity. Phosphorylation of the TARP γ8 CTD has been indicated to influence the magnitude of LTP (Park et al., 2016a), implicating other TARP interactions in AMPAR anchoring, yet the mechanism for this effect is completely unclear and unstudied.

It is peculiar that studies investigating TARP interactions in AMPAR anchoring have predominantly used TARP γ2, which does not play a major role in CA1 synaptic transmission (Hashimoto et al., 1999). Four TARPs appear to be present at hippocampal CA1 synapses (Tomita et al., 2003), with TARP γ3 and γ4 having little influence on AMPAR synaptic density (Yamasaki et al., 2016). In an elegant study, Yamasaki et al. (2016) showed that TARP γ2 predominantly localises to large, perforated synapses with a high AMPAR density, while TARP γ8 maintains a basal level of AMPARs in all spines and at extrasynaptic areas. This differential localisation raises questions over the role of the two TARP subtypes in these cells. Given that perforated synapses have been associated with LTP and long-term stability of spines (Dhanrajan et al., 2004; Hering and Sheng, 2001; Stewart et al., 2005), could TARP γ2 control the induction of LTP and the maintenance of AMPARs in a potentiated synapse? While basal transmission is unaffected at this synapse in the TARP γ2 knockout mouse (Hashimoto et al., 1999), LTP does not appear to have been studied to date.

Several key questions surrounding TARP-dependent AMPAR anchoring remain. What contribution to AMPAR synaptic transmission do TARPs provide, aside from its modulation of receptor gating? What role do individual TARP subtypes have on AMPAR function, and what mechanisms control receptor anchoring in each case?

The AMPAR CTD in synaptic anchoring

The CTD of the AMPAR has also been intensely studied, but due to conflicting interpretations of its influence on synaptic transmission, is less widely accepted as a synaptic anchoring mechanism.

The GluA1 CTD has been shown to interact with band 4.1 for surface delivery of receptors (Shen et al., 2000), yet this interaction is unlikely to control synaptic receptor anchoring. SAP97 binds the extreme C-terminus of GluA1 through its PDZ domain, with a suggested role in synaptic anchoring (Leonard et al., 1998). SAP97 is a MAGUK located at the postsynaptic density, with splicing controlling its lateral positioning (Waites et al., 2009), therefore could potentially control location specific accumulation of GluA1 containing receptors within synaptic areas. However, generation of a mouse line where the SAP97 interacting residues of GluA1 are deleted has little effect on either synaptic transmission or plasticity (Kim et al., 2005), and SAP97 removal appears not to substantially affect AMPAR transmission (Ehrlich and Malinow, 2004). This interaction therefore does not appear to have a significant role in AMPAR anchoring at the hippocampal CA1 synapse, and may have more significance in trafficking of GluA1 from the endoplasmic reticulum (Sans et al., 2001).

Phosphorylation of the GluA1 CTD has been widely reported as a mechanism controlling the delivery of GluA1 to the synapse (Esteban et al., 2003; Shepherd and Huganir, 2007), with the S845 phosphorylation by PKA being most prominent, and most likely required for the surface delivery of GluA1 containing receptors (Esteban et al., 2003; Man et al., 2007; Oh et al., 2006). Given that surface delivery of AMPARs is essential for the induction of late LTP (Makino and Malinow, 2009; Penn et al., 2017), the essential requirement for the GluA1 CTD in LTP is suggestive that GluA1 containing receptors are specifically delivered to the surface to mediate LTP, in a manner requiring their CTD, yet there is little substantial evidence that the CTD is directly involved in synaptic receptor anchoring at synaptic sites or receptor positioning within the PSD. It is also interesting to note that despite the intense study of GluA1 CTD phosphorylation, the actual function of this modification in affecting protein interactions or receptor conformations are completely unclear.

Granger et al. (2013) conclude that the GluA1 CTD is entirely dispensable for LTP, yet this result does not appear to be of the greatest physiological relevance, given that recent GluA1 CTD knockout mice (where GluA1 contains the CTD of GluA2) exhibit a complete lack of LTP (Zhou et al., 2018). The study of Zhou et al., while confirming a role for the GluA1

CTD in LTP, does not describe the mechanism for this function, therefore any of the reported interactions or phosphorylations could be the essential requirements.

The GluA2 CTD is also phosphorylated (Chung et al., 2000), with roles in regulating receptor endocytosis (Matsuda et al., 2000, 1999). This CTD interacts with a different subset of synaptic proteins to GluA1, with its PDZ ligand binding both GRIP/ABP and PICK1 (Xia et al., 1999). While GRIP interactions have been suggested to control synaptic localisation (Osten et al., 2000), evidence has suggested a more likely role in receptor recycling (Braithwaite et al., 2002). The interplay between GRIP and PICK1 binding has been demonstrated to elegantly control the endocytosis of the subunit (Lu, 2005), particularly in LTD (Takamiya et al., 2008; Xia et al., 2000) and may be of greater consequence at cerebellar synapses (Gallimore et al., 2016).

The ATPase NSF interacts with the GluA2 CTD in a manner that releases intracellular pools of AMPARs for surface delivery (Hanley et al., 2002). Key evidence for a role of the GluA2 CTD in synaptic transmission stems from the use of pep2m, a peptide derived from the GluA2 CTD which can block synaptic transmission by up to 80 % when used intracellularly (Lüthi et al., 1999; Nishimune et al., 1998). However, it is important to remember that this peptide could affect interactions of GluA2 binding partners with other synaptic proteins, so could feasibly have a more detrimental role on synaptic transmission than simply blocking the interactions of the GluA2 CTD. For this reason such techniques cannot be used to quantify the importance of particular CTD interactions in GluA2 synaptic anchoring.

The final, most recently identified domain controlling AMPAR synaptic anchoring is the NTD (see Chapter 4, 5 and Díaz-Alonso et al., 2017; Watson et al., 2017). As the critical role of this domain in synaptic transmission has only recently been demonstrated, the interplay of these interactions with CTD and TARP interactions is yet to be investigated or quantified. NTD deletion constructs act as dominant negatives, demonstrating an interplay with other receptor interactions in controlling synaptic transmission (Watson et al., 2017), while NTD removal does not affect the interaction with TARPs (see Chapter 4, 5) indicating that TARP interactions with the PSD alone are not sufficient for maintaining synaptic transmission. The precise requirements for each interaction in the accumulation of AMPARs at postsynaptic sites remains an open question of great significance.

6.2 Results

A plethora of AMPAR interaction proteins have been identified, which can be loosely categorised into three regions on the AMPAR which control synaptic transmission: the NTD, CTD and through auxiliary subunits (Figure 6.1). The interplay of these interactions in controlling synaptic transmission is yet to be clarified.

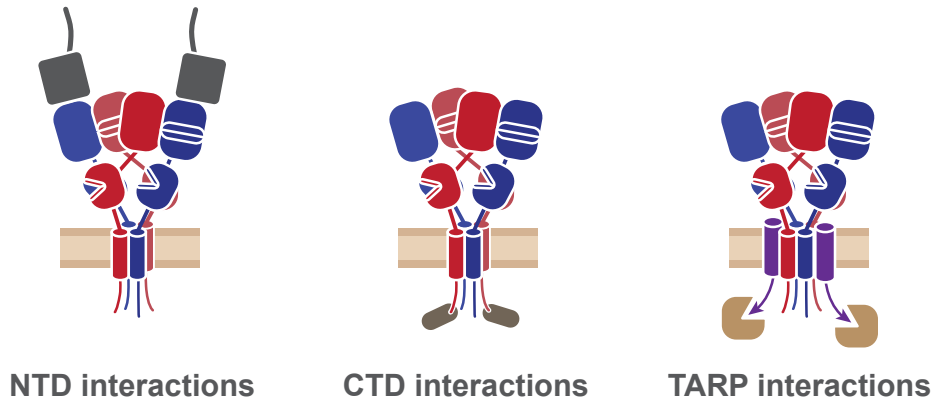

Figure 6.1 ***Three interaction sites control AMPAR synaptic anchoring.*** *AMPAR schematics highlighting the three sites of interactions which have been demonstrated to influence receptor anchoring at synaptic sites.*

6.2.1 The role of CTD interactors in GluA2Q synaptic anchoring.

The role of the NTD in synaptic transmission was demonstrated using NTD deletion constructs (see Chapter 4, 5 and Díaz-Alonso et al. (2017); Watson et al. (2017)). GluA2Q ΔNTD, while contributing to synaptic transmission, anchors poorly at synaptic sites, depressing synaptic responses on overexpression (Figure 6.2, see also Chapter 4 and Watson et al., 2017).

As synaptic transmission is depressed on overexpression, normal levels of transmission are not maintained by endogenous receptors present in the cells, and therefore GluA2Q ΔNTD acts as a dominant negative. For this to occur, this construct 1) must be poorly anchored at synaptic sites, which is explained by the requirement for NTD-dependent interactions, and 2) must also sequester other interactors which endogenous receptors require to maintain transmission in their stead. As GluA1 ΔNTD also cannot anchor at synaptic sites (see Chapter 5), yet does not act as a dominant negative, the sequestered interactors causing

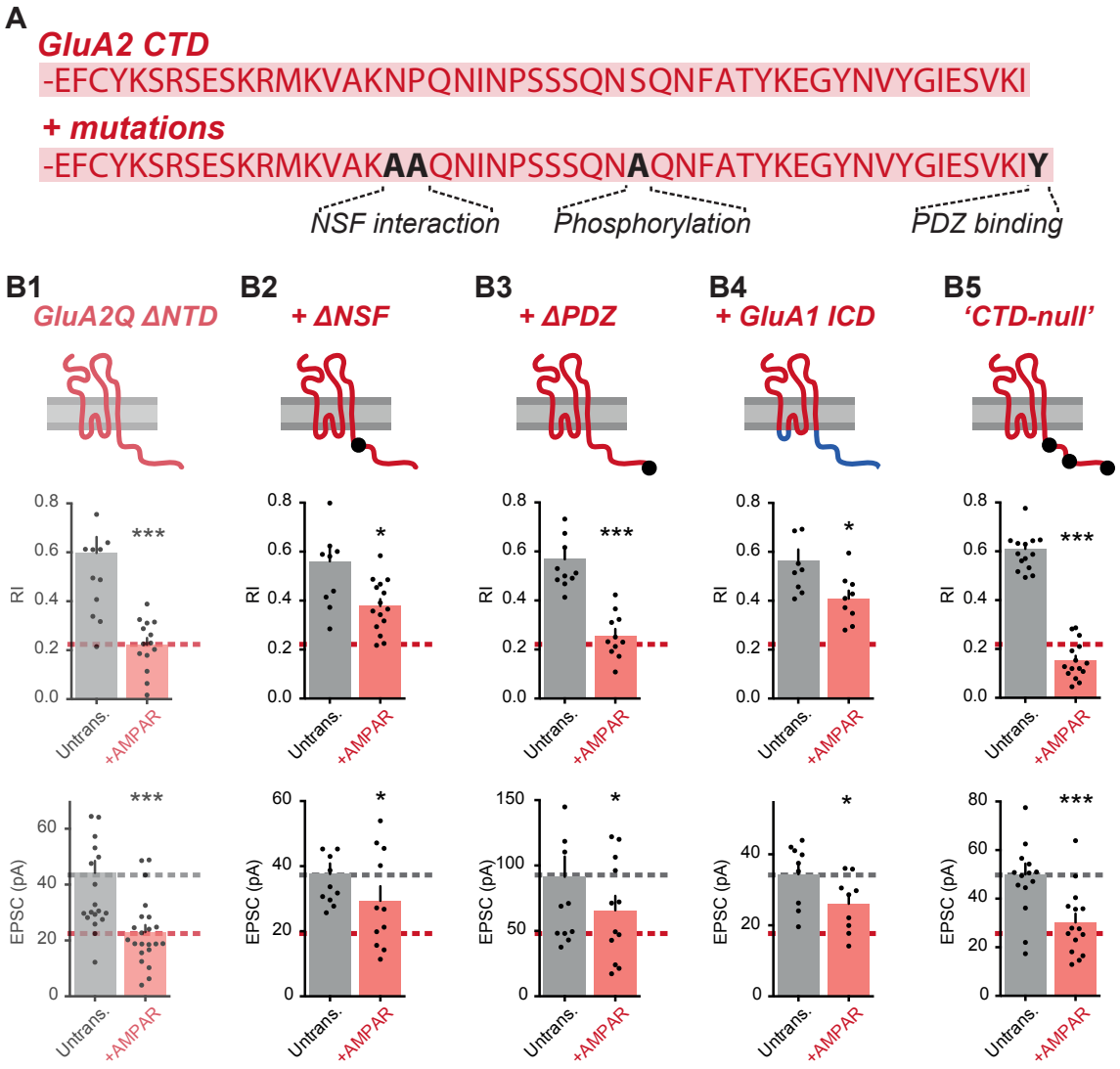

Figure 6.2 *The effect of CTD mutations on GluA2 ΔNTD.*

Figure 6.2 ***The effect of CTD mutations on GluA2 ΔNTD.*** *(**A**) Primary amino-acid sequence of the GluA2 CTD, and mutations used to prevent protein interactions or phosphorylations as indicated. (**B**) Synaptic rectification and AMPAR EPSC amplitudes between pairs of untransfected and cells transfected with indicated constructs. (**B1**) GluA2 ΔNTD causes synaptic rectification and decreased AMPAR EPSC amplitudes (reproduced from Chapter 4). (**B2**) NSF site mutation reduces both synaptic rectification and alleviates AMPAR EPSC depression (RI: untrans.: 0.55 ± 0.07; GluA2Q ΔNTD ΔNSF; 0.36 ± 0.03; paired t-test, p=0.036. EPSCs: untrans.: 37.6 ± 3.2 pA; GluA2Q ΔNTD ΔNSF: 29.4 ± 4.5 pA; paired t-test, p=0.019; n=11). (**B3**) PDZ-binding site mutated GluA2 ΔNTD causes strong synaptic rectification and some reduction in AMPAR EPSCs (RI: untrans.: 0.57 ± 0.04; GluA2Q ΔNTD ΔPDZ: 0.26 ± 0.03; paired t-test, p<0.0001. EPSCs: untrans.: 91.3 ± 15.4 pA; GluA2Q ΔNTD ΔNSF: 65.8 ± 11.0 pA; paired t-test, p=0.011; n=11). (**B4**) swapping the GluA2 intracellular domain (ICD) sequence for that of GluA1 limits both rectification and AMPAR EPSC depression (RI: untrans.: 0.56 ± 0.05; GluA2Q ΔNTD GluA1-ICD: 0.41 ± 0.03; paired t-test, p=0.018. EPSCs: untrans.: 34.4 ± 2.9 pA; GluA2Q ΔNTD GluA1-ICD: 26.1 ± 2.6 pA; paired t-test, p=0.027; n=9). (**B5**) Mutagenesis of both NSF and PDZ interaction sites and a phosphorylation site does not produce combinatorial limitation of GluA2 ΔNTD synaptic anchoring (RI: untrans.: 0.61 ± 0.02; GluA2Q ΔNTD CTD-null: 0.15 ± 0.02; paired t-test, p<0.0001. EPSCs: untrans.: 50.0 ± 4.5 pA; GluA2Q ΔNTD CTD-null: 30.2 ± 3.6 pA; paired t-test, p<0.0001; n=15).*

the dominant negative phenotype must be subunit specific for GluA2. As TARPs appear to have no subunit specific AMPAR binding, differential interactions with these auxiliary subunits are unlikely to cause the dominant negative effect, leaving CTD interactors the most promising candidate, given their strong subunit specific sequences (see Chapter 5).

Interactions of NSF and PDZ domain containing proteins with the GluA2 CTD have been shown to promote synaptic accumulation of this subunit, predominantly through enhanced surface trafficking (Araki et al., 2010; Braithwaite et al., 2002; Hanley et al., 2002). Mutations preventing these interactions have been reported previously (Kessels et al., 2009; Osten et al., 1998; Shi et al., 2001) (Figure 6.2A). Each interaction was prevented to assess its importance on GluA2 synaptic transmission by alleviating the dominant negative effect of GluA2Q ΔNTD. By mutating the NSF interaction site in GluA2Q ΔNTD, both the strong synaptic rectification and the depression of transmission are partially relieved (Figure 6.2B2 cf. B1). Prevention of PDZ domain interactions did not change the strong rectification of GluA2Q ΔNTD, and had only modest, if any, effect on AMPAR EPSCs (Figure 6.2B3). To confirm the role of the GluA2 CTD in the dominant negative effect, the intracellular domain (ICD, consisting of CTD and intracellular loop 1) was exchanged with that of GluA1, which alleviated both synaptic rectification and EPSC depression similarly to NSF site mutation (Figure 6.2B4). Interestingly, mutagenesis of both the NSF and PDZ sites and a reported phosphorylation site (Shepherd and Huganir, 2007), did not produce an aggregated alleviation of the synaptic changes, but instead this 'CTD-null' construct showed a similar synaptic phenotype to the original GluA2Q ΔNTD expression (Figure 6.2B5). This effect is likely produced by the complicated interplay of NSF and PDZ interactions in controlling GluA2 receptor recycling with intracellular pools (Braithwaite et al., 2002; Hanley et al., 2002; Shepherd and Huganir, 2007). While this data offers little insights into the role of CTD interactions on synaptic transmission, it demonstrates that this domain can influence the synaptic anchoring of GluA2 and sequestration of CTD interactors contributes to the synaptic depression observed on GluA2Q ΔNTD expression.

To investigate the interplay between NTD and CTD interactions, these CTD interacting protein mutations were introduced into full-length GluA2Q, which previously showed strong synaptic incorporation and results in elevated AMPAR EPSCs on overexpression (Figure 6.3A and Chapter 4). Mutation of the NSF interaction site, which showed a clear effect on GluA2Q ΔNTD synaptic anchoring did not alter full-length GluA2Q anchoring (Figure 6.3B1). In fact, mutation of the NSF interaction site (Figure 6.3B1), PDZ interaction site

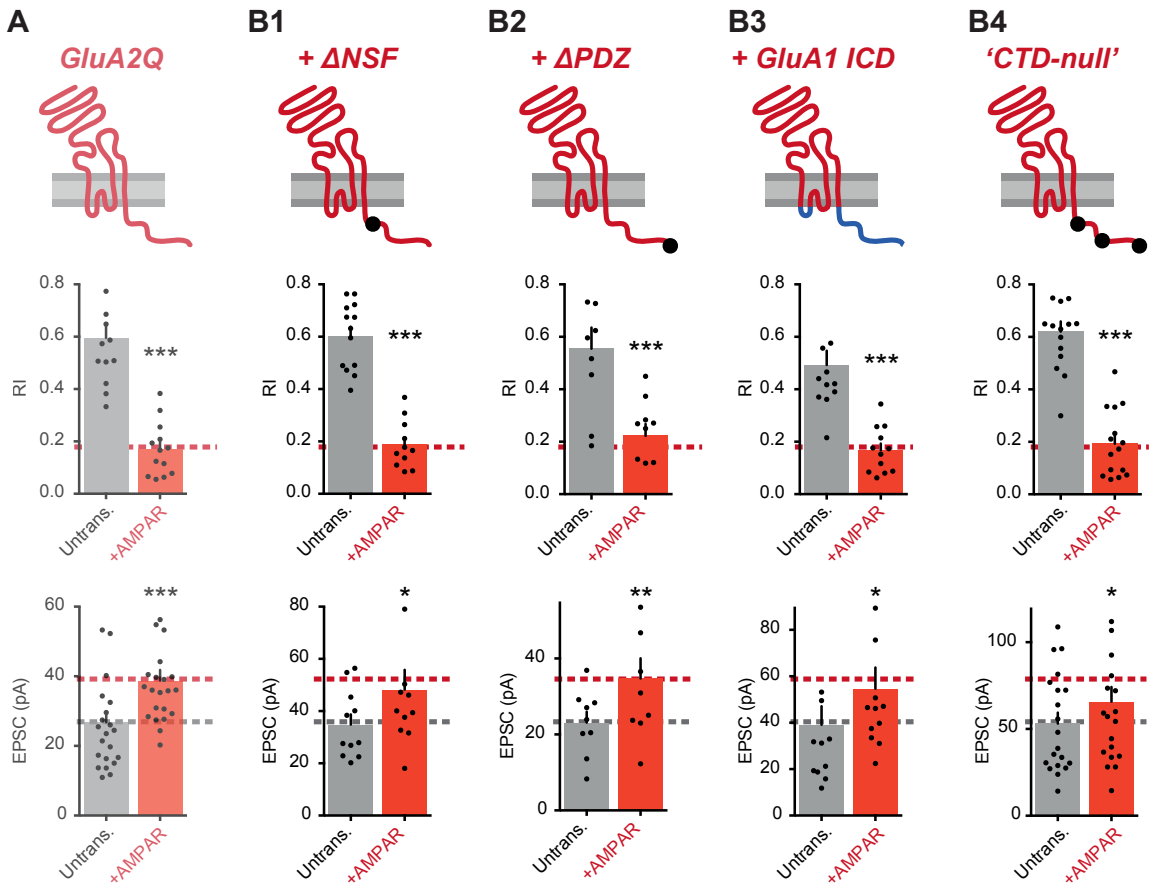

Figure 6.3 ***The effect of CTD mutations on full-length GluA2 synaptic anchoring.*** *(**A**) GluA2Q overexpression causes strong synaptic rectification and elevated AMPAR EPSC amplitudes (reproduced from Chapter 4). (**B**) No modification of the GluA2 CTD in the full length receptor prevents either synaptic rectification or AMPAR EPSC amplitude increase (ΔNSF - RI: untrans.: 0.60 ± 0.04; GluA2Q ΔNSF: 0.19 ± 0.03; paired t-test, p<0.0001. EPSCs: untrans.: 34.8 ± 3.9 pA; GluA2Q ΔNSF: 48.3 ± 7.5 pA; paired t-test, p=0.019; n=11) (ΔPDZ - RI: untrans.: 0.55 ± 0.08; GluA2Q ΔPDZ: 0.22 ± 0.05; paired t-test, p=0.0004. EPSCs: untrans.: 23.1 ± 2.9 pA; GluA2Q ΔPDZ: 34.7 ± 5.3 pA; paired t-test, p=0.006; n=9) (GluA1-ICD - RI: untrans.: 0.49 ± 0.05; GluA2Q GluA1-ICD: 0.17 ± 0.03; paired t-test, p<0.0001. EPSCs: untrans.: 39.1 ± 8.0 pA; GluA2Q GluA1-ICD: 54.6 ± 9.1 pA; paired t-test, p=0.024; n=12) (CTD-null - RI: untrans.: 0.62 ± 0.04; GluA2Q CTD-null: 0.19 ± 0.03; paired t-test: p<0.0001, EPSCs: untrans.: 53.1 ± 6.4 pA; GluA2Q CTD-null: 65.7 ± 8.5 pA; paired t-test, p=0.050; n=20).*

(Figure 6.3B2), exchanging the ICD for that of GluA1 (Figure 6.3B3) or constructing a CTD null construct (Figure 6.3B4, as per GluA2Q ΔNTD) all failed to prevent either the strong synaptic rectification or the elevated EPSC amplitudes of GluA2Q overexpression. While studying GluA2 ΔNTD demonstrated an influence of the CTD on synaptic anchoring, these effects cannot be recapitulated in the NTD-containing construct. Together, this data suggests a modulatory role for the CTD, which is not strictly essential to receptor anchoring, and that NTD-dependent interactions are dominant in controlling synaptic transmission under basal conditions.

6.2.2 The influence of the GluA1 CTD on synaptic anchoring.

The CTD of GluA1 also contains a PDZ interaction site at the extreme C-terminus (Figure 6.4A), as well as being multiply phosphorylated by CaMKII and PKA, which has been shown to influence receptor trafficking, particularly to the cell surface (Barria et al., 1997a; Man et al., 2007; Oh et al., 2006; Roche et al., 1996). Generation of GluA1 constructs where PDZ interactions were prevented by mutagenesis (see Shi et al. (2001)), or those lacking both PDZ-ligands and phosphorylation sites (CTD-null) did not affect GluA1 surface trafficking in this overexpression assay (Figure 6.4B).

Overexpressed GluA1 is able to anchor at synaptic sites, altering synaptic rectification, with little effect on the AMPAR EPSC amplitudes (Figure 6.4C1, and see Chapter 5), while NTD-deletion prevented this synaptic anchoring (Figure 6.4D1). Both PDZ mutated and CTD-null GluA1 caused synaptic rectification similarly to the full-length receptor (Figure 6.4C2, C3) indicating little influence of the CTD on full-length receptors, as seen for GluA2. Unsurprisingly, PDZ deletion had no influence on GluA1 ΔNTD, which already showed no synaptic anchoring (Figure 6.4D2). These results again suggest a prominent role for the NTD in AMPAR synaptic anchoring under basal conditions. The GluA1 CTD has been suggested to play a key role in plasticity induced receptor anchoring (Shi et al., 2001; Zhou et al., 2018), and GluA1 ΔNTD can act as a dominant negative construct in LTP (see Chapter 5), suggestive of a role for more interactions than just the NTD. Therefore the influence of the CTD mutations on GluA1 anchoring on tCaMKII overexpression would be of great interest, but is yet to be conducted.

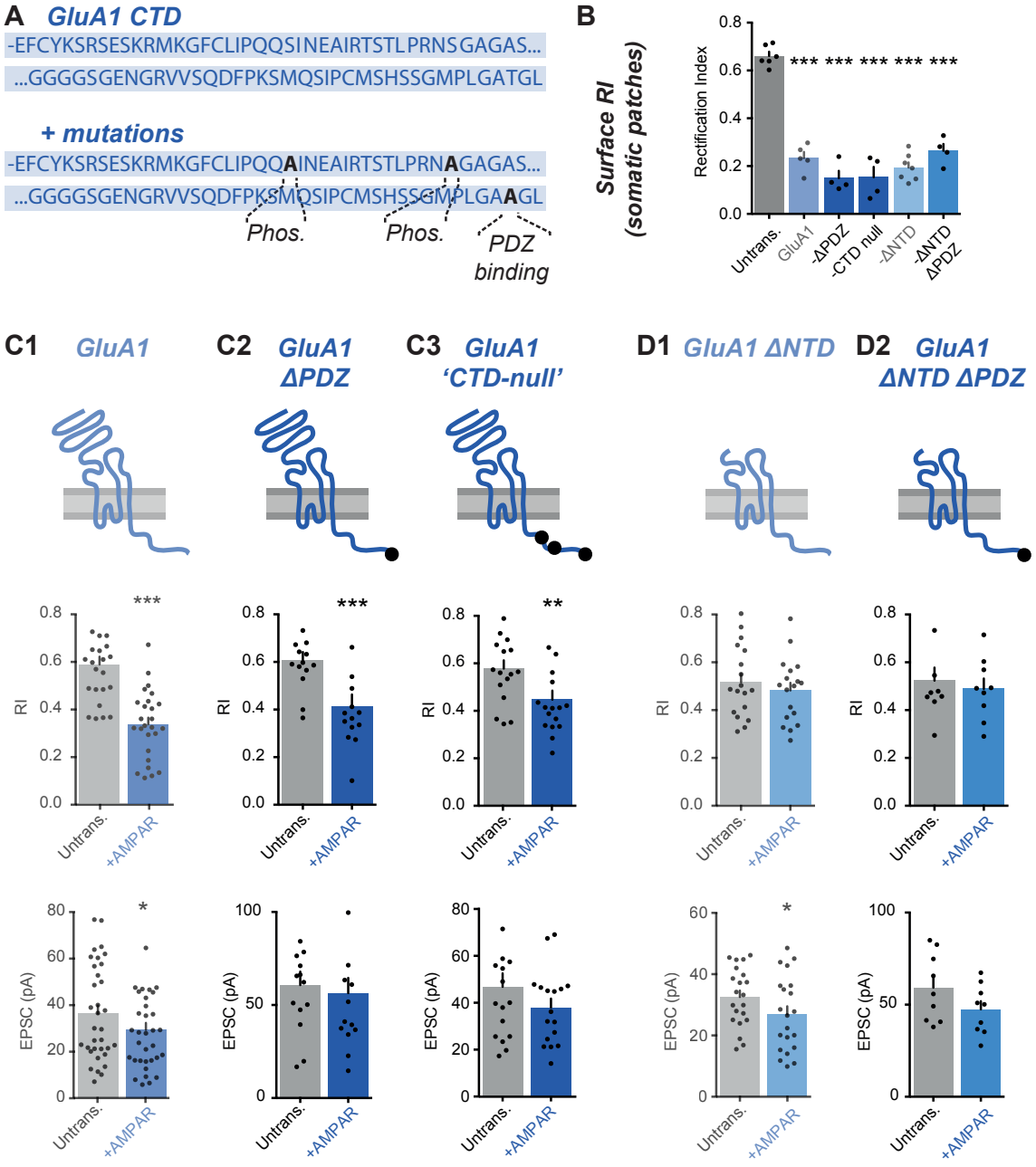

Figure 6.4 ***The effect of CTD mutations on GluA1 synaptic anchoring.***

Figure 6.4 ***The effect of CTD mutations on GluA1 synaptic anchoring.*** *(**A**) The GluA1 CTD primary sequence and mutations used to prevent protein interactions and phosphorylations. (**B**) Surface rectification of untransfected and GluA1 expressing cells shows no effect on GluA1 surface trafficking by CTD mutation (Untrans.: 0.66 ± 0.02; GluA1 reproduced from Chapter 5; GluA1 ΔPDZ: 0.15 ± 0.03; GluA1 CTD-null: 0.15 ± 0.03; GluA1 ΔNTD reproduced from Chapter 5; GluA1 ΔNTD ΔPDZ: 0.26 ± 0.03; One-way ANOVA, p<0.0001). (**C1**) The effect of GluA1 expression on synaptic transmission (reproduced from Chapter 5). (**C2**) Mutation of GluA1 PDZ interaction site does not affect synaptic anchoring of the subunit (RI: untrans.: 0.61 ± 0.04; GluA1 ΔPDZ: 0.41 ± 0.05; paired t-test, p=0.0004. EPSCs: untrans.: 60.8 ± 7.2 pA; GluA1 ΔPDZ: 56.4 ± 8.2 pA; paired t-test, p=0.66; n=14). (**C3**) Mutation of all indicated positions in **A** does not affect GluA1 synaptic anchoring (RI: untrans.: 0.58 ± 0.04; GluA1 CTD-null: 0.45 ± 0.04; paired t-test, p=0.0016. EPSCs: untrans.: 46.8 ± 5.8 pA; GluA1 CTD-null: 37.9 ± 3.8 pA; paired t-test, p=0.18; n=17). (**D1**) GluA1 ΔNTD does not cause synaptic rectification (reproduced from Chapter 5). (**D2**) GluA1 ΔNTD ± PDZ ligand mutation show no differences (RI: untrans.: 0.52 ± 0.05; GluA1 ΔNTD ΔPDZ: 0.49 ± 0.04; paired t-test, p=0.41. EPSCs: untrans.: 59.2 ± 6.1 pA; GluA1 ΔNTD ΔPDZ: 47.5 ± 4.4 pA; paired t-test, p=0.20; n=9).*

6.2.3 The interplay of NTD and TARP interactions at the synapse.

TARP interactions with the post-synaptic density are the best characterised synaptic anchor for the AMPAR (Opazo and Choquet, 2011). To study the interplay of NTD and TARP-dependent interactions in controlling the synaptic AMPAR content, fusion constructs were generated from GluA2Q and TARP γ8, the major TARP subunit in hippocampal CA1 cells (Rouach et al., 2005; Tomita et al., 2003). This construct was produced by cloning the TARP γ8 coding region in frame with, and downstream of GluA2Q, such that the GluA2 CTD is continuous with the N-terminus of the TARP (containing a GSGSG linking sequence). Such constructs have been previously used to control the TARP stoichiometry of AMPARs (Shi et al., 2009). By doing so, TARP dependent interactions with PSD-95 can be prevented by deletion of the C-terminal 'TTPV' motif of γ8, while NTD-dependent interactions can be prevented by NTD deletion as previously described. CTD interactions will likely be substantially limited in this fusion construct, however the influence of these interactions on receptor synaptic anchoring appears to be minimal at this synapse.

Four constructs were produced, a full length AMPAR-TARP tandem construct (GluA2Q-γ8), a TARP PDZ deleted (GluA2Q-γ8 ΔPDZ), NTD-deleted (GluA2Q-γ8 ΔNTD) and both NTD and PDZ deleted tandems (GluA2Q-γ8 ΔNTD ΔPDZ) (Figure 6.5A). Each construct was expressed in CA1 pyramidal neurons and the contribution to synaptic anchoring could be measured by assessing the rectification index and AMPAR EPSC amplitudes as previously described.

Overexpression of GluA2Q alone, without fused TARP γ8 gave rise to TARP-associated receptors through interaction of the overexpressed subunits with endogenous TARPs (see Chapter 4). Expression of this receptor caused synaptic rectification and elevated AMPAR ESPCs. In line with this result, expression of GluA2Q-γ8 caused a strongly reduced RI and an increase in the AMPAR EPSC amplitude of transfected cells (Figure 6.5B1). Overexpression of PDZ-deleted TARP γ2 in hippocampal neurons caused almost complete loss of synaptic AMPAR currents (Bats et al., 2007; Chen et al., 2000), indicating a dominant role for this interaction in controlling AMPAR transmission. However, in the present assay, expression of GluA2Q-γ8 ΔPDZ still substantially affected the synaptic RI, showing that receptor anchoring for synaptic transmission is not prevented (Figure 6.5B2). AMPAR EPSCs were not elevated as had been seen for GluA2Q-γ8 expression, indicative that the number of responding receptors was reduced on TARP PDZ deletion (Figure 6.5B2), yet anchoring was not prevented by loss of PSD interactions. Strikingly, NTD deletion completely prevented

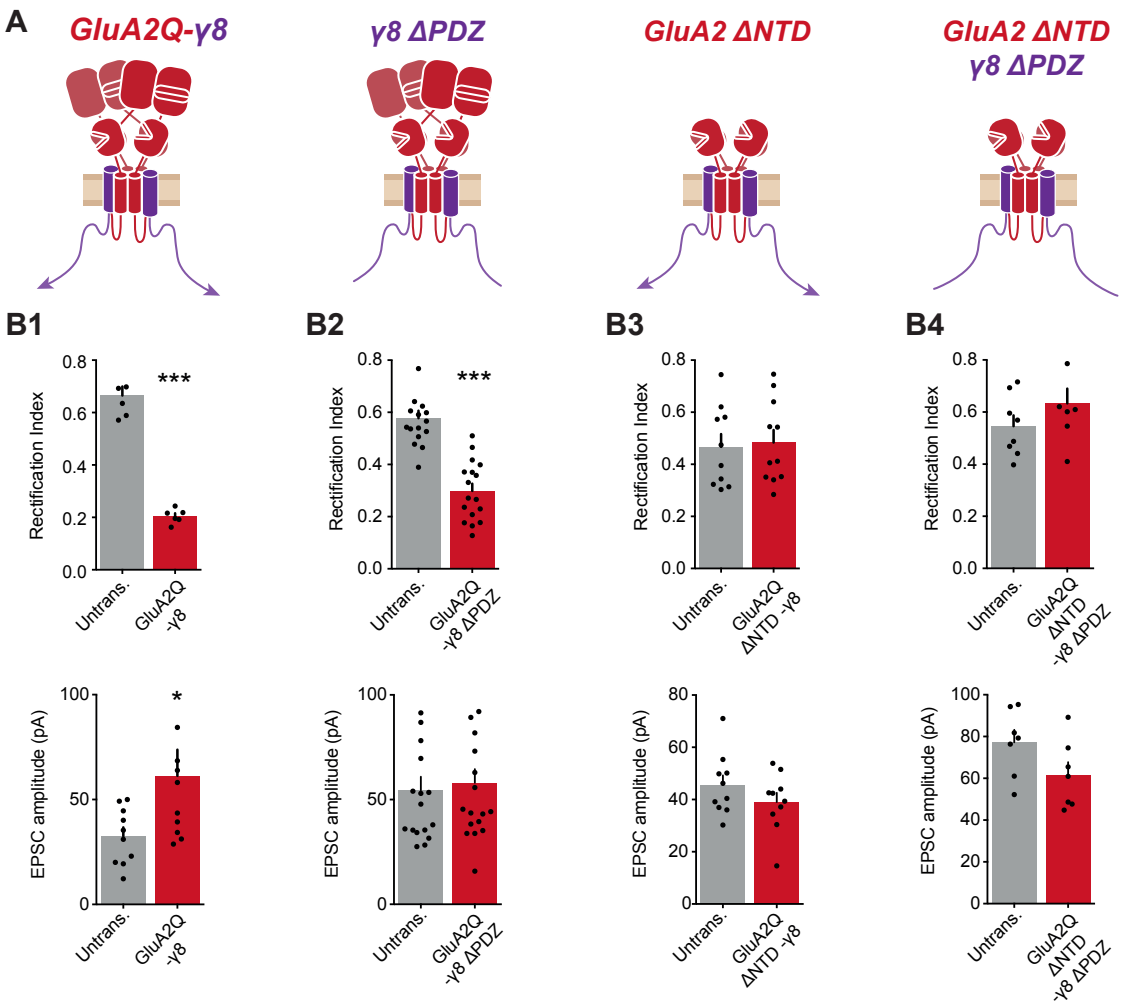

Figure 6.5 ***GluA2-TARP γ8 tandems demonstrate dominance of NTD interactions.*** *(**A**) Construct schematics for AMPAR-TARP fusions (two TARPs shown for clarity). Either TARP synaptic anchoring, or AMPAR synaptic anchoring can be limited by PDZ-ligand of NTD deletion respectively. (**B1**) GluA2Q fused to TARP γ8 (GluA2Q-γ8) contributes to synaptic transmission (RI: untrans.: 0.66 ± 0.03; GluA2Q-γ8: 0.20 ± 0.01; paired t-test, p<0.0001. EPSCs: untrans.: 32.5 ± 4.3 pA; GluA2Q-γ8: 62.3 ± 12.5 pA; paired t-test, p=0.19; n=10). (**B2**) TARP PDZ-ligand deletion does not prevent synaptic rectification (untrans.: 0.58 ± 0.03; GluA2Q-γ8 ΔPDZ: 0.30 ± 0.03; paired t-test, p<0.0001; n=16), but limits the increase in AMPAR EPSC amplitude (untrans.: 54.4 ± 6.6 pA; GluA2Q-γ8 ΔPDZ: 58.1 ± 6.5 pA; paired t-test, p=0.50; n=17). (**B3**) NTD deletion of GluA2Q-γ8 prevents synaptic anchoring (RI: untrans.: 0.47 ± 0.05; GluA2Q-γ8 ΔNTD: 0.48 ± 0.05; paired t-test, p=0.87. EPSCs: untrans.: 45.5 ± 3.7 pA; GluA2Q-γ8 ΔNTD: 39.0 ± 3.5 pA; paired t-test, p=0.20; n=10). (**B4**) Deletion of both synaptic anchors (NTD and TARP PDZ-ligand) prevents all receptor anchoring (RI: untrans.: 0.55 ± 0.04; GluA2Q-γ8 ΔNTD ΔPDZ: 0.63 ± 0.06; paired t-test, p=0.22. EPSCs: untrans.: 77.2 ± 6.0 pA; GluA2Q-γ8 ΔNTD ΔPDZ: 61.6 ± 6.2 pA; paired t-test, p=0.027; n=7).*

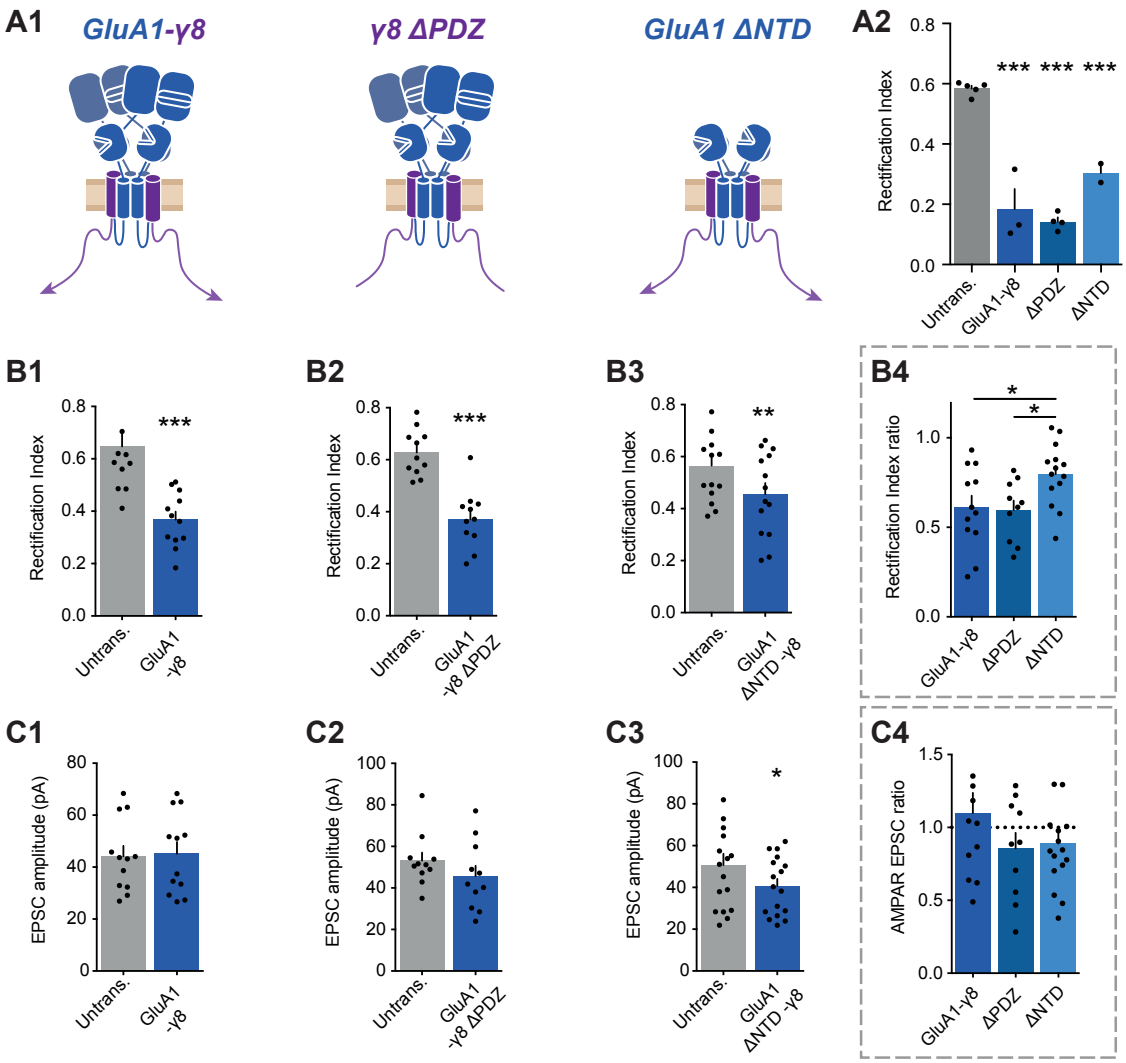

Figure 6.6 ***GluA1-TARP γ8 tandems confirm dominance of NTD interactions.*** *(**A1**) GluA1-TARP γ8 fusion schematics. (**A2**) RI confirms surface trafficking of all GluA1-γ8 constructs (Untrans.: 0.58 ± 0.01; GluA1-γ8: 0.18 ± 0.07; GluA1-γ8 ΔPDZ: 0.14 ±0.01; GluA1-γ8 ΔNTD: 0.30 ± 0.03; One-way ANOVA, p<0.0001). (**B**) Synaptic anchoring is selectively limited by NTD deletion ((**B1**) Untrans.: 0.65 ± 0.05; GluA1-γ8: 0.37 ± 0.03; p=0.001; n=12. (**B2**) Untrans.: 0.63 ± 0.03; GluA1-γ8 ΔPDZ: 0.37 ± 0.03; p<0.0001; n=11. (**B3**) Untrans.: 0.57 ± 0.04; GluA1-γ8 ΔNTD: 0.46 ± 0.04; p=0.001; n=14. All paired-t tests). (**B4**) RI normalised to untransfected cell of paired recordings demonstrates effect of NTD deletion on synaptic anchoring (A1-γ8: 0.61 ± 0.07; A1-γ8 ΔPDZ: 0.60 ± 0.05; A1-γ8 ΔNTD: 0.80 ± 0.05; One-way ANOVA, p=0.021). (**C**) No gross changes in AMPAR EPSC amplitude are observed on GluA1-γ8 expression ((**C1**) untrans.: 44.2 ± 4.0 pA; A1-γ8: 45.2 ± 4.5 pA; paired t-test, p=0.86. (**C2**) untrans.: 53.2 ± 3.8; A1-γ8 ΔPDZ: 45.6 ± 5.0 pA; paired t-test, p=0.17. (**C3**) untrans.: 50.7 ± 5.4 pA; A1-γ8 ΔNTD: 40.7 ± 3.4 pA; paired t-test, p=0.041. (**C4**) A1-γ8: 1.10 ± 0.14; A1-γ8 ΔPDZ: 0.86 ± 0.11; A1-γ8 ΔNTD: 0.89 ± 0.08; One-way ANOVA, p=0.26).*

synaptic anchoring of GluA2Q-γ8, blocking both RI and AMPAR EPSC changes (Figure 6.5B3). Combining NTD and PDZ deletions similarly did not affect synaptic currents (Figure 6.5B4). Together, this dataset indicates that NTD-deletion causes a more substantial effect on receptor anchoring than PDZ-deletion, and therefore that NTD-dependent receptor anchoring is more significant for controlling AMPAR contribution to synaptic transmission than TARP γ8 to PSD interactions.

The above experiment was performed using GluA2Q. The NTD of GluA1 is also important for synaptic anchoring (see Chapter 5), and therefore understanding the interplay of NTD and TARP interactions is valuable for this subunit. In a similar manner to GluA2, GluA1-TARP γ8 fusion constructs were produced (Figure 6.6A1), which all trafficked well to the cell surface (Figure 6.6A2). GluA1-γ8 reduced synaptic RI (Figure 6.6B1) in a similar manner to GluA1 overexpression (see Figure 6.4C1), without affecting EPSC amplitudes (Figure 6.6C1). Deletion of the TARP PDZ from this construct did not change the effect of receptor overexpression, with synaptic RI similarly altered (Figure 6.6B2), indicating that interactions of this region are not essential to synaptic anchoring. NTD deletion did not completely abolish changes to synaptic RI (Figure 6.6B3), but the change to RI was significantly reduced (Figure 6.6B4). Normalising the AMPAR EPSC amplitude of transfected cells to untransfected cells of paired recordings showed little change in any case (Figure 6.6C4). This data supports a model where NTD-dependent interactions are most influential in controlling AMPAR synaptic anchoring.

6.2.4 TARP subunit-specific synaptic anchoring.

While TARP γ8 is the major TARP associated with AMPARs in hippocampal CA1 pyramidal cells (Rouach et al., 2005; Tomita et al., 2003), TARP γ2 is also present in a subset of synapses in these neurons. predominantly localised at synapses with high AMPAR densities (Yamasaki et al., 2016). Therefore, it is possible that TARP subunits differentially anchor AMPARs in these cells by interacting with different postsynaptic proteins.

Performing a sequence alignment of γ2 and γ8 shows substantial differences between the two proteins (Figure 6.7). The N-terminus of γ8 is longer than that of γ2, and appears to have a role in controlling AMPAR transmission (Milstein and Nicoll, 2009). The TARPs contain two extracellular loops (*Ex1* and *Ex2*), which differentially modulate receptor gating (Riva et al., 2017), yet are unlikely to influence receptor anchoring, given their association

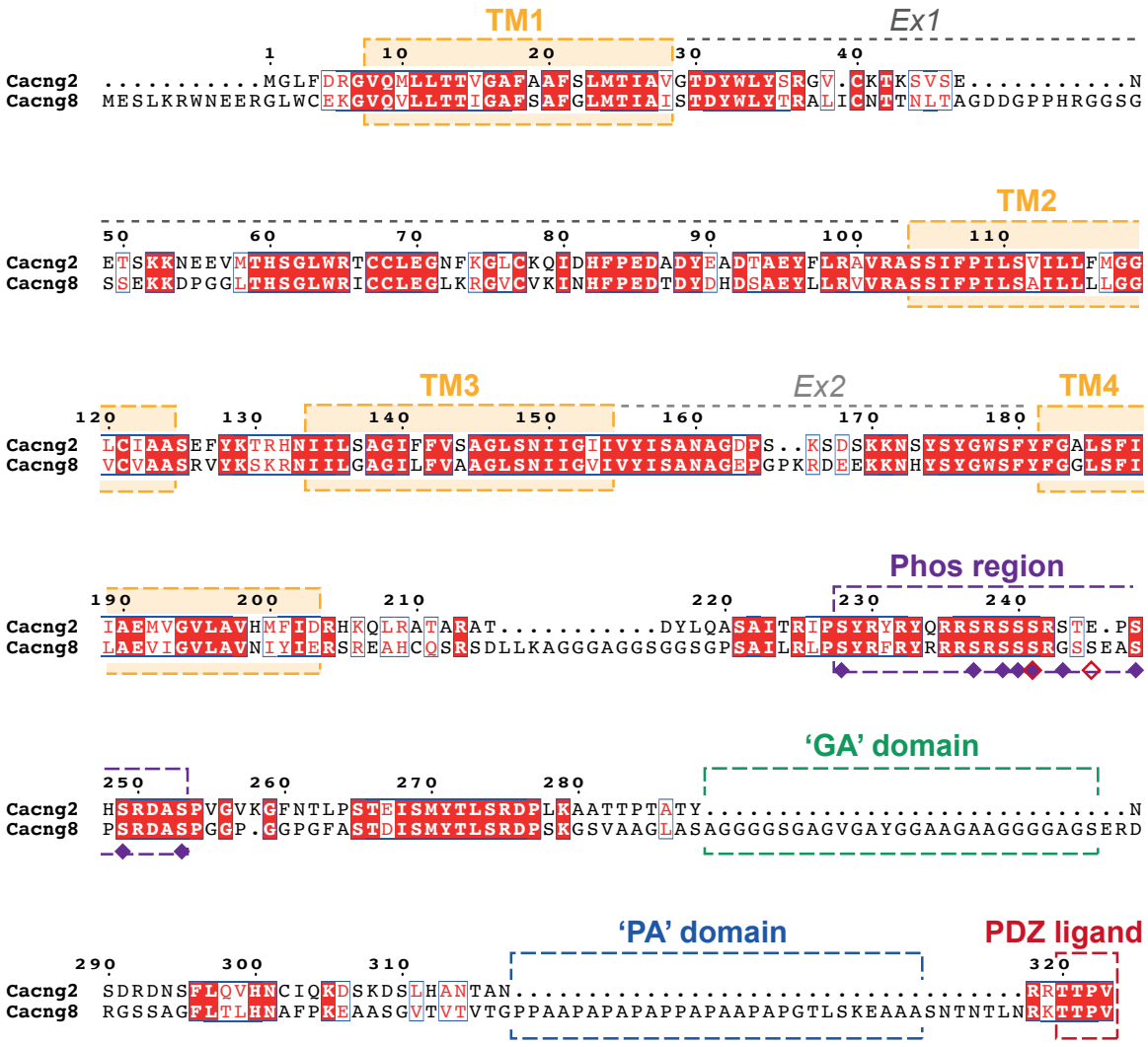

Figure 6.7 ***Primary protein sequence alignment of TARP γ2 and γ8.*** *Sequence alignment shows the increased length of TARP γ8 (Cacng8) compared to γ2 (Cacng2), with a longer intracellular N-terminus and an insertion in the first extracellular loop (Ex1). Transmembrane domains are marked 'TM'. Both intracellular C-termini contain a PDZ ligand 'TTPV' motif and a phosphorylated region containing many serine residues (Phos region), yet γ8 specifically contains insertions of a glycine and alanine rich ('GA') and a proline and alanine rich ('PA') domain. Reported phosphorylation sites from Tomita et al., 2005 and Park et al., 2016b are indicated by purple and red diamonds respectively.*

with the receptor extracellular domain and only slight protrusion from the membrane (Zhao et al., 2016). The CTD contains the greatest TARP subunit specific differences. While both contain a highly phosphorylated region (Park et al., 2016b; Tomita et al., 2005), the γ8 CTD is substantially longer, with two major insertions: one of a glycine and alanine rich (GA) region, and the other of a proline and alanine rich (PA) region, which has the potential to interact with SH3 domain containing proteins, which are abundant at the synapse (e.g. SHANK; Monteiro and Feng, 2017) through a PXXP motif (Saksela and Permi, 2012). The length of the TARP CTD has been hypothesised to control synaptic anchoring, by increased interaction with PDS-95 (Hafner et al., 2015). Phosphorylation of the TARP CTD reduces its association with the intracellular site of the plasma membrane, thus facilitating its interaction with PSD-95 and increasing receptor trapping at synapses (Opazo et al., 2010; Sumioka et al., 2010). This model was produced from accumulated evidence studying TARP γ2. As the TARP γ8 CTD is substantially longer than γ2, it could be expected that interactions with PSD-95 would be dominant for this subunit.

To understand the differential control of AMPAR anchoring by TARPs, GluA2Q fusions with either γ8 or γ2 were produced (Figure 6.8A). Interestingly, on overexpression, while both constructs were present on the surface of neurons, GluA2Q-γ2 appeared to traffic to a lesser extent than GluA2Q-γ8 or any other construct so far tested (Figure 6.8B). This difference should be appreciated in the interpretation of the subsequent data.

Overexpression of GluA2Q-γ2 significantly altered synaptic RI, indicating a substantial contribution to synaptic transmission (Figure 6.8C1). Interestingly, deletion of the PDZ-interaction site, in a similar manner to GluA2Q-γ8 shown previously (Figure 6.6), abolished this change to RI (Figure 6.8C2), suggesting that GluA2Q-γ2 is more dependent on PDZ interactions for synaptic anchoring than GluA2Q-γ8 (see Figure 6.5). This result also indicates that GluA2Q-γ8 may induce synaptic anchoring through alternative TARP interactions, for example the GA or PA domains of the γ8 CTD.

TARP γ2 appears to convert low AMPAR density synapses into high density ones (Yamasaki et al., 2016) and therefore may play a role in synaptic potentiation, where the AMPAR content of a synapse is increased (Nicoll, 2017). Coexpression of tCaMKII with GluA2Q-γ2 showed similar changes to synaptic RI, but dramatically potentiated synaptic currents (Figure 6.8C3), to a far greater extent than expression of GluA2Q-γ2 alone (Figure 6.8C1). This receptor anchoring was in part dependent on its PDZ-interaction site, with deletion of this

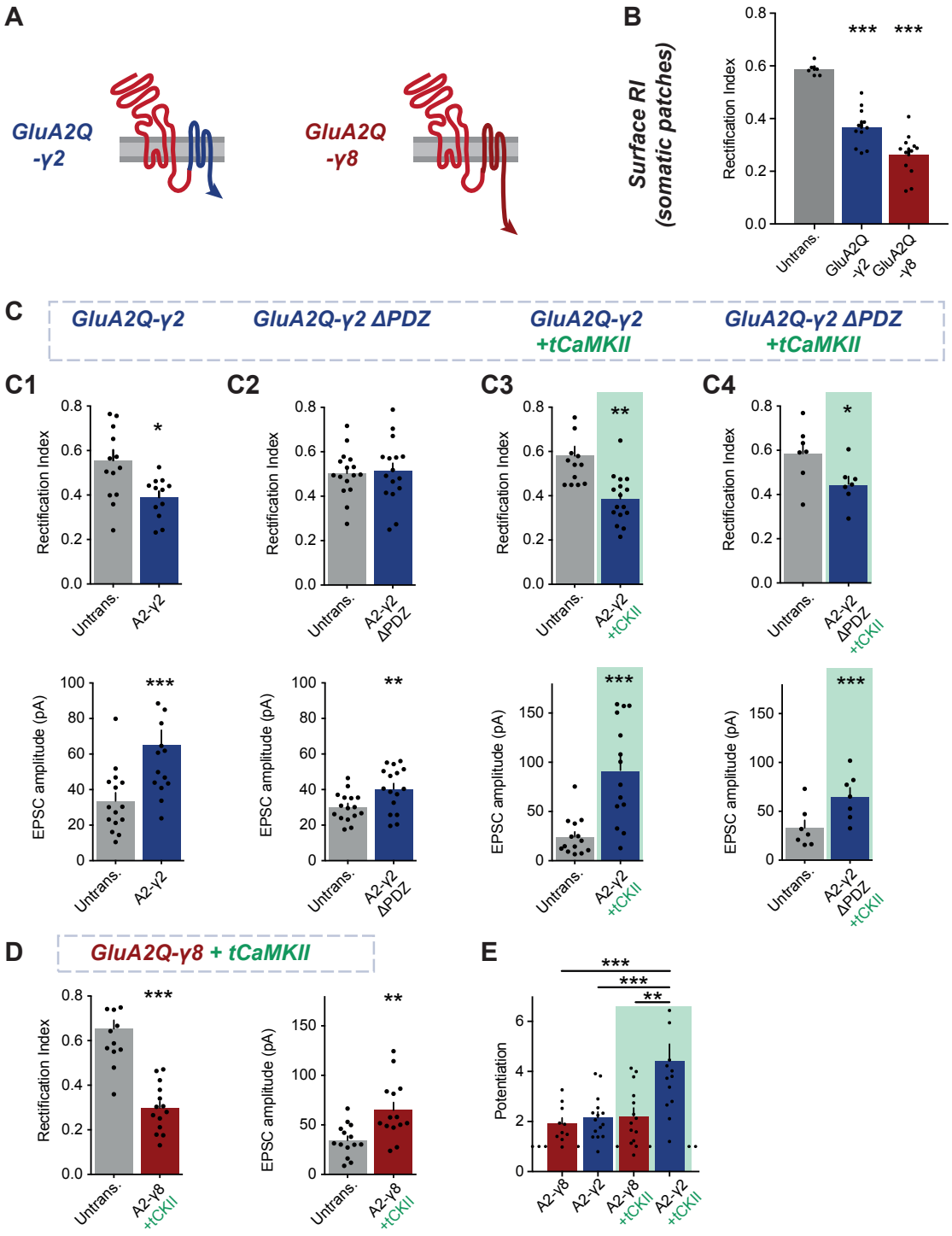

Figure 6.8 ***Differential effects of TARP tandems on synaptic transmission.***

Figure 6.8 ***Differential effects of TARP tandems on synaptic transmission.*** *(**A**) Schematics of AMPAR-TARP subunit fusions. (**B**) Surface RI demonstrates differential surface delivery of AMPAR-TARPs (untrans.: 0.59 ± 0.01, n=6; A2Q-γ2: 0.37 ± 0.02, n=11; A2Q-γ8: 0.26 ± 0.02, n=12; One-way ANOVA, p<0.0001). (**C**) Synaptic RI and AMPAR EPSC amplitudes from paired recordings. (**C1**) GluA2Q-γ2 alters synaptic rectification and increases AMPAR EPSC amplitudes (RI - untrans.: 0.56 ± 0.05; A2Q-γ2: 0.39 ± 0.03; paired t-test, p=0.016. EPSCs - untrans.: 33.6 ± 4.7 pA; A2Q-γ2: 65.2 ± 8.3 pA; paired t-test, p<0.0001). (**C2**) TARP PDZ-ligand deletion prevents synaptic rectification (untrans.: 0.50 ± 0.03; A2Q-γ2 ΔPDZ: 0.51 ± 0.04; paired t-test, p=0.83), but a slight increase in AMPAR EPSC amplitude remains (untrans.: 30.2 ± 2.0 pA; A2Q-γ2 ΔPDZ: 40.3 ± 3.1 pA; paired t-test, p=0.51). (**C3**) Constitutively active CaMKII expression (tCaMKII or tCKII) causes a substantial potentiation of cells expressing GluA2Q-γ2 (RI - untrans.: 0.58 ± 0.04; A2Q-γ2 +tCKII: 0.39 ± 0.03; paired t-test, p=0.007. EPSCs - untrans.: 24.3 ± 5.1 pA; A2Q-γ2 +tCKII: 91.9 ± 14.0 pA; paired t-test, p<0.0001). (**C4**) TARP PDZ site deletion limits the synaptic potentiation by tCaMKII, but does not prevent synaptic RI change (RI - untrans.: 0.59 ± 0.05; A2Q-γ2 ΔPDZ +tCKII: 0.45 ± 0.04; paired t-test, p=0.045. EPSCs - untrans.: 33.0 ± 7.8 pA; A2Q-γ2 ΔPDZ +tCKII: 65.0 ± 9.0 pA; paired t-test, p<0.0001). (**D**) GluA2Q-TARP γ8 coexpression with tCaMKII demonstrates strong synaptic rectification and AMPAR EPSC amplitude increase, similar to GluA2Q-TARP γ8 alone (RI - untrans.: 0.65 ± 0.04; A2Q-γ8 +tCKII: 0.30 ± 0.03; paired t-test, p<0.0001. EPSCs - untrans.: 58.6 ± 10.5 pA; A2Q-γ8 +tCKII: 73.4 ± 10.5 pA; paired t-test, p=0.002). (**E**) Normalisation of AMPAR EPSC amplitude changes to untransfected cells of paired recordings shows specific ability of tCaMKII to potentiate cells containing γ2 over γ8 fusion construct expression (A2Q-γ8: 1.91 ± 0.23; A2Q-γ2: 2.16 ± 0.23; A2Q-γ8 +tCKII: 2.23 ± 0.31; A2Q-γ2 +tCKII: 4.46 ± 0.63; One-way ANOVA, p<0.0001).*

region attenuating this increased potentiation to a large extent, but not preventing a change to synaptic RI (Figure 6.8C4).

Interestingly, coexpression of GluA2Q-γ8 with tCaMKII did not potentiate synaptic EPSCs significantly more than expression of the receptor construct alone (Figure 6.8D). By comparing the changes caused by TARP subunits (Figure 6.8E), only TARP γ2 is potentiated to a greater extent by coexpression of tCaMKII, indicating a preferential role for this kinase in driving the anchoring of TARP γ2 over TARP γ8 containing receptors. This data supports a role for γ2 associated AMPARs in synaptic potentiation.

6.3 Discussion

AMPAR synaptic anchoring is dependent on a raft of protein interactions (Shepherd and Huganir, 2007), and the strength of synaptic transmission is influenced not only by synaptic proteins, but also the multiple stages of regulation which controls the lifecycle of an AMPAR, from its biosynthesis in the endoplasmic reticulum, to its final localisation at the postsynaptic density when associated with a complement of auxiliary subunits (Greger et al., 2017; Jackson and Nicoll, 2011). This study has begun to investigate how the interactions of AMPAR regulatory proteins control the strength of excitatory synaptic transmission by associating with different domains of the receptor.

The role of the AMPAR CTD in synaptic transmission.

The AMPAR CTD has been extensively studied (Shepherd and Huganir, 2007), yet its significance is still debated (Granger et al., 2013; Panicker et al., 2008). GluA2Q ΔNTD causes synaptic depression despite altering the RI on overexpression (Chapter 4). At least part of this, is caused by the subunit-specific action of the GluA2 CTD, as replacement with the GluA1 intracellular sequence can alleviate both phenomena. But which interactions mediate this effect? Two regions of the CTD are known to meditate protein interactions: the membrane proximal region binds the ATPase NSF (Nishimune et al., 1998; Osten et al., 1998), with an overlapping AP2 interaction site for receptor endocytosis (Lee et al., 2002), the other at the extreme C-terminus, interacting with GRIP and PICK1 (Lu, 2005; Srivastava et al., 1998).

The synaptic depression caused by GluA2Q ΔNTD can be in part alleviated by NSF site mutation, supporting a role for this protein in maintaining a synaptic pool of receptors (Braithwaite et al., 2002; Hanley et al., 2002). While AP2 also interacts at this region, its role appears to be specific to AMPAR endocytosis in LTD (Lee et al., 2002), and therefore its influence under the recording conditions employed is expected to be minimal.

Mutation of the extreme CTD alone, preventing all interactions of this region, did not appear to have a substantial effect on GluA2Q ΔNTD transmission. This data indicates that the role of GRIP/ABP in stabilising AMPARs at synaptic sites is minimal at this neuronal connection. The interplay of PDZ interactions of GluA2 and NSF function has been studied previously, and is suggested to control the recycling of receptors between surface and intracellular synaptic pools (Braithwaite et al., 2002; Hanley et al., 2002). Simultaneous mutagenesis of NSF and PDZ interactions in this study could be interpreted to support this

model, however the results are far from clear-cut. While NSF mutation alleviates both RI and synaptic depression, additional mutation of the PDZ site returns the synaptic transmission phenotype to that of the original GluA2Q ΔNTD expression. One way to interpret this result is as follows. If mutation of PDZ site prevents any accumulation of receptors in intracellular pools, then the effect of NSF in releasing these receptors would be minimal. For this reason, any effect of NSF site mutation (as seen on NSF site mutation alone), would be negated by combination with PDZ site mutagenesis. Clearly the data presented above is insufficient to unequivocally support such a hypothesis without further investigation. What can be concluded is that CTD mutation influences GluA2 anchoring in some manner.

The effect of CTD mutations appears specific to GluA2Q ΔNTD studies, with no observable effect of any alteration on full-length GluA2 with an intact NTD. Together this data is suggestive of some modulatory role for the CTD in AMPAR trafficking, which is not of the greatest significance to GluA2 transmission, in agreement with previous studies (Panicker et al., 2008). Recent CTD mouse knock-in studies also demonstrated little role for the GluA2 CTD in basal transmission at the CA1 Schaffer collateral synapse (Zhou et al., 2018). It can be concluded that the interactions of the GluA2 NTD appear more significant than those of the CTD in controlling the synaptic anchoring of this subunit and the role of the CTD is not strictly essential.

Mutagenesis of the GluA1 CTD also showed no effect on synaptic transmission, which could be expected, given the clear necessity of NTD interactions only under basal transmission (see Chapter 5). Interactions of the CTD have been implicated more heavily in synaptic potentiation (Shi et al., 2001; Zhou et al., 2018), and whether CTD mutagenesis can alleviate the prevention of synaptic potentiation on GluA1 ΔNTD expression remains an important future direction of study.

TARP-dependent AMPAR anchoring

The binding of TARP PDZ ligands to PDS-95 is currently understood to be a critical regulator of AMPAR synaptic anchoring (Opazo and Choquet, 2011). In cerebellar granule cells, this mechanism appears concrete and essential for maintaining synaptic AMPARs (Chen et al., 2000; Hashimoto et al., 1999), however, at hippocampal CA1 synapses, this is not so clear-cut. The majority of AMPARs are associated with TARP γ8, as clearly demonstrated by the detrimental impact of γ8 knockout (Rouach et al., 2005), however deletion of the PDZ ligand of this protein does not prevent all synaptic transmission, only limiting it by 30 %

(Sumioka et al., 2011). Overexpression of PDZ-deleted TARP γ2 does appear to prevent the majority of transmission at this synapse (Bats et al., 2007; Chen et al., 2000), yet this TARP subtype is not present in the majority of synapses (Yamasaki et al., 2016), and therefore the detrimental effect of its overexpression is unlikely to be of great significance to understanding the mechanisms controlling AMPAR anchoring under basal transmission.

In this study, deletion of the TARP γ8 PDZ-ligand did not prevent synaptic anchoring of AMPAR-TARP fusions, indicating that it is not an essential AMPAR anchor point. These tandem receptors are highly unlikely to be compensated by association with endogenous, PDZ-ligand containing TARPs as each AMPAR tetramer is fused to four TARP subunits, the maximum number that appears to be able to associate with one receptor (Hastie et al., 2013; Zhao et al., 2016). The increase in AMPAR EPSCs observed on GluA2Q-TARP γ8 fusion expression is lost on PDZ-ligand deletion, suggesting that less AMPARs are contributing the synaptic transmission, and therefore agreeing with some role for TARP PDZ interactions in accumulating synaptic AMPARs, however its essential nature, as seen in cerebellar granule cells (Chen et al., 2000) is not so simple in the hippocampus.

TARP-fused AMPARs did show limited synaptic anchoring on NTD deletion, demonstrating a clear importance for the NTD in synaptic anchoring, as has been previously reported (see Chapter 4, 5; Díaz-Alonso et al., 2017; Watson et al., 2017). The ultimate requirement for a contribution to synaptic transmission appears to be mediated by NTD interactions that remain unidentified. Recent data has demonstrated an absolute requirement for glutamate receptor PDZ-ligands in their synaptic localisation, which is incongruent with the results presented above (Bemben et al., 2018). Clearly, much further work is required to unravel the fundamental basis of AMPAR localisation at the synapse.

One observation requires consideration when interpreting this data, in light of previous recordings. GluA2Q ΔNTD expressed alone, rather that TARP-fused, causes synaptic rectification and depressed AMPAR EPSCs, while GluA2Q ΔNTD-γ8 causes neither effect. Two mechanisms are likely at work here. As described above, the CTD of GluA2 has some influence on providing a pool of receptors available for transmission, and therefore by fusing the CTD of the AMPAR to the TARP N-terminus, such interactions are most likely prevented. A second possible explanation for this effect is that expression of GluA2Q ΔNTD alone sequesters endogenous TARPs, limiting their availability for endogenous receptors. On fusion,

this effect does not occur, and endogenous receptors are able to fully maintain transmission when synaptic anchoring of AMPAR-TARP fusions is affected by NTD-deletion.

Subtype-dependent TARP anchoring in synaptic potentiation.

The role of individual TARPs in hippocampal synaptic transmission remains largely unstudied. While TARP γ3 and γ4 may provide compensation in other TARP knockout lines (Rouach et al., 2005), on genetic deletion, no gross changes in AMPAR distribution in the synapse are observed (Yamasaki et al., 2016). TARP γ2 has been extensively studied for its role in AMPAR synaptic anchoring in dissociated hippocampal cultures (Bats et al., 2007; Constals et al., 2015; Hafner et al., 2015), despite not being present at the extrasynaptic membrane (Inamura et al., 2006), and causing little apparent change in the strength of transmission on genetic deletion (Hashimoto et al., 1999). Yamasaki et al. (2016) demonstrate that TARP γ2 appears to facilitate the formation of 'high-AMPAR-density synapses', associated with synapses with perforated postsynaptic densities, which would constitute strong synaptic connections. As TARP γ2 does not appear to exist at extrasynaptic sites (Inamura et al., 2006; Yamasaki et al., 2016), the diffusional trapping of extrasynaptic TARP γ2 associated AMPARs, as extensively investigated (Bats et al., 2007; Constals et al., 2015; Hafner et al., 2015; Opazo et al., 2010), is unlikely to be of significance under physiological conditions.

In this study, AMPAR-TARP tandem constructs were utilised to investigate the influence of TARP interactions on synaptic transmission. However, TARP γ2 tandems appear to express lower on the cell surface than γ8 tandems, complicating comparisons. While this difference could reflect their physiological locations, where TARP γ2 is not present on the extrasynaptic membrane in great abundance, similar expression of the two constructs cannot be assured.

Synaptic anchoring by TARP γ2, dependent on PDZ interactions, as reported previously (Bats et al., 2007; Chen et al., 2000), was observed in the present study. Strikingly, TARP-γ2 was able to potentiate synaptic transmission considerably on coexpression with tCaMKII, and to a far greater effect than TARP γ8, supporting a role in synaptic potentiation for this auxiliary subunit. While phosphorylation of TARP γ2 has been suggested to use CaMKII (Tomita et al., 2005, but see Inamura et al., 2006), mutagenesis of the CaMKII phosphorylation sites has been shown not to affect LTP (Park et al., 2016a), and therefore the direct action of CaMKII on TARP γ2 is unlikely to cause this large potentiation.

Expression of TARP γ2-fused AMPARs specifically potentiates synaptic currents to a greater

extent than TARP γ8-fused receptors on tCaMKII coexpression. This is suggestive that the synaptic rearrangements which occur on tCaMKII expression facilitate increased anchoring of TARP γ2 associated receptors, rather than TARP γ8 associated receptors which mediate the majority of basal transmission (Rouach et al., 2005). Differential synaptic anchoring of TARP subtypes has been demonstrated to be dependent on the intracellular portion of the protein (Milstein and Nicoll, 2009), and therefore studying the differential protein interactors of these domains could facilitate identification of the controllers of AMPAR synaptic content which is specific for long-term synaptic potentiation.

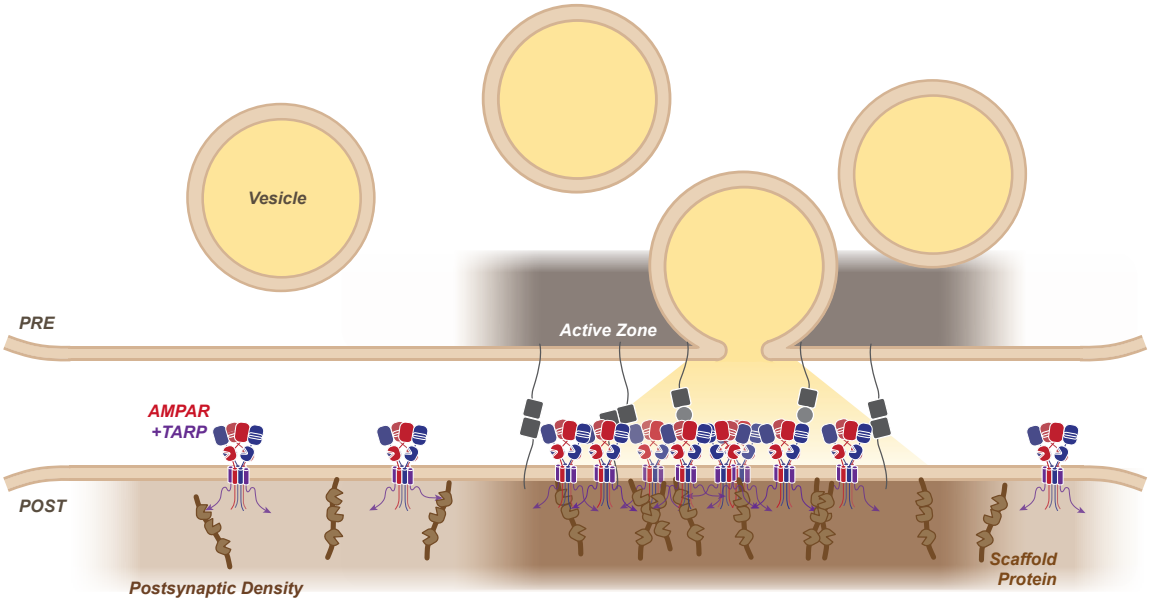

Figure 6.9 ***Model for the role of AMPAR interactions in controlling synaptic transmission.*** *Approximately scale representation of the synapse with AMPARs clustered opposite vesicle release sites by NTD interactions. CTD and TARP interactions allow postsynaptic AMPARs accumulation.*

The interplay of interactions controlling AMPAR synaptic transmission.

Together, this data suggests a model for AMPAR synaptic anchoring where the CTD has some role in receptor exchange between intracellular and extrasynaptic sites, which is not strictly of an essential nature for controlling the strength of synaptic transmission under the conditions studied in the present investigation. TARP interactions with the postsynaptic density do appear to influence the accumulation of synaptic receptors, yet is not the primary requirement for AMPAR anchoring in synaptic transmission. Interactions of the N-terminal

domain of the AMPAR appear to have the strongest influence on the ability of AMPARs to anchor at synaptic sites, and respond to presynaptically released glutamate. Identification of these interactions now becomes of great importance to our understanding of the synapse.

As AMPARs appear to align with presynaptic release sites (Tang et al., 2016), despite the relatively large size of the postsynaptic density, TARP interactions with postsynaptic intracellular proteins could accumulate receptors at the synaptic area, while NTD-dependent interactions are well placed to position AMPARs at vesicle release sites (Figure 6.9). Interaction of the AMPAR NTD with transsynaptically aligned proteins could be expected from this model. One candidate to mediate this would be LRRTMs, which bind AMPARs (Schwenk et al., 2012) and form a nanodomain arrangement in the synapse (Chamma et al., 2016), however this interaction appears particularly weak. Imaging the arrangement synaptic cleft components to identify possible AMPAR anchoring proteins, and biochemical identification of NTD-dependent AMPAR interactors would allow experimental investigation of this model by specific interaction disruption. By identifying the protein-protein interaction sites underlying NTD-dependent synaptic anchoring, precise modification of the receptor can be achieved to unequivocally confirm its dominance in controlling AMPAR synaptic anchoring for reliable transmission.

Chapter 7

Conclusions

This investigation has uncovered the importance of the AMPAR N-terminal domain in the synaptic function of the receptor. This domain provides a subunit-specific docking platform for protein interactions, which can control the positioning of the receptor within the synaptic cleft for efficient transmission. Removal of the AMPAR GluA2 subunit's NTD limits the number of receptors that contribute to synaptic transmission, by preventing their anchoring at synaptic sites, despite having little observable effect on the receptor's ability to pass glutamate-gated currents. These ΔNTD receptors show higher mobility in synaptic areas, demonstrating their impaired synaptic retention.

NTD-dependent anchoring appears to be a general principle for AMPARs, as interfering with the NTD of GluA1 can completely prevent synaptic anchoring of this subunit, and GluA1 ΔNTD receptors are unable to support synaptic potentiation. The interactions of each subunit appear to be unique, as exchange of NTDs between GluA2 and GluA1 can transfer synaptic anchoring phenotypes between subunits. These results demonstrate that a complex AMPAR interactome likely exists in the synaptic cleft, which controls the contribution of AMPAR subtypes to functional transmission. The identity of the protein partners involved in this action remains unknown, yet a multitude of proteins span the synaptic cleft, offering abundant opportunities for control of receptor anchoring and positioning. Identification of these partners is now of immediate importance.

Visualisation of receptor localisation using superresolution imaging shows mutant receptors that do not contribute to transmission are still localised and clustered at synaptic sites. Given the emerging importance of AMPAR alignment with presynaptic glutamate release sites, it is possible that regulation of AMPAR anchoring through its NTD is the mediator of this transsy-

naptic alignment. In comparison to previously investigated AMPAR anchoring mechanisms, such as the receptor's intracellular C-terminal domain, NTD-dependent interactions appear most crucial to maintaining a complement of receptors for transmission, however some modulatory role for the CTD in maintaining the availability of AMPARs for synaptic signalling can be observed. Interactions of the receptor's auxiliary subunit (TARPs) with postsynaptic scaffold molecules work in concert with NTD-dependent mechanisms. Revealing the unique requirements of these different anchoring methods remains an open question.

The AMPAR is unique in its association with such a plethora of interacting proteins and auxiliary subunits. Spatio-temporal regulation over the production and localisation of these signalling complexes is of utmost importance to neuronal communication. Understanding their distinct functions can reveal the fundamental properties of synaptic transmission, plasticity, and ultimately the mechanisms of neuronal information processing.

Bibliography

Abraham, W. C., B. Logan, J. M. Greenwood, and M. Dragunow
2002. Induction and experience-dependent consolidation of stable long-term potentiation lasting months in the hippocampus. *The Journal of neuroscience*, 22(21):9626–9634.

Adesnik, H. and R. A. Nicoll
2007. Conservation of Glutamate Receptor 2-Containing AMPA Receptors during Long-Term Potentiation. *Journal of Neuroscience*, 27(17):4598–4602.

Adesnik, H., R. A. Nicoll, and P. M. England
2005. Photoinactivation of native AMPA receptors reveals their real-time trafficking. *Neuron*, 48(6):977–85.

Ady, V., J. Perroy, L. Tricoire, C. Piochon, S. Dadak, X. Chen, I. Dusart, L. Fagni, B. Lambolez, and C. Levenes
2014. Type 1 metabotropic glutamate receptors (mGlu1) trigger the gating of GluD2 delta glutamate receptors. *EMBO Reports*, 15(1):103–109.

Allen, N. J., M. L. Bennett, L. C. Foo, G. X. Wang, C. Chakraborty, S. J. Smith, and B. A. Barres
2012. Astrocyte glypicans 4 and 6 promote formation of excitatory synapses via GluA1 AMPA receptors. *Nature*, 486(7403):410–414.

Almo, S. C. and J. D. Love
2014. Better and faster: Improvements and optimization for mammalian recombinant protein production. *Current Opinion in Structural Biology*, 26(1):39–43.

Ancona Esselmann, S. G., J. Díaz-Alonso, J. M. Levy, M. A. Bemben, and R. A. Nicoll
2017. Synaptic homeostasis requires the membrane-proximal carboxy tail of GluA2. *Proceedings of the National Academy of Sciences*, 114(50):201716022.

Andrásfalvy, B. K., M. A. Smith, T. Borchardt, R. Sprengel, and J. C. Magee
2003. Impaired regulation of synaptic strength in hippocampal neurons from GluR1-deficient mice. *Journal of Physiology*, 552(1):35–45.

Aoto, J., D. C. Martinelli, R. C. Malenka, K. Tabuchi, and T. C. Südhof
2013. Presynaptic neurexin-3 alternative splicing trans-synaptically controls postsynaptic AMPA receptor trafficking. *Cell*, 154(1):75–88.

Araki, Y., D.-T. Lin, and R. L. Huganir
2010. Plasma membrane insertion of the AMPA receptor GluA2 subunit is regulated by

NSF binding and Q/R editing of the ion pore. *Proceedings of the National Academy of Sciences*, 107(24):11080–11085.

Arendt, K. L., M. Royo, M. Fernández-Monreal, S. Knafo, C. N. Petrok, J. R. Martens, and J. A. Esteban
2010. PIP 3 controls synaptic function by maintaining AMPA receptor clustering at the postsynaptic membrane. *Nature Neuroscience*, 13(1):36–44.

Aricescu, A., R. Assenberg, R. Bill, D. Busso, V. Chang, S. Davis, A. Dubrovsky, L. Gustafsson, K. Hedfalk, U. Heinemann, I. Jones, D. Ksiazek, C. Lang, K. Maskos, A. Messerschmidt, S. Macieira, Y. Peleg, A. Perrakis, A. Poterszman, G. Schneider, T. Sixma, J. Sussman, G. Sutton, N. Tarboureich, T. Zeev-Ben-Mordehai, and E. Jones
2006a. Eukaryotic expression: developments for structural proteomics research papers. *Acta Crystallogr. D. Biol. Crystallogr*, 62:1114–1124.

Aricescu, A. R., W. Lu, and E. Y. Jones
2006b. A time- and cost-efficient system for high-level protein production in mammalian cells. *Acta Crystallographica Section D: Biological Crystallography*, 62(10):1243–1250.

Armstrong, N. and E. Gouaux
2000. Mechanisms for Activation and Antagonism of an AMPA-Sensitive Glutamate Receptor: Crystal Structures of the GluR2 Ligand Binding Core. *Neuron*, 28(1):165–181.

Ashby, M. C., S. R. Maier, A. Nishimune, and J. M. Henley
2006. Lateral Diffusion Drives Constitutive Exchange of AMPA Receptors at Dendritic Spines and Is Regulated by Spine Morphology. *Journal of Neuroscience*, 26(26):7046–7055.

Ashkenazy, H., S. Abadi, E. Martz, O. Chay, I. Mayrose, T. Pupko, and N. Ben-Tal
2016. ConSurf 2016: an improved methodology to estimate and visualize evolutionary conservation in macromolecules. *Nucleic acids research*, 44(W1):W344–W350.

Aslanidis, C. and P. J. de Jong
1990. Ligation-independent cloning of PCR products (LIC-PCR). *Nucleic Acids Research*, 18(20):6069–6074.

Ayalon, G. and Y. Stern-Bach
2001. Functional assembly of AMPA and kainate receptors is mediated by several discrete protein-protein interactions. *Neuron*, 31(1):103–13.

Backliwal, G., M. Hildinger, S. Chenuet, S. Wulhfard, M. De Jesus, and F. M. Wurm
2008. Rational vector design and multi-pathway modulation of HEK 293E cells yield recombinant antibody titers exceeding 1 g/l by transient transfection under serum-free conditions. *Nucleic Acids Research*, 36(15):e96.

Balik, A., A. C. Penn, Z. Nemoda, and I. H. Greger
2013. Activity-regulated RNA editing in select neuronal subfields in hippocampus. *Nucleic Acids Research*, 41(2):1124–1134.

Bannerman, D. M., M. A. Good, S. P. Butcher, and R. G. M. Morris
1995. Distinct components of spatial learning revealed by prior training and NMDA receptor blockade. *Nature*, 378(6553):182–186.

Barbour, B. and M. Häusser
1997. Intersynaptic diffusion of neurotransmitter. *Trends in neurosciences*, 20(9):377–84.

Barria, A., D. Muller, V. Derkach, L. C. Griffith, and T. R. Soderling
1997a. Regulatory phosphorylation of AMPA-type glutamate receptors by CaM-KII during long-term potentiation. *Science*, 276(5321):2042–2045.

Barria, A., D. Muller, V. Derkach, L. C. Griffith, and T. R. Soderling
1997b. Regulatory phosphorylation of AMPA-type glutamate receptors by CaM-KII during long-term potentiation. *Science*, 276(5321):2042–2045.

Bats, C., L. Groc, and D. Choquet
2007. The Interaction between Stargazin and PSD-95 Regulates AMPA Receptor Surface Trafficking. *Neuron*, 53(5):719–734.

Bats, C., D. Soto, D. Studniarczyk, M. Farrant, and S. G. Cull-Candy
2012. Channel properties reveal differential expression of TARPed and TARPless AMPARs in stargazer neurons. *Nature Neuroscience*, 15(6):853–861.

Bedoukian, M. A., A. M. Weeks, and K. M. Partin
2006. Different domains of the AMPA receptor direct stargazin-mediated trafficking and stargazin-mediated modulation of kinetics. *Journal of Biological Chemistry*, 281(33):23908–23921.

Bedoukian, M. A., J. D. Whitesell, E. J. Peterson, C. M. Clay, and K. M. Partin
2008. The stargazin C terminus encodes an intrinsic and transferable membrane sorting signal. *Journal of Biological Chemistry*, 283(3):1597–1600.

Bell, J. C. and S. C. Kowalczykowski
2016. RecA: Regulation and Mechanism of a Molecular Search Engine. *Trends in Biochemical Sciences*, 41(6):491–507.

Bemben, M. A., Y. S. Shi, R. A. Nicoll, N. Sheng, J. Díaz-Alonso, and W. Tao
2018. LTP requires postsynaptic PDZ-domain interactions with glutamate receptor/auxiliary protein complexes. *Proceedings of the National Academy of Sciences*, 115(15):3948–3953.

Benke, T. A., A. Lüthi, M. J. Palmer, M. A. Wikström, W. W. Anderson, J. T. Isaac, and G. L. Collingridge
2001. Mathematical modelling of non-stationary fluctuation analysis for studying channel properties of synaptic AMPA receptors. *Journal of Physiology*, 537(2):407–420.

Beyer, H. M., P. Gonschorek, S. L. Samodelov, M. Meier, W. Weber, and M. D. Zurbriggen
2015. AQUA cloning: A versatile and simple enzyme-free cloning approach. *PLoS ONE*, 10(9):e0137652.

Bi, G. Q. and M. M. Poo
1998. Synaptic modifications in cultured hippocampal neurons: dependence on spike timing, synaptic strength, and postsynaptic cell type. *The Journal of neuroscience*, 18(24):10464–10472.

Bi, X. and L. F. Liu
1994. recA-independent and recA-dependent intramolecular plasmid recombination. Differential homology requirement and distance effect. *Journal of Molecular Biology*, 235(2):414–423.

Biederer, T., P. S. Kaeser, and T. A. Blanpied
2017. Transcellular Nanoalignment of Synaptic Function. *Neuron*, 96(3):680–696.

Biou, V., S. Bhattacharyya, and R. C. Malenka
2008. Endocytosis and recycling of AMPA receptors lacking GluR2/3. *Proc Natl Acad Sci U S A*, 105(3):1038–1043.

Bliss, T. V. and G. L. Collingridge
2013. Expression of NMDA receptor-dependent LTP in the hippocampus: bridging the divide. *Molecular Brain*, 6(1):5.

Bliss, T. V. P. and G. L. Collingridge
1993. A synaptic model of memory: long-term potentiation in the hippocampus. *Nature*, 361(6407):31–39.

Bliss, T. V. P., G. L. Collingridge, and R. G. M. Morris
2003. Introduction. *Philosophical Transactions of the Royal Society B: Biological Sciences*, 358(1432):607–611.

Bliss, T. V. P. and T. Lømo
1973. Long-lasting potentiation of synaptic transmission in the dentate area of the anaesthetized rabbit following stimulation of the perforant path. *The Journal of Physiology*, 232(2):331–356.

Boehm, J., I. Ehrlich, H. Hsieh, and R. Malinow
2006. Two mutations preventing PDZ-protein interactions of GluR1 have opposite effects on synaptic plasticity. *Learning & Memory*, 13(5):562–565.

Bommarius, A. S. and B. R. Riebel
2004. *Biocatalysis*. Wiley-VCH.

Borgdorff, A. J. and D. Choquet
2002. Regulation of AMPA receptor lateral movements. *Nature*, 417(6889):649–653.

Bowen, A. B., A. M. Bourke, B. G. Hiester, C. Hanus, and M. J. Kennedy
2017. Golgi-Independent secretory trafficking through recycling endosomes in neuronal dendrites and spines. *eLife*, 6:e27362.

Bowie, D., E. P. Garcia, J. Marshall, S. F. Traynelis, and G. D. Lange
2003. Allosteric Regulation and Spatial Distribution of Kainate Receptors Bound to Ancillary Proteins. *The Journal of Physiology*, 547(2):373–385.

Bowie, D. and M. L. Mayer
1995. Inward rectification of both AMPA and kainate subtype glutamate receptors generated by polyamine-mediated ion channel block. *Neuron*, 15(2):453–462.

Braithwaite, S. P., H. Xia, and R. C. Malenka
2002. Differential roles for NSF and GRIP/ABP in AMPA receptor cycling. *Proceedings of the National Academy of Sciences*, 99(10):7096–7101.

Brechet, A., R. Buchert, J. Schwenk, S. Boudkkazi, G. Zolles, K. Siquier-Pernet, I. Schaber, W. Bildl, A. Saadi, C. Bole-Feysot, P. Nitschke, A. Reis, H. Sticht, N. Al-Sanna'a, A. Rolfs, A. Kulik, U. Schulte, L. Colleaux, R. Abou Jamra, and B. Fakler
2017. AMPA-receptor specific biogenesis complexes control synaptic transmission and intellectual ability. *Nature Communications*, 8:15910.

Brown, T. C., S. S. Correia, C. N. Petrok, and J. A. Esteban
2007. Functional Compartmentalization of Endosomal Trafficking for the Synaptic Delivery of AMPA Receptors during Long-Term Potentiation. *Journal of Neuroscience*, 27(48):13311–13315.

Bubeck, P., M. Winkler, and W. Bautsch
1993. Rapid cloning by homologous recombination in vivo. *Nucleic Acids Research*, 21(15):3601–3602.

Burnashev, N., H. Monyer, P. H. Seeburg, and B. Sakmann
1992. Divalent ion permeability of AMPA receptor channels is dominated by the edited form of a single subunit. *Neuron*, 8(1):189–198.

Cais, O., B. Herguedas, K. Krol, S. G. Cull-Candy, M. Farrant, and I. H. Greger
2014. Mapping the interaction sites between AMPA receptors and TARPs reveals a role for the receptor N-terminal domain in channel gating. *Cell Reports*, 9(2):728–740.

Carroll, R. C., R. A. Nicoll, and R. C. Malenka
1998. Effect of PKA and PKC on miniature excitatory postsynaptic currents in CA1 pyramidal cells. *Journal of Neurophysiology*, 80(5):2797.

Chamma, I., M. Letellier, C. Butler, B. Tessier, K. H. Lim, I. Gauthereau, D. Choquet, J. B. Sibarita, S. Park, M. Sainlos, and O. Thoumine
2016. Mapping the dynamics and nanoscale organization of synaptic adhesion proteins using monomeric streptavidin. *Nature Communications*, 7:10773.

Chang, M. C., J. M. Park, K. A. Pelkey, H. L. Grabenstatter, D. Xu, D. J. Linden, T. P. Sutula, C. J. McBain, and P. F. Worley
2010. Narp regulates homeostatic scaling of excitatory synapses on parvalbumin-expressing interneurons. *Nature Neuroscience*, 13(9):1090–1097.

Chatterton, J. E., M. Awobuluyi, L. S. Premkumar, H. Takahashi, M. Talantova, Y. Shin, J. Cui, S. Tu, K. A. Sevarino, N. Nakanishi, G. Tong, S. A. Lipton, and D. Zhang
2002. Excitatory glycine receptors containing the NR3 family of NMDA receptor subunits. *Nature*, 415(6873):793–798.

Chayot, R., B. Montagne, D. Mazel, and M. Ricchetti
2010. An end-joining repair mechanism in Escherichia coli. *Proceedings of the National Academy of Sciences*, 107(5):2141–2146.

Chen, B.-Y., H. W. Janes, and S. Chen
2002. Computer programs for PCR primer design and analysis. *Methods in molecular biology (Clifton, N.J.)*, 192(3):19–29.

Chen, G. Q., C. Cul, M. L. Mayer, and E. Gouaux
1999a. Functional characterization of a potassium-selective prokaryotic glutamate receptor. *Nature*, 402(6763):817–821.

Chen, L., S. Bao, X. Qiao, and R. F. Thompson
1999b. Impaired cerebellar synapse maturation in waggler, a mutant mouse with a disrupted neuronal calcium channel gamma subunit. *Proceedings of the National Academy of Sciences*, 96(21):12132–12137.

Chen, L., D. M. Chetkovich, R. S. Petralia, N. T. Sweeney, Y. Kawasaki, R. J. Wenthold, D. S. Bredt, and R. A. Nicoll
2000. Stargazin regulates synaptic targeting of AMPA receptors by two distinct mechanisms. *Nature*, 408(6815):936–943.

Chen, S., Y. Zhao, Y. Wang, M. Shekhar, E. Tajkhorshid, and E. Gouaux
2017. Activation and Desensitization Mechanism of AMPA Receptor-TARP Complex by Cryo-EM. *Cell*, 170(6):1234–1246.e14.

Chen, W., R. Prithviraj, A. H. Mahnke, K. E. McGloin, J. W. Tan, A. K. Gooch, and F. M. Inglis
2009. AMPA glutamate receptor subunits 1 and 2 regulate dendrite complexity and spine motility in neurons of the developing neocortex. *Neuroscience*, 159(1):172–182.

Chen, X., J. M. Levy, A. Hou, C. Winters, R. Azzam, A. A. Sousa, R. D. Leapman, R. A. Nicoll, and T. S. Reese
2015. PSD-95 family MAGUKs are essential for anchoring AMPA and NMDA receptor complexes at the postsynaptic density. *Proceedings of the National Academy of Sciences*, 112(50):E6983–E6992.

Cheng, D., C. C. Hoogenraad, J. Rush, E. Ramm, M. A. Schlager, D. M. Duong, P. Xu, S. R. Wijayawardana, J. Hanfelt, T. Nakagawa, M. Sheng, and J. Peng
2006. Relative and Absolute Quantification of Postsynaptic Density Proteome Isolated from Rat Forebrain and Cerebellum. *Molecular & Cellular Proteomics*, 5(6):1158–1170.

Chetkovich, D. M., L. Chen, T. J. Stocker, R. A. Nicoll, and D. S. Bredt
2002. Phosphorylation of the postsynaptic density-95 (PSD-95)/discs large/zona occludens-1 binding site of stargazin regulates binding to PSD-95 and synaptic targeting of AMPA receptors. *The Journal of Neuroscience*, 22(14):5791–5796.

Chih, B., H. Engelman, and P. Scheiffele
2005. Control of excitatory and inhibitory synapse formation by neuroligins. *Science*, 307(5713):1324–1328.

Chiu, S. L., G. H. Diering, B. Ye, K. Takamiya, C. M. Chen, Y. Jiang, T. Niranjan, C. E. Schwartz, T. Wang, and R. L. Huganir
2017. GRASP1 Regulates Synaptic Plasticity and Learning through Endosomal Recycling of AMPA Receptors. *Neuron*, 93(6):1405–1419.e8.

Cho, C. H., F. St-Gelais, W. Zhang, S. Tomita, and J. R. Howe
2007. Two Families of TARP Isoforms that Have Distinct Effects on the Kinetic Properties of AMPA Receptors and Synaptic Currents. *Neuron*, 55(6):890–904.

Choi, J., J. Ko, E. Park, J. R. Lee, J. Yoon, S. Lim, and E. Kim
2002. Phosphorylation of stargazin by protein kinase A regulates its interaction with PSD-95. *Journal of Biological Chemistry*, 277(14):12359–12363.

Choquet, D. and A. Triller
2013. The dynamic synapse. *Neuron*, 80(3):691–703.

Chu, P.-J., H. M. Robertson, and P. M. Best
2001. Calcium channel g subunits provide insights into the evolution of this gene family. *Gene*, 280(1-2):37–48.

Chung, H. J., J. Xia, R. H. Scannevin, X. Zhang, and R. L. Huganir
2000. Phosphorylation of the AMPA receptor subunit GluR2 differentially regulates its interaction with PDZ domain-containing proteins. *The Journal of neuroscience*, 20(19):7258–7267.

Clayton, A., C. Siebold, R. J. Gilbert, G. C. Sutton, K. Harlos, R. A. McIlhinney, E. Y. Jones, and A. R. Aricescu
2009. Crystal Structure of the GluR2 Amino-Terminal Domain Provides Insights into the Architecture and Assembly of Ionotropic Glutamate Receptors. *Journal of Molecular Biology*, 392(5):1125–1132.

Clements, J., R. Lester, G. Tong, C. Jahr, and G. Westbrook
1992. Science. *Science*, 243(4897):1474–1477.

Coleman, S. K., Y. Hou, M. Willibald, A. Semenov, T. Möykkynen, and K. Keinänen
2016. Aggregation limits surface expression of homomeric GluA3 receptors. *Journal of Biological Chemistry*, 291(16):8784–8794.

Coleman, S. K., T. Möykkynen, C. Cai, L. von Ossowski, E. Kuismanen, E. R. Korpi, and K. Keinänen
2006. Isoform-specific early trafficking of AMPA receptor flip and flop variants. *The Journal of neuroscience*, 26(43):11220–9.

Coleman, S. K., T. Möykkynen, S. Hinkkuri, L. Vaahtera, E. R. Korpi, O. T. Pentikäinen, and K. Keinänen
2010. Ligand-binding domain determines endoplasmic reticulum exit of AMPA receptors. *Journal of Biological Chemistry*, 285(46):36032–36039.

Collingridge, G. L., C. E. Herron, and R. A. Lester
1988. Synaptic activation of N-methyl-D-aspartate receptors in the Schaffer collateral-commissural pathway of rat hippocampus. *The Journal of Physiology*, 399(1):283–300.

Collingridge, G. L., S. J. Kehl, and H. McLennan
1983. The antagonism of amino acid-induced excitations of rat hippocampal CA1 neurones in vitro. *The Journal of physiology*, 334:19–31.

Collingridge, G. L. and R. A. Lester
1989. Excitatory amino acid receptors in the vertebrate central nervous system. *Pharmacol Rev*, 41(2):143–210.

Conley, E. C., V. A. Saunders, and J. R. Saunders
1986. Deletion and rearrangement of plasmid DNA during transformation of Escherichia coli with linear plasmid molecules. *Nucleic Acids Research*, 14(22):8905–8917.

Constals, A., A. Penn, B. Compans, E. Toulmé, A. Phillipat, S. Marais, N. Retailleau, A.-S. Hafner, F. Coussen, E. Hosy, and D. Choquet
2015. Glutamate-Induced AMPA Receptor Desensitization Increases Their Mobility and Modulates Short-Term Plasticity through Unbinding from Stargazin. *Neuron*, 85(4):787–803.

Contractor, A., C. Mulle, and G. T. Swanson
2011. Kainate receptors coming of age: Milestones of two decades of research. *Trends in Neurosciences*, 34(3):154–163.

Coombs, I. and S. Cull-Candy
2009. Transmembrane AMPA receptor regulatory proteins and AMPA receptor function in the cerebellum. *Neuroscience*, 162(3):656–665.

Coombs, I. D., D. M. MacLean, V. Jayaraman, M. Farrant, and S. G. Cull-Candy
2017. Dual Effects of TARP γ-2 on Glutamate Efficacy Can Account for AMPA Receptor Autoinactivation. *Cell Reports*, 20(5):1123–1135.

Cuadra, A. E.
2004. AMPA Receptor Synaptic Targeting Regulated by Stargazin Interactions with the Golgi-Resident PDZ Protein nPIST. *Journal of Neuroscience*, 24(34):7491–7502.

Dakoji, S., S. Tomita, S. Karimzadegan, R. A. Nicoll, and D. S. Bredt
2003. Interaction of transmembrane AMPA receptor regulatory proteins with multiple membrane associated guanylate kinases. *Neuropharmacology*, 45(6):849–856.

Dani, A., B. Huang, J. Bergan, C. Dulac, and X. Zhuang
2010. Superresolution Imaging of Chemical Synapses in the Brain. *Neuron*, 68(5):843–856.

Debanne, D., B. H. Gähwiler, and S. M. Thompson
1997. Bidirectional associative plasticity of unitary CA3-CA1 EPSPs in the rat hippocampus in vitro. *Journal of neurophysiology*, 77(5):2851–2855.

Deng, F., M. G. Price, C. F. Davis, M. Mori, and D. L. Burgess
2006. Stargazin and Other Transmembrane AMPA Receptor Regulating Proteins Interact with Synaptic Scaffolding Protein MAGI-2 in Brain. *Journal of Neuroscience*, 26(30):7875–7884.

Dereeper, A., V. Guignon, G. Blanc, S. Audic, S. Buffet, F. Chevenet, J.-F. Dufayard, S. Guindon, V. Lefort, M. Lescot, J.-M. Claverie, and O. Gascuel
2008. Phylogeny.fr: robust phylogenetic analysis for the non-specialist. *Nucleic Acids Research*, 36(Web Server):W465–W469.

Dev, K. K., A. Nishimune, J. M. Henley, and S. Nakanishi
1999. The protein kinase Cα binding protein PICK1 interacts with short but not long form alternative splice variants of AMPA receptor subunits. *Neuropharmacology*, 38(5):635–644.

Dhanrajan, T. M., M. A. Lynch, A. Kelly, V. I. Popov, D. A. Rusakov, and M. G. Stewart
2004. Expression of long-term potentiation in aged rats involves perforated synapses but dendritic spine branching results from high-frequency stimulation alone. *Hippocampus*, 14(2):255–264.

Diamond, J. S., D. E. Bergles, and C. E. Jahr
1998. Glutamate release monitored with astrocyte transporter currents during LTP. *Neuron*, 21(2):425–433.

Diamond, J. S. and C. E. Jahr
1997. Transporters buffer synaptically released glutamate on a submillisecond time scale. *The Journal of Neuroscience*, 17(12):4672–4687.

Díaz-Alonso, J., Y. J. Sun, A. J. Granger, J. M. Levy, S. M. Blankenship, and R. A. Nicoll
2017. Subunit-specific role for the amino-terminal domain of AMPA receptors in synaptic targeting. *Proceedings of the National Academy of Sciences*, 114(27):7136–7141.

Diering, G. H., S. Heo, N. K. Hussain, B. Liu, and R. L. Huganir
2016. Extensive phosphorylation of AMPA receptors in neurons. *Proceedings of the National Academy of Sciences*, 113(33):E4920–E4927.

Dodds, D. C., I. A. Omeis, S. J. Cushman, J. A. Helms, and M. S. Perin
1997. Neuronal pentraxin receptor, a novel putative integral membrane pentraxin that interacts with neuronal pentraxin 1 and 2 and taipoxin- associated calcium-binding protein 49. *Journal of Biological Chemistry*, 272(34):21488–21494.

Dong, H., R. J. O'Brien, E. T. Fung, A. A. Lanahan, P. F. Worley, and R. L. Huganir
1997. GRIP: A synaptic PDZ domain-containing protein that interacts with AMPA receptors. *Nature*, 386(6622):279–284.

Dürr, K. L., L. Chen, R. A. Stein, R. De Zorzi, I. M. Folea, T. Walz, H. S. McHaourab, and E. Gouaux
2014. Structure and dynamics of AMPA receptor GluA2 in resting, pre-open, and desensitized states. *Cell*, 158(4):778–792.

Dutra, B. E. and S. T. Lovett
2006. Cis and trans-acting effects on a mutational hotspot involving a replication template switch. *Journal of Molecular Biology*, 356(2):300–311.

Dutra, B. E., V. a. Sutera, and S. T. Lovett
2007. RecA-independent recombination is efficient but limited by exonucleases. *Proceedings of the National Academy of Sciences*, 104(1):216–221.

Egebjerg, J., V. Kukekov, and S. F. Heinemann
1994. Intron sequence directs RNA editing of the glutamate receptor subunit GluR2 coding sequence. *Proceedings of the National Academy of Sciences*, 91(22):10270–10274.

Ehrlich, I. and R. Malinow
2004. Postsynaptic Density 95 controls AMPA Receptor Incorporation during Long-Term Potentiation and Experience-Driven Synaptic Plasticity. *Journal of Neuroscience*, 24(4):916–927.

El-Husseini, A., E. Schnell, and D. Chetkovich
2000a. PSD-95 involvement in maturation of excitatory synapses. *Science*, 290(5495):1364–8.

El-Husseini, A. E., S. E. Craven, D. M. Chetkovich, B. L. Firestein, E. Schnell, C. Aoki, and D. S. Bredt
2000b. Dual palmitoylation of PSD-95 mediates its vesiculotubular sorting, postsynaptic targeting, and ion channel clustering. *Journal of Cell Biology*, 148(1):159–171.

El-Husseini, A. E., J. R. Topinka, J. E. Lehrer-Graiwer, B. L. Firestein, S. E. Craven, C. Aoki, and D. S. Bred
2000c. Ion channel clustering by membrane-associated guanylate kinases: Differential regulation by N-terminal lipid and metal binding motifs. *Journal of Biological Chemistry*, 275(31):23904–23910.

El-Husseini, A. E. D., E. Schnell, S. Dakoji, N. Sweeney, Q. Zhou, O. Prange, C. Gauthier-Campbell, A. Aguilera-Moreno, R. A. Nicoll, and D. S. Bredt
2002. Synaptic strength regulated by palmitate cycling on PSD-95. *Cell*, 108(6):849–863.

Elegheert, J., W. Kakegawa, J. E. Clay, N. F. Shanks, E. Behiels, K. Matsuda, K. Kohda, E. Miura, M. Rossmann, N. Mitakidis, J. Motohashi, V. T. Chang, C. Siebold, I. H. Greger, T. Nakagawa, M. Yuzaki, and A. R. Aricescu
2016. Structural basis for integration of GluD receptors within synaptic organizer complexes. *Science*, 353(6296):295–300.

Elias, G. M., L. Funke, V. Stein, S. G. Grant, D. S. Bredt, and R. A. Nicoll
2006. Synapse-Specific and Developmentally Regulated Targeting of AMPA Receptors by a Family of MAGUK Scaffolding Proteins. *Neuron*, 52(2):307–320.

Emptage, N. J., C. A. Reid, A. Fine, and T. V. Bliss
2003. Optical quantal analysis reveals a presynaptic component of LTP at hippocampal Schaffer-associational synapses. *Neuron*, 38(5):797–804.

Engler, C., R. Gruetzner, R. Kandzia, and S. Marillonnet
2009. Golden gate shuffling: A one-pot DNA shuffling method based on type ils restriction enzymes. *PLoS ONE*, 4(5):e5553.

Engler, C., R. Kandzia, and S. Marillonnet
2008. A one pot, one step, precision cloning method with high throughput capability. *PLoS ONE*, 3(11):e3647.

Enoki, R., Y. ling Hu, D. Hamilton, and A. Fine
2009. Expression of Long-Term Plasticity at Individual Synapses in Hippocampus Is Graded, Bidirectional, and Mainly Presynaptic: Optical Quantal Analysis. *Neuron*, 62(2):242–253.

Erlenhardt, N., H. Yu, K. Abiraman, T. Yamasaki, J. I. Wadiche, S. Tomita, and D. S. Bredt
2016. Porcupine Controls Hippocampal AMPAR Levels, Composition, and Synaptic Transmission. *Cell Reports*, 14(4):782–794.

Eroglu, C. and B. A. Barres
2010. Regulation of synaptic connectivity by glia. *Nature*, 468(7321):223–231.

Esteban, J. A.
2008. Intracellular machinery for the transport of AMPA receptors. *British Journal of Pharmacology*, 153(SUPPL. 1):S35–S43.

Esteban, J. A., S. H. Shi, C. Wilson, M. Nuriya, R. L. Huganir, and R. Malinow
2003. PKA phosphorylation of AMPA receptor subunits controls synaptic trafficking underlying plasticity. *Nature Neuroscience*, 6(2):136–143.

Esteves da Silva, M., M. Adrian, P. Schätzle, J. Lipka, T. Watanabe, S. Cho, K. Futai, C. J. Wierenga, L. C. Kapitein, and C. C. Hoogenraad
2015. Positioning of AMPA Receptor-Containing Endosomes Regulates Synapse Architecture. *Cell Reports*, 13(5):933–943.

Evan, G. I., G. K. Lewis, G. Ramsay, and J. M. Bishop
1985. Isolation of monoclonal antibodies specific for human c-myc proto-oncogene product. *Molecular and cellular biology*, 5(12):3610–6.

Farhy-Tselnicker, I., A. C. van Casteren, A. Lee, V. T. Chang, A. R. Aricescu, and N. J. Allen
2017. Astrocyte-Secreted Glypican 4 Regulates Release of Neuronal Pentraxin 1 from Axons to Induce Functional Synapse Formation. *Neuron*, 96(2):428–445.e13.

Farrow, P., K. Khodosevich, Y. Sapir, A. Schulmann, M. Aslam, Y. Stern-Bach, H. Monyer, and J. von Engelhardt
2015. Auxiliary subunits of the CKAMP family differentially modulate AMPA receptor properties. *eLife*, 4(December2015):e09693.

Feng, W. and M. Zhang
2009. Organization and dynamics of PDZ-domain-related supramodules in the postsynaptic density. *Nature Reviews Neuroscience*, 10(2):87–99.

Fisher, A. B., Z. B. Canfield, L. C. Hayward, S. S. Fong, and G. H. McArthur
2013. Ex vivo DNA Assembly. *Frontiers in Bioengineering and Biotechnology*, 1:12.

Fiuza, M., C. M. Rostosky, G. T. Parkinson, A. M. Bygrave, N. Halemani, M. Baptista, I. Milosevic, and J. G. Hanley
2017. PICK1 regulates AMPA receptor endocytosis via direct interactions with AP2 α-appendage and dynamin. *Journal of Cell Biology*, 216(10):3323–3338.

Fujino, T., J. H. Leslie, R. Eavri, J. L. Chen, W. C. Lin, G. H. Flanders, E. Borok, T. L. Horvath, and E. Nedivi
2011. CPG15 regulates synapse stability in the developing and adult brain. *Genes and Development*, 25(24):2674–2685.

Fukata, Y., A. Dimitrov, G. Boncompain, O. Vielemeyer, F. Perez, and M. Fukata
2013. Local palmitoylation cycles define activity-regulated postsynaptic subdomains. *Journal of Cell Biology*, 202(1):145–161.

Fukata, Y., A. V. Tzingounis, J. C. Trinidad, M. Fukata, A. L. Burlingame, R. A. Nicoll, and D. S. Bredt
2005. Molecular constituents of neuronal AMPA receptors. *Journal of Cell Biology*, 169(3):399–404.

Fukaya, M., M. Tsujita, M. Yamazaki, E. Kushiya, M. Abe, K. Akashi, R. Natsume, M. Kano, H. Kamiya, M. Watanabe, and K. Sakimura
2006. Abundant distribution of TARP γ-8 in synaptic and extrasynaptic surface of hippocampal neurons and its major role in AMPA receptor expression on spines and dendrites. *European Journal of Neuroscience*, 24(8):2177–2190.

Fukaya, M., M. Yamazaki, K. Sakimura, and M. Watanabe
2005. Spatial diversity in gene expression for VDCC gamma subunit family in developing and adult mouse brains. *Neuroscience research*, 53(4):376–83.

Futai, K., M. J. Kim, T. Hashikawa, P. Scheiffele, M. Sheng, and Y. Hayashi
2007. Retrograde modulation of presynaptic release probability through signaling mediated by PSD-95-neuroligin. *Nature Neuroscience*, 10(2):186–195.

Gallimore, A. R., A. R. Aricescu, M. Yuzaki, and R. Calinescu
2016. A Computational Model for the AMPA Receptor Phosphorylation Master Switch Regulating Cerebellar Long-Term Depression. *PLoS Computational Biology*, 12(1):e1004664.

Ganai, R. A. and E. Johansson
2016. DNA Replication-A Matter of Fidelity. *Molecular Cell*, 62(5):745–755.

García-Nafría, J., B. Herguedas, J. F. Watson, and I. H. Greger
2016a. The dynamic AMPA receptor extracellular region: a platform for synaptic protein interactions. *Journal of Physiology*, 594(19):5449–5458.

García-Nafría, J., J. F. Watson, and I. H. Greger
2016b. IVA cloning: A single-tube universal cloning system exploiting bacterial In Vivo Assembly. *Scientific Reports*, 6(May):27459.

Gardner, S. M., L. O. Trussell, and D. Oertel
1999. Time course and permeation of synaptic AMPA receptors in cochlear nuclear neurons correlate with input. *The Journal of neuroscience*, 19(20):8721–8729.

Geiger, J. R., T. Melcher, D. S. Koh, B. Sakmann, P. H. Seeburg, P. Jonas, and H. Monyer
1995. Relative abundance of subunit mRNAs determines gating and Ca2+ permeability of AMPA receptors in principal neurons and interneurons in rat CNS. *Neuron*, 15(1):193–204.

Gibson, D. G., L. Young, R. Y. Chuang, J. C. Venter, C. A. Hutchison, and H. O. Smith
2009. Enzymatic assembly of DNA molecules up to several hundred kilobases. *Nature Methods*, 6(5):343–345.

Gill, M. B., A. S. Kato, M. F. Roberts, H. Yu, H. Wang, S. Tomita, and D. S. Bredt
2011. Cornichon-2 Modulates AMPA Receptor-Transmembrane AMPA Receptor Regulatory Protein Assembly to Dictate Gating and Pharmacology. *Journal of Neuroscience*, 31(18):6928–6938.

Granger, A. J. and R. A. Nicoll
2013. Expression mechanisms underlying long-term potentiation: a postsynaptic view, 10 years on. *Philosophical Transactions of the Royal Society B: Biological Sciences*, 369(1633):20130136–20130136.

Granger, A. J., Y. Shi, W. Lu, M. Cerpas, and R. A. Nicoll
2013. LTP requires a reserve pool of glutamate receptors independent of subunit type. *Nature*, 493(7433):495–500.

Gray, E. E., A. E. Fink, J. Sariñana, B. Vissel, and T. J. O'Dell
2007. Long-term potentiation in the hippocampal CA1 region does not require insertion and activation of GluR2-lacking AMPA receptors. *Journal of neurophysiology*, 98(July 2007):2488–92.

Greger, I. H. and J. A. Esteban
2007. AMPA receptor biogenesis and trafficking. *Current Opinion in Neurobiology*, 17(3):289–297.

Greger, I. H., L. Khatri, and E. B. Ziff
2002. RNA editing at Arg607 controls AMPA receptor exit from the endoplasmic reticulum. *Neuron*, 34(5):759–772.

Greger, I. H., J. F. Watson, and S. G. Cull-Candy
2017. Structural and Functional Architecture of AMPA-Type Glutamate Receptors and Their Auxiliary Proteins. *Neuron*, 94(4):713–730.

Gupta, R., D. Barkan, G. Redelman-Sidi, S. Shuman, and M. S. Glickman
2011. Mycobacteria exploit three genetically distinct DNA double-strand break repair pathways. *Molecular Microbiology*, 79(2):316–330.

Gupta, R., M. Ryzhikov, O. Koroleva, M. Unciuleac, S. Shuman, S. Korolev, and M. S. Glickman
2013. A dual role for mycobacterial RecO in RecA-dependent homologous recombination and RecA-independent single-strand annealing. *Nucleic Acids Research*, 41(4):2284–2295.

Gutierrez-Castellanos, N., C. M. Da Silva-Matos, K. Zhou, C. B. Canto, M. C. Renner, L. M. Koene, O. Ozyildirim, R. Sprengel, H. W. Kessels, and C. I. De Zeeuw
2017a. Motor Learning Requires Purkinje Cell Synaptic Potentiation through Activation of AMPA-Receptor Subunit GluA3. *Neuron*, 93(2):409–424.

Gutierrez-Castellanos, N., N. R. Reinders, E. H. Albers, H. Xiong, H. W. Kessels, A. N. van Huijstee, T. R. Lodder, and M. C. Renner
2017b. Synaptic plasticity through activation of GluA3-containing AMPA-receptors. *eLife*, 6:e25462.

Hafner, A.-S. S., A. C. Penn, D. Grillo-Bosch, N. Retailleau, C. Poujol, A. Philippat, F. Coussen, M. Sainlos, P. Opazo, and D. Choquet
2015. Lengthening of the stargazin cytoplasmic tail increases synaptic transmission by promoting interaction to deeper domains of PSD-95. *Neuron*, 86(2):475–489.

Hanley, J. G., L. Khatri, P. I. Hanson, and E. B. Ziff
2002. NSF ATPase and α-/β-SNAPs disassemble the AMPA receptor-PICK1 complex. *Neuron*, 34(1):53–67.

Hanus, C., H. Geptin, G. Tushev, S. Garg, B. Alvarez-Castelao, S. Sambandan, L. Kochen, A.-S. Hafner, J. D. Langer, and E. M. Schuman
2016. Unconventional secretory processing diversifies neuronal ion channel properties. *eLife*, 5:e20609.

Hartveit, E. and M. L. Veruki
2007. Studying properties of neurotransmitter receptors by non-stationary noise analysis of spontaneous postsynaptic currents and agonist-evoked responses in outside-out patches. *Nature Protocols*, 2(2):434–448.

Hashimoto, K., M. Fukaya, X. Qiao, K. Sakimura, M. Watanabe, and M. Kano
1999. Impairment of AMPA Receptor Function in Cerebellar Granule Cells of Ataxic Mutant Mouse Stargazer. *J. Neurosci.*, 19(14):6027–6036.

Hastie, P., M. H. Ulbrich, H.-L. Wang, R. J. Arant, A. G. Lau, Z. Zhang, E. Y. Isacoff, and L. Chen
2013. AMPA receptor/TARP stoichiometry visualized by single-molecule subunit counting. *Proceedings of the National Academy of Sciences*, 110(13):5163–8.

Hawken, N. M., E. I. Zaika, and T. Nakagawa
2017. Engineering defined membrane-embedded elements of AMPA receptor induces opposing gating modulation by cornichon 3 and stargazin. *Journal of Physiology*, 595(20):6517–6539.

Hayashi, Y., S. H. Shi, J. A. Esteban, A. Piccini, J. C. Poncer, and R. Malinow
2000. Driving AMPA receptors into synapses by LTP and CaMKII: Requirement for GluR1 and PDZ domain interaction. *Science*, 287(5461):2262–2267.

Hebb, D. O.
1949. *The organisation of behaviour*.

Heine, M., L. Groc, R. Frischknecht, J. C. Béïque, B. Lounis, G. Rumbaugh, R. L. Huganir, L. Cognet, and D. Choquet
2008. Surface mobility of postsynaptic AMPARs tunes synaptic transmission. *Science*, 320(5873):201–205.

Hell, J. W.
2014. CaMKII: Claiming center stage in postsynaptic function and organization. *Neuron*, 81(2):249–265.

Henke, W., K. Herdel, K. Jung, D. Schnorr, and S. A. Loening
1997. Betaine improves the PCR amplification of GC-rich DNA sequences. *Nucleic Acids Res.*, 25:3957–3958.

Herguedas, B., J. García-Nafría, O. Cais, R. Fernández-Leiro, J. Krieger, H. Ho, and I. H. Greger
2016. Structure and organization of heteromeric AMPA-type glutamate receptors. *Science*, 3873:aad3873.

Herguedas, B., J. Krieger, and I. H. Greger
2013. Receptor heteromeric assembly - How it works and why it matters: The case of ionotropic glutamate receptors. *Progress in Molecular Biology and Translational Science*, 117:361–386.

Hering, H. and M. Sheng
2001. Dentritic spines: structure, dynamics and regulation. *Nature Reviews Neuroscience*, 2(12):880–888.

Herring, B. E., Y. Shi, Y. H. Suh, C. Y. Zheng, S. M. Blankenship, K. W. Roche, and R. A. Nicoll
2013. Cornichon Proteins Determine the Subunit Composition of Synaptic AMPA Receptors. *Neuron*, 77(6):1083–1096.

Higuchi, M., S. Maas, F. N. Single, J. Hartner, A. Rozov, N. Burnashev, D. Feldmeyer, R. Sprengel, and P. H. Seeburg
2000. Point mutation in an AMPA receptor gene rescues lethality in mice deficientin the RNA-editing enzyme ADAR2. *Nature*, 406(6791):78–81.

Hirbec, H., J. C. Francis, S. E. Lauri, S. P. Braithwaite, F. Coussen, C. Mulle, K. K. Dev, V. Couthino, G. Meyer, J. T. Isaac, G. L. Collingridge, and J. M. Henley
2003. Rapid and differential regulation of AMPA and kainate receptors at hippocampal mossy fibre synapses by PICK1 and GRIP. *Neuron*, 37(4):625–638.

Hollmann, M., M. Hartley, and S. Heinemann
1991. Ca2+permeability of KA-AMPA - gated glutamate receptor channels depends on subunit composition. *Science*, 252(5007):851–853.

Hosokawa, T., D. Mitsushima, R. Kaneko, and Y. Hayashi
2015. Stoichiometry and Phosphoisotypes of Hippocampal AMPA-Type Glutamate Receptor Phosphorylation. *Neuron*, 85(1):60–68.

Howard, M. A., G. M. Elias, L. A. B. Elias, W. Swat, and R. A. Nicoll
2010. The role of SAP97 in synaptic glutamate receptor dynamics. *Proceedings of the National Academy of Sciences*, 107(8):3805–3810.

Howorka, S. and H. Bayley
1998. Improved protocol for high-throughput cysteine scanning mutagenesis. *BioTechniques*, 25(5):764–772.

Huang, F., J. R. Spangler, and A. Y. Huang
2017. In vivo cloning of up to 16 kb plasmids in E. coli is as simple as PCR. *PLoS ONE*, 12(8):e0183974.

Huganir, R. L. and R. A. Nicoll
2013. AMPARs and synaptic plasticity: The last 25 years. *Neuron*, 80(3):704–717.

Hultman, T., M. Murby, S. Ståhl, E. Hornes, and M. Uhlén
1990. Solid phase in vitro mutagenesis using plasmid DNA template. *Nucleic Acids Research*, 18(17):5107–12.

Hume, R. I., R. Dingledine, and S. F. Heinemann
1991. Identification of a site in glutamate receptor subunits that controls calcium permeability. *Science*, 253(5023):1028–31.

Iacobucci, G. J. and G. K. Popescu
2017. NMDA receptors: Linking physiological output to biophysical operation. *Nature Reviews Neuroscience*, 18(4):236–249.

Inamura, M., M. Itakura, H. Okamoto, S. Hoka, A. Mizoguchi, Y. Fukazawa, R. Shigemoto, S. Yamamori, and M. Takahashi
2006. Differential localization and regulation of stargazin-like protein, γ-8 and stargazin in the plasma membrane of hippocampal and cortical neurons. *Neuroscience Research*, 55(1):45–53.

Irie, M., Y. Hata, M. Takeuchi, K. Ichtchenko, A. Toyoda, K. Hirao, Y. Takai, T. W. Rosahl, and T. C. Südhof
1997. Binding of neuroligins to PSD-95. *Science*, 277(5331):1511–1515.

Isaac, J. T., M. C. Ashby, and C. J. McBain
2007. The Role of the GluR2 Subunit in AMPA Receptor Function and Synaptic Plasticity. *Neuron*, 54(6):859–871.

Isaac, J. T., R. A. Nicoll, and R. C. Malenka
1995. Evidence for silent synapses: Implications for the expression of LTP. *Neuron*, 15(2):427–434.

Itakura, M., I. Watanabe, T. Sugaya, and M. Takahashi
2014. Direct association of the unique C-terminal tail of transmembrane AMPA receptor regulatory protein γ-8 with calcineurin. *FEBS Journal*, 281(5):1366–1378.

Ives, J. H., S. Fung, P. Tiwari, H. L. Payne, and C. L. Thompson
2004. Microtubule-associated protein light chain 2 is a stargazin-AMPA receptor complex-interacting protein in vivo. *Journal of Biological Chemistry*, 279(30):31002–31009.

Jackman, S. L. and W. G. Regehr
2017. The Mechanisms and Functions of Synaptic Facilitation. *Neuron*, 94(3):447–464.

Jackson, A. C. and R. A. Nicoll
2011. The Expanding Social Network of Ionotropic Glutamate Receptors: TARPs and Other Transmembrane Auxiliary Subunits. *Neuron*, 70(2):178–199.

Jacob, A. L. and R. J. Weinberg
2015. The organization of AMPA receptor subunits at the postsynaptic membrane. *Hippocampus*, 25(7):798–812.

Jacobus, A. P. and J. Gross
2015. Optimal cloning of PCR fragments by homologous recombination in Escherichia coli. *PLoS ONE*, 10(3):e0119221.

Jia, Z., N. Agopyan, P. Miu, Z. Xiong, J. Henderson, R. Gerlai, F. A. Taverna, A. Velumian, J. MacDonald, P. Carlen, W. Abramow-Newerly, and J. Roder
1996. Enhanced LTP in mice deficient in the AMPA receptor GluR2. *Neuron*, 17(5):945–956.

Jin, R., S. K. Singh, S. Gu, H. Furukawa, A. I. Sobolevsky, J. Zhou, Y. Jin, and E. Gouaux
2009. Crystal structure and association behaviour of the GluR2 amino-terminal domain. *EMBO Journal*, 28(12):1812–1823.

Jonas, P., G. Major, and B. Sakmann
1993. Quantal components of unitary EPSCs at the mossy fibre synapse on CA3 pyramidal cells of rat hippocampus. *The Journal of Physiology*, 472(1):615–663.

Jonas, P. and N. Spruston
1994. Mechanisms shaping glutamate-mediated excitatory postsynaptic currents in the CNS. *Current Opinion in Neurobiology*, 4(3):366–372.

Jones, D. G.
1993. Synaptic plasticity and perforated synapses: their relevance for an understanding of abnormal synaptic organization. *APMIS. Supplementum*, 40:25–34.

Jones, D. H. and B. H. Howard
1991. A rapid method for recombination and site-specific mutagenesis by placing homologous ends on DNA using polymerase chain reaction. *BioTechniques*, 10(1):62–66.

Jones, D. H. and S. C. Winistorfer
1993. Use of Polymerase Chain Reaction for Making Recombinant Constructs. In *PCR Protocols*, volume 15, Pp. 241–250. New Jersey: Humana Press.

Jones, D. H. and S. C. Winistorfer
1997. Recombination and site-directed mutagenesis using recombination PCR. *Methods in molecular biology (Clifton, N.J.)*, 67:131–40.

Jones, D. H. and S. C. Winistorfer
2003. Recombination and site-directed mutagenesis using recombination PCR. *Methods in molecular biology (Clifton, N.J.)*, 226:517–24.

Joska, T. M., A. Mashruwala, J. M. Boyd, and W. J. Belden
2014. A universal cloning method based on yeast homologous recombination that is simple, efficient, and versatile. *Journal of Microbiological Methods*, 100(1):46–51.

Kakegawa, W., T. Miyazaki, K. Emi, K. Matsuda, K. Kohda, J. Motohashi, M. Mishina, S. Kawahara, M. Watanabe, and M. Yuzaki
2008. Differential Regulation of Synaptic Plasticity and Cerebellar Motor Learning by the C-Terminal PDZ-Binding Motif of GluR 2. *Journal of Neuroscience*, 28(6):1460–1468.

Kakegawa, W., T. Miyazaki, H. Hirai, J. Motohashi, M. Mishina, M. Watanabe, and M. Yuzaki
2007. Ca2+ permeability of the channel pore is not essential for the $\delta 2$ glutamate receptor to regulate synaptic plasticity and motor coordination. *Journal of Physiology*, 579(3):729–735.

Kakegawa, W., Y. Miyoshi, K. Hamase, S. Matsuda, K. Matsuda, K. Kohda, K. Emi, J. Motohashi, R. Konno, K. Zaitsu, and M. Yuzaki
2011. D-Serine regulates cerebellar LTD and motor coordination through the $\delta 2$ glutamate receptor. *Nature Neuroscience*, 14(5):603–611.

Kalashnikova, E., R. A. Lorca, I. Kaur, G. A. Barisone, B. Li, T. Ishimaru, J. S. Trimmer, D. P. Mohapatra, and E. Díaz
2010. SynDIG1: An Activity-Regulated, AMPA- Receptor-Interacting Transmembrane Protein that Regulates Excitatory Synapse Development. *Neuron*, 65(1):80–93.

Kamboj, S. K., G. T. Swanson, and S. G. Cull-Candy
1995. Intracellular spermine confers rectification on rat calcium-permeable AMPA and kainate receptors. *The Journal of Physiology*, 486(2):297–303.

Karakas, E. and H. Furukawa
2014. Crystal structure of a heterotetrameric NMDA receptor ion channel. *Science*, 344(6187):992–7.

Kato, A. S., M. B. Gill, M. T. Ho, H. Yu, Y. Tu, E. R. Siuda, H. Wang, Y. W. Qian, E. S. Nisenbaum, S. Tomita, and D. S. Bredt
2010. Hippocampal AMPA Receptor Gating Controlled by Both TARP and Cornichon Proteins. *Neuron*, 68(6):1082–1096.

Kato, A. S., E. R. Siuda, E. S. Nisenbaum, and D. S. Bredt
2008. AMPA Receptor Subunit-Specific Regulation by a Distinct Family of Type II TARPs. *Neuron*, 59(6):986–996.

Kauer, J. A. and R. C. Malenka
2007. Synaptic plasticity and addiction. *Nature Reviews Neuroscience*, 8(11):844–858.

Kauer, J. A., R. C. Malenka, and R. A. Nicoll
1988. A persistent postsynaptic modification mediates long-term potentiation in the hippocampus. *Neuron*, 1(10):911–917.

Kavalali, E. T.
2015. The mechanisms and functions of spontaneous neurotransmitter release. *Nature Reviews Neuroscience*, 16(1):5–16.

Keinänen, K., W. Wisden, B. Sommer, P. Werner, A. Herb, T. A. Verdoorn, B. Sakmann, and P. H. Seeburg
1990. A family of AMPA-selective glutamate receptors. *Science*, 249(4968):556–60.

Kennedy, M. B.
1995. Origin of PDZ (DHR, GLGF) domains. *Trends in Biochemical Sciences*, 20(9):350.

Kerr, J. M. and T. A. Blanpied
2012. Subsynaptic AMPA Receptor Distribution Is Acutely Regulated by Actin-Driven Reorganization of the Postsynaptic Density. *Journal of Neuroscience*, 32(2):658–673.

Kerschensteiner, D.
2017. Aligning a Synapse. *Neuron*, 93(6):1241–1243.

Kessels, H. W., C. D. Kopec, M. E. Klein, and R. Malinow
2009. Roles of stargazin and phosphorylation in the control of AMPA receptor subcellular distribution. *Nature Neuroscience*, 12(7):888–896.

Kessels, H. W. and R. Malinow
2009. Synaptic AMPA Receptor Plasticity and Behavior. *Neuron*, 61(3):340–350.

Khodosevich, K., E. Jacobi, P. Farrow, A. Schulmann, A. Rusu, L. Zhang, R. Sprengel, H. Monyer, and J. von Engelhardt
2014. Coexpressed Auxiliary Subunits Exhibit Distinct Modulatory Profiles on AMPA Receptor Function. *Neuron*, 83(3):601–615.

Kibbe, W. A.
2007. OligoCalc: An online oligonucleotide properties calculator. *Nucleic Acids Research*, 35(SUPPL.2):W43–W46.

Kim, C. H., K. Takamiya, R. S. Petralia, R. Sattler, S. Yu, W. Zhou, R. Kalb, R. Wenthold, and R. Huganir
2005. Persistent hippocampal CA1 LTP in mice lacking the C-terminal PDZ ligand of GluR1. *Nature Neuroscience*, 8(8):985–987.

Kim, Y. G. and S. Maas
2000. Multiple site mutagenesis with high targeting efficiency in one cloning step. *BioTechniques*, 28(2):196–198.

Kingston, A. W., C. Roussel-Rossin, C. Dupont, and E. A. Raleigh
2015. Novel recA-independent horizontal gene transfer in Escherichia coli K-12. *PLoS ONE*, 10(7):e0130813.

Klaassen, R. V., J. Stroeder, F. Coussen, A.-S. Hafner, J. D. Petersen, C. Renancio, L. J. M. Schmitz, E. Normand, J. C. Lodder, D. C. Rotaru, P. Rao-Ruiz, S. Spijker, H. D. Mansvelder, D. Choquet, and A. B. Smit
2016. Shisa6 traps AMPA receptors at postsynaptic sites and prevents their desensitization during synaptic activity. *Nature Communications*, 7:10682.

Klock, H. E., E. J. Koesema, M. W. Knuth, and S. A. Lesley
2008. Combining the polymerase incomplete primer extension method for cloning and mutagenesis with microscreening to accelerate structural genomics efforts. *Proteins: Structure, Function and Genetics*, 71(2):982–994.

Klöcker, N., R. C. Bunn, E. Schnell, G. Caruana, A. Bernstein, R. A. Nicoll, and D. S. Bredt
2002. Synaptic glutamate receptor clustering in mice lacking the SH3 and GK domains of SAP97. *European Journal of Neuroscience*, 16(8):1517–1522.

Koh, D. S., N. Burnashev, and P. Jonas
1995. Block of native Ca(2+)-permeable AMPA receptors in rat brain by intracellular polyamines generates double rectification. *The Journal of Physiology*, 486(2):305–312.

Kohda, K., W. Kakegawa, S. Matsuda, T. Yamamoto, H. Hirano, and M. Yuzaki
2013. The 2 glutamate receptor gates long-term depression by coordinating interactions between two AMPA receptor phosphorylation sites. *Proceedings of the National Academy of Sciences*, 110(10):E948–E957.

Kohler, M., H. C. Kornau, and P. H. Seeburg
1994. The organization of the gene for the functionally dominant alpha-amino- 3-hydroxy-5-methylisoxazole-4-propionic acid receptor subunit GluR-B. *Journal of Biological Chemistry*, 269(26):17367–17370.

Kolleker, A., J. J. Zhu, B. J. Schupp, Y. Qin, V. Mack, T. Borchardt, G. Köhr, R. Malinow, P. H. Seeburg, and P. Osten
2003. Glutamatergic plasticity by synaptic delivery of GluR-B long- containing AMPA receptors. *Neuron*, 40(6):1199–1212.

Kostylev, M., A. E. Otwell, R. E. Richardson, and Y. Suzuki
2015. Cloning should be simple: Escherichia coli DH5α-mediated assembly of multiple DNA fragments with short end homologies. *PLoS ONE*, 10(9):1–15.

Krantz Lab and University of California; Berkley
2002. Oligo Calculator.

Krieger, J., I. Bahar, and I. H. Greger
2015. Structure, Dynamics, and Allosteric Potential of Ionotropic Glutamate Receptor N-Terminal Domains. *Biophysical Journal*, 109(6):1136–1148.

Kristensen, A. S., M. A. Jenkins, T. G. Banke, A. Schousboe, Y. Makino, R. C. Johnson, R. Huganir, and S. F. Traynelis
2011. Mechanism of Ca2+/calmodulin-dependent kinase II regulation of AMPA receptor gating. *Nature Neuroscience*, 14(6):727–735.

Kuner, T., C. Beck, B. Sakmann, and P. H. Seeburg
2001. Channel-lining residues of the AMPA receptor M2 segment: structural environment of the Q/R site and identification of the selectivity filter. *The Journal of neuroscience*, 21(12):4162–4172.

Lai, D., X. Zhu, and S. Pestka
1993. A simple and efficient method for site-directed mutagenesis with double-stranded plasmid DNA. *Nucleic Acids Research*, 21(17):3977–3980.

Lee, H. K., K. Takamiya, J. S. Han, H. Man, C. H. Kim, G. Rumbaugh, S. Yu, L. Ding, C. He, R. S. Petralia, R. J. Wenthold, M. Gallagher, and R. L. Huganir
2003. Phosphorylation of the AMPA receptor GluR1 subunit is required for synaptic plasticity and retention of spatial memory. *Cell*, 112(5):631–643.

Lee, H.-K., K. Takamiya, K. He, L. Song, and R. L. Huganir
2010. Specific Roles of AMPA Receptor Subunit GluR1 (GluA1) Phosphorylation Sites in Regulating Synaptic Plasticity in the CA1 Region of Hippocampus. *Journal of Neurophysiology*, 103(1):479–489.

Lee, S. H., C. Jin, E. Cai, P. Ge, Y. Ishitsuka, K. W. Teng, A. A. De Thomaz, D. Nall, M. Baday, O. Jeyifous, D. Demonte, C. M. Dundas, S. Park, J. Y. Delgado, W. N. Green, and P. R. Selvin
2017. Super-resolution imaging of synaptic and extra-synaptic AMPA receptors with Different-Sized fluorescent probes. *eLife*, 6:e27744.

Lee, S. H., L. Liu, Y. T. Wang, and M. Sheng
2002. Clathrin adaptor AP2 and NSF interact with overlapping sites of GluR2 and play distinct roles in AMPA receptor trafficking and hippocampal LTD. *Neuron*, 36(4):661–74.

Lei, N., J. E. Mellem, P. J. Brockie, D. M. Madsen, and A. V. Maricq
2017. NRAP-1 Is a Presynaptically Released NMDA Receptor Auxiliary Protein that Modifies Synaptic Strength. *Neuron*, 96(6):1303–1316.e6.

Leonard, A. S., M. A. Davare, M. C. Horne, C. C. Garner, and J. W. Hell
1998. SAP97 is associated with the α-amino-3-hydroxy-5-methylisoxazole-4- propionic acid receptor GluR1 subunit. *Journal of Biological Chemistry*, 273(31):19518–19524.

Letts, V. A., R. Felix, G. H. Biddlecome, J. Arikkath, C. L. Mahaffey, A. Valenzuela, F. S. Bartlett, Y. Mori, K. P. Campbell, and W. N. Frankel
1998. The mouse stargazer gene encodes a neuronal Ca2+-channel γ subunit. *Nature Genetics*, 19(4):340–347.

Leuschner, W. D. and W. Hoch
1999. Subtype-specific assembly of α-amino-3-hydroxy-5-methyl-4-isoxazole propionic acid receptor subunits is mediated by their N-terminal domains. *Journal of Biological Chemistry*, 274(24):16907–16916.

Levy, J. M., X. Chen, T. S. Reese, and R. A. Nicoll
2015. Synaptic Consolidation Normalizes AMPAR Quantal Size following MAGUK Loss. *Neuron*, 87(3):534–48.

Li, C., A. Wen, B. Shen, J. Lu, Y. Huang, and Y. Chang
2011. FastCloning: A highly simplified, purification-free, sequence- and ligation-independent PCR cloning method. *BMC Biotechnology*, 11(1):92.

Li, M. Z. and S. J. Elledge
2007. Harnessing homologous recombination in vitro to generate recombinant DNA via SLIC. *Nature Methods*, 4(3):251–256.

Li, T. P., Y. Song, H. D. MacGillavry, T. A. Blanpied, and S. Raghavachari
2016. Protein Crowding within the Postsynaptic Density Can Impede the Escape of Membrane Proteins. *Journal of Neuroscience*, 36(15):4276–4295.

Liao, D., N. A. Hessler, and R. Malinow
1995. Activation of postsynaptically silent synapses during pairing-induced LTP in CA1 region of hippocampal slice. *Nature*, 375(6530):400–404.

Lim, I. A., M. A. Merrill, Y. Chen, and J. W. Hell
2003. Disruption of the NMDA receptor-PSD-95 interaction in hippocampal neurons with no obvious physiological short-term effect. *Neuropharmacology*, 45(6):738–754.

Lisman, J. and S. Raghavachari
2006. A unified model of the presynaptic and postsynaptic changes during LTP at CA1 synapses. *Science Signalling*, 2006(356):re11.

Lisman, J. E.
2009. The Pre/Post LTP Debate. *Neuron*, 63(3):281–284.

Lisman, J. E., S. Raghavachari, and R. W. Tsien
2007. The sequence of events that underlie quantal transmission at central glutamatergic synapses. *Nature Reviews Neuroscience*, 8(8):597–609.

Liu, G., S. Choi, and R. W. Tsien
1999. Variability of neurotransmitter concentration and nonsaturation of postsynaptic AMPA receptors at synapses in hippocampal cultures and slices. *Neuron*, 22(2):395–409.

Liu, S. J. and R. S. Zukin
2007. Ca2+-permeable AMPA receptors in synaptic plasticity and neuronal death. *Trends in Neurosciences*, 30(3):126–134.

Lomeli, H., J. Mosbacher, T. Melcher, T. Höger, R. P. Jörg, T. Kuner, H. Monyer, M. Higuchi, A. Bach, P. H. Seeburg, H. Lomeli, J. Mosbacher, T. Melcher, T. Hoger, J. R. P. Geiger, T. Kuner, H. Monyer, M. Higuchi, A. Bach, and P. H. Seeburgt
1994. Control of Kinetic Properties of AMPA Receptor Channels by Nuclear RNA Editing. *Science*, 266(5191):1709–1713.

Lovero, K. L., S. M. Blankenship, Y. Shi, and R. A. Nicoll
2013. SynDIG1 Promotes Excitatory Synaptogenesis Independent of AMPA Receptor Trafficking and Biophysical Regulation. *PLoS ONE*, 8(6):e66171.

Lovett, S. T., R. L. Hurley, V. A. Sutera, R. H. Aubuchon, and M. A. Lebedeva
2002. Crossing over between regions of limited homology in Escherichia coli: RecA-dependent and RecA-independent pathways. *Genetics*, 160(3):851–859.

Lu, Q.
2005. Seamless cloning and gene fusion. *Trends in Biotechnology*, 23(4):199–207.

Lu, W., Y. Shi, A. C. Jackson, K. Bjorgan, M. J. During, R. Sprengel, P. H. Seeburg, and R. A. Nicoll
2009. Subunit Composition of Synaptic AMPA Receptors Revealed by a Single-Cell Genetic Approach. *Neuron*, 62(2):254–268.

Lu, W. and E. B. Ziff
2005. PICK1 interacts with ABP/GRIP to regulate AMPA receptor trafficking. *Neuron*, 47(3):407–421.

Lučić, V., T. Yang, G. Schweikert, F. Förster, and W. Baumeister
2005. Morphological characterization of molecular complexes present in the synaptic cleft. *Structure*, 13(3):423–434.

Luo, F., X. Du, T. Weng, X. Wen, J. Huang, and L. Chen
2012. Efficient multi-site-directed mutagenesis directly from genomic template. *Journal of Biosciences*, 37(6):965–969.

Lüthi, A., R. Chittajallu, F. Duprat, M. J. Palmer, T. A. Benke, F. L. Kidd, J. M. Henley, J. T. Isaac, and G. L. Collingridge
1999. Hippocampal LTD expression involves a pool of AMPARs regulated by the NSF-GluR2 interaction. *Neuron*, 24(2):389–399.

MacGillavry, H. D., Y. Song, S. Raghavachari, and T. A. Blanpied
2013. Nanoscale scaffolding domains within the postsynaptic density concentrate synaptic ampa receptors. *Neuron*, 78(4):615–622.

Mack, V., N. Burnashev, K. M. Kaiser, A. Rozov, V. Jensen, Hvalby, P. H. Seeburg, B. Sakmann, and R. Sprengel
2001. Conditional restoration of hippocampal synaptic potentiation in GluR-A-deficient mice. *Science*, 292(5526):2501–2504.

Mahajan, S. S. and E. B. Ziff
2007. Novel toxicity of the unedited GluR2 AMPA receptor subunit dependent on surface trafficking and increased Ca2+-permeability. *Molecular and Cellular Neuroscience*, 35(3):470–481.

Mainen, Z. F., Z. Jia, J. Roder, and R. Malinow
1998. Use-dependent AMPA receptor block in mice lacking GluR2 suggests postsynaptic site for LTP expression. *Nature Neuroscience*, 1(7):579–586.

Makino, H. and R. Malinow
2009. AMPA Receptor Incorporation into Synapses during LTP: The Role of Lateral Movement and Exocytosis. *Neuron*, 64(3):381–390.

Malinow, R., Z. F. Mainen, and Y. Hayashi
2000. LTP mechanisms: From silence to four-lane traffic. *Current Opinion in Neurobiology*, 10(3):352–357.

Mammen, A. L., K. Kameyama, K. W. Roche, and R. L. Huganir
1997. Phosphorylation of the α-amino-3-hydroxy-5-methylisoxazole-4-propionic Acid receptor GluR1 subunit by calcium/calmodulin-dependent kinase II. *Journal of Biological Chemistry*, 272(51):32528–32533.

Man, H.-Y., Y. Sekine-Aizawa, and R. L. Huganir
2007. Regulation of alpha-amino-3-hydroxy-5-methyl-4-isoxazolepropionic acid receptor trafficking through PKA phosphorylation of the Glu receptor 1 subunit. *Proceedings of the National Academy of Sciences*, 104(9):3579–3584.

Martenson, J. S. and S. Tomita
2015. Synaptic localization of neurotransmitter receptors: comparing mechanisms for AMPA and GABAA receptors. *Current Opinion in Pharmacology*, 20:102–108.

Martin, A., E. Toselli, M. françoise Rosier, C. Auffray, and M. dominique Devignes
1995. Rapid and high efficiency site-directed mutagenesis by improvement of the homologous recombination technique. *Nucleic Acids Research*, 23(9):1642–1643.

Mashruwala, A. A. and J. M. Boyd
2016. De novo assembly of plasmids using yeast recombinational cloning. *Methods in Molecular Biology*, 1373:33–41.

Matsuda, K., T. Budisantoso, N. Mitakidis, Y. Sugaya, E. Miura, W. Kakegawa, M. Yamasaki, K. Konno, M. Uchigashima, M. Abe, I. Watanabe, M. Kano, M. Watanabe, K. Sakimura,

A. R. Aricescu, and M. Yuzaki
2016. Transsynaptic Modulation of Kainate Receptor Functions by C1q-like Proteins. *Neuron*, 90(4):752–767.

Matsuda, K., E. Miura, T. Miyazaki, W. Kakegawa, K. Emi, S. Narumi, Y. Fukazawa, A. Itolshida, T. Kondo, R. Shigemoto, M. Watanabe, and M. Yuzaki
2010. Cbln1 is a ligand for an orphan glutamate receptor $\delta 2$, a bidirectional synapse organizer. *Science*, 328(5976):363–368.

Matsuda, S., T. Launey, S. Mikawa, and H. Hirai
2000. Disruption of AMPA receptor GluR2 clusters following long-term depression induction in cerebellar Purkinje neurons. *The EMBO journal*, 19(12):2765–74.

Matsuda, S., S. Mikawa, and H. Hirai
1999. Phosphorylation of serine-880 in GluR2 by protein kinase C prevents its C terminus from binding with glutamate receptor-interacting protein. *Journal of neurochemistry*, 73(4):1765–8.

Matsuzaki, M., G. C. R. Ellis-Davies, T. Nemoto, Y. Miyashita, M. Iino, and H. Kasai
2001. Dendritic spine geometry is critical for AMPA receptor expression in hippocampal CA1 pyramidal neurons. *Nature Neuroscience*, 4(11):1086–1092.

Matsuzaki, M., N. Honkura, G. C. Ellis-Davies, and H. Kasai
2004. Structural basis of long-term potentiation in single dendritic spines. *Nature*, 429(6993):761–766.

Matt, L., L. M. Kirk, G. Chenaux, D. J. Speca, K. R. Puhger, M. C. Pride, M. Qneibi, T. Haham, K. E. Plambeck, Y. Stern-Bach, J. L. Silverman, J. N. Crawley, J. W. Hell, and E. Díaz
2018. SynDIG4/Prrt1 Is Required for Excitatory Synapse Development and Plasticity Underlying Cognitive Function. *Cell Reports*, 22(9):2246–2253.

Mattison, H. A., A. A. Bagal, M. Mohammadi, N. S. Pulimood, C. G. Reich, B. E. Alger, J. P. Y. Kao, and S. M. Thompson
2014. Evidence of calcium-permeable AMPA receptors in dendritic spines of CA1 pyramidal neurons. *Journal of Neurophysiology*, 112(2):263–275.

Mayer, M. L.
2006. Glutamate receptors at atomic resolution. *Nature*, 440(7083):456–462.

Mayer, M. L., G. L. Westbrook, and P. B. Guthrie
1984. Voltage-dependent block by Mg2+of NMDA responses in spinal cord neurones. *Nature*, 309(5965):261–263.

Mayford, M., S. A. Siegelbaum, E. R. Kandel, N. R.-d. Long-term, C. Lüscher, R. C. Malenka, K. M. Harris, R. J. Weinberg, T. G. Smart, P. Paoletti, and C. Südhof
2012. Synapses and Memory Storage. *Cold Spring Harbor perspectives in biology*, 4(6):1–18.

McAllister, K. A. and C. F. Stevens
2000. Nonsaturation of AMPA and NMDA receptors at hippocampal synapses. *Proceedings of the National Academy of Sciences*, 97(11):6173–6178.

Mccullum, E. O., B. a. R. Williams, J. Zhang, and J. C. Chaput
2002. In Vitro Mutagenesis Protocols. *Methods in Molecular Biology*, 634(3):103–109.

McInerney, P., P. Adams, and M. Z. Hadi
2014. Error Rate Comparison during Polymerase Chain Reaction by DNA Polymerase. *Molecular Biology International*, 2014:1–8.

Medvedev, N. I., J. J. Rodríguez-Arellano, V. I. Popov, H. A. Davies, C. M. Tigaret, R. Schoepfer, and M. G. Stewart
2008. The glutamate receptor 2 subunit controls post-synaptic density complexity and spine shape in the dentate gyrus. *European Journal of Neuroscience*, 27(2):315–325.

Menuz, K., G. A. Kerchner, J. L. O'Brien, and R. A. Nicoll
2009. Critical role for TARPs in early development despite broad functional redundancy. *Neuropharmacology*, 56(1):22–29.

Menuz, K., J. L. O'Brien, S. Karmizadegan, D. S. Bredt, and R. A. Nicoll
2008. TARP Redundancy Is Critical for Maintaining AMPA Receptor Function. *Journal of Neuroscience*, 28(35):8740–8746.

Meyerson, J. R., S. Chittori, A. Merk, P. Rao, T. H. Han, M. Serpe, M. L. Mayer, and S. Subramaniam
2016. Structural basis of kainate subtype glutamate receptor desensitization. *Nature*, 537(7621):567–571.

Meyerson, J. R., J. Kumar, S. Chittori, P. Rao, J. Pierson, A. Bartesaghi, M. L. Mayer, and S. Subramaniam
2014. Structural mechanism of glutamate receptor activation and desensitization. *Nature*, 514(7522):328–334.

Mi, R., X. Tang, R. Sutter, D. Xu, P. Worley, and R. J. O'Brien
2002. Differing Mechanisms for Glutamate Receptor Aggregation on Dendritic Spines and Shafts in Cultured Hippocampal Neurons. *J. Neurosci.*, 22(17):7606–7616.

Miesenböck, G., D. A. De Angelis, and J. E. Rothman
1998. Visualizing secretion and synaptic transmission with pH-sensitive green fluorescent proteins. *Nature*, 394(6689):192–195.

Migaud, M., P. Charlesworth, M. Dempster, L. C. Webster, A. M. Watabe, M. Makhinson, Y. He, M. F. Ramsay, R. G. Morris, J. H. Morrison, T. J. O'Dell, and S. G. Grant
1998. Enhanced long-term potentiation and impaired learning in mice with mutant postsynaptic density-95 protein. *Nature*, 396(6710):433–439.

Milstein, A. D. and R. A. Nicoll
2009. TARP modulation of synaptic AMPA receptor trafficking and gating depends on multiple intracellular domains. *Proceedings of the National Academy of Sciences*, 106(27):11348–11351.

Milstein, A. D., W. Zhou, S. Karimzadegan, D. S. Bredt, and R. A. Nicoll
2007. TARP Subtypes Differentially and Dose-Dependently Control Synaptic AMPA Receptor Gating. *Neuron*, 55(6):905–918.

Mishina, M., K. Sakimura, H. Mori, E. Kushiya, M. Harabayashi, S. Uchino, and K. Nagahari
1991. A single amino acid residue determines the Ca2+permeability of AMPA-selective glutamate receptor channels. *Biochemical and Biophysical Research Communications*, 180(2):813–821.

Mitchell, L. A., Y. Cai, M. Taylor, A. M. Noronha, J. Chuang, L. Dai, and J. D. Boeke
2013. Multichange isothermal mutagenesis: A new strategy for multiple site-directed mutations in plasmid DNA. *ACS Synthetic Biology*, 2(8):473–477.

Molnár, E.
2013. Are Neto1 and APP auxiliary subunits of NMDA receptors? *Journal of Neurochemistry*, 126(5):551–553.

Monaco, A. P. and Z. Larin
1994. YACs, BACs, PACs and MACs: Artificial chromosomes as research tools. *Trends in Biotechnology*, 12(7):280–286.

Monaghan, D. T. and D. E. Jane
2009. *Pharmacology of NMDA Receptors*. CRC Press/Taylor & Francis.

Monteiro, P. and G. Feng
2017. SHANK proteins: Roles at the synapse and in autism spectrum disorder. *Nature Reviews Neuroscience*, 18(3):147–157.

Morimoto-Tomita, M., W. Zhang, C. Straub, C. H. Cho, K. S. Kim, J. R. Howe, and S. Tomita
2009. Autoinactivation of Neuronal AMPA Receptors via Glutamate-Regulated TARP Interaction. *Neuron*, 61(1):101–112.

Motohashi, K.
2015. A simple and efficient seamless DNA cloning method using SLiCE from Escherichia coli laboratory strains and its application to SLiP site-directed mutagenesis. *BMC Biotechnology*, 15(1):47.

Möykkynen, T., S. K. Coleman, A. Semenov, and K. Keinänen
2014. The N-terminal Domain Modulates α-Amino-3-hydroxy-5-methyl-4-isoxazolepropionic acid (AMPA) Receptor Desensitization. *Journal of Biological Chemistry*, 289(19):13197–13205.

Muller, D., M. Joly, and G. Lynch
1988. Contributions of quisqualate and NMDA receptors to the induction and expression of LTP. *Science*, 242(4886):1694–7.

Muller, D. and G. Lynch
1989. Evidence that changes in presynaptic calcium currents are not responsible for long-term potentiation in hippocampus. *Brain Research*, 479(2):290–299.

Murphy, K. C. and M. G. Marinus
2010. RecA-independent single-stranded DNA oligonucleotide-mediated mutagenesis. *F1000 Biology Reports*, 2:56.

Nabavi, S., R. Fox, S. Alfonso, J. Aow, and R. Malinow
2013. GluA1 trafficking and metabotropic NMDA: addressing results from other laboratories inconsistent with ours. *Philosophical Transactions of the Royal Society B: Biological Sciences*, 369(1633):20130145–20130145.

Nabavi, S., R. Fox, C. D. Proulx, J. Y. Lin, R. Y. Tsien, and R. Malinow
2014. Engineering a memory with LTD and LTP. *Nature*, 511(7509):348–352.

Nair, D., E. Hosy, J. D. Petersen, A. Constals, G. Giannone, D. Choquet, and J.-B. Sibarita
2013. Super-Resolution Imaging Reveals That AMPA Receptors Inside Synapses Are Dynamically Organized in Nanodomains Regulated by PSD95. *Journal of Neuroscience*, 33(32):13204–13224.

Nakagawa, T., Y. Cheng, E. Ramm, M. Sheng, and T. Walz
2005. Structure and different conformational states of native AMPA receptor complexes. *Nature*, 433(7025):545–549.

Nakano, Y. J. and H. K. Kuramitsu
1992. Mechanism of Streptococcus mutans glucosyltransferases: Hybrid-enzyme analysis. *Journal of Bacteriology*, 174(17):5639–5646.

Ng, D., G. M. Pitcher, R. K. Szilard, A. Sertié, M. Kanisek, S. J. Clapcote, T. Lipina, L. V. Kalia, D. Joo, C. McKerlie, M. Cortez, J. C. Roder, M. W. Salter, and R. R. McInnes
2009. Neto1 is a novel CUB-domain NMDA receptor-interacting protein required for synaptic plasticity and learning. *PLoS Biology*, 7(2):0278–0300.

Nicoll, R. A.
2017. A Brief History of Long-Term Potentiation. *Neuron*, 93(2):281–290.

Nicoll, R. A. and R. C. Malenka
1995. Contrasting properties of two forms of long-term potentiation in the hippocampus. *Nature*, 377(6545):115–118.

Nicoll, R. A., S. Tomita, and D. S. Bredt
2006. Auxiliary subunits assist AMPA-type glutamate receptors. *Science*, 311(5765):1253–1256.

Nishikura, K.
2016. A-to-I editing of coding and non-coding RNAs by ADARs. *Nature Reviews Molecular Cell Biology*, 17(2):83–96.

Nishimune, A., J. T. Isaac, E. Molnar, J. Noel, S. R. Nash, M. Tagaya, G. L. Collingridge, S. Nakanishi, and J. M. Henley
1998. NSF binding to GluR2 regulates synaptic transmission. *Neuron*, 21(1):87–97.

Niswender, C. M. and P. J. Conn
2010. Metabotropic Glutamate Receptors: Physiology, Pharmacology, and Disease. *Annual Review of Pharmacology and Toxicology*, 50(1):295–322.

Noel, J., G. S. Ralph, L. Pickard, J. Williams, E. Molnar, J. B. Uney, G. L. Collingridge, and J. M. Henley
1999. Surface expression of AMPA receptors in hippocampal neurons is regulated by an NSF-dependent mechanism. *Neuron*, 23(2):365–376.

Nowak, L., P. Bregestovski, P. Ascher, A. Herbet, and A. Prochiantz
1984. Magnesium gates glutamate-activated channels in mouse central neurones. *Nature*, 307(5950):462–465.

O'Brien, R., D. Xu, R. Mi, X. Tang, C. Hopf, and P. Worley
2002. Synaptically targeted narp plays an essential role in the aggregation of AMPA receptors at excitatory synapses in cultured spinal neurons. *The Journal of neuroscience*, 22(11):4487–4498.

O'Brien, R. J., X. Desheng, R. S. Petralia, O. Steward, R. L. Huganir, and P. Worley
1999. Synaptic clustering of AMPA receptors by the extracellular immediate- early gene product Narp. *Neuron*, 23(2):309–323.

Oh, M. C., V. A. Derkach, E. S. Guire, and T. R. Soderling
2006. Extrasynaptic membrane trafficking regulated by GluR1 serine 845 phosphorylation primes AMPA receptors for long-term potentiation. *Journal of Biological Chemistry*, 281(2):752–758.

Oliner, J. D., K. W. Kinzler, and B. Vogelstein
1993. In vivo cloning of PCR products in E.coli. *Nucleic Acids Research*, 21(22):5192–5197.

Olsen, D. B. and F. Eckstein
1989. Incomplete primer extension during in vitro DNA amplification catalyzed by Taq polymerase; exploitation for DNA sequencing. *Nucleic Acids Research*, 17(23):9613–9620.

Opazo, P. and D. Choquet
2011. A three-step model for the synaptic recruitment of AMPA receptors. *Molecular and Cellular Neuroscience*, 46(1):1–8.

Opazo, P., S. Labrecque, C. M. Tigaret, A. Frouin, P. W. Wiseman, P. De Koninck, and D. Choquet
2010. CaMKII triggers the diffusional trapping of surface AMPARs through phosphorylation of stargazin. *Neuron*, 67(2):239–252.

Opazo, P., M. Sainlos, and D. Choquet
2012. Regulation of AMPA receptor surface diffusion by PSD-95 slots. *Current Opinion in Neurobiology*, 22(3):453–460.

Orth, A., D. Tapken, and M. Hollmann
2013. The delta subfamily of glutamate receptors: Characterization of receptor chimeras and mutants. *European Journal of Neuroscience*, 37(10):1620–1630.

Osten, P., L. Khatri, J. L. Perez, G. Köhr, G. Giese, C. Daly, T. W. Schulz, A. Wensky, L. M. Lee, and E. B. Ziff
2000. Mutagenesis reveals a role for ABP/GRIP binding to GluR2 in synaptic surface accumulation of the AMPA receptor. *Neuron*, 27(2):313–325.

Osten, P., S. Srivastava, G. J. Inman, F. S. Vilim, L. Khatri, L. M. Lee, B. A. States, S. Einheber, T. A. Milner, P. I. Hanson, and E. B. Ziff
1998. The AMPA receptor GluR2 C terminus can mediate a reversible, ATP- dependent interaction with NSF and α- and β-SNAPs. *Neuron*, 21(1):99–110.

Otmakhov, N., L. Khibnik, N. Otmakhova, S. Carpenter, S. Riahi, B. Asrican, and J. Lisman
2004. Forskolin-Induced LTP in the CA1 Hippocampal Region Is NMDA Receptor Dependent. *Journal of Neurophysiology*, 91(5):1955–1962.

Otmakhova, N. A., N. Otmakhov, L. H. Mortenson, and J. E. Lisman
2000. Inhibition of the cAMP pathway decreases early long-term potentiation at CA1 hippocampal synapses. *The Journal of neuroscience*, 20(12):4446–51.

Padamsey, Z. and N. Emptage
2013. Two sides to long-term potentiation: a view towards reconciliation. *Philosophical Transactions of the Royal Society B: Biological Sciences*, 369(1633):20130154–20130154.

Pandya, N. J., F. Koopmans, J. A. Slotman, I. Paliukhovich, A. B. Houtsmuller, A. B. Smit, and K. W. Li
2017. Correlation profiling of brain sub-cellular proteomes reveals co-assembly of synaptic proteins and subcellular distribution. *Scientific Reports*, 7(1):12107.

Panicker, S., K. Brown, and R. A. Nicoll
2008. Synaptic AMPA receptor subunit trafficking is independent of the C terminus in the GluR2-lacking mouse. *Proceedings of the National Academy of Sciences*, 105(3):1032–1037.

Paoletti, P., C. Bellone, and Q. Zhou
2013. NMDA receptor subunit diversity: impact on receptor properties, synaptic plasticity and disease. *Nature Reviews Neuroscience*, 14(6):383–400.

Park, J., A. E. Chávez, Y. S. Mineur, M. Morimoto-Tomita, S. Lutzu, K. S. Kim, M. R. Picciotto, P. E. Castillo, and S. Tomita
2016a. CaMKII Phosphorylation of TARPγ-8 Is a Mediator of LTP and Learning and Memory. *Neuron*, 92(1):75–83.

Park, P., T. M. Sanderson, M. Amici, S.-L. Choi, Z. A. Bortolotto, M. Zhuo, B.-K. Kaang, and G. L. Collingridge
2016b. Calcium-Permeable AMPA Receptors Mediate the Induction of the Protein Kinase A-Dependent Component of Long-Term Potentiation in the Hippocampus. *Journal of Neuroscience*, 36(2):622–631.

Parrish, J. R., T. Limjindaporn, J. A. Hines, J. Liu, G. Liu, and R. L. Finley
2004. High-throughput cloning of Campylobacter jejuni ORFs by in vivo recombination in Escherichia coli. *Journal of Proteome Research*, 3(3):582–586.

Pasieka, T. J., L. Maresova, and C. Grose
2003. A functional YNKI motif in the short cytoplasmic tail of varicella-zoster virus glycoprotein gH mediates clathrin-dependent and antibody-independent endocytosis. *Journal of virology*, 77(7):4191–4204.

Passafaro, M., T. Nakagawa, C. Sala, and M. Sheng
2003. Induction of dendritic spines by an extracellular domain of AMPA receptor subunit GluR2. *Nature*, 424(6949):677–681.

Passafaro, M., V. Piãch, and M. Sheng
2001. Subunit-specific temporal and spatial patterns of AMPA receptor exocytosis in hippocampal neurons. *Nature Neuroscience*, 4(9):917–926.

Pasternack, A., S. K. Coleman, A. Jouppila, D. G. Mottershead, M. Lindfors, M. Pasternack, and K. Keinänen
2002. α-amino-3-hydroxy-5-methyl-4-isoxazolepropionic acid (AMPA) receptor channels lacking the N-terminal domain. *Journal of Biological Chemistry*, 277(51):49662–49667.

Peijnenburg, A. A., S. Bron, and G. Venema
1987. Structural plasmid instability in recombination- and repair-deficient strains of Bacillus subtilis. *Plasmid*, 17(2):167–170.

Pelkey, K. A., E. Barksdale, M. T. Craig, X. Yuan, M. Sukumaran, G. A. Vargish, R. M. Mitchell, M. S. Wyeth, R. S. Petralia, R. Chittajallu, R. M. Karlsson, H. A. Cameron, Y. Murata, M. T. Colonnese, P. F. Worley, and C. J. McBain
2015. Pentraxins coordinate excitatory synapse maturation and circuit integration of parvalbumin interneurons. *Neuron*, 85(6):1257–1272.

Pellegrini-Giampietro, D. E., J. A. Gorter, M. V. Bennett, and R. S. Zukin
1997. The GluR2 (GluR-B) hypothesis: Ca2+-permeable AMPA receptors in neurological disorders. *Trends in Neurosciences*, 20(10):464–470.

Penn, A. C., A. Balik, C. Wozny, O. Cais, and I. H. Greger
2012. Activity-Mediated AMPA Receptor Remodeling, Driven by Alternative Splicing in the Ligand-Binding Domain. *Neuron*, 76(3):503–510.

Penn, A. C., C. L. Zhang, F. Georges, L. Royer, C. Breillat, E. Hosy, J. D. Petersen, Y. Humeau, and D. Choquet
2017. Hippocampal LTP and contextual learning require surface diffusion of AMPA receptors. *Nature*, 549(7672):384–388.

Perez de Arce, K., N. Schrod, S. W. Metzbower, E. Allgeyer, G. K. Kong, A. H. Tang, A. J. Krupp, V. Stein, X. Liu, J. Bewersdorf, T. A. Blanpied, V. Lucić, and T. Biederer
2015. Topographic Mapping of the Synaptic Cleft into Adhesive Nanodomains. *Neuron*, 88(6):1165–1172.

Pernía-Andrade, A., S. Goswami, Y. Stickler, U. Fröbe, A. Schlögl, and P. Jonas
2012. A Deconvolution-Based Method with High Sensitivity and Temporal Resolution for Detection of Spontaneous Synaptic Currents In Vitro and In Vivo. *Biophysical Journal*, 103(7):1429–1439.

Pinheiro, P. and C. Mulle
2006. Kainate receptors. *Cell and Tissue Research*, 326(2):457–482.

Plant, K., K. A. Pelkey, Z. A. Bortolotto, D. Morita, A. Terashima, C. J. McBain, G. L. Collingridge, and J. T. Isaac
2006. Transient incorporation of native GluR2-lacking AMPA receptors during hippocampal long-term potentiation. *Nature Neuroscience*, 9(5):602–604.

Priel, A., A. Kolleker, G. Ayalon, M. Gillor, P. Osten, and Y. Stern-Bach
2005. Stargazin Reduces Desensitization and Slows Deactivation of the AMPA-Type Glutamate Receptors. *Journal of Neuroscience*, 25(10):2682–2686.

Prybylowski, K., K. Chang, N. Sans, L. Kan, S. Vicini, and R. J. Wenthold
2005. The synaptic localization of NR2B-containing NMDA receptors is controlled by interactions with PDZ proteins and AP-2. *Neuron*, 47(6):845–857.

Raghavachari, S. and J. E. Lisman
2004. Properties of Quantal Transmission at CA1 Synapses. *Journal of Neurophysiology*, 92(4):2456–2467.

Rathenberg, J., T. Nevian, and V. Witzemann
2003. High-efficiency transfection of individual neurons using modified electrophysiology techniques. *Journal of Neuroscience Methods*, 126(1):91–98.

Rebola, N., M. Carta, and C. Mulle
2017. Operation and plasticity of hippocampal CA3 circuits: Implications for memory encoding. *Nature Reviews Neuroscience*, 18(4):209–221.

Ripley, B., S. Otto, K. Tiglio, M. E. Williams, and A. Ghosh
2011. Regulation of synaptic stability by AMPA receptor reverse signaling. *Proceedings of the National Academy of Sciences*, 108(1):367–372.

Riva, I., C. Eibl, R. Volkmer, A. L. Carbone, and A. J. Plested
2017. Control of AMPA receptor activity by the extracellular loops of auxiliary proteins. *eLife*, 6:e28680.

Robinson, H. P., Y. Sahara, and N. Kawai
1991. Nonstationary fluctuation analysis and direct resolution of single channel currents at postsynaptic sites. *Biophysical Journal*, 59(2):295–304.

Roche, K. W., R. J. O'Brien, A. L. Mammen, J. Bernhardt, and R. L. Huganir
1996. Characterization of multiple phosphorylation sites on the AMPA receptor GluR1 subunit. *Neuron*, 16(6):1179–1188.

Rossmann, M., M. Sukumaran, A. C. Penn, D. B. Veprintsev, M. M. Babu, and I. H. Greger
2011. Subunit-selective N-terminal domain associations organize the formation of AMPA receptor heteromers. *EMBO Journal*, 30(5):959–971.

Rothman, J. E., S. S. Krishnakumar, K. Grushin, and F. Pincet
2017. Hypothesis - buttressed rings assemble, clamp, and release SNAREpins for synaptic transmission. *FEBS Letters*, 591(21):3459–3480.

Rouach, N., K. Byrd, R. S. Petralia, G. M. Elias, H. Adesnik, S. Tomita, S. Karimzadegan, C. Kealey, D. S. Bredt, and R. A. Nicoll
2005. TARP γ-8 controls hippocampal AMPA receptor number, distribution and synaptic plasticity. *Nature Neuroscience*, 8(11):1525–1533.

Rozov, A., R. Sprengel, and P. H. Seeburg
2012. GluA2-lacking AMPA receptors in hippocampal CA1 cell synapses: evidence from gene-targeted mice. *Frontiers in Molecular Neuroscience*, 5:22.

Rubio, M. E., Y. Fukazawa, N. Kamasawa, C. Clarkson, E. Molnár, and R. Shigemoto
2014. Target- and input-dependent organization of AMPA and NMDA receptors in synaptic connections of the cochlear nucleus. *Journal of Comparative Neurology*, 522(18):4023–4042.

Rumbaugh, G., J. P. Adams, J. H. Kim, and R. L. Huganir
2006. SynGAP regulates synaptic strength and mitogen-activated protein kinases in cultured neurons. *Proceedings of the National Academy of Sciences*, 103(12):4344–4351.

Sabzghabaee, A., F. Moazen, Z. Mousavian, and H. M. Sadeghi
2014. Polymerase chain reaction amplification of a GC rich region by adding 1,2 propanediol. *Advanced Biomedical Research*, 3(1):65.

Saglietti, L., C. Dequidt, K. Kamieniarz, M. C. Rousset, P. Valnegri, O. Thoumine, F. Beretta, L. Fagni, D. Choquet, C. Sala, M. Sheng, and M. Passafaro
2007. Extracellular Interactions between GluR2 and N-Cadherin in Spine Regulation. *Neuron*, 54(3):461–477.

Sainlos, M., C. Tigaret, C. Poujol, N. B. Olivier, L. Bard, C. Breillat, K. Thiolon, D. Choquet, and B. Imperiali
2011. Biomimetic divalent ligands for the acute disruption of synaptic AMPAR stabilization. *Nature chemical biology*, 7(2):81–91.

Saksela, K. and P. Permi
2012. SH3 domain ligand binding: What's the consensus and where's the specificity? *FEBS Letters*, 586(17):2609–2614.

Sanderson, J. L., J. A. Gorski, and M. L. Dell'Acqua
2016. NMDA Receptor-Dependent LTD Requires Transient Synaptic Incorporation of Ca2+-Permeable AMPARs Mediated by AKAP150-Anchored PKA and Calcineurin. *Neuron*, 89(5):1000–1015.

Sans, N., C. Racca, R. S. Petralia, Y. X. Wang, J. McCallum, and R. J. Wenthold
2001. Synapse-associated protein 97 selectively associates with a subset of AMPA receptors early in their biosynthetic pathway. *The Journal of neuroscience*, 21(19):7506–7516.

Sans, N., B. Vissel, R. R. S. Petralia, Y.-X. Wang, K. Chang, G. A. Royle, C.-Y. Wang, S. O'Gorman, S. F. Heinemann, and R. J. Wenthold
2003. Aberrant formation of glutamate receptor complexes in hippocampal neurons of mice lacking the GluR2 AMPA receptor subunit. *The Journal of neuroscience*, 23(28):9367–9373.

Sawano, A. and A. Miyawaki
2000. Directed evolution of green fluorescent protein by a new versatile PCR strategy for site-directed and semi-random mutagenesis. *Nucleic Acids Research*, 28(16):78e–78.

Schlüter, O. M., W. Xu, and R. C. Malenka
2006. Alternative N-terminal domains of PSD-95 and SAP97 govern activity-dependent regulation of synaptic AMPA receptor function. *Neuron*, 51(1):99–111.

Schmid, S. M., S. Kott, C. Sager, T. Huelsken, and M. Hollmann
2009. The glutamate receptor subunit delta2 is capable of gating its intrinsic ion channel as revealed by ligand binding domain transplantation. *Proceedings of the National Academy of Sciences*, 106(25):10320–10325.

Schmitt, W. B., R. Sprengel, V. Mack, R. W. Draft, P. H. Seeburg, R. M. Deacon, J. N. Rawlins, and D. M. Bannerman
2005. Restoration of spatial working memory by genetic rescue of GluR-A - Deficient mice. *Nature Neuroscience*, 8(3):270–272.

Schmitz, L. J., R. V. Klaassen, M. Ruiperez-Alonso, A. E. Zamri, J. Stroeder, P. Rao-Ruiz, J. C. Lodder, R. J. van der Loo, H. D. Mansvelder, A. B. Smit, and S. Spijker
2017. The AMPA receptor-associated protein Shisa7 regulates hippocampal synaptic function and contextual memory. *eLife*, 6:e24192.

Schneider, C. A., W. S. Rasband, and K. W. Eliceiri
2012. NIH Image to ImageJ: 25 years of image analysis. *Nature Methods*, 9(7):671–675.

Schnell, E., M. Sizemore, S. Karimzadegan, L. Chen, D. S. Bredt, and R. A. Nicoll
2002. Direct interactions between PSD-95 and stargazin control synaptic AMPA receptor number. *Proceedings of the National Academy of Sciences*, 99(21):13902–13907.

Schulga, A. A., L. V. Levichkin, F. T. Kurbanov, A. L. Lokorokov, G. E. Pozmogova, and M. P. Kirpichnikov
1994. An approach to construction of hybrid polypeptide molecules - homologue recombination method. *Nucleic Acids Research*, 22(18):3808–3810.

Schwenk, J., D. Baehrens, A. Haupt, W. Bildl, S. Boudkkazi, J. Roeper, B. Fakler, and U. Schulte
2014. Regional diversity and developmental dynamics of the AMPA-receptor proteome in the mammalian brain. *Neuron*, 84(1):41–54.

Schwenk, J., N. Harmel, A. Brechet, G. Zolles, H. Berkefeld, C. S. Müller, W. Bildl, D. Baehrens, B. Hüber, A. Kulik, N. Klöcker, U. Schulte, and B. Fakler
2012. High-Resolution Proteomics Unravel Architecture and Molecular Diversity of Native AMPA Receptor Complexes. *Neuron*, 74(4):621–633.

Schwenk, J., N. Harmel, G. Zolles, W. Bildl, A. Kulik, B. Heimrich, O. Chisaka, P. Jonas, U. Schulte, B. Fakler, and N. Klöcker
2009. Functional proteomics identify cornichon proteins as auxiliary subunits of AMPA receptors. *Science*, 323(5919):1313–1319.

Seidenman, K. J., J. P. Steinberg, R. Huganir, and R. Malinow
2003. Glutamate receptor subunit 2 Serine 880 phosphorylation modulates synaptic transmission and mediates plasticity in CA1 pyramidal cells. *The Journal of neuroscience*, 23(27):9220–9228.

Semenov, A., T. Möykkynen, S. K. Coleman, E. R. Korpi, and K. Keinänen
2012. Autoinactivation of the stargazin-AMPA receptor complex: subunit-dependency and independence from physical dissociation. *PloS one*, 7(11):e49282.

Shanks, N. F., T. Maruo, A. N. Farina, M. H. Ellisman, and T. Nakagawa
2010. Contribution of the Global Subunit Structure and Stargazin on the Maturation of AMPA Receptors. *Journal of Neuroscience*, 30(7):2728–2740.

Shanks, N. F., J. N. Savas, T. Maruo, O. Cais, A. Hirao, S. Oe, A. Ghosh, Y. Noda, I. H. Greger, J. R. Yates, and T. Nakagawa
2012. Differences in AMPA and Kainate Receptor Interactomes Facilitate Identification of AMPA Receptor Auxiliary Subunit GSG1L. *Cell Reports*, 1(6):590–598.

Shen, L., F. Liang, L. D. Walensky, and R. L. Huganir
2000. Regulation of AMPA receptor GluR1 subunit surface expression by a 4. 1N-linked actin cytoskeletal association. *The Journal of neuroscience*, 20(21):7932–7940.

Shepherd, J. D. and R. L. Huganir
2007. The Cell Biology of Synaptic Plasticity: AMPA Receptor Trafficking. *Annual Review of Cell and Developmental Biology*, 23(1):613–643.

Shetty, R. P., D. Endy, and T. F. Knight
2008. Engineering BioBrick vectors from BioBrick parts. *Journal of Biological Engineering*, 2:5.

Shi, S. H., Y. Hayashi, J. A. Esteban, and R. Malinow
2001. Subunit-specific rules governing AMPA receptor trafficking to synapses in hippocampal pyramidal neurons. *Cell*, 105(3):331–343.

Shi, S.-H., Y. Hayashi, R. S. Petralia, S. H. Zaman, R. J. Wenthold, K. Svoboda, and R. Malinow
1999. Rapid Spine Delivery and Redistribution of AMPA Receptors After Synaptic NMDA Receptor Activation. *Science*, 284(5421):1811–1816.

Shi, Y., W. Lu, A. D. Milstein, and R. A. Nicoll
2009. The Stoichiometry of AMPA Receptors and TARPs Varies by Neuronal Cell Type. *Neuron*, 62(5):633–640.

Sia, G. M., J. C. Béïque, G. Rumbaugh, R. Cho, P. F. Worley, and R. L. Huganir
2007. Interaction of the N-Terminal Domain of the AMPA Receptor GluR4 Subunit with the Neuronal Pentraxin NP1 Mediates GluR4 Synaptic Recruitment. *Neuron*, 55(1):87–102.

Silva, A. J., C. F. Stevens, and S. Tonegawa
1992. Deficient hippocampal long-term potentiation in α-calcium- calmodulin kinase II mutant mice. *Science*, 257(July):201–206.

Sleight, S. C., B. A. Bartley, J. A. Lieviant, and H. M. Sauro
2010. In-Fusion BioBrick assembly and re-engineering. *Nucleic acids research*, 38(8):2624–36.

Smith, T. C. and J. R. Howe
2000. Concentration-dependent substate behavior of native AMPA receptors. *Nature neuroscience*, 3(10):992–997.

Sobolevsky, A. I., M. P. Rosconi, and E. Gouaux
2009. X-ray structure, symmetry and mechanism of an AMPA-subtype glutamate receptor. *Nature*, 462(7274):745–756.

Soler-Llavina, G. J., P. Arstikaitis, W. Morishita, M. Ahmad, C. Südhof, R. C. Malenka, and T. C. Südhof
2013. Leucine-Rich Repeat Transmembrane Proteins Are Essential for Maintenance of Long-Term Potentiation. *Neuron*, 79(3):439–46.

Soler-Llavina, G. J., M. V. Fuccillo, J. Ko, T. C. Sudhof, and R. C. Malenka
2011. The neurexin ligands, neuroligins and leucine-rich repeat transmembrane proteins, perform convergent and divergent synaptic functions in vivo. *Proceedings of the National Academy of Sciences*, 108(40):16502–16509.

Sommer, B., K. Keinanen, T. Verdoorn, W. Wisden, N. Burnashev, A. Herb, M. Kohler, T. Takagi, B. Sakmann, and P. Seeburg
1990. Flip and flop: a cell-specific functional switch in glutamate-operated channels of the CNS. *Science*, 249(4976):1580–1585.

Sommer, B., M. Köhler, R. Sprengel, and P. H. Seeburg
1991. RNA editing in brain controls a determinant of ion flow in glutamate-gated channels. *Cell*, 67(1):11–19.

Song, I., S. Kamboj, J. Xia, H. Dong, D. Liao, and R. L. Huganir
1998. Interaction of the N-ethylmaleimide-sensitive factor with AMPA receptors. *Neuron*, 21(2):393–400.

Soto, D., I. D. Coombs, L. Kelly, M. Farrant, and S. G. Cull-Candy
2007. Stargazin attenuates intracellular polyamine block of calcium-permeable AMPA receptors. *Nature Neuroscience*, 10(10):1260–1267.

Spruston, N.
2008. Pyramidal neurons: Dendritic structure and synaptic integration. *Nature Reviews Neuroscience*, 9(3):206–221.

Srivastava, S., P. Osten, F. S. Vilim, L. Khatri, G. Inman, B. States, C. Daly, S. DeSouza, R. Abagyan, J. G. Valtschanoff, R. J. Weinberg, and E. B. Ziff
1998. Novel anchorage of GluR2/3 to the postsynaptic density by the AMPA receptor-binding protein ABP. *Neuron*, 21(3):581–591.

Stein, V., D. R. C. House, D. S. Bredt, and R. A. Nicoll
2003. Postsynaptic density-95 mimics and occludes hippocampal long-term potentiation and enhances long-term depression. *The Journal of neuroscience*, 23(13):5503–6.

Stern-Bach, Y., B. Bettler, M. Hartley, P. O. Sheppard, P. J. O'Hara, and S. F. Heinemann
1994. Agonist selectivity of glutamate receptors is specified by two domains structurally related to bacterial amino acid-binding proteins. *Neuron*, 13(6):1345–1357.

Stewart, M. G., N. I. Medvedev, V. I. Popov, R. Schoepfer, H. A. Davies, K. Murphy, G. M. Dallérac, I. V. Kraev, and J. J. Rodríguez
2005. Chemically induced long-term potentiation increases the number of perforated and complex postsynaptic densities but does not alter dendritic spine volume in CA1 of adult mouse hippocampal slices. *European Journal of Neuroscience*, 21(12):3368–3378.

Stoppini, L., P.-A. Buchs, and D. Muller
1991. A simple method for organotypic cultures of nervous tissue. *Journal of Neuroscience Methods*, 37(2):173–182.

Straub, C., D. L. Hunt, M. Yamasaki, K. S. Kim, M. Watanabe, P. E. Castillo, and S. Tomita
2011. Distinct functions of kainate receptors in the brain are determined by the auxiliary subunit Neto1. *Nature Neuroscience*, 14(7):866–873.

Sturgill, J. F., P. Steiner, B. L. Czervionke, and B. L. Sabatini
2009. Distinct Domains within PSD-95 Mediate Synaptic Incorporation, Stabilization, and Activity-Dependent Trafficking. *Journal of Neuroscience*, 29(41):12845–12854.

Südhof, T. C.
2017. Synaptic Neurexin Complexes: A Molecular Code for the Logic of Neural Circuits. *Cell*, 171(4):745–769.

Sukumaran, M., M. Rossmann, I. Shrivastava, A. Dutta, I. Bahar, and I. H. Greger
2011. Dynamics and allosteric potential of the AMPA receptor N-terminal domain. *EMBO Journal*, 30(5):972–982.

Sumioka, A., T. E. Brown, A. S. Kato, D. S. Bredt, J. A. Kauer, and S. Tomita
2011. PDZ binding of TARPγ-8 controls synaptic transmission but not synaptic plasticity. *Nature Neuroscience*, 14(11):1410–1412.

Sumioka, A., D. Yan, and S. Tomita
2010. TARP Phosphorylation Regulates Synaptic AMPA Receptors through Lipid Bilayers. *Neuron*, 66(5):755–767.

Swanson, G. T., S. K. Kamboj, and S. G. Cull-Candy
1997. Single-channel properties of recombinant AMPA receptors depend on RNA editing, splice variation, and subunit composition. *The Journal of neuroscience*, 17(1):58–69.

Swingle, B., E. Markel, N. Costantino, M. G. Bubunenko, S. Cartinhour, and D. L. Court
2010. Oligonucleotide recombination in Gram-negative bacteria. *Molecular Microbiology*, 75(1):138–148.

Takamiya, K., L. Mao, R. L. Huganir, and D. J. Linden
2008. The glutamate receptor-interacting protein family of GluR2-binding proteins is required for long-term synaptic depression expression in cerebellar Purkinje cells. *The Journal of neuroscience*, 28(22):5752–5.

Takeuchi, Y., J. Morise, I. Morita, H. Takematsu, and S. Oka
2015. Role of Site-Specific N-Glycans Expressed on GluA2 in the Regulation of Cell Surface Expression of AMPA-Type Glutamate Receptors. *PLOS ONE*, 10(8):e0135644.

Tang, A. H., H. Chen, T. P. Li, S. R. Metzbower, H. D. MacGillavry, and T. A. Blanpied
2016. A trans-synaptic nanocolumn aligns neurotransmitter release to receptors. *Nature*, 536(7615):210–214.

Tao, H. W. and M. Poo
2001. Retrograde signaling at central synapses. *Proceedings of the National Academy of Sciences*, 98(20):11009–15.

Tomita, S., L. Chen, Y. Kawasaki, R. S. Petralia, R. J. Wenthold, R. A. Nicoll, and D. S. Bredt
2003. Functional studies and distribution define a family of transmembrane AMPA receptor regulatory proteins. *Journal of Cell Biology*, 161(4):805–816.

Tomita, S., M. Fukata, R. A. Nicoll, and D. S. Bredt
2004. Dynamic Interaction of Stargazin-like TARPs with Cycling AMPA Receptors at Synapses. *Science*, 303(5663):1508–1511.

Tomita, S., V. Stein, T. J. Stocker, R. A. Nicoll, and D. S. Bredt
2005. Bidirectional synaptic plasticity regulated by phosphorylation of stargazin-like TARPs. *Neuron*, 45(2):269–277.

Tønnesen, J., G. Katona, B. Rózsa, and U. V. Nägerl
2014. Spine neck plasticity regulates compartmentalization of synapses. *Nature Neuroscience*, 17(5):678–685.

Tracy, T. E., J. J. Yan, and L. Chen
2011. Acute knockdown of AMPA receptors reveals a trans-synaptic signal for presynaptic maturation. *EMBO Journal*, 30(8):1577–1592.

Traynelis, S. F., L. P. Wollmuth, C. J. McBain, F. S. Menniti, K. M. Vance, K. K. Ogden, K. B. Hansen, H. Yuan, S. J. Myers, and R. Dingledine
2010. Glutamate Receptor Ion Channels: Structure, Regulation, and Function. *Pharmacological Reviews*, 62(3):405–496.

Trehan, A., M. Kiełbus, J. Czapinski, A. Stepulak, I. Huhtaniemi, and A. Rivero-Müller
2016. REPLACR-mutagenesis, a one-step method for site-directed mutagenesis by recombineering. *Scientific Reports*, 6:19121.

Trussell, L. O., S. Zhang, and I. M. Ramant
1993. Desensitization of AMPA receptors upon multiquantal neurotransmitter release. *Neuron*, 10(6):1185–1196.

Turetsky, D., E. Garringer, and D. K. Patneau
2005. Stargazin modulates native AMPA receptor functional properties by two distinct mechanisms. *The Journal of Neuroscience*, 25(32):7438–48.

Turrigiano, G.
2012. Homeostatic synaptic plasticity: Local and global mechanisms for stabilizing neuronal function. *Cold Spring Harbor Perspectives in Biology*, 4(1):a005736.

Twomey, E. C., M. V. Yelshanskaya, R. A. Grassucci, J. Frank, and A. I. Sobolevsky
2016. Elucidation of AMPA receptor-stargazin complexes by cryo-electron microscopy. *Science*, 353(6294):83–86.

Twomey, E. C., M. V. Yelshanskaya, R. A. Grassucci, J. Frank, and A. I. Sobolevsky
2017. Channel opening and gating mechanism in AMPA-subtype glutamate receptors. *Nature*, 549(7670):60–65.

van Leeuwen, J., B. Andrews, C. Boone, and G. Tan
2015. Rapid and Efficient Plasmid Construction by Homologous Recombination in Yeast. *Cold Spring Harbor protocols*, 2015(9):pdb.prot085100.

Vandenberghe, W., R. A. Nicoll, and D. S. Bredt
2005. Stargazin is an AMPA receptor auxiliary subunit. *Proceedings of the National Academy of Sciences*, 102(2):485–90.

Verdoorn, T. A., N. Burnashev, H. Monyer, P. H. Seeburg, and B. Sakmann
1991. Structural determinants of ion flow through recombinant glutamate receptor channels. *Science*, 252(5013):1715–1718.

Verheijen, J. H., N. M. E. Nieuwenbroek, B. Beekman, R. Hanemaaijer, H. W. Verspaget, H. K. Ronday, and A. H. F. Bakker
1997. Modified proenzymes as artificial substrates for proteolytic enzymes: colorimetric assay of bacterial collagenase and matrix metalloproteinase activity using modified pro-urokinase. *Biochem. J*, 323:603–609.

Viswanathan, M. and S. T. Lovett
1998. Single-strand DNA-specific exonucleases in Escherichia coli: Roles in repair and mutation avoidance. *Genetics*, 149(1):7–16.

Von Engelhardt, J., V. Mack, R. Sprengel, N. Kavenstock, K. W. Li, Y. Stern-Bach, A. B. Smit, P. H. Seeburg, and H. Monyer
2010. CKAMP44: A brain-specific protein attenuating short-term synaptic plasticity in the dentate gyrus. *Science*, 327(5972):1518–1522.

Vyleta, N. P., C. Borges-Merjane, and P. Jonas
2016. Plasticity-dependent, full detonation at hippocampal mossy fiber–CA3 pyramidal neuron synapses. *eLife*, 5:e17977.

Waites, C. L., C. G. Specht, K. Hartel, S. Leal-Ortiz, D. Genoux, D. Li, R. C. Drisdel, O. Jeyifous, J. E. Cheyne, W. N. Green, J. M. Montgomery, and C. C. Garner
2009. Synaptic SAP97 Isoforms Regulate AMPA Receptor Dynamics and Access to Presynaptic Glutamate. *Journal of Neuroscience*, 29(14):4332–4345.

Wakayama, S., S. Kiyonaka, I. Arai, W. Kakegawa, S. Matsuda, K. Ibata, Y. L. Nemoto, A. Kusumi, M. Yuzaki, and I. Hamachi
2017. Chemical labelling for visualizing native AMPA receptors in live neurons. *Nature Communications*, 8:14850.

Wang, Y., K. E. Fehlhaber, I. Sarria, Y. Cao, N. T. Ingram, D. Guerrero-Given, B. Throesch, K. Baldwin, N. Kamasawa, T. Ohtsuka, A. P. Sampath, and K. A. Martemyanov
2017. The Auxiliary Calcium Channel Subunit $\alpha 2\delta 4$ Is Required for Axonal Elaboration, Synaptic Transmission, and Wiring of Rod Photoreceptors. *Neuron*, 93(6):1359–1374.e6.

Wang, Y., Y. Liu, J. Chen, M. J. Tang, S. L. Zhang, L. N. Wei, C. H. Li, and D. B. Wei
2015. Restriction-ligation-free (RLF) cloning: A high-throughput cloning method by in vivo homologous recombination of PCR products. *Genetics and Molecular Research*, 14(4):12306–12315.

Watson, J. F., H. Ho, and I. H. Greger
2017. Synaptic transmission and plasticity require AMPA receptor anchoring via its N-terminal domain. *eLife*, 6:e23024.

Weber, E., R. Gruetzner, S. Werner, C. Engler, and S. Marillonnet
2011. Assembly of designer tal effectors by golden gate cloning. *PLoS ONE*, 6(5):e19722.

Wei, H., J. Hu, L. Wang, F. Xu, and S. Wang
2012. Rapid gene splicing and multi-sited mutagenesis by one-step overlap extension polymerase chain reaction. *Analytical Biochemistry*, 429(1):76–78.

Wenthold, R. J., R. S. Petralia, I. I. Blahos J, and A. S. Niedzielski
1996. Evidence for multiple AMPA receptor complexes in hippocampal CA1/CA2 neurons. *The Journal of Neuroscience*, 16(6):1982–9.

Werner, S., C. Engler, E. Weber, R. Gruetzner, and S. Marillonnet
2012. Fast track assembly of multigene constructs using golden gate cloning and the MoClo system. *Bioeng. Bugs*, 3:38–43.

Wisden, W. and P. H. Seeburg
1993. A complex mosaic of high-affinity kainate receptors in rat brain. *The Journal of neuroscience*, 13(8):3582–3598.

Won, S., J. M. Levy, R. A. Nicoll, and K. W. Roche
2017. MAGUKs: multifaceted synaptic organizers. *Current Opinion in Neurobiology*, 43:94–101.

Wright, A. and B. Vissel
2012. The essential role of AMPA receptor GluR2 subunit RNA editing in the normal and diseased brain. *Frontiers in Molecular Neuroscience*, 5:34.

Wu, D., T. Bacaj, W. Morishita, D. Goswami, K. L. Arendt, W. Xu, L. Chen, R. C. Malenka, and T. C. Südhof
2017. Postsynaptic synaptotagmins mediate AMPA receptor exocytosis during LTP. *Nature*, 544(7650):316–321.

Xia, J., H. J. Chung, C. Wihler, R. L. Huganir, and D. J. Linden
2000. Cerebellar long-term depression requires PKC-regulated interactions between GluR2/3 and PDZ domain-containing proteins. *Neuron*, 28(2):499–510.

Xia, J., X. Zhang, J. Staudinger, and R. L. Huganir
1999. Clustering of AMPA Receptors by the Synaptic PDZ Domain–Containing Protein PICK1. *Neuron*, 22(1):179–187.

Xia, Y., W. Chu, Q. Qi, and L. Xun
2015. New insights into the QuikChange™ process guide the use of Phusion DNA polymerase for site-directed mutagenesis. *Nucleic Acids Research*, 43(2):e12–e12.

Xu, G., H. Lu, L. Wang, H. Chen, Z. Xu, Y. Hu, B. Tian, and Y. Hua
2010. DdrB stimulates single-stranded DNA annealing and facilitates RecA-independent DNA repair in Deinococcus radiodurans. *DNA Repair*, 9(7):805–812.

Xu, W., O. M. Schlüter, P. Steiner, B. L. Czervionke, B. Sabatini, and R. C. Malenka
2008. Molecular Dissociation of the Role of PSD-95 in Regulating Synaptic Strength and LTD. *Neuron*, 57(2):248–262.

Yamasaki, M., M. Fukaya, M. Yamazaki, H. Azechi, R. Natsume, M. Abe, K. Sakimura, and M. Watanabe
2016. TARP γ-2 and γ-8 Differentially Control AMPAR Density Across Schaffer Collateral/Commissural Synapses in the Hippocampal CA1 Area. *The Journal of Neuroscience*, 36(15):4296–312.

Yamazaki, M., K. Araki, A. Shibata, and M. Mishina
1992. Molecular cloning of a cDNA encoding a novel member of the mouse glutamate receptor channel family. *Biochemical and biophysical research communications*, 183(2):886–892.

Yamazaki, M., T. Ohno-Shosaku, M. Fukaya, M. Kano, M. Watanabe, and K. Sakimura
2004. A novel action of stargazin as an enhancer of AMPA receptor activity. *Neuroscience Research*, 50(4):369–374.

Yao, Z., D. H. Jones, and C. Grose
1992. Site-directed mutagenesis of herpesvirus glycoprotein phosphorylation sites by recombination polymerase chain reaction. *Genome Research*, 1(3):205–207.

York, A. L. and J. Q. Zheng
2017. Super-Resolution Microscopy Reveals a Nanoscale Organization of Acetylcholine Receptors for Trans-Synaptic Alignment at Neuromuscular Synapses. *eneuro*, 4(4):ENEURO.0232–17.2017.

Yuan, H., K. B. Hansen, K. M. Vance, K. K. Ogden, and S. F. Traynelis
2009. Control of NMDA Receptor Function by the NR2 Subunit Amino-Terminal Domain. *Journal of Neuroscience*, 29(39):12045–12058.

Yuzaki, M. and A. R. Aricescu
2017. A GluD Coming-Of-Age Story. *Trends in Neurosciences*, 40(3):138–150.

Zachariassen, L. G., L. Katchan, A. G. Jensen, D. S. Pickering, A. J. R. Plested, and A. S. Kristensen
2016. Structural rearrangement of the intracellular domains during AMPA receptor activation. *Proceedings of the National Academy of Sciences*, 113(27):E3950–E3959.

Zamanillo, D., R. Sprengel, Ø. Hvalby, V. Jensen, N. Burnashev, A. Rozov, K. M. Kaiser, H. J. Köster, T. Borchardt, P. Worley, J. Lübke, M. Frotscher, P. H. Kelly, B. Sommer, P. Andersen, P. H. Seeburg, and B. Sakmann
1999. Importance of AMPA receptors for hippocampal synaptic plasticity but not for spatial learning. *Science*, 284(5421):1805–1811.

Zaret, K. S., J. K. Liu, and C. M. DiPersio
1990. Site-directed mutagenesis reveals a liver transcription factor essential for the albumin transcriptional enhancer. *Proceedings of the National Academy of Sciences*, 87(14):5469–5473.

Zhang, H., L. A. Etherington, A. S. Hafner, D. Belelli, F. Coussen, P. Delagrange, F. Chaouloff, M. Spedding, J. J. Lambert, D. Choquet, and L. Groc
2013. Regulation of AMPA receptor surface trafficking and synaptic plasticity by a cognitive enhancer and antidepressant molecule. *Molecular Psychiatry*, 18(4):471–484.

Zhang, W., F. St-Gelais, C. P. Grabner, J. C. Trinidad, A. Sumioka, M. Morimoto-Tomita, K. S. Kim, C. Straub, A. L. Burlingame, J. R. Howe, and S. Tomita
2009. A Transmembrane Accessory Subunit that Modulates Kainate-Type Glutamate Receptors. *Neuron*, 61(3):385–396.

Zhang, Y., L. Matt, T. Patriarchi, Z. A. Malik, D. Chowdhury, D. K. Park, A. Renieri, J. B. Ames, and J. W. Hell
2014a. Capping of the N-terminus of PSD-95 by calmodulin triggers its postsynaptic release. *EMBO Journal*, 33(12):1341–1353.

Zhang, Y., J. P. Muyrers, G. Testa, and A. F. Stewart
2000. DNA cloning by homologous recombination in Escherichia coli. *Nature biotechnology*, 18(12):1314–1317.

Zhang, Y., U. Werling, and W. Edelmann
2012. SLiCE: A novel bacterial cell extract-based DNA cloning method. *Nucleic Acids Research*, 40(8):1–10.

Zhang, Y., U. Werling, and W. Edelmann
2014b. Seamless Ligation Cloning Extract (SLiCE) cloning method. *Methods in Molecular Biology*, 1116:235–244.

Zhao, H., S. Lomash, S. Chittori, C. Glasser, M. L. Mayer, and P. Schuck
2017. Preferential assembly of heteromeric kainate and AMPA receptor amino terminal domains. *eLife*, 6:e32056.

Zhao, Y., S. Chen, C. Yoshioka, I. Baconguis, and E. Gouaux
2016. Architecture of fully occupied GluA2 AMPA receptor-TARP complex elucidated by cryo-EM. *Nature*, 536(7614):1–18.

Zheng, L., U. Baumann, and J. L. Reymond
2004. An efficient one-step site-directed and site-saturation mutagenesis protocol. *Nucleic Acids Research*, 32(14):e115–e115.

Zheng, Y., P. J. Brockie, J. E. Mellem, D. M. Madsen, C. S. Walker, M. M. Francis, and A. V. Maricq
2006. SOL-1 is an auxiliary subunit that modulates the gating of GLR-1 glutamate receptors in Caenorhabditis elegans. *Proceedings of the National Academy of Sciences*, 103(4):1100–1105.

Zhou, Z., A. Liu, S. Xia, C. Leung, J. Qi, Y. Meng, W. Xie, P. Park, G. L. Collingridge, and Z. Jia
2018. The C-terminal tails of endogenous GluA1 and GluA2 differentially contribute to hippocampal synaptic plasticity and learning. *Nature Neuroscience*, 21(1):50–65.

Zhu, S., R. A. Stein, C. Yoshioka, C. H. Lee, A. Goehring, H. S. McHaourab, and E. Gouaux
2016. Mechanism of NMDA Receptor Inhibition and Activation. *Cell*, 165(3):704–714.

Zuo, J., P. L. De Jager, K. A. Takahashi, W. Jiang, D. J. Linden, and N. Heintz
1997. Neurodegeneration in Lurcher mice caused by mutation in $\delta 2$ glutamate receptor gene. *Nature*, 388(6644):769–773.

Appendix A

Primer Sequences for IVA cloning development.

Primer sequence regions in regular font denote template binding regions.

Primer sequence regions in *italics* denote homologous regions.

Primer sequence regions in **bold** denote new codons for mutagenesis.

Template opt.		**Function**
OPT1-F	AATGACAGCTCATCCTCAGAGAACCGG	Amplify pRK5 without recombination
OPT1-R	TCCTCCGTGAGAATGACCCAAAAGCC	

Length opt.		Length (bp)	
OPT2-F	*CGCCCGGCGG* AATGACAGCTCATCCTCAGAGAACCGG	10	Delete GluA3 NTD region in pRK5
OPT2-R	*CCGCCGGGCG* TCCTCCGTGAGAATGACCCAAAAGCC	10	
OPT3-F	*CACGTCCAGAAGAAT* AATGACAGCTCATCCTCAGAGAACCGG	15	
OPT3-R	*ATTCTTCTGGACGTG* TCCTCCGTGAGAATGACCCAAAAGCC	15	
OPT4-F	*ATTCTTATGGACATTAATTA* AATGACAGCTCATCCTCAGAGAACCGG	20	
OPT4-R	*TAATTAATGTCCATAAGAAT* TCCTCCGTGAGAATGACCCAAAAGCC	20	
OPT5-F	*ATTATAATATTTACTATATATTATT* AATGACAGCTCATCCTCAGAGAACCGG	25	
OPT5-R	*AATAATATATAGTAAATATTATAAT* TCCTCCGTGAGAATGACCCAAAAGCC	25	

Tm opt.		Tm (°C)	
OPT6-F	*ATTATTAATTATTTA* AATGACAGCTCATCCTCAGAGAACCGG	20	Delete GluA3 NTD region in pRK5
OPT6-R	*TAAATAATTAATAAT* TCCTCCGTGAGAATGACCCAAAAGCC	20	
OPT7-F	*GTCATCAGTTCTTTC* AATGACAGCTCATCCTCAGAGAACCGG	36	
OPT7-R	*GAAAGAACTGATGAC* TCCTCCGTGAGAATGACCCAAAAGCC	36	
OPT8-F	*GACGTCAGCGTGGTA* AATGACAGCTCATCCTCAGAGAACCGG	45	
OPT8-R	*TACCACGCTGACGTC* TCCTCCGTGAGAATGACCCAAAAGCC	45	
OPT9-F	*GGCGTCAGCGCGGTC* AATGACAGCTCATCCTCAGAGAACCGG	53	
OPT9-R	*GACCGCGCTGACGCC* TCCTCCGTGAGAATGACCCAAAAGCC	53	

Figure A.1 ***Primer sequences for Method Optimisation.***

Delete/Insert		
INS1-F	*GAACAAAAACTCATCTCAGAAGAGGATCTG* TTCCCCAACACCATCAGCATAGGTGG	Inserting myc tag at GluA3 N-terminus in pRK5-GluA3 (IVA)
INS1-R	*TCTTCTGAGATGAGTTTTTGTTTC* TCCTCCGTGAGAATGACCCAAAAGCC	
INS2-F	**(P)**-TCAGAAGAGGATCTG TTCCCCAACACCATCAGCATAGGTGG	Inserting myc tag at GluA3 N-terminus (phosphorylated primers)
INS2-R	**(P)**-GATGAGTTTTTGTTC TCCTCCGTGAGAATGACCCAAAAGCC	
DEL1-F	*TGGGTCATTCTCACGGAGGA* AATGACAGCTCATCCTCAGAGAACCGG	Deleting GluA3 N-terminal domain in pRK5-GluA3
DEL1-R	TCCTCCGTGAGAATGACCCAAAAGCC	
DEL2-F	*CTGATTTTTGGTGTC* TCTTCTAACAGCATACAGATAGGGGGG	Deleting myc tag at GluA2 N-terminus in plRES-GluA2
DEL2-R	GACACCAAAAATCAGTCCCCATAAAACAG	
DELINS1-F	*GAAAACCTGTACTTCCAGTCC* ATG GTG AGC AAG GGC GAG GAG CTG	Replacing IRES with linker in plRES-GluA2 EGFP
DELINS1-R	*GGACTGGAAGTACAGGTTTTC* CTTCATTCGTTTCGCCTCGGCCCTTG	
Subcloning		
SUB1-F	*ACCGTCAGATCCGGTAGC* ATGAAGACGAGCCGCCGCGGC	Amplifies GSG1L for plRES vector
SUB1-R	*GATCTGAGTCCGGTAGC* TCACACCCAGTGCCCCAGGACCC	
SUB2-F	GCTACCGGACTCAGATCTCGAGC	Amplifies plRES vector for GSG1L
SUB2-R	GCTAGCGGATCTGACGGTTCACTAAAC	
SUB3-F	*TGGTACCGAGCTCGGATCC* ATGCAAAAGATTATGCATATTTCTGTCCTCCTTTCTC	Amplifies GluA2 for pcDNA4/TO
SUB3-R	*GTGCTGGATATCTGCAGAATTC* CTAAATTTTAACACTCTCGATGCCATATACGTTGTAAC	
SUB4-F	GAATTCTGCAGATATCCAGCACAGTGGC	Amplifies pcDNA4/TO vector for GluA2
SUB4-R	GGATCCGAGCTCGGTACCAAGCTTAAG	
SUB5-F	*ATCGATAAGCTTGATTCGAGCTAGCC* ACCATGGTGAGCAAGGGCG	Amplifies EGFP-Homer1c for AAV-CW3SL vector
SUB5-R	*CTCGAGATAATCAACCTCTGGATTA* TTAGCTGCATTCTAGTAGCTTGGCCAAATTATCC	

Figure A.2 ***Primer sequences for Insertions, Deletions and Subcloning.***

Mutagenesis	**IVA cloning**	
MUT1-F	*CCAGATCGTGAAGCTA* **TGC** AAGAATGGCATCGGGTACCACTACATCC	GluA1 E202C mutation in pIRES-GluA1
MUT1-R	**GCA**TAGCTTCACGATCTGGCCCAGGATG	
MUT2-F	*ACTGAAGCATTCCGT* **TCC**CTTCGGAAGCAGAGGATTGAAATATCCCG	GluA2 N292S mutation in pIRES-GluA2
MUT2-R	GGAACGGAA TGCTTCAGTCATCACTTGGACAG	
MUT3-F	*ACAAATTGTGAGTGTT* **TGC** AAGCATGTCAAAGGCTACCATTATATCATC	GluA4 G208C mutation in pRK5-GluA4
MUT3-R	**GCA**AACACTCACAATTTGTTCTAAAATGTTTTGAAGC	
MUT4-F	*ACCGACTACCTCCAG* **TAG**TCGGCCATCACCCGCATCCCC	!2 A219STOP mutation in pGW1-γ2
MUT4-R	**CTA**CTGGAGGTAGTCGGTGGCACGG	

QuikChange mutagenesis		
MUT5-F	CCAGATCGTGAAGCTA**TGC**AAGAATGGCATCG	GluA1 E202C mutation in pIRES-GluA1
MUT5-R	CGATGCCATTCTT**GCA**TAGCTTCACGATCTGG	
MUT6-F	GACTGAAGCATTCCGT**TCC**CTTCGGAAGCAGAGG	GluA2 N292S mutation in pIRES-GluA2
MUT6-R	CCTCTGCTTCCGAAG**GGA**ACGGAATGCTTCAGTC	
MUT7-R	GAACAAATTGTGAGTGTT**TGC**AAGCATGTCAAAGGCTAC	GluA4 G208C mutation in pRK5-GluA4
MUT7-F	GTAGCCTTTGACATGCTT**GCA**AACACTCACAATTTGTTC	
MUT8-F	CCGACTACCTCCAG**TAG**TCCGCCATCACCCG	!2 A219STOP mutation in pGW1-γ2
MUT8-R	CGGGTGATGGCGGA**CTA**CTGGAGGTAGTCGG	

Multi-site		
INS3-F	*GACTACAAGGACGACGATGACAAG* TCTTCTAACAGCATACAGATAGGGGGC	Inserts FLAG at GluA2 N-terminus in pCustom vector
INS3-R	*TCATCGTCGTCCTTGTAGTC* GACACCAAAAATCAGTCCCCATAAAACAGGAGA	
DEL3-F	*TTCCCAGAATTTTGCAACTTAT* AAGGAAGGTTACAACGTATATGGCATCGAGAG	Deletes FLAG at GluA2 C-terminus in pCustom vector
DEL3-R	ATAAGTTGCAAAATTCTGGAATTCTGCGAGGAAG	
DELINS2-F	*AAGGATGACGACGATAAG* AATGACAGCTCATCCTCAGAGAACCGG	Exchanges GluA3 NTD for FLAG at in pRK5-GluA3
DELINS2-R	ATCGTCGTCATCCTTGTAATCTCCGTGAGA	
SUB6-F	*AGATCGGAAGCGGAAGCGGC* GGGCTGTTTGATCGAGGTGTTCAAATGC	Amplifies !2 for GluA3-γ2 tandem construct
SUB6-R	*CTTCTGGTGGGAAGGATCC* TCATACGGGCGTGGTCCGGCGG	
SUB7-F	GGATCCCTTCCCACCAGAAGCATG	Amplifies pRK5-GluA3 vector for GluA3-γ2 tandem construct
SUB7-R	*GCCGCTTCCGCTTCC* GATCTTAACACTTTCTGTTCCATACACGTTGTAG	

Figure A.3 ***Primer sequences for Mutagenesis and Multi-site modifications.***

XhoI sites		
MUT9-F	*ATGGGGCAAAGCGTGCTC* **GAG** GCGGTCTTCTTTTAGTCCTGGGGC	XhoI site 1 in pRK5-GluA3
MUT9-R	**CTC** GAGCACGCTTTGCCCCATTTTCTTCTG	
MUT10-F	*ACTGGAAAGAGTCATGCATG* **CTC** GAGCCAACATTACAGGTTTCCAGATTGTCAAC	XhoI site 2 in pRK5-GluA3
MUT10-R	**GAG** CATGCATGACTCTTTCCAGTAAAATGTCAGTAAAAC	
MUT11-F	*GCAAGGATGTGATATTTCTC* **GAG** GATCACTTTCTGGGCGCATTGTTGGAG	XhoI site 3 in pRK5-GluA3
MUT11-R	**CTC** GAGAAATATCACATCCTTGCTGCATGAAAGCA	
MUT12-R	*CCTGATGCGGTATTTTCTC* **GAG** ACGCATCTGTGCGGTATTTCACACCG	XhoI site 4 in pRK5-GluA3
MUT12-F	**CTC** GAGAAAATACCGCATCAGGCGCCATTC	
MUT13-R	*ACAAGCTGTGACCGT* **CTC** GAGCTGCATGTGTCAGAGGTTTTCACC	XhoI site 5 in pRK5-GluA3
MUT13-F	**GAG** ACGGTCACAGCTTGTCTGTAAGC	
MUT14-R	*GACCAAAATCCCTTAACTC* **CTC** GAGTTTTCGTTCCACTGAGCGTCAGAC	XhoI site 6 in pRK5-GluA3
MUT14-F	**GAG** TTAAGGGATTTTGGTCATGAGATTATCAAAAAGGATCTTC	
Assembly		
ASS1-F	*GCAGTGAGCGCAACGCAA* TGCTTAGGGTTAGGCGTTTTGCGC	Amplifies CMVtet for Assembly
ASS1-R	*CTATGGAGGTCAAAACAGCG* TCTCTATCACTGATAGGGAGATCTCTATCAC	
ASS2-F	*CGCTGTTTTGACCTCCATAG* ATGGTGAGCAAGGGCGAGGAGC	Amplifies EGFP for Assembly
ASS2-R	*GATGGTGTTGGGGAATCC* CTTGTACAGCTCGTCCATGCCGAG	
ASS3-F	GGATTCCCCAACACCATCAGCATAGG	Amplifies GluA3 for Assembly
ASS3-R	*GCCGCTTCCGCTTCC* GATCTTAACACTTTCTGTTCCATACACGTTGTAG	
ASS4-F	*CGAAGCTTGAGCTCGAG* TCATACGGGCGTGGTCCGGC	Amplifies v2 for Assembly
ASS4-R	*AGATCGGAAGCGGAAGCGGC* GGGCTGTTTGATCGAGGTGTTCAAATGC	
ASS5-F	TGGCCGCCATGGCCCAACTTG	Amplifies pRK5-GluA4 vector for Assembly
ASS5-R	ATTGCGTTGCGCTCACTGCCCG	
Library Formation		
LIB1-F	TGGCCGCCATGGCCCAACTTG	Amplifies pRK5-GluA3 vector for Library
LIB1-F	ATTGCGTTGCGCTCACTGCCCG	
LIB2-F	*GCAGTGAGCGCAACGCAAT* GCTCGCCCGACATTGATTATTGACTAG	Amplifies CMV promoter for Library
LIB2-F	*CTATGGAGGTCAAAACAGCG* AGCTCTGCTTATATAGACCTCCCACCG	
LIB3-F	*GCAGTGAGCGCAACGCAAT* CACTTGTGGACTAAGTTTGTTCGCATCC	Amplifies CamKII promoter for Library
LIB3-F	*CTATGGAGGTCAAAACAGCG* GCTGCCCCCAGAACTAGGGG	
LIB4-F	*CGCTGTTTTGACCTCCATAG* CGAATTCGAATATGCCGTACATCTTTGCC	Amplifies GluA1 for Library from pIRES-GluA1
LIB4-F	*GGGCCATGGCGGCCA* TTACAATCCTGTGGCTCCCAAGGGC	
LIB5-F	*CGCTGTTTTGACCTCCATAG* GCTAGCGGATTCTTCTGCCTTCACTTC	Amplifies GluA2 for Library from pIRES-GluA2
LIB5-F	*GGGCCATGGCGGCCA* CTCGAGGCACTCAGAAGGTTCCTATC	
LIB6-F	*CGCTGTTTTGACCTCCATAG* GAATTCGGCACGAGGTTGCGCC	Amplifies GluA3 for Library from pIRES-GluA3
LIB6-F	*GGGCCATGGCGGCCA* GGATCCCTAGATCTTAACACTTTCTGTTCC	

Figure A.4 ***Primers for XhoI mutations, Plasmid Assembly and Library Creation.***